3. SITE 801[1]

Shipboard Scientific Party[2]

HOLE 801A

Date occupied: 6 December 1989

Date departed: 9 December 1989

Time on hole: 2 days, 10 hr, 00 min

Position: 18°38.568′N, 156°21.57′E

Bottom felt (rig floor, m; drill-pipe measurement): 5685.0

Distance between rig floor and sea level (m): 11.20

Water depth (drill-pipe measurement from sea level, m): 5673.8

Total depth (rig floor; m): 5879.00

Penetration (m): 194.0

Number of cores (including cores with no recovery): 20

Total length of cored section (m): 186.0

Total core recovered (m): 31.49

Core recovery (%): 16

Oldest sediment cored:
Depth (mbsf): 194.0
Nature: Radiolarian claystone
Age: Cenomanian

HOLE 801B

Date occupied: 9 December 1989

Date departed: 17 December 1989

Time on hole: 7 days, 8 hr, 45 min

Position: 18°38.52′N, 156°21.582′E

Bottom felt (rig floor; m: drill-pipe measurement): 5685.0

Distance between rig floor and sea level (m): 11.20

Water depth (drill-pipe measurement from sea level, m): 5673.8

Total depth (rig floor; m): 6196.20

Penetration (m): 511.20

Number of cores (including cores with no recovery): 44

Total length of cored section (m): 317.20

Total core recovered (m): 59.17

Core recovery (%): 18

Oldest sediment cored:
Depth (mbsf): 511.20
Nature: Calcareous silicified tuff and radiolarian metasiltstone
Earliest age: Callovian-Bathonian
Latest age: Oxfordian

Basement:
Depth (mbsf): 461.6
Nature: Basalt

HOLE 801C

Date occupied: 18 December 1989

Date departed: 16 January 1990

Time on hole: 16 days, 2 hr, 00 min

Position: 18°38.538′N, 156°21.588′E

Bottom felt (rig floor; m; drill-pipe measurement): 5685.0

Distance between rig floor and sea level (m): 11.00

Water depth (drill-pipe measurement from sea level, m): 5674.0

Total depth (rig floor; m): 6279.30

Penetration (m): 594.30

Number of cores (including cores with no recovery): 12

Total length of cored section (m): 100.60

Total core recovered (m): 60.60

Core recovery (%): 60

Basement:
Depth (mbsf): 493.7
Nature: Basalt

Comments: Revisited site for fishing and reentry.

Principal Results: This is the first Deep Sea Drilling Project/Ocean Drilling Program (DSDP/ODP) drill site ever to recover Jurassic-age sediments and oceanic crust from the Pacific plate or Pacific Ocean Basin. Site 801 is located in the central Pigafetta Basin on a magnetic quiet zone southeast of, and presumably older than, the M25–M37 magnetic lineation sequence. Holes 801A, 801B, and 801C consist of the following stratigraphic sequence:

8.0–64.0 mbsf: Tertiary to Campanian brown pelagic clay.

64.0–126.5 mbsf: Campanian to Turonian brown chert and porcellanite.

126.5–318.3 mbsf: Cenomanian and Albian volcaniclastic turbidites with minor radiolarite near the base.

318.3–442.9 mbsf: Lower Cretaceous (Valanginian) to Upper Jurassic (Oxfordian) brown radiolarite with dark brown chert and abundant manganese.

442.9–461.6 mbsf: Middle Jurassic (Callovian-Bathonian) umber-colored radiolarite and claystone with strong hematite enrichment, probably indicative of hydrothermal activity during or just after deposition. The oldest dated sediment is interbedded with the basalts in the underlying unit at 473 m where the *Tricolocapsa conexa* zone of Matsuoka and Yao (1986) has been identified. This radiolarian assemblage is the same as the basal radiolarian sequence of DSDP Site 534 that has been recalibrated by Baumgartner (1987) to lie at the Callovian/Bathonian boundary, ~170 Ma. No carbonate in this ridge-crest, equatorial-paleolatitude sedimentary facies suggests that the Late/Middle Jurassic superocean was characterized by extremely low carbonate production and/or preservation.

461.6–590.9 mbsf: Middle Jurassic basement. Interbedded basaltic thin flows, possibly some thin sills, and silicified claystone are at the top of the sequence. Pillow basalts begin at 495 mbsf that exhibit concave pillow structures with chilled margins, variolitic textures, and microcrystalline interiors. A remarkable hydrothermal concretion occurs between 522 and 531 mbsf that is chrome yellow and silica cemented. It is underlain by pillow basalts that are extremely altered directly beneath the hydrothermal deposit,

[1] Lancelot, Y., Larson, R. L., et al., 1990. *Proc. ODP, Init. Repts.*, 129: College Station, TX (Ocean Drilling Program).

[2] Shipboard Scientific Party is as given in the list of participants preceding the contents.

and become less altered towards the bottom of the hole. A summary of coring statistics is present in Table 1.

Standard logging was completed, including a repeat formation microscanner run with the wireline heave compensator operating, from 56 to about 460 mbsf.

BACKGROUND AND OBJECTIVES

Site 801 (proposed site PIG-3A) is located within the so-called "Jurassic magnetic quiet zone" in the central part of the Pigafetta Basin, approximately 150 nautical miles (nmi) southeast of the last well-defined magnetic anomaly (M37) (Figs. 1 and 2). The main objective at this site was to recover Jurassic sediment and oceanic crust that might be the oldest in the Pacific Ocean and possibly in the world ocean.

The main reason for interest in Jurassic sediments from the Pacific is that they chronicle the paleoenvironment of the Jurassic superocean, which covered two-thirds of the Earth at that time, but for which we have no direct record. The only samples of pelagic "deep-sea" Jurassic sediments come from the fold belts surrounding the Tethys paleo-ocean and from DSDP sites in the proto-Atlantic, both of which correspond to relatively restricted marine conditions mostly from continental margin environments.

Previous attempts to recover Jurassic sediments in the Pacific prior to Leg 129 all have failed in cherts or extraordinarily thick lava flows, sills, or volcaniclastics of middle to Late Cretaceous age that proved impossible to penetrate (DSDP Site 461 in the Nauru Basin and Site 585 in the East Mariana Basin). The most recent attempt was the previous site on Leg 129 (Site 800), where again volcanic rocks of probable Early Cretaceous age were found above the top of the oceanic crust, as inferred from seismic data. The oldest sediments that we recovered at that site, before encountering a series of thick dolerite sills, were claystones of Berriasian age, and although that discovery was indeed a disappointment, it did not seriously alter our hopes to find the Jurassic basement in the Pigafetta Basin. The results from the sonobuoys in the area of Site 801, as well as the much clearer image of the acoustic basement on reflection profiles, were very encouraging in that respect. Furthermore, since the acoustic basement at Site 801 was visible near 8.0 to 8.1 seconds two-way traveltime (s twt), chances appeared good that this reflector would coincide with the top of the oceanic crust because that depth is approximately the level at which crust of Jurassic age is expected (approximately 6200 mbsl).

The lowermost reflector observed on both the multichannel seismic profile from the MESOPAC II cruise (see "Site Geophysics and Seismic Stratigraphy" section, this chapter) and the single-channel profile recorded while approaching the site lies at approximately 8.0 s twt beneath sea level. Its exhibits a "hummocky" character that strongly suggests its correspondence to the top of seismic layer 2. Based on this observation, the total sediment thickness at Site 801 was estimated at about 460 m assuming an average sound velocity of about 2.0 km/s for the whole sedimentary section, a value derived both from site survey data (sonobuoys from MESOPAC II and *Fred H. Moore* 35-12 cruises) and from drilling results from Site 800.

A simple, straightforward extrapolation of ages and spreading rates of the magnetic anomalies observed in the northwestern part of the Pigafetta Basin (M20–M25), predicts the basement to be of Middle to Late Jurassic age at Site 801 (Fig. 3). The sediment section was believed to consist mostly of pelagic deposits, although chances remained good to encounter volcaniclastic turbidites again since the seismic interval corresponding to these sediments could be traced all the way

Table 1. Coring summary for Site 801.

Core	Date	Time	Depth (mbsf)	Length cored (m)	Length recovered (m)	Recovery (%)
129-801A-						
1R[a]	7 Dec 1989	1145	14.5	6.5	1.30	20.0
2R	7 Dec	1545	20.4	5.9	0.50	8.5
3R	7 Dec	1645	30.0	9.6	5.29	55.1
4R	7 Dec	2025	39.6	9.6	2.45	25.5
5R	7 Dec	2125	49.3	9.7	8.50	87.6
6R	8 Dec	0020	59.0	9.7	0.02	0.2
7R	8 Dec	0210	68.6	9.6	5.15	53.6
8R	8 Dec	0400	78.2	9.6	0.27	2.8
9R	8 Dec	0545	87.5	9.3	0.16	1.7
10R	8 Dec	0735	97.1	9.6	0.42	4.4
11R	8 Dec	0920	106.8	9.7	0.17	1.8
12R	8 Dec	1115	116.5	9.7	0.22	2.3
13R	8 Dec	1320	126.2	9.7	0.35	3.6
14R	8 Dec	1520	135.9	9.7	0.63	6.5
15R	8 Dec	1720	145.6	9.7	0.42	4.3
16R	8 Dec	1940	155.2	9.6	1.59	16.5
17R	8 Dec	2130	165.0	9.8	0.74	7.6
18R	8 Dec	2350	174.7	9.7	1.69	17.4
19R	9 Dec	0205	184.4	9.7	1.25	12.9
20R	9 Dec	0450	194.0	9.6	0.37	3.9
		Coring totals		186.0	31.49	16.9
129-801B-						
1R	10 Dec	0320	203.5	9.5	6.45	67.9
2R	10 Dec	0610	212.9	9.4	1.31	13.9
3R	10 Dec	0830	222.3	9.4	1.29	13.7
4R	10 Dec	1025	231.7	9.4	0.44	4.7
5R	10 Dec	1315	241.3	9.6	4.01	41.8
6R	10 Dec	1500	251.0	9.7	5.67	58.4
7R	10 Dec	1655	260.7	9.7	1.21	12.5
8R	10 Dec	1845	270.3	9.6	7.92	82.5
9R	10 Dec	2040	280.0	9.7	0.01	0.1
10R	10 Dec	2250	289.7	9.7	0.75	7.7
11R	11 Dec	0055	299.3	9.6	0.19	2.0
12R	11 Dec	0305	309.0	9.7	0.86	8.9
13R	11 Dec	0600	318.3	9.3	1.17	12.6
14R	11 Dec	0815	327.7	9.4	0.49	5.2
15R	11 Dec	1030	337.2	9.5	0.12	1.3
16R	11 Dec	1245	346.6	9.4	0.49	5.2
17R	11 Dec	1520	355.8	9.2	0.38	4.1
18R	11 Dec	1730	365.3	9.5	0.46	4.8
19R	11 Dec	1920	374.5	9.2	0.25	2.7
20R	11 Dec	2135	383.7	9.2	0.29	3.2
21R	12 Dec	0005	389.8	6.1	0.21	3.4
22R	12 Dec	0215	395.9	6.1	0.05	0.8
23R	12 Dec	0620	400.6	4.7	0.16	3.4
24R	12 Dec	0825	405.2	4.6	0.68	14.8
25R	12 Dec	1025	410.0	4.8	0.62	12.9
26R	12 Dec	1230	414.7	4.7	0.10	2.1
27R	12 Dec	1425	419.4	4.7	1.02	21.7
28R	12 Dec	1625	424.2	4.8	0.11	2.3
29R	12 Dec	1815	428.9	4.7	0.14	3.0
30R	12 Dec	2000	433.6	4.7	0.16	3.4
31R	12 Dec	2155	438.2	4.6	0.28	6.1
32R	12 Dec	2340	442.8	4.6	0.07	1.5
33R	13 Dec	0115	447.6	4.8	2.18	45.4
34R	13 Dec	0325	452.3	4.7	0.72	15.3
35R	13 Dec	0515	456.9	4.6	3.43	74.5
36R	13 Dec	0710	461.5	4.6	0.06	1.3
37R	13 Dec	0930	466.1	4.6	0.58	12.6
38R	13 Dec	1205	470.7	4.6	0.20	4.4
39R	13 Dec	1425	476.9	6.2	0.29	4.7
40R	13 Dec	1845	483.0	6.1	0.94	15.4
41R	13 Dec	2355	487.6	4.6	2.66	57.8
42R	14 Dec	0305	492.2	4.6	2.39	51.9
43R	14 Dec	0905	501.7	9.5	5.00	52.6
44R	14 Dec	1625	511.2	9.5	3.36	35.3
		Coring totals		317.2	59.17	18.7
129-801C-						
1R	9 Jan 1990	1145	511.0	9.3	7.43	79.9
2R	9 Jan	1835	520.2	9.2	6.69	72.7
3R	9 Jan	2200	529.7	9.5	0.95	10.0
4R	10 Jan	0100	539.2	9.5	2.42	25.5
5R	10 Jan	0607	548.5	9.3	6.36	68.4
6R	10 Jan	1615	558.1	9.6	6.52	67.9
7R	11 Jan	0005	567.5	9.4	5.87	62.4
8R	11 Jan	0830	571.2	3.7	2.22	60.0
9R	14 Jan	1300	577.0	5.8	5.83	100.0
10R	14 Jan	2050	585.9	8.9	8.42	94.6
11R	15 Jan	0320	595.3	9.4	4.25	45.2
12R	15 Jan	1830	602.3	7.0	3.64	52.0
		Coring totals		100.6	60.60	60.2

[a] Top of Core 129-801A-1R is 8 mbsf.

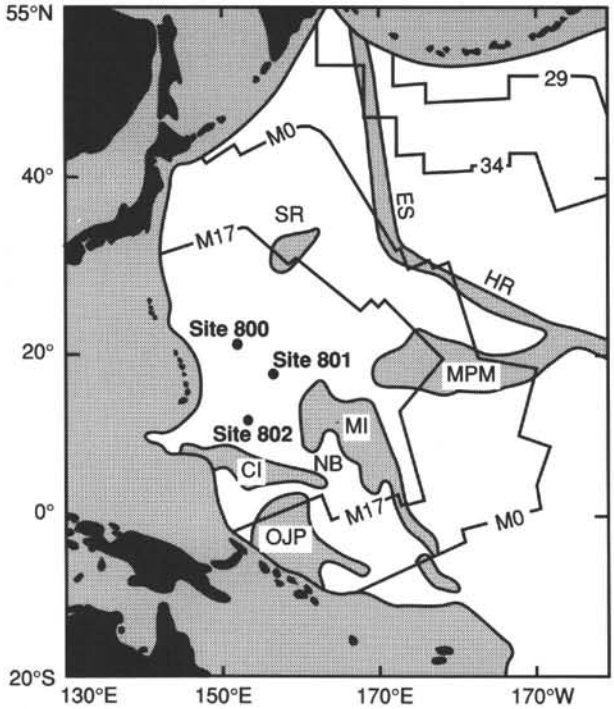

Figure 1. Location of Site 801. Bedrock isochrons are determined from magnetic anomaly lineation mapping on the Pacific plate (after Larson et al., 1985) and superimposed on groups of islands, atolls, and guyots in the western Pacific Ocean. Feature abbreviations are as follows: Caroline Islands (CI), Ontong Java Plateau (OJP), Marshall Islands (MI), Nauru Basin (NB), Mid-Pacific Mountains (MPM), Shatshy Rise (SR), Hawaiian Ridge (HR), and Emperor Seamounts (ES). Jagged contours represent normal Pacific oceanic crust. Shaded areas represent volcanic edifices with thickened crustal sections as well as younger areas beyond the Pacific subduction zones.

through the Pigafetta Basin from Site 800 to Site 801. Abundant chert was also expected at this site both in the upper and in the lower parts of the sediment column, corresponding to two successive crossings of the equatorial zone. The youngest of these crossings is believed to have occurred, from south to north, during the Late Cretaceous (Lancelot and Larson, 1975; Lancelot, 1978) and should correspond with abundant deposition of biogenic silica, later diagenetically altered into chert and/or porcellanite. These layers are probably responsible for the uppermost strong reflector observed at about 60 milliseconds below seafloor (ms bsf), both on the 3.5-kHz and water-gun seismic profiles.

The results from drilling at Site 800 have confirmed that the motion of the Pacific plate was such that the spreading ridge that generated the seafloor of the Pigafetta Basin was probably located north of the equator prior to the earliest Cretaceous, accounting for the oldest equatorial crossing from north to south, as suggested by Larson and Lowrie (1975). If productivity at the equator was comparable to what is observed for the subsequent times, this older equatorial crossing would certainly have been also characterized by abundant deposition of silica. The lowermost part of the sediment section was thus expected to be composed of chert and possibly limestone, depending on the level of the carbonate compensation depth (CCD) at the time. These deposits could be responsible for the rather strong regional reflector observed on most seismic profiles just above the horizon that we interpret as the top of the oceanic crust.

In summary, because of (1) the location of Site 801 on seafloor presumably older than the M30–M37 magnetic lineation sequence, (2) the "hummocky" character of the acoustic basement, and (3) comparison with results obtained from drilling at Sites 307 and 800, this site appeared to offer the best chance to sample Jurassic sediments and the underlying oceanic crust and hence to achieve the primary objectives of Leg 129.

If indeed the results from the single-bit pilot hole confirmed our hopes, then the site obviously would become the first choice for a major attempt at deep basement penetration with reentry. The plan, therefore, was to continuously core the pilot hole to basement, obtain a complete suite of logs in the sediment section, drill and case another hole into basement, and try to reach at least 100 to 150 m into the oceanic crust in the reentry hole. After logging the lower part of the hole and running a packer/permeability test into the crust, we intended to leave a clean-cased hole, open for future downhole experiments, as well as for further penetration into what is believed to be the oldest crust of the world ocean.

OPERATIONS

Approach to the Site

We approached Site 801 from the northwest on a course of 127°, parallel to MESOPAC II line 6, at 6 knots (kt), shooting a seismic line with two 80-in.^{3} water guns (Fig. 4). Our target was a point at 0600 hr (Universal Time Coordinated, or UTC), 26 August 1989, on MESOPAC II line 10 that is perpendicular to our approach direction. At 1600 hr UTC, 6 December 1989, we crossed MESOPAC II line 6 at the target location (18°38.5′N, 154°211.6′E) and launched a beacon over a very clear seismic target on the system of the *JOIDES Resolution* corresponding exactly to MESOPAC II lines 6 and 10 (see Figs. 51, 52, and 53, "Site Geophysics and Seismic Stratigraphy," this chapter). We continued this profile on this heading until 1655 hr, when we retrieved the seismic gear, returned to the beacon location, and discovered the beacon was inoperable. Having no global positioning system (GPS) available for navigation, we hove to, acquired a transit satellite fix, and dead-reckoned back to the original drop site to deploy a second beacon, which was also a dud. This procedure was repeated again, and we finally placed a working beacon on bottom, but GPS eventually proved its location to be 1180 m south of the intended drill site. An 1180-m offset from this beacon provided marginal positioning in calm weather, so we dropped a fourth beacon at the drill site just prior to spudding into the seafloor.

Hole 801A

The bottom-hole assembly (BHA) for Hole 801A was identical to that for Hole 800A (see "Operations" section, "Site 800" chapter, this volume). The depth to the rig floor, measured by precision depth recorder, was 5696 m. The first mud-line coring attempt was at 5698 m, and provided a core liner completely covered with soupy brown clay. We raised the bit 8 m and recovered a completely clean and empty core liner. We lowered the bit to 5699 m and recovered 6 m of soupy brown clay, establishing the mud line at 5693 m below the rig floor. A jet-in test from this depth met slight resistance at 35 mbsf and a hard layer that could not be washed through at 53 mbsf. These sub-bottom depths are about 10 m too shallow when compared with reflector depths on the 3.5-kHz records. This discrepancy was also present at Sites 800 and 307 in similar geologic environments. It might be explained by an extremely soupy seafloor that would reflect 3.5-kHz sound, but whose sediment would not be retained by the core catcher or adhere to the plastic core liner. This speculation was confirmed at Hole 801C by TV observation

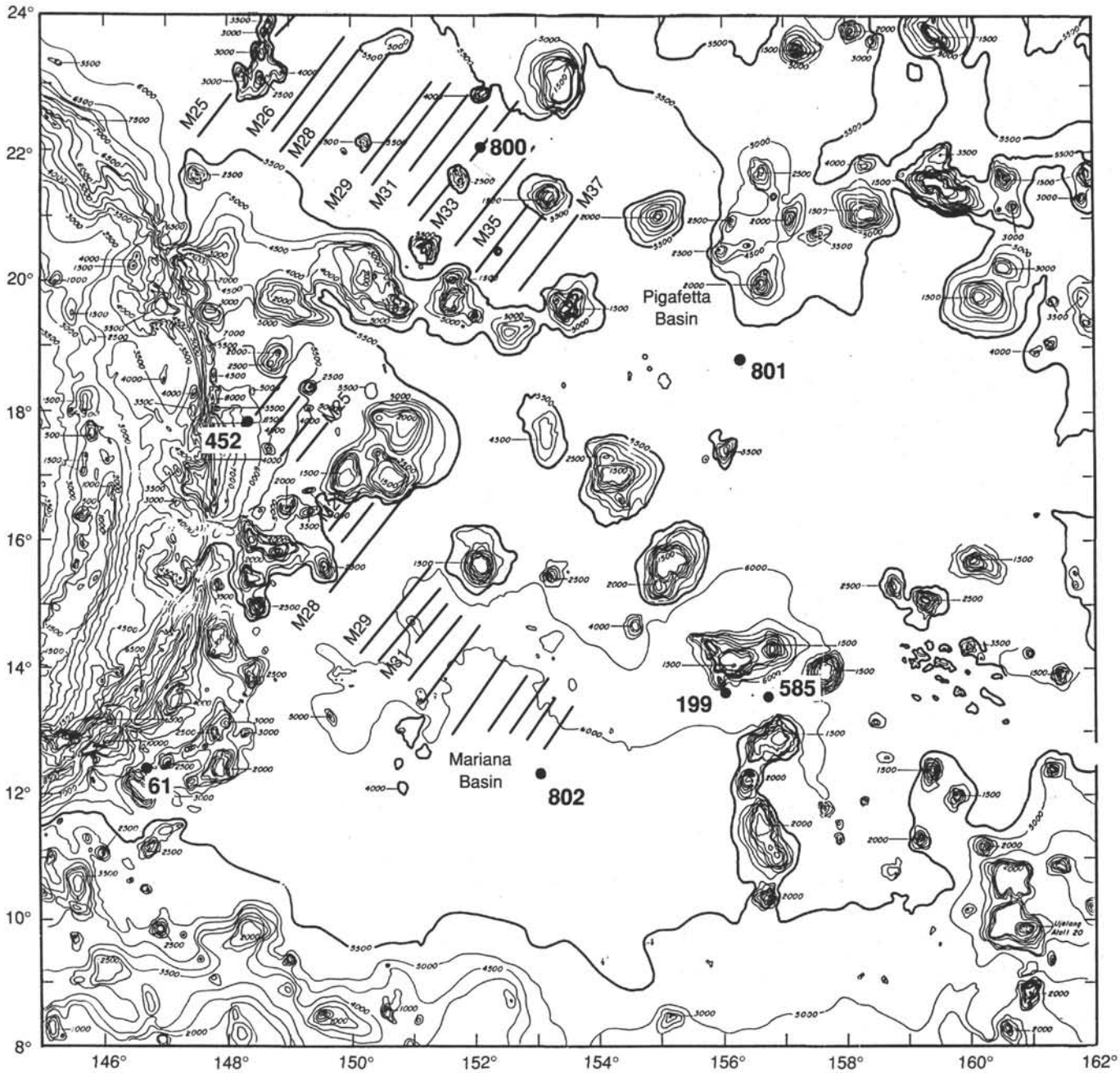

Figure 2. Bathymetry (in meters) of the central western Pacific (from M. Angell and C. Brenner, pers. comm., 1990) with location of drill sites. Magnetic anomalies modified from Handschumacher and Gettrust (1985), Tamaki et al. (1987), and Handschumacher et al. (1988).

of the impact on the seafloor of the end of the drill string. Observation showed a depth below rig floor of 5685 m, 8 m shallower than at Hole 801A. All depths below rig floor or seafloor for Holes 801A and 801B have been recalibrated to the mud-line depth measured by TV observation at Hole 801C for the following discussion and all other descriptions of Site 801. A further discussion of this TV observation is included in the subsequent part of this section describing operations at Hole 801C.

Coring proceeded without pumping or rotation for Cores 129-801A-1R through -6R. The hard layer at 61 mbsf (listed at 53 in the previous paragraph, but now corrected by the addition of 8 m as discussed above) proved to be red chert in Core 129-801A-7R and required moderate pumping and bit weight for penetration. Recovery was relatively good for Cores 129-801A-3R through -7R with the exception of Core 129-801A-6R. All but a core-catcher sample was washed out of this core possibly because of the lack of a soft-sediment, flapper-type core catcher, and because the core was retrieved too rapidly. Cores 129-801A-1R through -7R contained zeolitic brown clay grading down into nannofossil clay and a sharply bounded bed of nannofossil chalk. Temperature measurements were attempted after recovery of Cores 129-801A-3R and -5R. Both attempts were unsuccessful owing to a faulty thermistor.

Coring continued in cherts from Cores 129-801A-7R through -13R. The bit then met a sequence of claystones and mudstones with interbedded turbidites containing mainly volcaniclastic de-

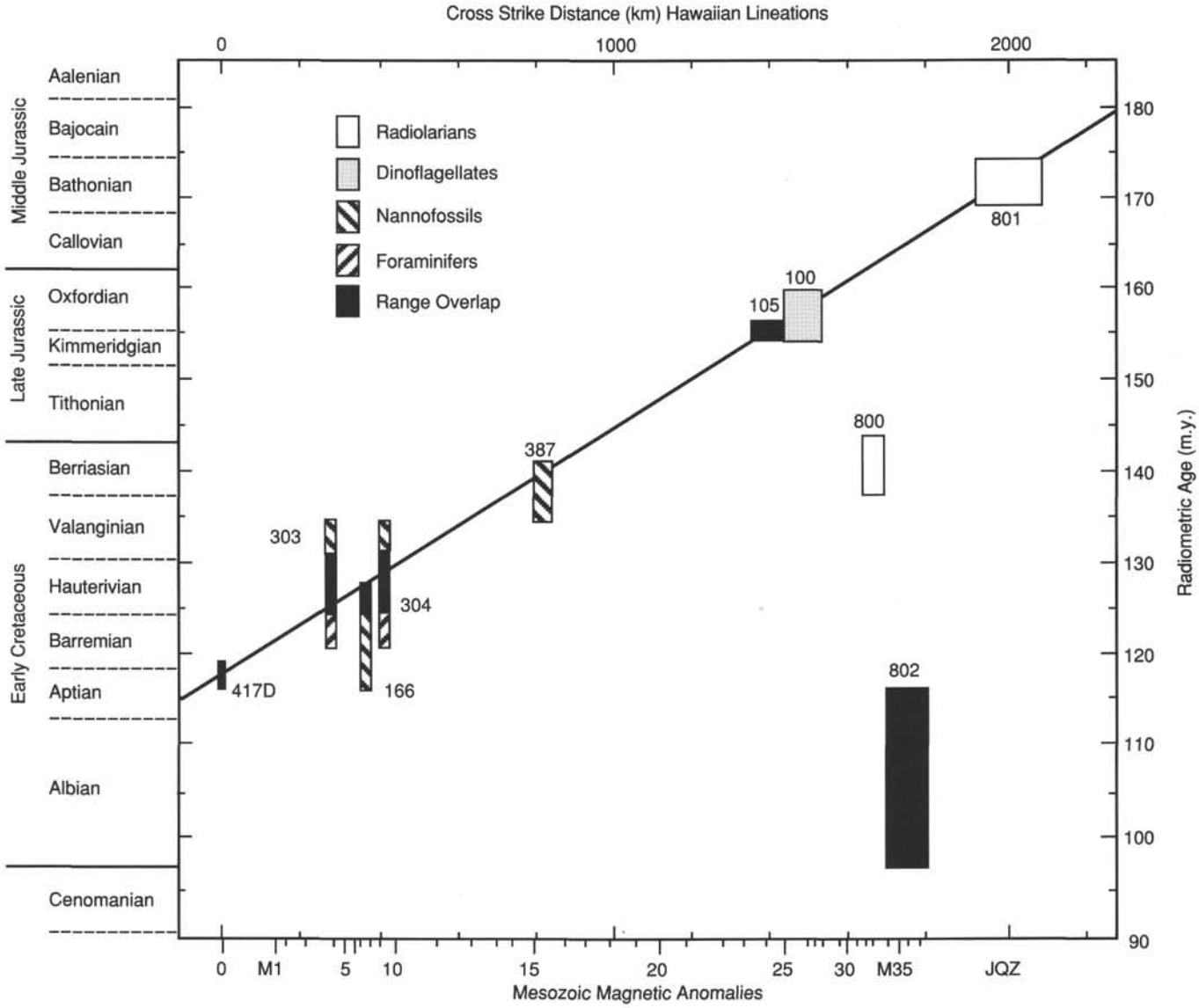

Figure 3. Time calibration plot of the Mesozoic anomalies M0 to M37 and the preceding Jurassic magnetic quiet zone (JQZ). Magnetic anomalies are plotted as cross-strike distance across the Hawaiian lineations for M0 to M25. Anomalies M25 to M37 are normalized to that parameter after Handschumacher et al. (1988). Geologic time scale and radiometric ages are from Harland et al. (1982), as modified by Kent and Gradstein (1985) at the Tithonian/Kimmeridgian boundary. Diagonal line indicates a predicted time scale constrained prior to Leg 129 that closely fits the calibration points. Oldest paleontologic ages in various DSDP holes (numbered) are shown as rectangles. Vertical lengths of rectangles show paleontological age ranges from DSDP *Initial Reports,* except for 100 (Zotto et al., 1987) and 105 (Gradstein and Sheridan, 1983). Horizontal lengths show magnetic age ranges from Larson and Hilde (1975) for DSDP Sites 303, 304, 166, 100, and 105, and from DSDP *Initial Reports* for Sites 387 and 417D. Age ranges from Sites 800, 801, and 802 are also shown.

bris. Hole inclination surveys were taken after Cores 129-801A-16R, -18R, and -19R, with the first two showing 8° of deviation from the vertical at the bottom of the hole. This was further verified on the last inclination survey that also showed the drill pipe vertical above the mud line. Most of this excessive hole deviation probably occurred at the top of the chert sequence at 61 mbsf, either due to the bit glancing off the edge of a chert ledge or to excessive weight on bit (15,000 lb) when first penetrating the cherts.

We decided to terminate this hole after Core 129-801A-20R due to the hole deviation, offset a short distance, and spud-in Hole 801B with the same bit and BHA.

Hole 801B

We pulled the bit approximately 20 m above the mud line and offset from Hole 801A 15 m east and 46 m south. Hole 801B was spudded at 0945 hr UTC, 9 December 1989, and drilled to the total depth of Hole 801A (194.0 m), where we measured 2.5° of hole inclination and proceeded to core ahead. It took almost an identical amount of rotating time (10 hr) to redrill this interval as it had taken in the same interval in Hole 801A.

At 194 mbsf we began continuous coring in the middle Cretaceous volcaniclastic sequence that we had recovered

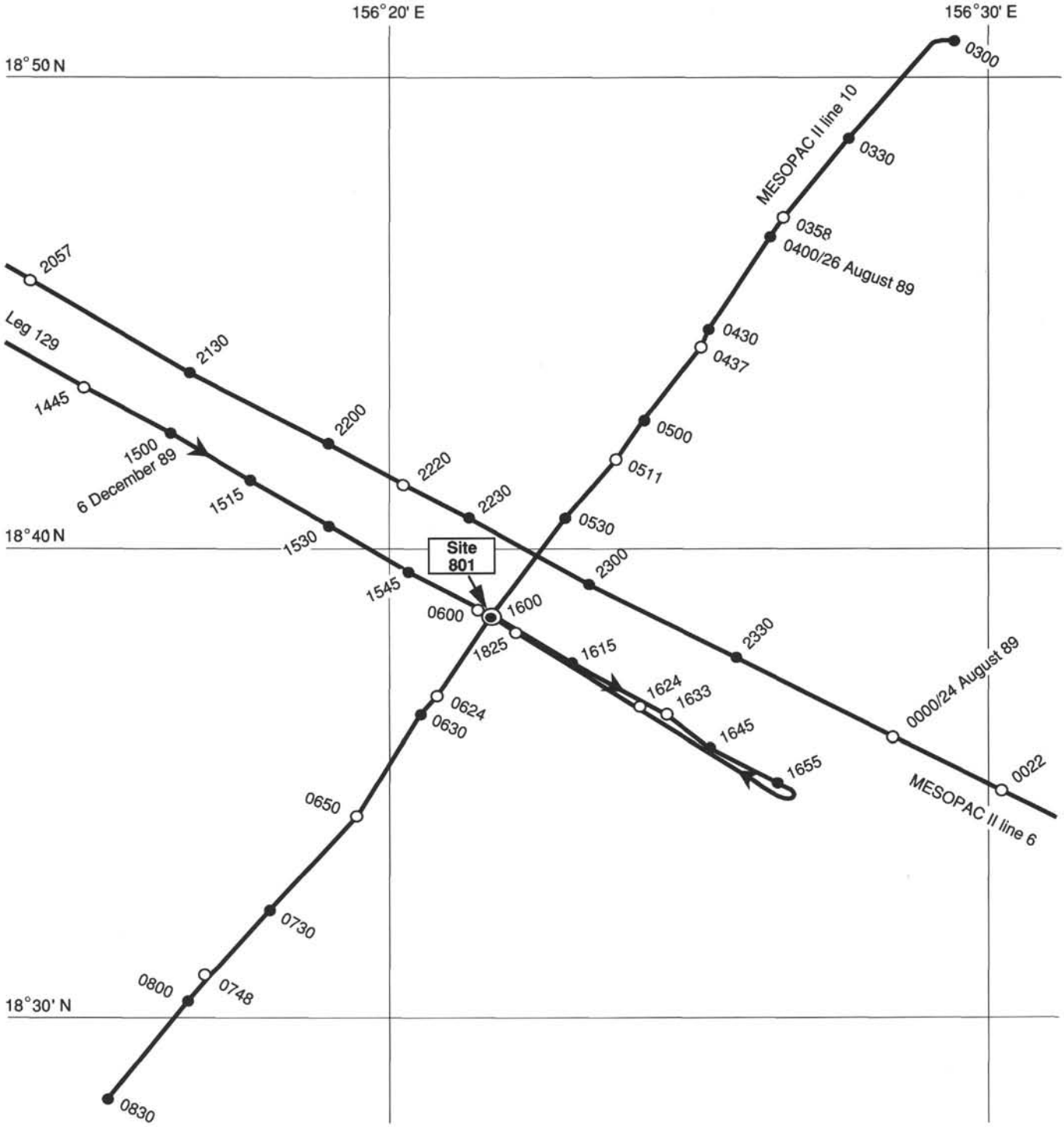

Figure 4. Track chart of the expeditions MESOPAC II and Leg 129 showing the location of Site 801. Note that the Leg 129 track shown here is the initial approach to Site 801, whereas that shown in Figure 51 in the "Site Geophysics and Seismic Stratigraphy" section (this chapter) is a reshoot line run essentially coincident with the approach track after Hole 801B was completed.

from the bottom 63 m of Hole 801A. We continued in this sequence to 280 mbsf for a total thickness of 149 m of volcaniclastics. Below 280 mbsf we encountered 34 m of mixed volcaniclastics and chert from Cores 129-801B-10R through -13R, where we encountered 2 m of extremely hard drilling that correlates with a prominent seismic reflector at 300 ms twt. None of the material believed to be responsible for this reflector was recovered. Below this level (315 mbsf) we recovered only minor amounts of chert for 128 m down through Core 129-801B-32R at 443 mbsf. Half-cores were pulled from the lower portion of this interval in an effort to increase recovery. From 443 to 461 mbsf we recovered a much greater percentage of iron-enriched, umber-colored radiolarite in Cores 129-801B-33R through -36R. Basalt was then encountered interbedded with chert from 461 to 483 mbsf in Cores 129-801B-37R through -40R. Essentially solid basalt was

encountered from there to the bottom of the hole at 511 mbsf, although a minor amount of baked claystone was recovered in the lowest core (Core 129-801B-44R).

This entire coring operation was conducted with no hole problems of any consequence with the exception of extremely low recovery in the chert sequence. We terminated the hole so that the sedimentary sequence could be logged while the hole was in good condition, and with the expectation of setting a reentry cone and casing to basalt at a short offset distance for an attempt at deeper penetration into basement. At total depth the bit had 55 hr of wear with no core gauge or torquing problems. However, the penetration rate in basalt had slowed to less than 2 m/hr, suggesting that the cutting structure was wearing out.

A complete wiper trip was made and mud was pumped in preparation for logging. The bit was then dropped at the bottom of the hole and the pipe bottom raised to 70 mbsf. Standard logging was conducted using exactly the same tool strings as at Hole 800A. All logs were run up to 64 mbsf, which is just below the top of the upper chert sequence. The quad combination logs bottomed at 474 mbsf, the geochemical string at 482 mbsf, and the formation microscanner (FMS) at 456 mbsf. The FMS log was run twice in the hope that the second run would be slightly rotated relative to the first, which was indeed the case. The wireline heave compensator was operational for both of the FMS runs, but not for the other runs. Logging took a total of 26 hr, after which we pulled out of the hole and began to assemble reentry hardware for Hole 801C.

Hole 801C

We assembled a full-sized reentry cone with fixed sonar reflectors, floating sonar reflectors on 2-m-long tethers, and a fixed acoustic beacon, all for relocation purposes, and latched in 51.13 m of 16-in. conductor casing at approximately 0130 hr on 17 December 1989. The base of the conductor casing was intended to land 1 or 2 m above the top of the upper chert sequence. The drill pipe and BHA were terminated with a 14¾-in. standard oil field drill bit with no coring capability for rapid penetration through the sedimentary sequence. This entire apparatus was lowered away through the moon pool directly after latch-in of the conductor casing. Spud-in was achieved with the drilling vessel offset 20 m north of Hole 801B. The casing washed in easily to 44 mbsf where considerable pumping was required to achieve further penetration. Penetration ceased at 51 mbsf, essentially equivalent to the length of the conductor casing.

After unlatching, we proceeded to drill a casing hole through the remainder of the sedimentary section into solid basalt to a total depth of 491 mbsf. This should have provided an adequate casing seat for the main casing string, and 20 m of overlap section with the previous hole. We experienced moderate torque conditions during this drilling operation and were stuck temporarily after the hole was about half completed. Hole conditions improved when basalt was reached and most of the chert cuttings had been flushed from the hole. After drilling, a wiper trip was run to the base of the conductor casing and the hole was swept with mud. Rotation was required to regain the bottom of the hole, so it was decided to fill the lower portion of the hole with high-viscosity mud in an effort to prevent further fill. The drill string was tripped to the rig floor, and the bit was recovered intact. Two cones had undergone initial bearing failure and the third had suffered serious shirt-tail wear. About 30% of the cutting teeth were badly abraded or missing from extended drilling through chert gravel.

An 11¾-in. casing string, 479 m long, with one 3-m-long slip joint, was made up and run in. The cone was located easily with the TV camera, and less certainly with the scanning sonar. The cone was easily reentered and the casing string run into the hole without obstruction until about 25 m above the latch-in depth. Pumping and multiple raising and lowering of the pipe gained 5 m towards the bottom of the hole where a ledge that we could not pass, probably near the top of basement, was encountered. The top drive was picked up and the drill string rotated slowly to the right in an attempt to "screw past" this ledge without disconnecting the casing string at the lefthand disconnect thread. While the drill string was rotated, the casing disconnect joint was observed on the TV camera in order to verify that the casing string was also rotating with the drill pipe. The ledge was passed while allowing a maximum of about 60,000 lb to come off the total drill-string weight. We then continued to lower the drill string for an additional 5 to 10 m and to rotate it slowly with about the same weight fluctuations until the TV cable parted about 15 m below the drilling vessel with the casing shoe about 10 m from the latch-in depth.

The TV cable had most probably become wrapped around the drill pipe during lowering because its compass was seen to rotate at least 4 times during this operation. Rotation of the drill pipe may have caused additional wraps to be taken around the pipe; however, the camera was not observed to rotate during this operation. A more likely scenario is that rotating the drill string caused the previously acquired wraps to be tightened around the drill pipe so that it could not be lowered without eventually breaking the TV cable. In hindsight, it appears that the TV cable was indeed holding back the drill-string lowering, because the casing lowered much more easily into the casing seat immediately after the cable broke. It is likely that a significant fraction of the weight loss observed on the drill-pipe weight indicator prior to the cable break was the result of tension on the TV cable, which has a breaking strength of 30,000 lb.

The casing latched into the cone with the casing shoe at about 481 mbsf. This was well into the basalt which was first observed in the pilot hole 20 m away at 461 mbsf. The casing was disconnected easily by allowing the cone to support the casing string weight (120,000 lb) while rotating the drill pipe 10 turns to the right. We then cemented the casing into place and pulled out of the hole.

The pipe was brought on deck free of any junked TV cable or the TV camera frame itself. Since the wire broke when the pipe was still in the hole, we assumed that the camera fell into the cone and was still there, with 5600 m or more of camera wire attached to it. Because the spare camera flooded and was not reparable, we could not conduct the relatively simple fishing job of removing this junk from the cone until we obtained another video camera. Thus, we conducted a short post-site survey and got underway for East Mariana Basin proposed site EMB-2A, while contacting ODP headquarters to request resupply with another video system.

After successfully coring Site 802 (proposed site EMB-2A) and receiving a new TV camera by tug boat transfer, we returned to Hole 801C to fish for the lost TV system and to core ahead into the Jurassic basement. We approached the site without operating the seismic system, and acquired two weak but operational beacons when we hove to. One of these was the beacon mounted on the reentry cone, so its position was fixed. We dropped a new beacon for a stronger signal in the windy weather, detorqued the new TV cable, magnafluxed the BHA, and ran in the pipe. When the cone was viewed with the TV, we observed that it was free of all parts of the lost TV system. On orders from ODP headquarters we then spent the next 9 hr searching for the lost system in the vicinity of the cone. The camera frame itself was never spotted, but we

thought we recognized the camera wire on several occasions. In three attempts to snag the wire with our fishing tool (a double-pronged fish hook designed to lock onto the camera frame), we lowered the pipe about 1 m into the mud and then offset away from the cone, "plowing" a furrow across the target area. Although we stirred up a lot of mud, we were unsuccessful in hooking onto the TV camera wire or frame. We did document the ability of a "steering jet" bored into the side of the fishing tool sub to offset the drill pipe when water was pumped through the jet with the mud pumps. After determining that it was futile to continue this exercise, we recovered the operational TV camera and the drill string in preparation for a reentry attempt with a coring bit in place.

We also documented a mud-line depth below the rig floor of 5685 m by direct observation with the TV camera of the impact on the seafloor with the fishing tool at the end of the drill pipe. This is 8 m shallower than the mud-line depth documented earlier at Hole 801A by the level of the uppermost mud smeared on the core liner of the uppermost core. Although Holes 801A and 801C are physically separated by about 30 m, our survey of the immediate area around the reentry cone indicates that the seafloor is essentially horizontal. Thus, we concluded that the mud-line depth at Holes 801A and 801B is also 5685 m below rig floor, substantiating our earlier speculation that the extremely soupy seafloor is not retained on the core liner at the seafloor level itself. Only when (in this case) 8 m of penetration had been accomplished was mud retained on the core liner. This discrepancy has been corrected throughout the Leg 129 reports by calibrating all depths below rig floor or sea level to the depth observed with the TV camera at Hole 801C.

The BHA for coring at Hole 801C was the same as that used at Holes 801A and 801B, with the addition of three stabilizers within 25 m of its base to help maintain the bit in place at the bottom of the hole, and a Rock Bit International C4 bit as the coring tool. The BHA was made up and run in to just above the seafloor, and the TV camera/scanning sonar was lowered on the exterior camera frame. The reentry cone was just coming into view on both of these instruments when they stopped working simultaneously with dead shorts to both tools. We retrieved the system after suffering some initial trepidation that we had lost a second camera frame and the attached instruments. Instead, we discovered a flooded cable connector as the cause of the malfunction. With the cable connector repaired, but the scanning sonar still on deck because of an additional electronic problem, we relowered the TV system alone on the camera frame. Reentry was eventually accomplished this time after 4 hr of efforts to minutely offset the drilling vessel in the presence of gusting 30- to 40-kt winds.

Coring proceeded without serious delays, and with the best percentage of basement recovery for the leg due to the massive and/or weathered nature of the basalts. The weather did not improve, with the winds continuing in the presence of two distinct swells forming an interference pattern that resulted in large (10°) rolls during the coring process. This, plus the large dynamic loads, large heave-compensator stroke, and marginal acoustic conditions, placed us at the use limits of several systems at once.

Core 129-801C-7R was cut at a rate of only 1.5 m/hr, and Core 129-801C-8R was cutting at less than 1 m/hr when the bit locked with a large amount of torque after 35 hr of bit life. The bit was retrieved and discovered to have lost three of its four cones, along with the shanks attached to two of the cones (Fig. 5). The hole was thus junked with about 10 kg of steel and tungsten carbide in at least three large pieces. Opinions varied as to the cause of the failure. We noted that large

Figure 5. Broken bit used in Hole 801C. All the missing junk metal was recovered in subsequent fishing operations.

portions of the tungsten carbide that had made up the middle stabilizer were missing, suggesting that the bit wore out prematurely as a result of excess grinding on fragments of the missing stabilizer. This is supported by the condition of the remaining, and eventually recovered, bit cones that had all their cutting teeth nearly worn off. We also noted that one of the shank "sockets" was much more badly worn than the other, suggesting that its weld had fractured early. It had eventually fallen off and taken the rest of the lost material with it. Although the exact causes of the specific failure(s) are unknown, they are almost certainly related to the rough weather conditions we experienced during coring. The 35- to 40-kt winds, and in particular the 4- to 5-m swells, undoubtedly caused large fluctuations in weight on bit, which eventually resulted in premature failures. The lesson for future drillers is that coring during rough weather in a basalt formation will almost certainly reduce bit life by more than 50%.

We decided to make one fishing run in an attempt to pick up the lost fragments. We employed a recirculating junk basket that allows circulation water to be diverted out of the bit sub and reverse-circulated up into the throat of the junk basket in order to pick up the junk. We ran in this assembly and after considerable effort regained the bottom of the hole, where we rotated with light bit weight and circulated both water and mud for about 1 hr. Amazingly, when the BHA was brought on deck, all three of the main broken parts were recovered, one cone/shank inside the junk basket and the other cone/shank and cone wedged tightly into its throat. We lacked only one small piece of throat-guide metal from the broken bit, and decided that would not impede subsequent coring operations.

We assembled a coring BHA, this time without the stabilizers, with a re-bearinged, F-99-CK, button-toothed coring bit, originally of Smith manufacture, that was equipped with a "boot basket" at the bit sub to trap remaining small metal parts. The drill string was run in and reentry was made without incident, and without the extreme wind conditions present at previous reentries. Coring proceeded at a slow rate of penetration but with excellent recovery. This bit run was terminated by the end of the leg with 18.5 hr of bit life. The recovered bit had broken teeth and two leaking bearing seals. The throat-guide metal from the broken bit was recovered in the boot basket, so the hole was left entirely clean for deepening on future expeditions.

LITHOSTRATIGRAPHY AND SEDIMENTOLOGY

Lithostratigraphy

The sedimentary section recovered at Site 801 is divided into six lithologic units based on composition, color, and presence of volcanics (Fig. 6; Table 2).

Unit I (8.0–63.8 mbsf, Cenozoic and Upper Cretaceous) is composed of pelagic clay and is subdivided into two subunits according to color. Subunit IA (8.0–41.0 mbsf, Tertiary) is dark reddish brown clay and Subunit IB (41.0–63.8 mbsf, Maestrichtian-Campanian?) is brown clay with light-colored streaks.

Unit II (63.8–126.5 mbsf, Campanian-Cenomanian) is predominantly composed of brown chert and porcellanite.

Unit III (126.5–318.3 mbsf, Cenomanian-Albian) consists of volcaniclastic turbidites with minor pelagic intervals.

Unit IV (318.3–442.9 mbsf, Valanginian-Oxfordian) consists of brown radiolarite with dark brown chert and is subdivided into two subunits according to clay content; Subunit IVA (318.3–400.6 mbsf, Valanginian-upper Tithonian) is brown radiolarite and Subunit IVB (400.6–442.9 mbsf, upper Tithonian-Oxfordian) is brown, clayey radiolarite.

Unit V (442.9–461.6 mbsf, Callovian-Bathonian) consists of alternating red radiolarite and claystone.

Unit VI (461.6–590.9 mbsf, Callovian-Bathonian) consists of basaltic sills and pillows with interbedded, silicified claystone.

Placement of the boundaries of these major lithologic units, which were generally based upon low rates of core recovery, is supported by analysis of geochemical logs from Hole 801B.

Unit I. Core 129-801A-1R to Section 129-801A-7R-4, 29 cm (8.0–63.8 mbsf): Brown Pelagic Clay; Cenozoic to Maestrichtian-Campanian?

This unit is composed of pelagic clay with different colorations. Age-diagnostic microfossils are generally lacking. The rotary coring has completely obliterated any original sedimentary structures of the soft deposits.

Subunit IA. Dark Reddish Brown Pelagic Clay with Zeolites; Tertiary (Core 129-801A-1R to Section 129-801A-5R-2, 0 cm; 8.0–41.0 mbsf)

Subunit IA extends 33 m from the first recovery at 8 mbsf to the top of underlying lighter-colored Subunit IB. This dark reddish brown, ferruginous pelagic clay contains some silt-sized globules or aggregates of iron oxyhydroxides, and zeolite (phillipsite), minor quantities of micronodules, quartz silt and rare benthic foraminifers. This facies is typical of condensed sediments deposited below the CCD.

The dark reddish brown color is derived from an abundance of fine, silt- to clay-sized globules or aggregates of iron oxyhydroxides (20%–45% of the sediment as estimated from smear slides). These semi-opaque, isotropic, or weakly birefringent dark red particles, described by Yeats, Hart, et al. (1976) as "red brown semi-opaque objects" or "RSO's," are common at other deep Pacific sites. The co-occurrence of zeolites with numerous iron oxyhydroxides indicates an intense early diagenetic process during periods of low sedimentation rates (Karpoff, 1989, and references therein).

Pale yellow to light olive brown nannofossil ooze intervals occur in the lower portion of this subunit (Sections 129-801A-4R-2 to 129-801A-5R-1). The mixed assemblages of late Paleocene and Late Cretaceous nannofossils, and the sharp contacts of pelagic clay with the layers of calcareous ooze, suggest that the layers represent redeposition events.

Subunit IB. Brown Pelagic Clay with Light-colored Streaks; Paleocene-Campanian (Sections 129-801A-5R-2, 0 cm, to 129-801A-7R-4, 29 cm; 41.0–63.8 mbsf)

Subunit IB is distinguished by lighter color, a much lower abundance of the iron oxyhydroxides aggregates, and by a generally lower abundance of zeolites. At Site 800, a similar change in the color of the pelagic clay coincides with a hiatus between Tertiary and Campanian deposits (see "Lithostratigraphy and Sedimentology" section, "Site 800' chapter, this volume). At Site 801, the uppermost portion of this subunit contains nannofossils of late Paleocene age (lower part of Core 129-801A-5R) and there are inadequate biostratigraphic data to identify a possible hiatus between the Tertiary and Cretaceous.

The pelagic clay is brown to dark reddish gray with streaks, mottles, and thin bands of reddish yellow to light yellow and is composed of clay with variable abundances of zeolites (traces to 20%) and iron oxyhydroxides aggregates (3%–5%) and with minor amounts of micronodules, radiolarian fragments, and quartz silt. The main composition difference between the brown and the light-colored streaks is the concentration of aggregates and micronodules. In the basal portion of this subunit (Section 129-801A-7R-3 and upper Section 129-801A-7R-4), there are several bands of brown radiolarian clay which progressively increase in thickness from 2 to 15 cm. These beds contain 40%–50% radiolarians and mark a transition to the underlying Unit II, which consists of brown chert and porcellanite.

Unit II. Sections 129-801A-7R-4, 29 cm, to 129-801A-14R-1, 35 cm (63.8–126.5 mbsf): Brown Chert and Porcellanite; Campanian-Cenomanian

The sediments recovered from Unit II consist of pieces of brown radiolarian chert with porcellanite. No core from this 62.7-m-thick unit recovered more than 5% of its drilled interval; therefore, the following characterization of Unit II probably applies only to the more resistant beds.

The radiolarian chert and porcellanite are generally moderate brown to light brown, commonly with darker laminations. Several pieces display a variable degree of chertification with alternating bands of lighter-colored chert and darker-colored porcellanite (Fig. 7). Textures range from planar laminated to moderately bioturbated. Fracture surfaces commonly have manganese oxide fillings or dendrites. Chalcedony- or opal-CT-filled radiolarians and siliceous spines range in abundance from 20%–35% in thin sections and occur in a matrix made of micro- to cryptocrystalline silica, along with variable amounts of clay (Fig. 8).

Except for the lower transition zone to the underlying lithologic Unit III, Unit II is non-calcareous. Also recovered were light brown to dusky brown claystone (Cores 129-801A-8R to -11R), and light brownish gray calcareous radiolarian porcellanite (silicified clayey limestone; Core 129-801A-13R), which is 20% chalcedony-filled radiolarians, spines, and sponge spicules in a mixed matrix of micrite, clay, and silica.

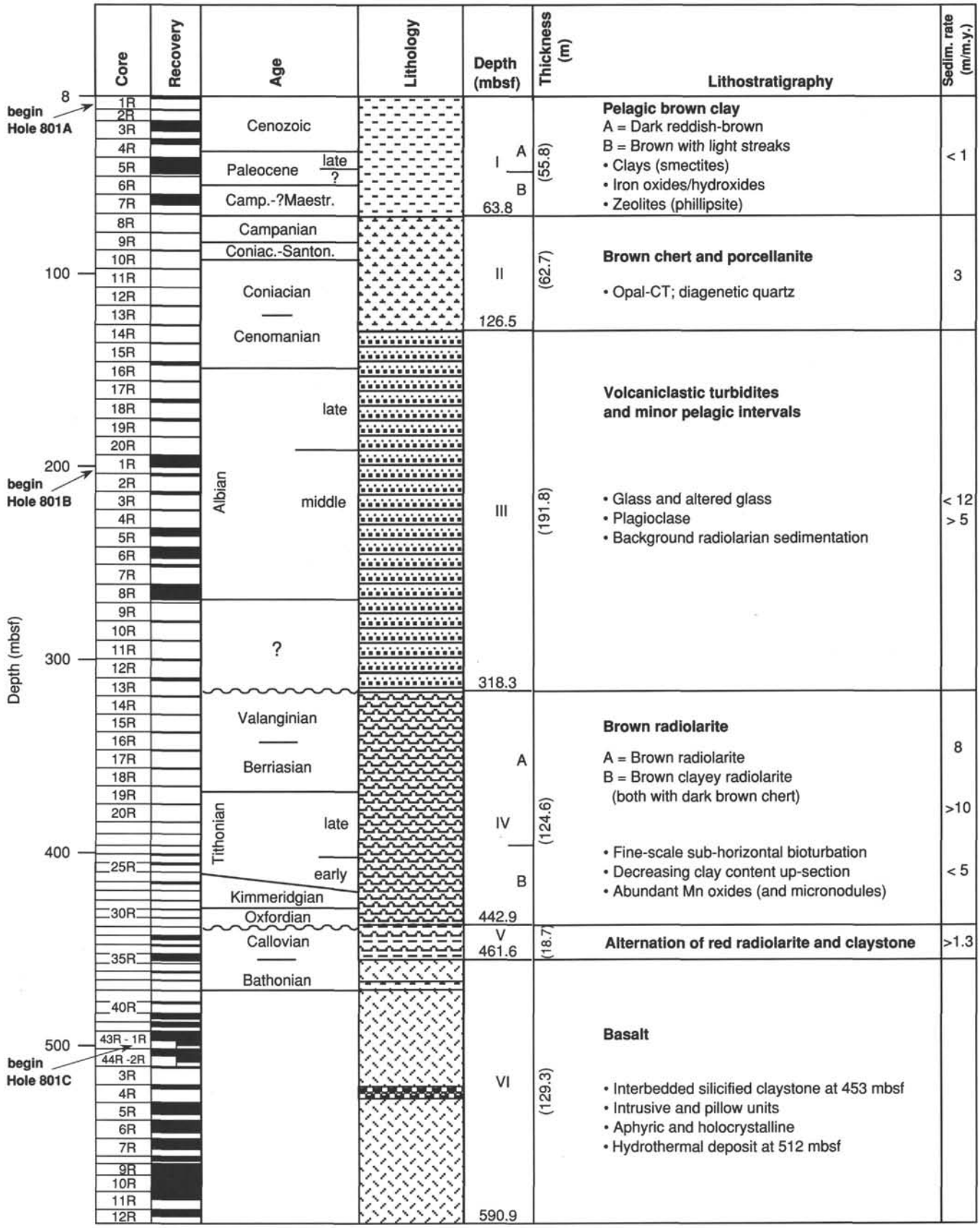

Figure 6. Lithostratigraphy of Site 801. (Note: No recovery from 0 to 8 mbsf. Total depth is 5675 mbsl.)

These minor lithologies may be representative of poorly recovered, less competent beds.

Two trends mark a gradual transition to the underlying lithologic Unit III (volcaniclastic turbidites). First, the color of the radiolarian porcellanite changes downward from brown to gray near the top of Section 129-801A-13R-1 (116.5 mbsf), and the underlying clayey radiolarian porcellanites become progressively grayer and slightly greener with increasing abundance of interbedded volcaniclastic turbidites. Second, the abundance of calcareous beds increase downward. Core 129-801A-13R includes a piece of calcareous radiolarian porcellanite (silicified limestone), and Cores 129-801A-14R and -15R include pieces of tuffaceous nannofossil claystone and chalk with a Cenomanian nannofossil assemblage. Within this transition zone, the boundary between Units II and III was set arbitrarily as the top of the highest recovered turbidite, a piece of a feldspathic radiolarian volcaniclastic turbidite of sandy texture (Sample 129-801A-14R-1, 35–37 cm).

Unit III. Sections 129-801A-14R-1, 35 cm, to 129-801B-14R-1, 0 cm (126.5–318.3 mbsf): Volcaniclastic Turbidites with Minor Pelagic Intervals; Cenomanian-Albian

This 191.8-m-thick unit consists of volcaniclastic turbidites with scattered pelagic beds of radiolarian claystone to radiolarite, radiolarian porcellanite and chert, and nannofossil claystone to chalk. The relative abundance of turbidites and pelagic interbeds varies considerably downcore. The initiation and termination of the turbidite input appears to be gradational; the top of Unit III was set at the top of the highest volcaniclastic turbidite (Core 129-801A-14R) and the base was set at the bottom of the lowest volcaniclastic deposit (between Cores 129-801B-13R and -14R).

The deposits are dark greenish gray to medium bluish gray beds, which darken and fine upward and range from sandstone to claystone in texture. Turbidite beds in cores with good recovery display typical sequences that include basal scour, graded sediments, scattered rip-up clasts, ripple- and cross-laminations, lower bed planar lamination, and bioturbation in their uppermost portions. Consequently, sections of similar volcaniclastic sandstone to claystone are interpreted as incomplete recovery of turbidites beds.

The recovered turbidite series displays a peak in bed thickness (5 m), grain size (coarse-sand), rip-up clast concentration, and rate of accumulation (debris or fluidized flow vs. turbidite flow) in the interval from 165 to 214 mbsf (Cores 129-801A-18R to 129-801B-1R). This section of the unit includes the most "proximal" turbidite facies observed (Fig. 9). Thin sections from these highest energy turbidites contain minor amounts of red algae and echinoderm fragments, implying contributions from shallow-water sources.

The volcaniclastic turbidites are composed of glass and volcanic fragments, feldspar, pyroxene, smectites, and other clay minerals with minor iron oxides, zeolites, quartz, secondary calcite, and accessory minerals (Fig. 10). Some of the volcanic glass has been altered or palagonitized and some of these sandstones now have a clayey matrix, a precursor to a greywacke texture. The finer-grained upper layers also contain rare radiolarians, foraminifers, and nannofossils. Cores 129-801A-18R and 129-801B-5R contain calcitic sandstones with abundant calcite-replaced and -filled radiolarians, in places defining discrete through cross-laminations within the otherwise volcaniclastic sandstone. A bed of black, well-sorted sandstone in Core 129-801A-16R may represent a coarse ash-tuff deposit.

Pelagic interbeds within the uppermost four cores of the turbidite unit (Cores 129-801A-14R through -18R, 126–165 mbsf) consist mainly of grayish olive to dark gray clayey radiolarite to radiolarian porcellanite, and of dusky green to gray nannofossil claystone to tuffaceous nannofossil chalk. Fine-grained pelagic intervals through Core 129-801A-20R are finely laminated or display irregular, discontinuous laminations and weak bioturbation. Pelagic interbeds are less common in the central portion of the volcaniclastic unit (Cores 129-801A-18R through 129-801B-9R, 165–280 mbsf) and consist of pieces of dark gray chert (Core 129-801B-6R) or thin, olive gray layers of radiolarite (Core 129-801B-8R).

The four lowest cores of Unit III (Cores 129-801B-10R to -13R, 280–318 mbsf) comprise a transition zone to the underlying brown radiolarite of Unit IV. The poorly recovered sediments of Cores 129-801B-10R and -11R consist of pieces of calcareous claystone and radiolarite without volcaniclastic beds. Core 129-801B-12R is mainly fine-grained volcaniclastic turbidites. Core 129-801B-13R consists of closely spaced, 2-cm-thick, fine-grained "distal" siltstone/claystone turbidites interbedded with millimetric layers of pelagic radiolarian claystone (Fig. 11).

Unit IV. Sections 129-801B-14R-1, 0 cm, to 129-801B-33R-1, 10 cm (318.3–442.9 mbsf): Brown Radiolarite; Valanginian-Oxfordian

The Upper Jurassic and Lower Cretaceous strata of this unit consist of 125 m of brown radiolarite with scattered dark brown chert or porcellanite bands or nodules. With the exception of rare nannofossils in Cores 129-801B-25R and -26R, this siliceous facies lacks a calcareous component. The unit is subdivided into an upper, clay-poor radiolarite with abundant chert (Subunit IVA) and a lower, clay-rich radiolarite with lesser amounts of chert (Subunit IVB).

Subunit IVA. Brown Radiolarite with Abundant Dark Brown Chert; Valanginian-Upper Tithonian (Sections 129-801B-14R-1, 0 cm, to 129-801B-24R-1, 0 cm; 318.3–400.6 mbsf)

Subunit IVA consists of 81 m of brown radiolarite with abundant porcellanite and chert. Recovery was less than 5% for all cores; therefore, the following description is probably biased toward the relatively resistant lithologies. A downcore increase in the proportion of hard chert to radiolarite also corresponded to decreased core recovery.

The radiolarite is characterized by varied shades of brown from tan to dusky yellowish brown to very dark gray. Ferromanganiferous oxyhydroxides occur as spotted deposits on most natural fractures, as discontinuous microlaminations within the radiolarite and as tiny black flecks. Precipitation of manganese oxide along some fractures preceded quartz or opal fracture-filling. The radiolarite generally displays a finely laminated texture, but the discontinuous or elongate, flaser nature of these laminations suggest that they may be caused by compacted, subhorizontal bioturbation (Fig. 12). Some of the recovered pieces within Cores 129-801B-16R through -18R have a vague rhythmic banding of clay content, color darkness, radiolarian abundance, and/or degree of silicification at intervals of approximately 5 cm (Fig. 12). The poor recovery precludes identification of cyclicity, such as that observed in the coeval Lower Cretaceous radiolarite unit at Site 800 (see "Lithostratigraphy and Sedimentology" section, "Site 800" chapter, this volume).

Porcellanite or chert occurs within the radiolarite as bands of preferential silicification (Fig. 12A) or less commonly as cross-cutting nodules (Fig. 12B). These bands or nodules are dusky yellowish brown to very dark grayish brown and darker than the host radiolarite. Some pieces display tan or reddish brown mottles, thin lenses, or discoloration near fractures. Some light-colored layers in chert show many hollow radio-

Table 2. Lithofacies of cores from Holes 801A, 801B, and 801C.

Core	Depth (mbsf)	Length cored (m)	Length recovered (m)	Lithology	Age
Unit I—Brown pelagic clay					
Subunit IA—Dark brown pelagic clay; 129-801A-1R-1, 0 cm; 8 mbsf; uppermost recovered sediment					
Hole 801A					
1R	8.0–14.5	6.5	1.30	Pelagic clay with zeolites	?Cenozoic
2R	14.5–20.4	5.9	0.50	Pelagic clay with zeolites	?Cenozoic
3R	20.4–30.0	9.6	5.29	Pelagic clay with zeolites	?Cenozoic
4R	30.0–39.6	9.6	2.45	Pelagic clay and minor nannofossil ooze	late Paleocene
5R	39.6–49.3	9.7	8.50	Pelagic clay and minor nannofossil ooze	Paleocene
Subunit IB—Brown clay with light streaks; 129-801A-5R-2, 0 cm; 41.6 mbsf					
6R	49.3–59.0	9.7	0.02	Pelagic clay	?Maestrichtian-Campanian
7R	59.0–68.6	9.6	5.15	Pelagic clay with zeolites	?Maestrichtian-Campanian
Unit II—Brown chert and porcellanite; 129-801A-7R-4, 29 cm; 63.8 mbsf; highest chert					
8R	68.6–78.2	9.6	0.27	Chert, porcellanite	Campanian
9R	78.2–87.5	9.3	0.16	Chert	Coniacian-Santonian
10R	87.5–97.1	9.6	0.42	Porcellanite, chert	Coniacian-Santonian
11R	97.1–106.8	9.7	0.17	Chert, porcellanite	Coniacian-Santonian
12R	106.8–116.5	9.7	0.22	Chert, porcellanite	Coniacian-Santonian
13R	116.5–126.2	9.7	0.35	Calcareous porcellanite	Cenomanian-Coniacian
				Transition zone: gray cherts, below 13R-1, 2.5 cm; 116.5 mbsf	Cenomanian-Coniacian
14R	126.2–135.9	9.7	0.63	Porcellanite, minor volcaniclastic sandstone	Cenomanian-Coniacian
Unit III—Volcaniclastic turbidites and pelagic intervals; 124-801A-14R-1, 35 cm; 126.5 mbsf; uppermost volcaniclastic turbidite					
15R	135.9–145.6	9.7	0.42	Volcaniclastic sandstone, porcellanite	Cenomanian-Coniacian
16R	145.6–155.2	9.6	1.59	Volcaniclastic sandstone to claystone	Cenomanian-Coniacian
17R	155.2–165.0	9.8	0.74	Clayey radiolarite, calcareous claystone	upper Albian
18R	165.0–174.7	9.7	1.69	Volcaniclastic sandstone	upper Albian
19R	174.7–184.4	9.7	1.25	Volcaniclastic siltstone	upper Albian
20R	184.4–194.0	9.6	0.37	Silty radiolarian claystone	upper Albian
Hole 801B					
1R	194.0–203.5	9.5	6.45	Volcaniclastic sandstone and silty claystone	upper Albian
2R	203.5–212.9	9.4	1.31	Volcaniclastic silty sandstone	upper Albian
3R	212.9–222.3	9.4	1.29	Volcaniclastic silty sandstone and clayey siltstone	upper Albian
4R	222.3–231.7	9.4	0.44	Volcaniclastic sandy claystone and sandstone	upper Albian
5R	231.7–241.3	9.6	4.01	Volcaniclastic claystone and turbidites	upper Albian
6R	241.3–251.0	9.7	5.67	Volcaniclastic turbidites	middle Albian
7R	251.0–260.7	9.7	1.21	Volcaniclastic claystone and turbidites	middle Albian
8R	260.7–270.3	9.6	7.92	Volcaniclastic turbidites	middle Albian
Transition zone					
10R	280.0–289.7	9.7	0.75	Calcareous claystone, radiolarite	middle Albian
11R	289.7–299.3	9.6	0.19	Radiolarite, porcellanite	middle Albian
12R	299.3–309.0	9.7	0.86	Volcaniclastic turbidites, radiolarite and chert	middle Albian
13R	309.0–318.3	9.3	1.17	Volcaniclastic turbidites, radiolarian claystone	middle Albian
Unit IV—Brown radiolarite					
Subunit IVA—Brown radiolarite with dark chert; 129-801B-14R-1, 0 cm; 318.3 mbsf; top of radiolarite prevalence					
14R	318.3–327.7	9.4	0.49	Clayey radiolarite, procellanite	Valanginian-Berriasian
15R	327.7–337.2	9.5	0.12	Radiolarite to chert	Valanginian-Berriasian
16R	337.2–346.6	9.4	0.49	Chert, radiolarite	Valanginian-Berriasian
17R	346.6–355.8	9.2	0.38	Radiolarite, chert	Valanginian-Berriasian
18R	355.8–365.3	9.5	0.46	Radiolarite, chert	Valanginian-Berriasian
19R	365.3–374.5	9.2	0.25	Radiolarite, chert	Valanginian-Berriasian
20R	374.5–383.7	9.2	0.29	Chert, radiolarite	Valanginian-Berriasian
21R	383.7–389.8	6.1	0.21	Chert	Valanginian-Berriasian
22R	389.8–395.9	6.1	0.05	Chert	Valanginian-Berriasian
23R	395.9–400.6	4.7	0.16	Chert, porcellanite	upper Tithonian
Subunit IVB—"Woody" brown clayey radiolarite and chert; 129-801B-24R-1, 0 cm; 400.6 mbsf; highest dominance of clayey radiolarite					
24R	400.6–405.2	4.6	0.68	Clayey radiolarte, chert	upper Tithonian
25R	405.2–410.0	4.8	0.62	Clayey radiolarite, chert	upper Tithonian
26R	410.0–414.7	4.7	0.10	Clayey radiolarite, chert	lower Tithonian
27R	414.7–419.4	4.7	1.02	Chert, clayey radiolarite	lower Tithonian
28R	419.4–424.2	4.8	0.11	Chert, clayey radiolarite	lower Tithonian
29R	424.2–428.9	4.7	0.14	Chert, clayey radiolarite	Kimmeridgian
30R	428.9–433.6	4.7	0.16	Chert, clayey radiolarite	Kimmeridgian
31R	433.6–438.2	4.6	0.28	Chert, clayey radiolarite	Kimmeridgian
32R	438.2–442.8	4.6	0.07	Brown clayey radiolarite	Oxfordian
Unit V—Alternations of red radiolarite and claystone; 129-801B-33R-1, 10 cm; 442.9 mbsf; highest red coloration					
33R	442.8–447.6	4.8	2.18	Red radiolarite, claystone	Callovian

Table 2 (continued).

Core	Depth (mbsf)	Length cored (m)	Length recovered (m)	Lithology	Age
34R	447.6–452.3	4.7	0.72	Claystone, red radiolarite	Callovian-Bathonian
35R	452.3–456.9	4.6	3.43	Claystone, red radiolarite	
36R	456.9–461.5	4.6	0.06	Red radiolarite, claystone	
Unit VI—Interbedded basalt and silicified claystone; 122-801B-37R-1, 7 cm; 461.6 mbsf; highest brecciated chert					
37R	461.5–466.1	4.6	0.58	Brecciated chert, basalt	
38R	466.1–470.7	4.6	0.20	Basalt, brecciated chert	
39R	470.7–476.9	6.2	0.29	Basalt, chertified radiolarian claystone	
40R	476.9–483.0	6.1	0.94	Basalt	
41R	483.0–487.6	4.6	2.66	Basalt	
42R	487.6–492.2	4.6	2.39	Basalt	
43R	492.2–501.7	9.5	5.00	Basalt, limestone fragment	
44R	501.7–511.2	9.5	3.36	Basalt, claystone	
Hole 801C					
1R	493.7–503.0	9.3	7.43	Basalt	
2R	503.0–512.2	9.2	6.69	Basalt	
3R	512.2–521.7	9.5	0.95	Basalt	
4R	521.7–531.2	9.5	2.42	Silica and iron hydrothermal deposit	
5R	531.2–540.5	9.3	6.36	Basalt, minor calcareous claystone	
6R	540.5–550.1	9.6	6.52	Basalt, minor calcareous claystone	
7R	550.1–559.5	9.4	5.87	Basalt	
8R	559.5–563.2	3.7	2.22	Basalt, minor metalliferous claystone	
9R	563.2–569.0	5.8	5.83	Basalt, minor siliceous claystone	
10R	569.0–577.9	8.9	8.42	Basalt	
11R	577.9–587.3	9.4	4.25	Basalt	
12R	587.3–594.3	7.0	3.64	Basalt	

larian molds, in contrast to the chalcedony-filled radiolarians common in the darker chert or radiolarite.

Thin-section analyses reveal that the radiolarite, chert, porcellanite, and radiolarian claystone differ only in the relative proportions of the main components: radiolarians, silica, clay, and iron-manganese oxides. Layers of radiolarians are alternately grain- or matrix-supported, making up 10%–60% of the bulk lithology. These radiolarians, usually completely replaced by microcrystalline quartz or chalcedony, are difficult to distinguish from the matrix, which is composed of iron-manganese oxides, clay, and silica. Silica does not include opal-CT below Core 129-801B-20R. Radiolarians and rare foraminifers are often sites of precipitation of oxides (Fig. 13). Interstitial iron-manganese oxides comprise 5%–20% of most thin sections.

Brecciation of chert progressively intensifies from Cores 129-801B-16R through -21R, then becomes less important in Core 129-801B-22R and below. Most fractures in this interval are filled by one or more generations of macroquartz or chalcedony; drusy, quartz-lined, open voids, up to 3 by 8 mm, occur in Cores 129-801B-20R and -21R (Fig. 14). In some breccias, fragments of siliceous radiolarite are separated from adjacent chert with similar texture by the quartz-filled fractures, suggesting that the brecciation and quartz-filling of resulting fractures occurred prior to full chertification, differentially affecting the rates of silicification of each piece.

Subunit IVB: Brown Clayey Radiolarite; Upper Tithonian-Oxfordian (Sections 129-801B-24R-1, 0 cm, to 129-801B-33R-1, 10 cm; 400.6–442.9 mbsf)

The lowermost 42 m of Unit IV consist of a brown clayey radiolarite with approximately equal amounts of clay and radiolarians. The contact between Subunits IVA and IVB was placed at the top of the highest core in clayey radiolarite was recovered (Core 129-801B-24R). The estimated average clay content of Subunit IVB is 40%–50% vs. 10%–20% in Subunit IVA. The transition between clay-rich and clay-poor strata appears to be sharp in the cores. The recovery of this subunit was enhanced by a combination of a decrease in the size of each core (4.7 m/core vs. 9.4 m/core for overlying units), and by a lesser amount of chert.

The clayey radiolarite is dark brown, mottled or banded by light yellowish brown to pink. The mottling commonly cuts across burrows and laminations and is probably due to mobilization and differential staining by iron-manganese oxyhydroxides (Fig. 15A). Slightly lighter-colored bands seem to be richer in radiolarians, whereas darker-colored bands seem to be richer in clay and minor amounts of volcanic glass. Most radiolarians are filled by microquartz (Fig. 16), with calcite-filled radiolarian casts present in Core 129-801B-29R.

Manganese micronodules, 1–2 mm in diameter, which occur scattered in the radiolarite or in clusters subparallel to the laminated fabric, are less common in the chert. However, the presence of micronodules in porcellanite and chert indicates that their formation partially predates silicification. Oxides also occur as black flecks or streaks, as replacement of microfossil tests, and as dendritic spots on fractures (Fig. 15A).

The clayey radiolarite has a distinctive "woody" texture of subhorizontal streaks, discontinuous planar to irregular laminations and thin, elongate lenses (Fig. 15A). This texture could be the result of subhorizontal burrows and bioturbation that underwent considerable and differential compaction. Continuous laminations are much less common.

Chert or radiolarian porcellanite occurs as secondary lenses within the clayey radiolarite, or was recovered as separate pieces (Fig. 15B). The chert is typically very dark brown, commonly with reddish brown coloration in layers, lenses, burrows, mottles, and adjacent to fractures. Quartz-filled fractures display multiple generations of silica precipitation and locally influence the degree of oxidation of the host rock (Cores 129-801B-27R to -30R). A higher abundance of chert relative to clayey radiolarite in the lower half of Subunit IVB may be an artifact of recovery.

In Core 129-801B-27R (414.7 mbsf) and below, the recovered blocks have an apparent dip of 10°, increasing to 30° in

Figure 7. Brown radiolarian porcellanite with bands of lighter-colored chert typical of lithologic Unit II (Campanian-Cenomanian). Moderate bioturbation. Interval 129-801A-10R-1, 8–15 cm.

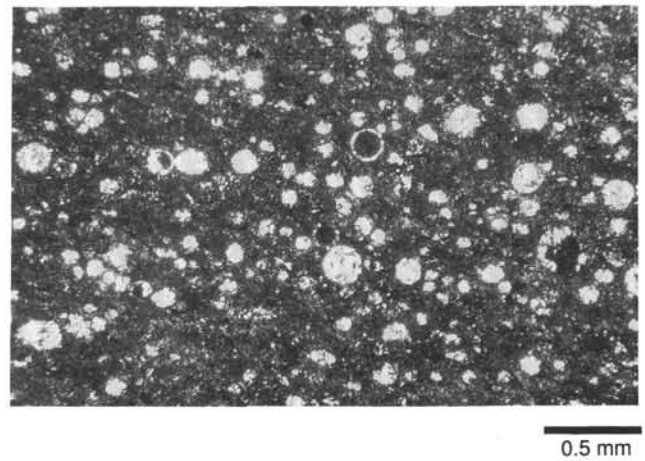

Figure 8. Photomicrograph of radiolarian porcellanite typical of lithologic Unit II, Campanian-Cenomanian. Radiolarians are commonly infilled with opal-CT or chalcedony. Crossed nicols. Sample 129-801A-13R-1, 18–20 cm.

Core 129-801B-33R. This apparent dip exceeds the measured 2¼° deviation of the drilling from vertical, indicating that the strata have a moderate tectonic or depositional dip.

Unit V. Sections 129-801B-33R-1, 10 cm, to 129-801B-37R-1, 7 cm (442.9–461.6 mbsf): Alternations of Red Radiolarite and Claystone; Callovian-Bathonian

The lowest major sedimentary unit at Site 801 consists of 18 m of red, interbedded radiolarite and claystone. The boundary between Units IV and V was placed at the highest appearance of red coloration. This color boundary, which appears as a sharp contrast in a piece of radiolarite in the uppermost portion of Core 129-801B-33R, also corresponds to a change in degree of lithification.

Alternations of radiolarite and claystone average about 5 cm, but have irregular spacing. Contacts between the two lithologies are generally sharp (Fig. 17). However, thin sections show that the boundaries are gradual on a millimeter scale, suggesting that the lithologic variations reflect changes in primary sedimentation deposition or the intensity of winnowing, rather than redeposition events (Fig. 18).

Radiolarite layers are generally yellowish red to brick red, silty in texture, vaguely laminated to weakly bioturbated, and contain intervals with anastomosing clay-rich seams or lenses of partial silicification (Fig. 17). Claystone layers are slightly darker red with respect to adjacent radiolarite bands, and are featureless to moderately bioturbated. They lack the distinctive "woody" texture of Unit IV.

Several types of alteration features are common in both lithologies. Reduction mottles (patches of light greenish gray to white) cut across layering and bioturbation, occur adjacent to some fractures, or are present as elongate lenses parallel to bedding. Zones of diffuse brownish yellow are adjacent to some fractures. White, translucent, silica-lined fractures are common whereas manganese oxides coat rare fractures, and are much less common than in overlying Unit IV. Pieces of varicolored chert and breccia were recovered only in the uppermost portion of Core 129-801B-34R, and probably represent contamination from strata uphole.

The bedding has an apparent dip of 27°–30° (pieces of Core 129-801B-33R) and one large intact block in Core 129-801B-35R (at 99–110 cm) has an apparent dip of 60°.

The base of this unit was placed above the uppermost reddish brown chert, representative of silicified sediments interbedded with basalts, at Core 129-801B-37R, 7 cm. The uppermost sediment piece of Core 129-801B-37R is a pink radiolarite with brown porcellanite, similar to the "woody" textured, brown radiolarite of Subunit IVB. However, its Callovian-Bathonian radiolarian assemblage (see "Biostratigraphy" section, this chapter), suggests that this pink radiolarite may represent a lithology which was not recovered in the 4.6-m interval spanned by Core 129-801B-36R. Regardless, the division of Site 801 into lithologic units must rely on the actual recovered sediments; therefore, the very distinct lithologic change between radiolarite and underlying chert near the top of Core 129-801B-37R is used as the base of Unit V.

Unit VI. Sections 129-801B-37R-1, 7 cm, to 129-801B-44R-3, 47 cm, and Cores 129-801C-1R to 129-801C-12R (461.6–590.9 mbsf): Interbedded Basalt and Silicified Claystone (Chert); Callovian-Bathonian

The lowermost 133 m drilled at Site 801 consist of fine-grained basalt and microdolerite flows and sills (see "Igneous Petrology" section, this chapter), interbedded with red to brown chert and metasediments.

Above the highest recovered basalts (Section 129-801B-37R-1), and also occurring as probable cavings at the top of Core 129-801B-38R, are fragments of silica-cemented and -replaced claystone breccia, approaching chert in hardness (Fig. 19). The reddish brown claystone is intensely crackle brecciated, such that in places the pieces would fit back together (Fig. 20A, -B). Drusy quartz fills most of the fractures between clasts, but some open voids exist. Brecciation probably occurred during rapid dewatering or fluid injection associated with the heating of soft clay by the adjacent basalt. Similar breccia pieces occur at the tops of Cores 129-801B-40R and -41R. These may be contamination from the same breccia zone of Core 129-801B-37R.

Interflow sediments in Core 129-801B-39R consist mainly of dark brown chert with grayer mottles and dark, silicified radiolarite (Fig. 20C, -D). Faint burrow-mottling is marked by silica-filled radiolarians.

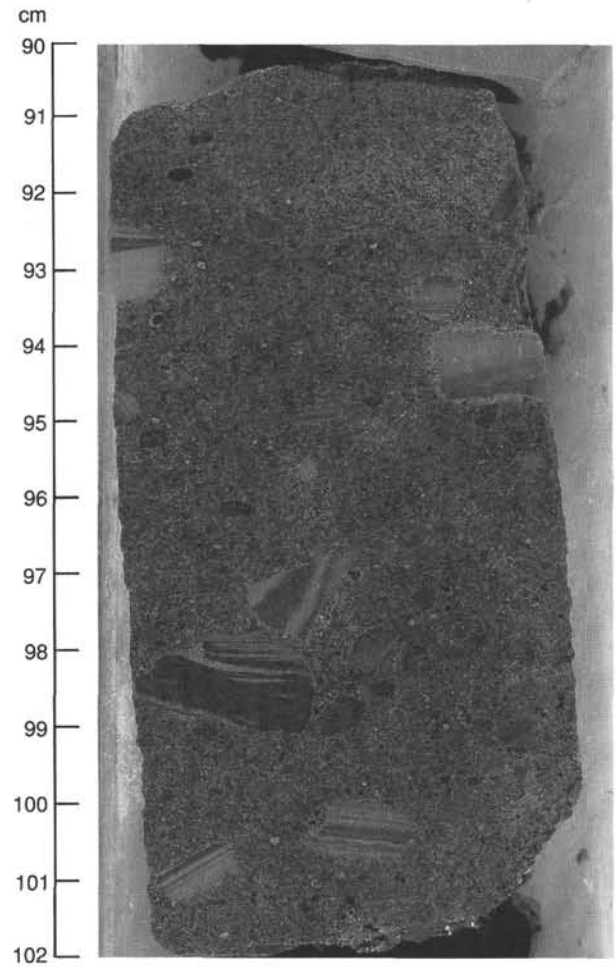

Figure 9. Portion of a coarse-grained volcaniclastic turbidite containing rip-up clasts of laminated and cross-laminated, fine-grained sandstone. This sediment records a high-energy redeposition event of Albian age. Interval 129-801B-1R-4, 90–102 cm.

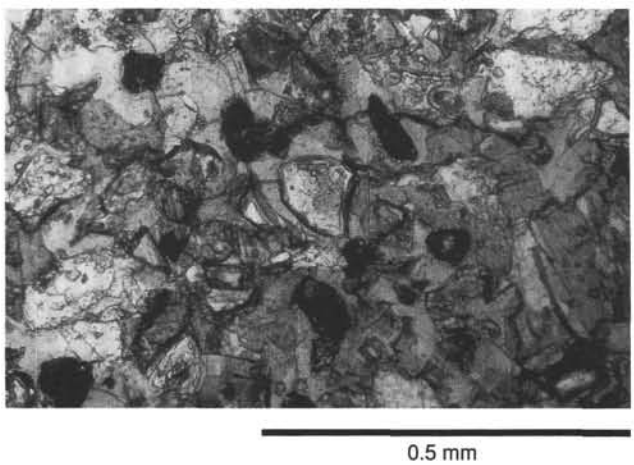

Figure 10. Photomicrograph of volcaniclastic sandstone (lithologic Unit III) with volcanic glass and igneous fragments with minor feldspar, opaques and oxides, pyroxene, and calcite. Crossed nicols. Sample 129-801A-19R-1, 1–4 cm.

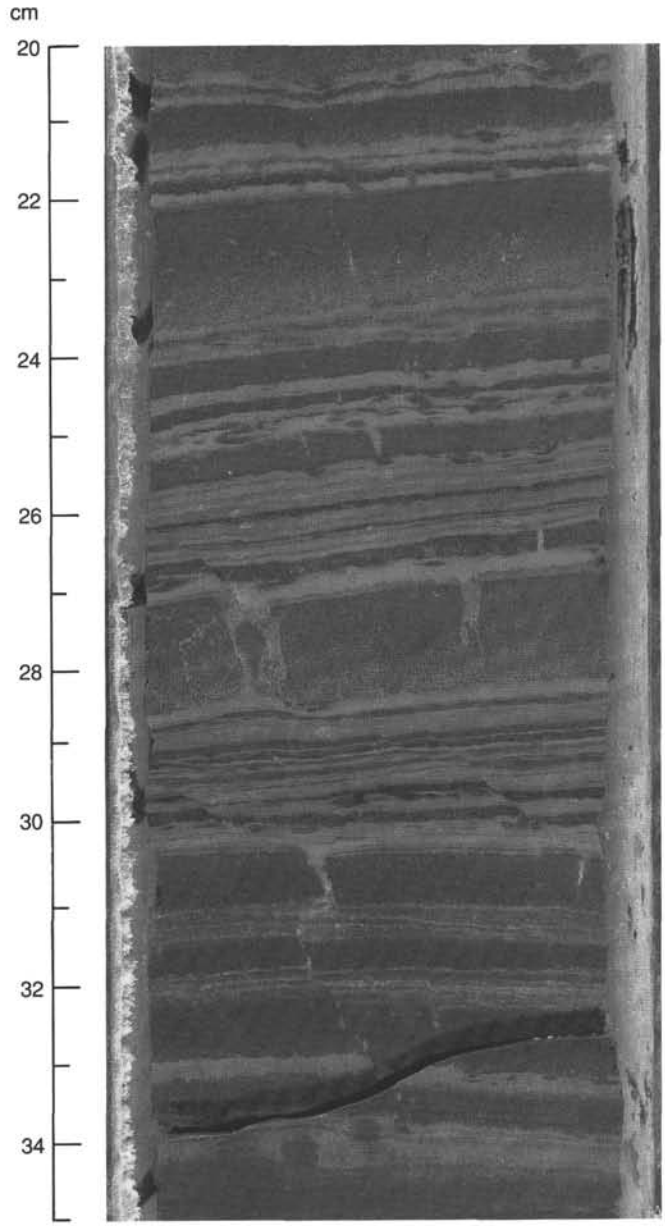

Figure 11. Fine-grained, fining-upward volcaniclastic turbidites (base of lithologic Unit III; middle Cretaceous) consisting mainly of altered volcanic glass and igneous rock fragments, interbedded with lighter-colored radiolarian claystone containing rare nannofossils. Interval 129-801B-13R-1, 20–35 cm.

Recrystallized limestone occurs between basalt flows in interval 129-801B-43R-3, 76–81 cm (Fig. 20E). Irregular pods of gray crystalline calcite are in a matrix of relatively porous white calcite. The piece contains rare nannofossils and very small (<0.3 mm) patches of lapilli partially replaced by calcite.

Between the basalt pillows in Cores 129-801B-40R to -44R are 1- to 5-cm-thick beds of red claystone. Core 129-801B-44R also contains volcaniclastic metasediments with recrystallized microfossils(?) overlain by iron-rich radiolarian metasiltstone (Fig. 20F).

Core 129-801C-4R consists of a yellow hydrothermal deposit of iron hydroxide (goethite) associated with silica. Thin-section observations indicate a multi-stage diagenetic history as yellow iron hydroxide deposits grew outward as radially

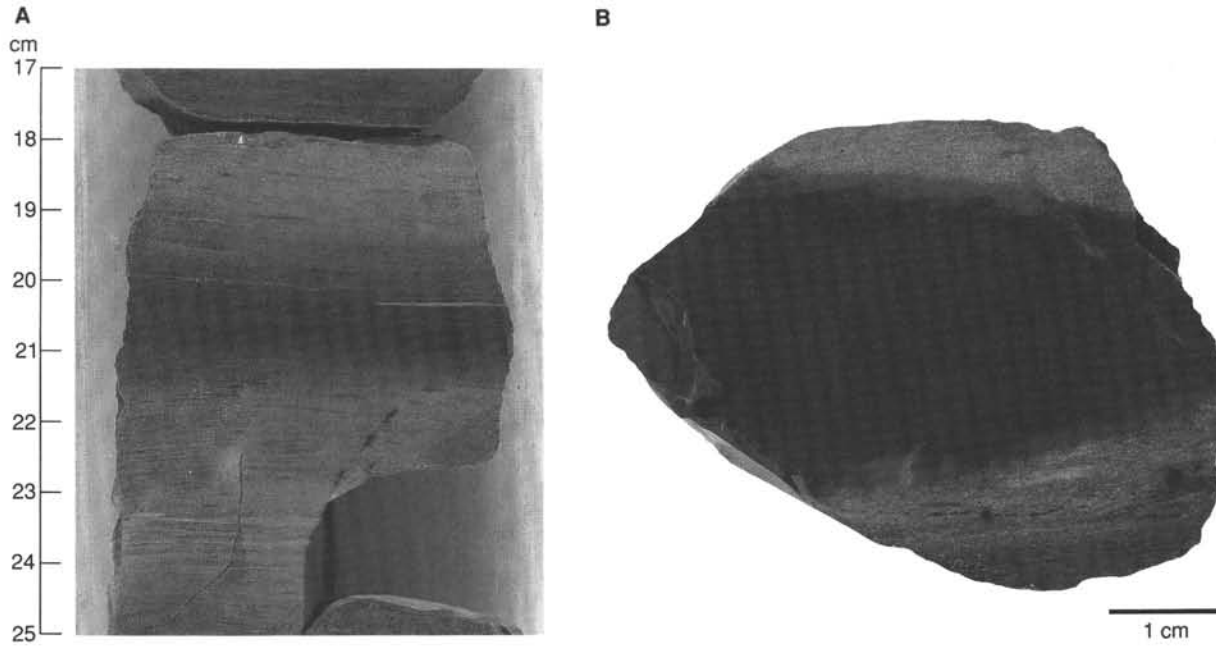

Figure 12. Typical brown radiolarite and dark brown chert of lithologic Subunit IVA. **A.** Radiolarite with discontinuous streaks and wispy, elongate flaser laminations subparallel to bedding that may be partially caused by compaction of fine subhorizontal bioturbation. Black streaks and spots are concentrations of iron-manganese oxides; dark layer in middle of center piece is silicified to chert. Note light-colored reduction mottles. Interval 129-801B-18R-1, 17–25 cm (Berriasian-Valanginian). **B.** Progressive chertification with radiolarite. An irregular, thin zone of lighter-colored porcellanite is between the dark brown chert and the outer radiolarite. Interval 129-801B-17R-1, 29–33 cm (Berriasian-Valanginian).

fibrous, coalescing, botryoidal masses, commonly zoned, then divided into platelets, followed by partial replacement by triple-junctioned quartz crystals. Larger quartz crystals fill secondary veins that traverse the deposit.

Red calcareous claystone, siliceous claystone, and chert occur between basalt flows throughout the lower portion of Hole 801C, with thicker intervals having depositional contacts to chill margins of basalt pillows recovered in intervals 129-801C-5R-4, 8–31 cm, and 129-801C-8R, 17–32 cm.

Carbonate Analyses

The percentage of carbonate remains very low throughout all these sedimentary facies (Table 3, Fig. 21). The few exceptions consist of rare nannofossils chalk beds in Unit II and some volcaniclastic turbidites beds of Unit III which contain shallow-water carbonate debris or nannofossils.

Sedimentation History of Site 801

The recovered sedimentary record of Site 801, when integrated with geophysical data on the motion and subsidence of this portion of the Pacific plate and with sedimentary facies data from nearby DSDP and ODP sites, provides a preliminary synthesis of the main features of its sedimentation history.

From the paleomagnetic data for Site 801 (see "Paleomagnetics" section, this chapter), the estimated paleolatitudes imply that the site was within or near the zone of equatorial divergence and upwelling during most of its Mesozoic history.

Callovian-Bathonian to Basal Oxfordian: The Interflow Sediments and Hydrothermal Deposit, and the Red Radiolarite and Claystone

During the formation of the basal igneous complex, various deposits were trapped between pillows or thin sheet flows of aphyric basalt and underwent significant recrystallization. The metasediments include silicified red claystone and radiolarian claystone, recrystallized gray limestone, and reddish calcareous and silicified tuff (Fig. 20). Hydrothermal processes produced an interval of at least 3 m of yellow siliceous iron oxyhydroxide deposit (Core 129-801C-4R).

The occurrence of calcareous layers and scarce nannofossils suggests either that the ridge site was above the CCD or that peculiar conditions of local chemistry enabled pockets of calcareous sediments to be preserved.

The biogenic siliceous and clayey sediments have a high content of metal oxides as hematite. The lowest silicified claystone breccia above the basalt (Section 129-801B-37R-1) probably resulted from rapid dewatering or fluid injection associated with the emplacement of the adjacent basalt.

Callovian-Bathonian sediments (Unit V) consist of red, hematite-rich alternations of claystone and radiolarite with an average repetition at intervals of approximately 5 cm (Fig. 17). A minimum sedimentation rate of 1.3 m/m.y. for this unit can be calculated assuming that sedimentation extended continuously through the Bathonian and Callovian. This implies that the alternations have a maximum average duration of 38,000 yr. The distinct radiolarian concentration and sharp contacts between the radiolarite and claystone layers are similar to radiolarian sand horizons observed in the Callovian of Atlantic Site 534 (Ogg et al., 1983) and in the upper Cenomanian of Atlantic Sites 386 and 387 (McCave, 1979). Three main hypotheses have been suggested to explain the contrast between these layers at Atlantic occurrences: (1) episodic blooms of high radiolarian productivity, (2) radiolarian-rich redeposition events, and (3) bottom-current winnowing and concentration of radiolarians followed by differential silica dissolution between radiolarian-enriched and -depleted layers. According to a thin-

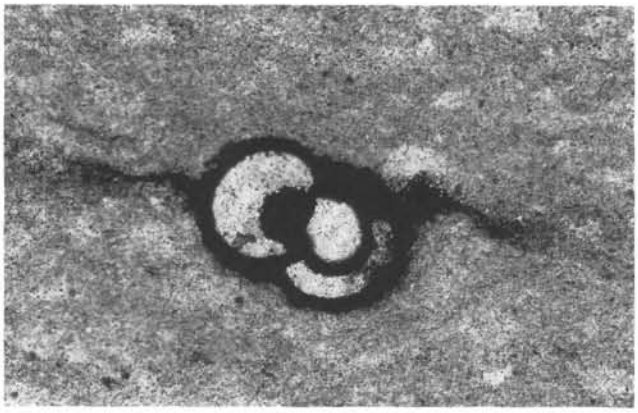

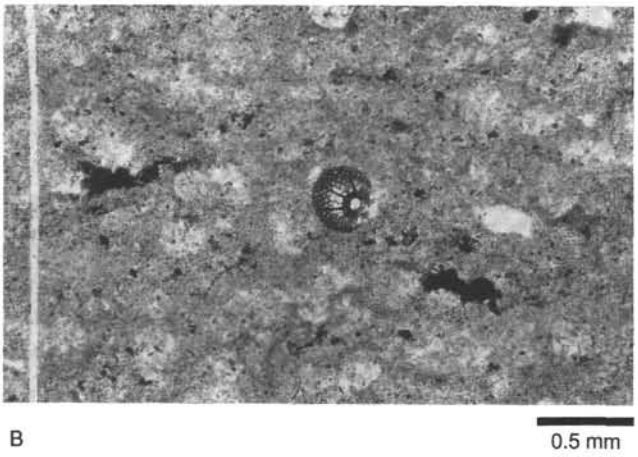

Figure 13. Photomicrographs of microfossils replaced or stained by iron-manganese oxide and filled by chalcedony in radiolarian chert (Subunit IVA; upper Tithonian). Most of the former radiolarians are now microcrystalline-filled ghosts within the chert; black regions are iron-manganese oxide concentrations. Crossed nicols. **A.** Foraminifer from Sample 129-801A-20R-1, 6–7 cm. **B.** Radiolarian from Sample 129-801A-21R-1, 17–18 cm.

section observation of one transition between radiolarite and claystone (Fig. 18) and pending further investigations, the models of episodic productivity-preservation or winnowing of radiolarians are favored.

Hematite enrichment of the Callovian strata may result from the combined effect of well-oxygenated bottom waters and the proximity of the site to the effluent of metal-rich hydrothermal waters produced at the active spreading ridge (Boström and Peterson, 1965; Bonatti, 1981). Localized reduction mottles post-date oxidation of the sediment that occurred at the surface. Low sedimentation rates and proximity to the ridge axis contributed to the iron and manganese enrichment of these sediments.

The Callovian-Oxfordian Boundary

The distinct lithologic boundary between the Callovian red radiolarite and claystone (Unit V) and the Oxfordian brown clayey radiolarite (Unit IVB) is probably a hiatus or a condensed section marked by: (1) a distinct upward color change from red to brown with corresponding enrichment in oxides, (2) a change in style of sedimentation from alternating layers to a more homogeneous clayey radiolarite, (3) a change in average apparent dip of bedding from about 30° in Callovian-Bathonian strata to about 10° in Upper Jurassic strata, and (4) a gap in radiolarian zones. The change in apparent dip suggests that tectonic tilting may have occurred. Worldwide, the contact between Oxfordian and Callovian marine sediments is commonly a hiatus, with upper Callovian and/or lower Oxfordian sediments being absent or extremely condensed. The presence of a hiatus between Callovian-Bathonian and Oxfordian at Site 801 may also be a manifestation of the general global events demarcating the Middle/Late Jurassic boundary, and not solely a local tectonic coincidence.

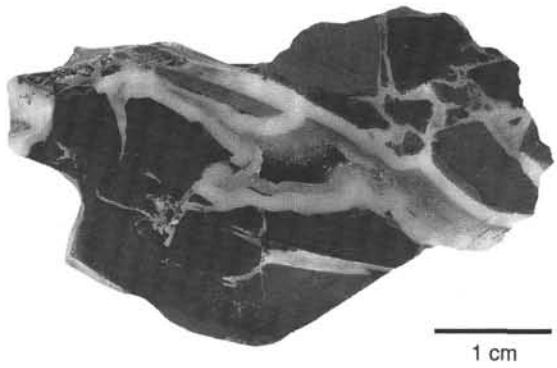

Figure 14. Brecciated radiolarian chert from the lower part of Subunit IVA (upper Tithonian). Fractures in the dark brown chert are completely filled with multiple generations of quartz; an open void is lined by drusy quartz. Siliceous radiolarite is separated from adjacent chert with similar texture. Sample 129-801B-21R-1, 19–22 cm.

Oxfordian to Valanginian: The Brown Radiolarite Deposition and Diagenesis

Depositional Environment and Change of Sedimentation of the Siliceous and Clayey Facies

Variations on the scale of several centimeters occur in the relative radiolarian concentration, in the development of porcellanite or chert, and in the character of the quasi-laminated texture. These small-scale variations suggest the possibility of periodic changes in siliceous productivity; however, recovery was inadequate to unequivocally demonstrate cyclicity, such as that described in coeval sediments at nearby sites: the Berriasian-Valanginian of Site 800 (see "Lithostratigraphy" section, "Site 800" chapter, this volume) and in the Lower Cretaceous limestones at Site 167 on Magellan Plateau (Winterer, Ewing, et al., 1973; Cotillon, 1984, 1985).

The less silicified radiolarites generally exhibit a streaky, discontinuous-laminated, "woody" texture, which is interpreted as the result of compaction of sub-horizontal bioturbation. Less distorted bioturbation occurs in some intervals. No definite evidence either of low-oxygen bottom water or of bottom-current activity was noted, which suggests that deposition was on a quiet, but oxygenated, seafloor.

Within the brown radiolarite sequence (Unit IV) the relative abundance of radiolarians increases upward, reaching a maximum in the upper Tithonian sediments. The Oxfordian-lower Tithonian clayey radiolarite (Subunit IVB) implies an average sedimentation rate of less than 5 m/m.y. In contrast, the thickened upper Tithonian-Valanginian radiolarite (Subunit IVA) has an apparent sedimentation rate of about 8 m/m.y. (Fig. 24). In between, the upper Tithonian,

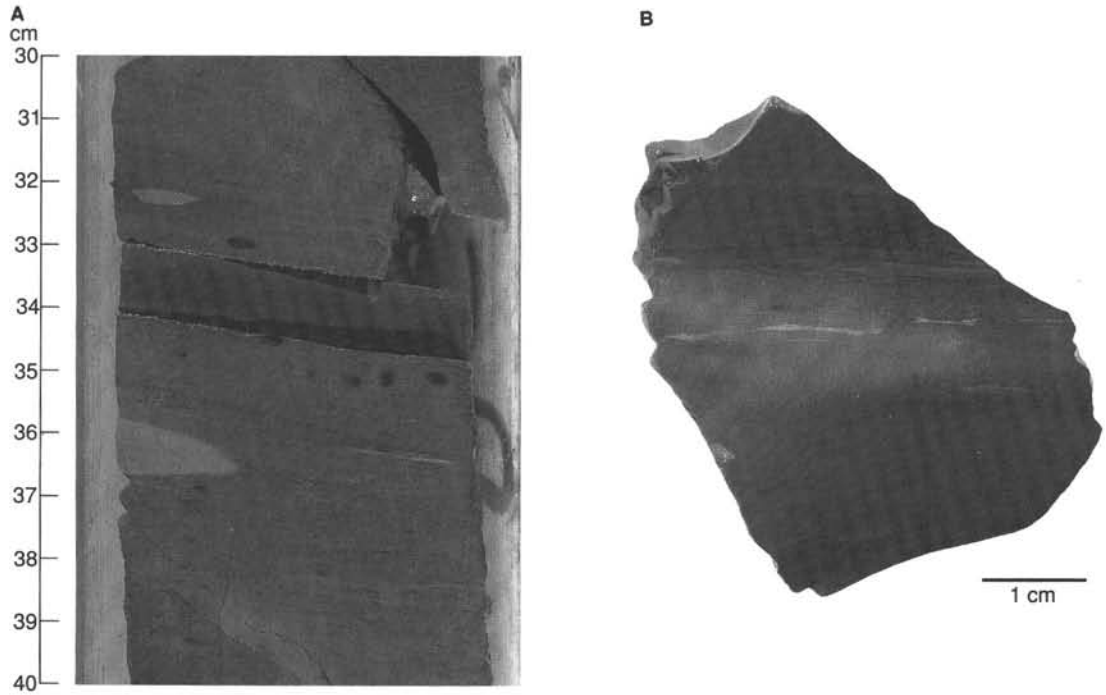

Figure 15. Typical clayey radiolarite and radiolarian chert of lithologic Subunit IVB. **A.** Clayey radiolarite. Discontinuous streaks and wispy, elongate flaser laminations subparallel to bedding may be partially caused by compaction of fine subhorizontal bioturbation. Black spots and streaks are concentration of iron-manganese oxide; reduction mottling is also present. Interval 129-801B-27R-1, 30–40 cm (lower Tithonian). **B.** Radiolarian chert formed by silicification of clayey radiolarite. The dark brown chert has weak bioturbation to wispy laminations, black spots of concentrated iron-manganese oxide, and a reduction mottle of reddish brown in the center. Interval 129-801B-28R-1, 10–14 cm (Kimmeridgian-lower Tithonian).

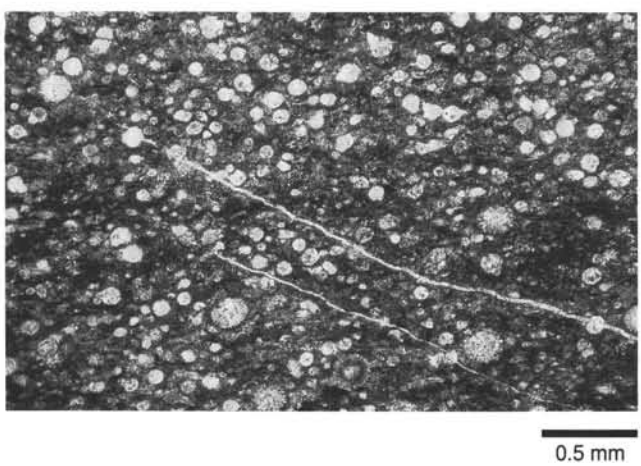

Figure 16. Photomicrograph of typical clayey radiolarite from lithologic Subunit IVB. Radiolarians are chalcedony-filled and commonly coated with iron-manganese oxide. Plain light. Scale bar is 0.5 mm. From sample 129-801B-23R-CC, 1–4 cm (middle Tithonian).

more siliceous sediments record a higher sedimentation rate of about 10 m/m.y. or greater (Cores 129-801B-20R through -23R). Silica abundance and the silicon/aluminum ratio, as measured by the geochemical logging of the site, attains a distinctive peak in this interval (370–395 mbsf) (Fig. 47). The increase in silica content also correlates with an assemblage of sparse nannofossils indicative of high fertility in the lowest upper Tithonian strata of Site 801 (see "Biostratigraphy" section, this chapter). The change between lower Tithonian clayey radiolarite and upper Tithonian radiolarite and chert is sharp in both the recovered sediments and in the geochemical logs; this sudden transition marks the boundary between Subunits IVB and IVA.

The upper Tithonian burst in radiolarian abundance can be partially explained by the near-equatorial position of the site (see "Paleomagnetics" section, this chapter); the equatorial current system is a likely area for preferential radiolarite deposition throughout the Mesozoic (Lancelot and Larson, 1975; Lancelot, 1978; Baumgartner, 1987).

The upward decrease in the abundance of radiolarians relative to clay in Berriasian through Valanginian strata (upper Subunit IVA) probably reflects a slow decline in radiolarian productivity and preservation due to the steady southward drift of the site from the equatorial high-fertility zone.

Diagenetic and Deformation Features

Primary textural differences of the facies have been enhanced by later diagenesis, especially by dissolution and reprecipitation of silica. In some intervals, radiolarians have been silica-infilled in the darker, partially silicified layers and left as molds in the adjacent, more porous, light-colored layers. Most of the dark brown chert occurs as bands parallel to bedding, but discordant diagenetic boundaries are also common (Fig. 12B).

Fracturing of the chert beds and the associated formation of quartz-lined voids decrease uphole from Cores 129-801B-22R to -16R, suggesting that early chertification of the radiolarian-enriched mid-Tithonian strata resulted in horizons susceptible to later brittle deformation (Fig. 14). The early-formed quartz fillings of some fractures served as permeability barriers and resulted in isolated "compartments" in the

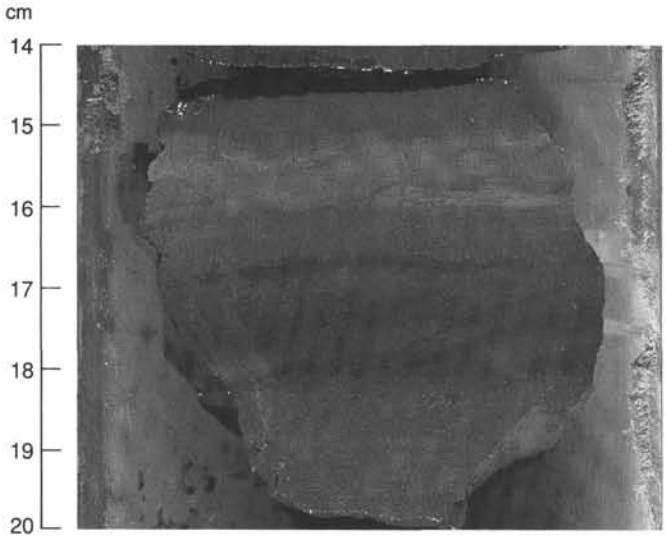

Figure 17. Alternating red radiolarite and claystone of lithologic Unit V. Central block has a dark band of radiolarian-poor claystone between two lighter-colored bands of concentrated radiolarians. Upper radiolarite band displays flaser or lenticular structures of radiolarian concentrations between discontinuous, wavy, clay-rich laminations. Interval 129-801B-33R-1, 14–20 cm (Callovian).

radiolarite which experienced different degrees of chertification.

The brown radiolarite of Unit IV has abundant brown staining and black micronodules, fracture coatings, and internal flecks of oxides (Figs. 12 and 15). In mottles where brown coloration is absent, the sediment is reddish, indicating the continued presence of iron oxide. Some of the micronodules appear to have begun as manganiferous replacement or coatings of biogenic tests (Figs. 13 and 16). Growth of micronodules preceded silicification as indicated by their occurrence within chert nodules of probable low permeability. The high abundance of manganese in Unit IV, in contrast to the underlying red claystone and radiolarite of Callovian-Bathonian Unit V, may be the result of post-burial, slow, upward

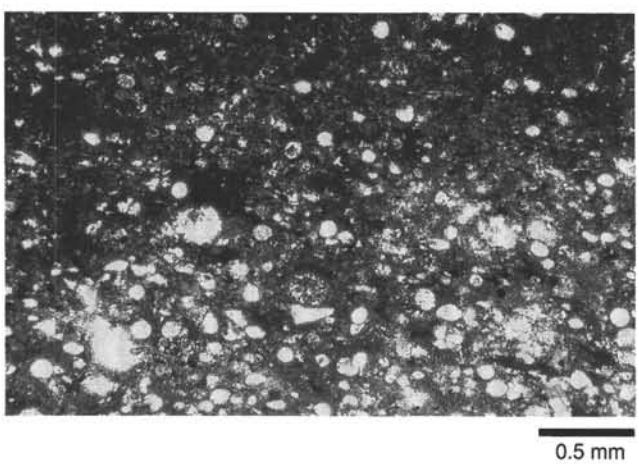

Figure 18. Photomicrograph of a transition between a radiolarite band and a claystone band in lithologic Unit V. In this thin section, the transition is narrow, but not abrupt. The claystone and the radiolarite are rich in hematite. Plain light. Scale bar is 0.5 mm. Sample 129-801B-35R-1, 62–65 cm (Callovian).

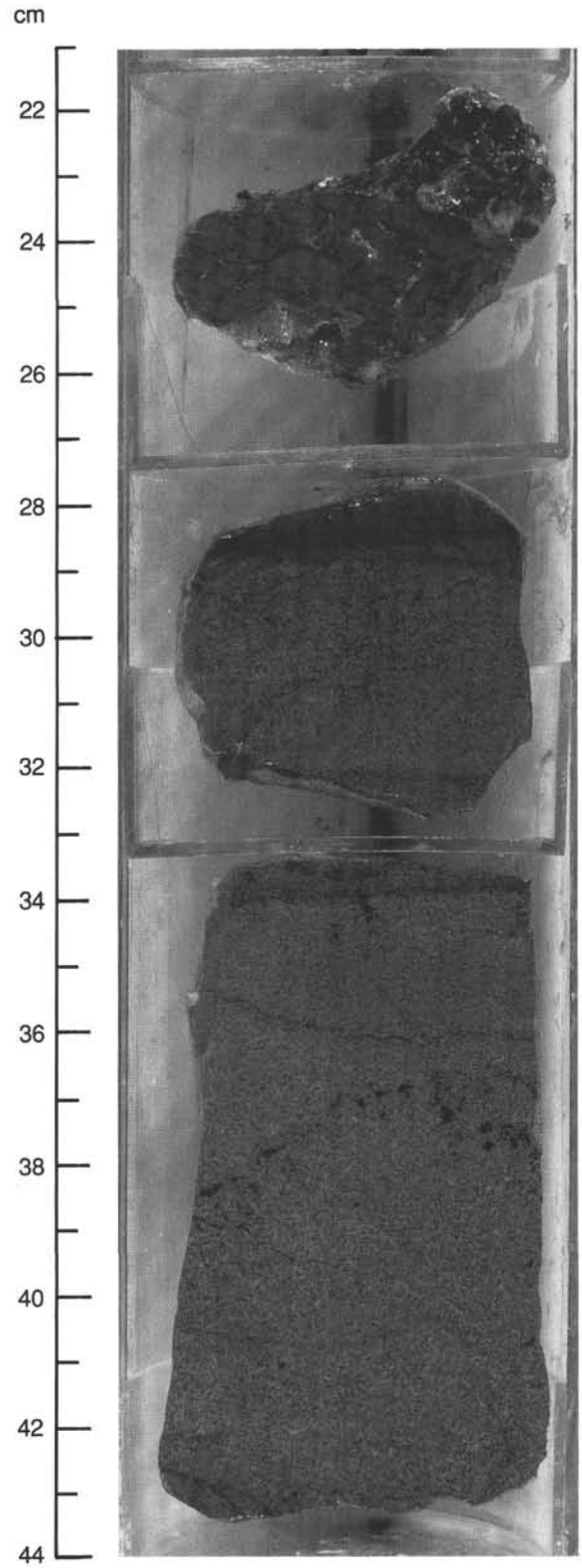

Figure 19. Uppermost recovered flow or thin-sill aphyric basalt underlying brecciated chert. Top of basalt has a fine-grained chill margin, but actual sediment/basalt contact was not recovered. Interval 129-801B-37R-1, 22–43 cm. (Callovian-Bathonian).

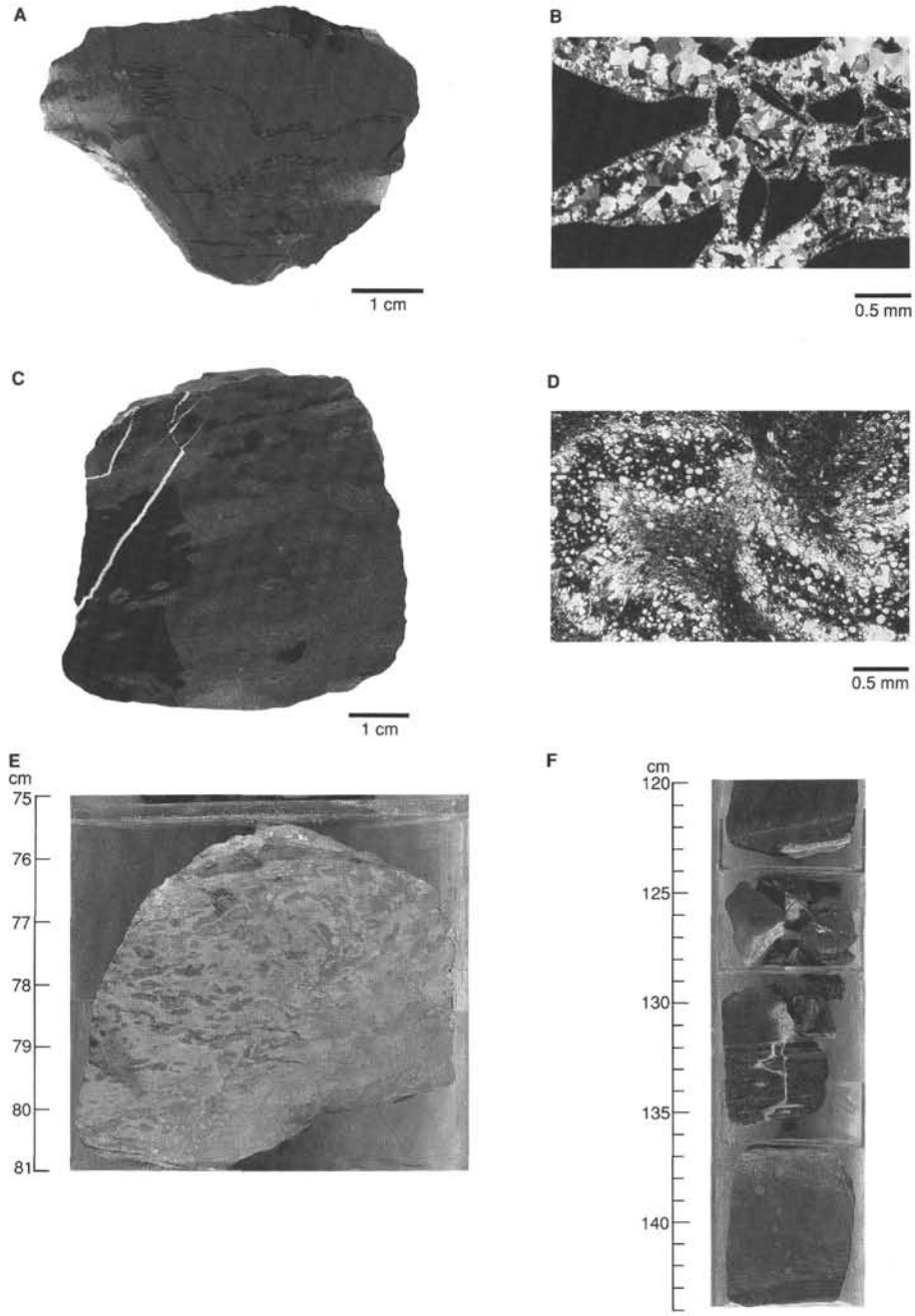

Figure 20. Representative lithologies of basal and interpillow sediments, the oldest sediments recovered from the Pacific plate (Callovian-Bathonian). **A.** Reddish brown chert crackle breccia. Brecciation occurred in soft clay, by rapid dehydration or fluid injection associated with heating by the adjacent basalt, which is suggested by quartz-filled fractures that have curved, non-parallel surfaces that taper into the host siliceous claystone with a feathery or horsetail appearance. Interval 129-801B-37R-1, 11–16 cm. Centimeter scale bar is parallel to bedding. **B.** Photomicrograph of reddish brown chert breccia similar to (A). Metalliferous siliceous claystone clasts are separated by quartz-filled fracture fillings. Crossed nicols. Sample 129-801B-38R-1, 4–7 cm. **C.** Interflow silicified radiolarite. Radiolarite is dark reddish gray with moderate bioturbation. Radiolarians are replaced by opaque white silica, making some burrow-fillings clearly evident. Darker area on the left is more silicified. Interval 129-801B-39R-1, 27–32 cm. **D.** Photomicrograph of silicified radiolarite similar to (B). Silica-filled radiolarians are most abundant or best preserved within the burrow-fillings. Interburrow sediment is a metalliferous claystone with radiolarians. Plain light. Sample 129-801B-39R-1, 15–16 cm. **E.** Interflow gray limestone. Irregular pods of darker gray, densely crystalline calcite are contained within a matrix of more porous calcite in a fabric which may represent disruption or injection. Interval 129-801B-43R-3, 75–81 cm. **F.** Interflow reddish gray, calcareous, silicified tuff (two lowest pieces) that is depositionally overlain by dark reddish brown, bioturbated, radiolarian metasiltstone (second piece from top). Calcareous, silicified tuff has a finely laminated, aphanitic groundmass; the upper piece contains 1- to 3-mm calcareous ovoids with coarser, crystalline calcite centers, which are possibly biogenic tests. Radiolarian metasiltstone has a cryptocrystalline to microcrystalline siliceous matrix containing ghosts of radiolarians and rich in iron-manganese oxides. Interval 129-801B-44R-1, 120–144 cm.

Table 3. Carbonate, organic carbon, and sulfur content of samples from Site 801.

Core, section, interval (cm)	Depth (mbsf)	$CaCO_3$ (wt%)	C_{org} (wt%)	S (wt%)	Lithology
129-801A-					
4R-1, 76–78	30.76	0.5	8.50		Pelagic clay
5R-1, 74–76	40.34	73.9			Nannofossil ooze
5R-5, 57–58	46.17	0.2			Pelagic clay
5R-5, 74–76	46.34	0.4			Pelagic clay
7R-1, 75–77	59.75	0.2			Pelagic clay
7R-CC, 11–13	64.06	0.2			Chert
9R-1, 17–19	78.37	0.1			Chert
12R-1, 0–2	106.80	0.1			Chert, porcellanite
13R-1, 13–15	116.63	5.4			Calcareous porcellanite
14R-1, 51–53	126.71	0.2			Radiolarian porcellanite
15R-1, 10–12	136.00	1.2			Volcaniclastic sandstone
16R-1, 44–46	146.04	2.8			Volcaniclastic sandstone
17R-1, 64–66	155.84	0.2			Chert with porcellanite
18R-1, 49–51	165.49	3.4			Volcaniclastic sandstone
19R-1, 33–35	175.03	7.7			Volcaniclastic calcareous claystone
20R-1, 15–17	184.55	0.2			Radiolarian claystone
129-801B-					
1R-1, 60–62	194.60	0.2			Radiolarian silty claystone
1R-3, 81–83	197.81	3.2			Volcaniclastic sandstone
2R-1, 92–94	204.42	1.2			Volcaniclastic silty sandstone
3R-1, 76–79	213.66	0.3			Volcaniclastic silty sandstone
3R-1, 79–81	213.69	1.1			Volcaniclastic silty sandstone
3R-CC, 0–2	214.06	1.2			Volcaniclastic silty sandstone
4R-1, 17–19	222.47	3.7			Volcaniclastic clayey sandstone
5R-2, 0–10	233.20	4.3			Volcaniclastic silty claystone
5R-2, 145–147	234.65	15.2			Calcareous volcaniclastic sandstone
6R-4, 10–12	245.90	2.3			Volcaniclastic clayey siltstone
7R-1, 3–5	251.03	15.5			Calcareous volcaniclastic claystone
8R-3, 115–125	264.85	4.0			Volcaniclastic silty claystone
8R-4, 126–128	266.46	2.8			Volcaniclastic silty claystone
10R-1, 22–24	280.22	0.1			Calcareous claystone
10R-1, 29–31	280.29	5.7			Calcareous siltstone
11R-1, 21–23	289.91	0.2			Clayey radiolarite
12R-1, 13–17	299.43	0.6			Volcaniclastic turbidite
13R-1, 46–51	309.46	1.4			Volcaniclastic turbidite
14R-1, 15–24	318.45	0.2			Clayey radiolarite
16R-1, 30–32	337.50	0.4			Radiolarite
17R-1, 1–3	346.61	0.2			Radiolarite
18R-1, 17–19	355.97	0.3			Radiolarite
19R-1, 26–28	365.56	0.2			Radiolarian chert
20R-1, 21–23	374.71	0.2			Radiolarian chert
21R-1, 10–12	383.80	0.1			Radiolarian chert
23R-CC, 13–15	396.03	0.1			Radiolarian chert
25R-1, 41–43	405.61	0.2			Radiolarite with chert
27R-1, 37–39	415.07	0.2			Clayey radiolarite with chert
31R-1, 25–27	433.85	0.2			Radiolarian chert
33R-1, 55–57	443.35	0.2			Clayey radiolarite
35R-1, 131–133	453.61	0.2			Radiolarite
37R-1, 54–56	462.04	0.4	0.0	0.1	Basalt
37R-1, 66–71	462.16	0.5			Basalt
38R-1, 22–25	466.32	1.9			Basalt
39R-1, 9–11	470.79	0.4			Basalt
40R-1, 20–23	477.10	0.2			Basalt
40R-1, 38–40	477.28	1.7	0.0	0.1	Basalt
40R-1, 85–91	477.75	9.1			Basalt
41R-1, 26–31	483.26	6.8			Basalt
41R-1, 95–97	485.45	8.2	0.0	0.0	Basalt
42R-2, 93–95	489.98	1.2	0.0	0.1	Basalt
43R-1, 42–44	492.62	2.0	0.0	0.0	Basalt
43R-3, 119–121	496.17	23.0	0.1	0.0	Basalt
44R-1, 52–54	502.22	8.8	0.0	0.0	Basalt

diffusion of reduced manganese into overlying Upper Jurassic strata, which had sufficiently oxidizing conditions for the manganese to reprecipitate. A similar model of upward diffusion of manganese and precipitation at the sediment surface explains the formation of manganese-rich nodules and segregation between iron and manganese oxides during early diagenesis of pelagic sediments (Lynn and Bonatti, 1965; Tsunogai and Kusakabe, 1982; Karpoff, 1989, and references therein).

Underlying lower Tithonian and Kimmeridgian strata (Cores 129-801B-24R through -27R) have apparent dips of 5°–10°, in contrast to the relatively horizontal strata of upper Tithonian and higher, in which the apparent dip is indistinguishable from the 2°–3° deviation of the drill string from vertical. The simultaneous upward decrease in the clay content in Core 129-801B-24R (boundary between Subunits IVB and IVA, which is also sharply delimited on the geochemical logs) and in the apparent dip of bedding suggests the possibil-

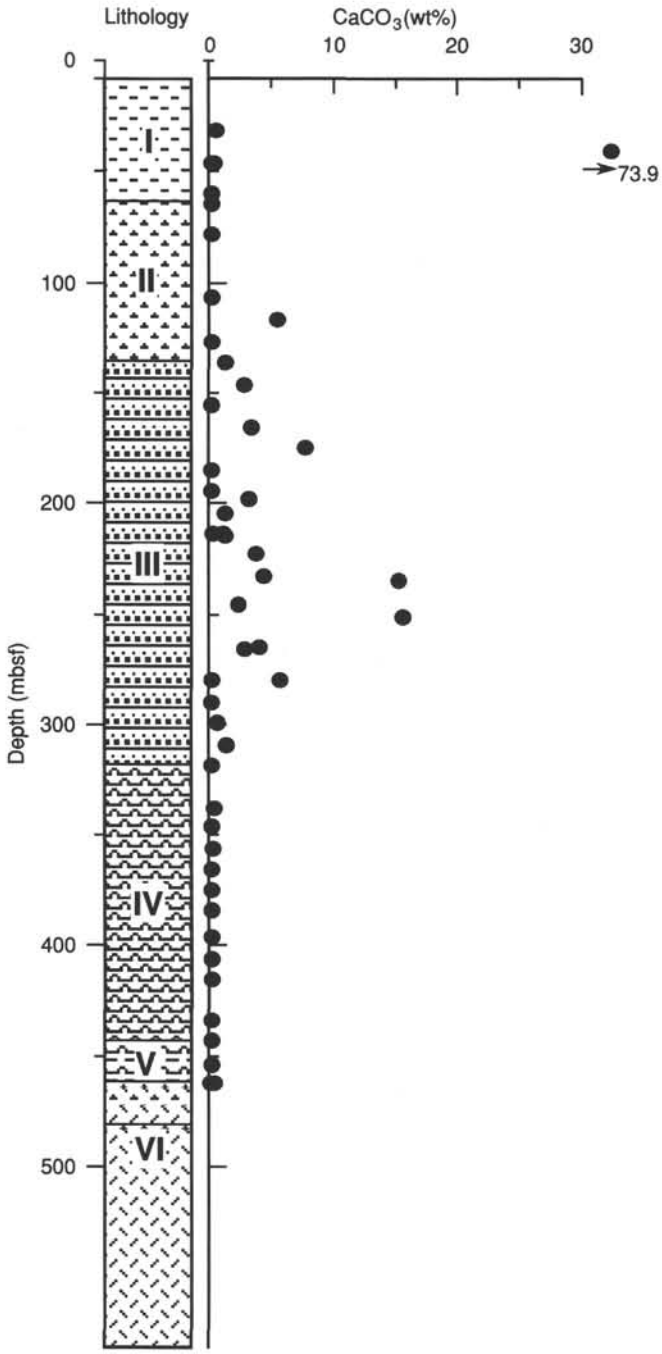

Figure 21. Stratigraphic plot of carbonate percentages (Table 3) and lithologic units of Holes 801A and 801B. Lithologic symbols are the same as for Figure 6.

ity of a minor, tectonically induced unconformity at the base of the upper Tithonian strata.

The Hiatus between Valanginian and Albian Deposits

The sharp lithologic and geochemical-log boundary between the Valanginian radiolarites of Core 129-801B-14R and the Albian distal volcaniclastic turbidites of Core 129-801B-13R (318 mbsf; Unit III) is either a hiatus or condensed interval in sedimentation. A hiatus within this same age span is also suspected at nearby Site 800 (see "Paleomagnetics" and "Biostratigraphy" sections, "Site 800" chapter, this volume).

Aptian-Cenomanian: The Origin and Pulses of the Volcaniclastic Turbidites and Associated Pelagic Sediments

The first pulse of volcaniclastic input is recorded at Site 801 as distal, fine-grained turbidites interbedded with radiolarian claystone (Cores 129-801B-13R and -12R). This initial herald of local seamount formation had not been precisely dated at the time of preparation of this report. The lack of magnetic reversals suggests an Aptian age (see "Paleomagnetics" section, this chapter). After an interval of siliceous pelagic sedimentation (Cores 129-801-11R and -10R), a second sustained pulse of volcaniclastic input began in the middle Albian with thick fine-grained turbidites.

Despite their apparent source in seamounts located over 100 km from the site, individual volcaniclastic turbidite beds at Site 801 exceed 4 m in thickness and can approach a debris flow texture in their abundance of rip-up clasts. The seamounts which were the source of these turbidites had built up to neritic depths by the late Albian, as shown by occurrence of fragments of red algae and echinoderms.

Pelagic intervals occur mainly as minor interbeds between turbidites, except for a brief, pelagic-dominated interval during the upper Albian (Cores 129-801A-20R to -17R). The pelagic facies primarily range from nannofossil-bearing siliceous clay to radiolarian ooze.

A third pulse of volcaniclastic turbidites and tuffaceous beds of latest Albian and Cenomanian age (Cores 129-801A-17R to -14R) completed the volcanic sequence.

At Site 800, the Albian and Cenomanian is represented by 150 m of siliceous limestone, a lithology virtually absent at Site 801. Many of the Albian-Cenomanian pelagic interbeds at Site 801 contain minor amounts of nannofossils and carbonate, but clay and radiolarians remain the dominant components. Site 801 was 3° farther south from the paleoequator and perhaps slightly deeper; hence, it may have received and preserved less calcareous input. However, such effects would seem relatively insignificant considering the 5°–10° of northward drift of the Pacific plate through this time interval (see "Paleomagnetic" section, this chapter). Other alternate explanations include locally enhanced carbonate productivity associated with proximity of seamounts, erosional removal of carbonate strata, and post-burial dissolution; however, our favored explanation is that the low carbonate content of Albian-Cenomanian deposits at Site 801 reflects the geographic variation of a redeposited facies. Albian to Cenomanian radiolarian-rich limestones at Sites 800 and 802 are largely muddy turbidites (see "Lithostratigraphy and Sedimentology" sections, "Site 800" and "Site 802" chapters, this volume). At Sites 800 and 801, the change from calcareous-bearing pelagic sediment to noncalcareous radiolarian cherts and porcellanites occurs approximately during Turonian time, suggesting a regional rise in the CCD.

Cenomanian to Campanian: Brown Chert and Porcellanite

There was very poor recovery of the Upper Cretaceous brown chert and porcellanite Unit II. Those recovered facies probably represent some of the more silicified layers within a host radiolarian clay. This interpretation of the *in-situ* unrecovered lithology is supported by the common occurrence of "rinds" of lighter brown siliceous claystone on the some edges of the tumbled chert fragments, by the recovery of some pieces of softer clayey radiolarian porcellanite (e.g., within Core 129-801A-10R), and by the interbedded radiolarite and claystone character of the upper portion of this unit (lower Core 129-801A-7R).

Although some chert or porcellanite fragments display minor bioturbation, most of the sediment retains an original

banding undisrupted by bioturbation. The brown to reddish coloration, probably related to iron-manganese oxides, suggests that the bottom waters were oxidizing, but that either oxygen or nutrient levels were not conducive to an abundance of bottom life. The primary compositional differences, such as relative content of minor amounts of clay, partially controlled the chertification processes (Lancelot, 1973) and result in thin bands of porcellanite in the chert.

The decrease in radiolarian content of the sediments at the end of the Campanian, and the corresponding termination of the chert-rich Unit II, may represent the passage of Site 801 into the low-fertility waters of the North Pacific gyre. Brown pelagic clay deposition completes the Mesozoic sedimentation history of Site 801. There is a probable hiatus between Campanian-Maestrichtian and Paleocene sediments, as occurs at other nearby sites.

The brown pelagic clay of the latest Cretaceous and Tertiary are typical deep-sea clay deposits formed below the CCD, such as those described in deep basins from Pacific and Atlantic realm. Some redepositional events, expressed as calcareous ooze layers, are recorded in the deep Pigafetta Basin.

Main Aspects of Mesozoic Sedimentation

Several main aspects of the sedimentation at Site 801 in the deep Pigafetta Basin can be established from the preliminary lithologic observations.

Mesozoic pelagic sedimentation at Site 801 was dominated by radiolarians and clay. The siliceous deposits were dominant, with high sedimentation rates during the late Tithonian-early Berriasian and the Cenomanian-Campanian, coincident with times of equatorial paleolatitudes. Jurassic and Cretaceous pelagic sediments preserved on circum-Pacific terrains consist mainly of ribbon radiolarite cherts (e.g., Baumgartner, 1987). In contrast, sediments recovered at Site 801 and other Pacific Mesozoic sites have never displayed such sharply bedded and cherty ribbon radiolarites.

Calcareous biogenic phases are rare components of Mesozoic sediments at Site 801. At DSDP Sites 303 and 304, about 21° north of the Site 801, Lower Cretaceous basal calcareous sediments were recovered. Therefore, during the Early Cretaceous the CCD could be estimated to lie between the paleodepths of Sites 801, 303, and 304, between 3.5 and 4.5 km. The scarce nannofossils suggest high-fertility surface conditions during the Jurassic (see "Biostratigraphy" section, this chapter), although calcareous nannoplankton were probably not an important component of near-equatorial sedimentation. Pelagic limestones are scarce in the Atlantic and western Tethys basins below the Upper Tithonian (Bernoulli, 1972; Lancelot et al., 1972) and in circum-Pacific terrains younger than Upper Cretaceous (Baumgartner, 1987). Siliceous epochs are often contemporaneous with periods of fast oceanic spreading and volcanism (Garrison, 1974; Adachi et al., 1986). The absence of a calcareous sequence of Callovian through Kimmeridgian age at Site 801 may be the result of selectively siliceous, high surface-productivity, rather than a shallow CCD.

Mesozoic pelagic deposits at Site 801 are weakly to moderately bioturbated, devoid of organic carbon, and rich in iron oxide. This character is quite comparable to most other sites drilled in the deep Pacific, and indicates continually oxygenated bottom waters during the Cretaceous.

The basal and interpillow sediments at Site 801 have been affected to varying degrees by hydrothermalism and thermal effects accompanying emplacement of the basalt flows. The iron, manganese, and even silica-rich deposits from this hydrothermal activity at the nearby spreading ridge axis may be compared to metalliferous deposits described in the Tethyan realm at the Oman and Cyprus ophiolites (e.g., Karpoff et al., 1988, and references therein).

BIOSTRATIGRAPHY

Sediment was cored in two holes (801A and 801B) at this site. Twenty rotary cores were taken from Hole 801A, and a sequence of sediments was recovered and dated as latest Paleocene to late Albian. In contrast to the Santonian-Campanian to late Tertiary hiatus suspected at Site 800, continuous sedimentation is believed to have taken place from the Late Cretaceous to the early Tertiary at Site 801, although the exact position of the Cretaceous/Tertiary (K/T) boundary in the hole could not be determined because of insufficient core recovery.

Hole 801B was drilled in response to an 8° deviation of the drill string at the bottom of Hole 801A, and was washed down to the depth at which Hole 801A was terminated. The sediments recovered from 44 rotary cores in Hole 801B are dated as middle Albian to Bathonian. Core-catcher samples were routinely analyzed for calcareous nannofossils, foraminifers, radiolarians, and palynomorphs, and where necessary, additional samples from within the cores were also examined for these microfossils.

Radiolarians are the most abundant and persistent group throughout the cored sequence, whereas the distribution of calcareous nannofossils is sporadic and their abundance is usually lower. Planktonic foraminifers occur rarely in the sequence, and benthic foraminifers are of low to moderate abundance in the Campanian to Paleocene pelagic clay. Amorphous organic matter was found at some levels, but dinoflagellate cysts were absent.

Cores from Holes 801A and 801B were dated using calcareous nannofossils, foraminifers and radiolarians. The calcareous nannofossils provide useful datums in the Tertiary and middle Cretaceous, and the presence of single specimens in two deeper cores in Hole 801B are in agreement with Jurassic ages determined by radiolarians. The agglutinated foraminifers allow approximate determination of the Late Cretaceous and early Tertiary from their occurrence in Site 800. The planktonic foraminifers, although rare and only moderately well preserved, provide middle Cretaceous ages. Radiolarians are poorly preserved in the Cretaceous intervals, although late Albian to Campanian biozones may be recognized, supported by evidence from planktonic foraminifers. The radiolarians also provide detailed stratigraphic resolution of the Lower Cretaceous and Middle Jurassic intervals and indicate a possible hiatus in the early Oxfordian. A summary of the biostratigraphy of Site 801 is provided in Figure 22.

The paleoenvironment of Site 801 is interpreted as abyssal with deposition below the calcium carbonate compensation depth during the late Cenomanian through early Tertiary, based primarily on the presence of deep-water agglutinated foraminifer assemblages. It is hard to speculate on the paleobathymetry for the Albian through Bathonian interval at this site since sedimentation rates, likely affected by changing paleolatitude, volcanism, and gravity flows, will have had an important influence on the abundance trends of the nannofossils and radiolarians.

Calcareous Nannofossils

Forty-one core-catcher and 50 additional samples from Site 801 were investigated. Nannofossil distribution is very uneven (Fig. 23). Total abundance fluctuates from barren to very abundant, and preservation varies from poor to good. Diver-

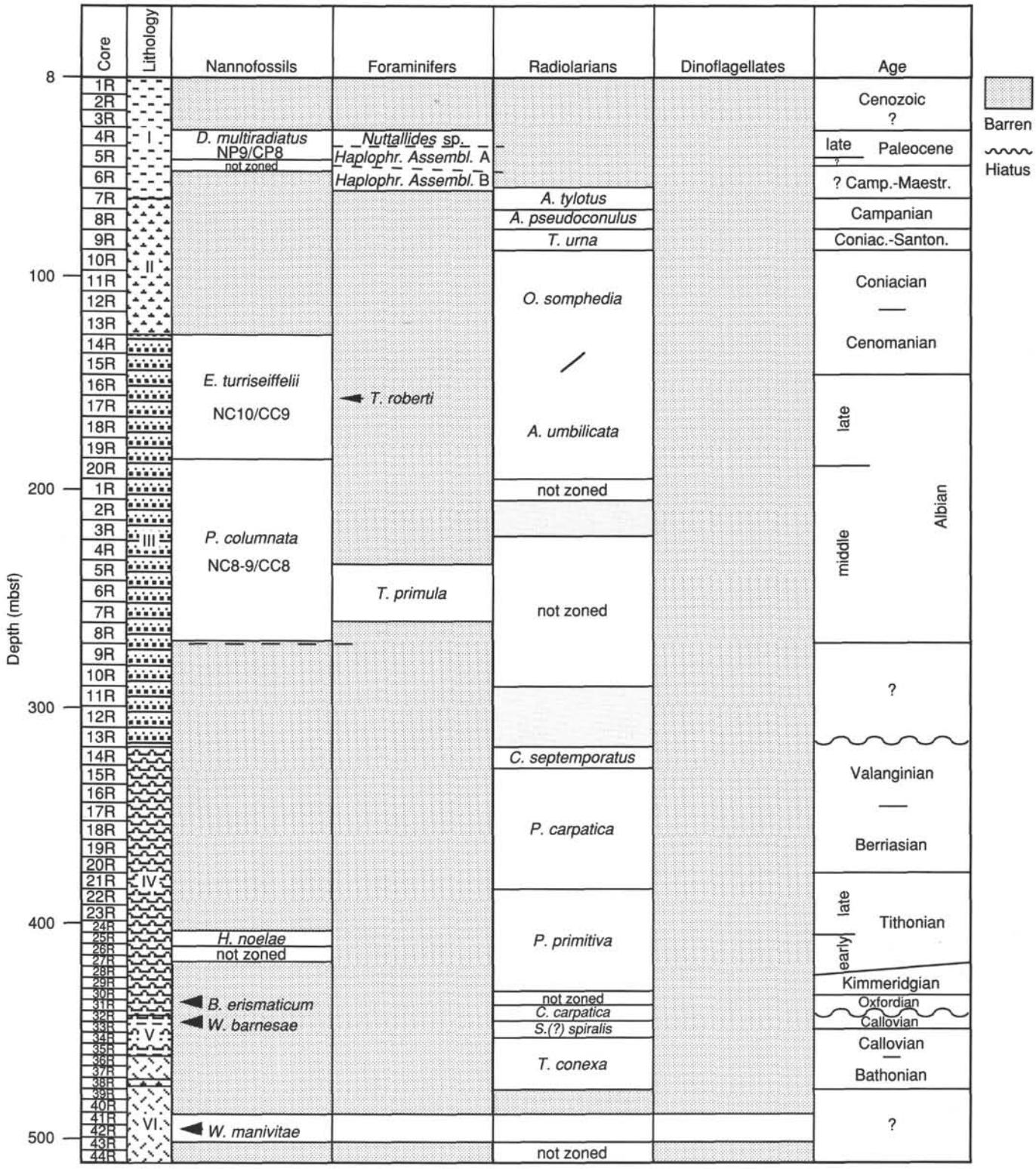

Figure 22. Summary of the biostratigraphy for Holes 801A and 801B. (Note: No recovery between 0 and 8 mbsf.)

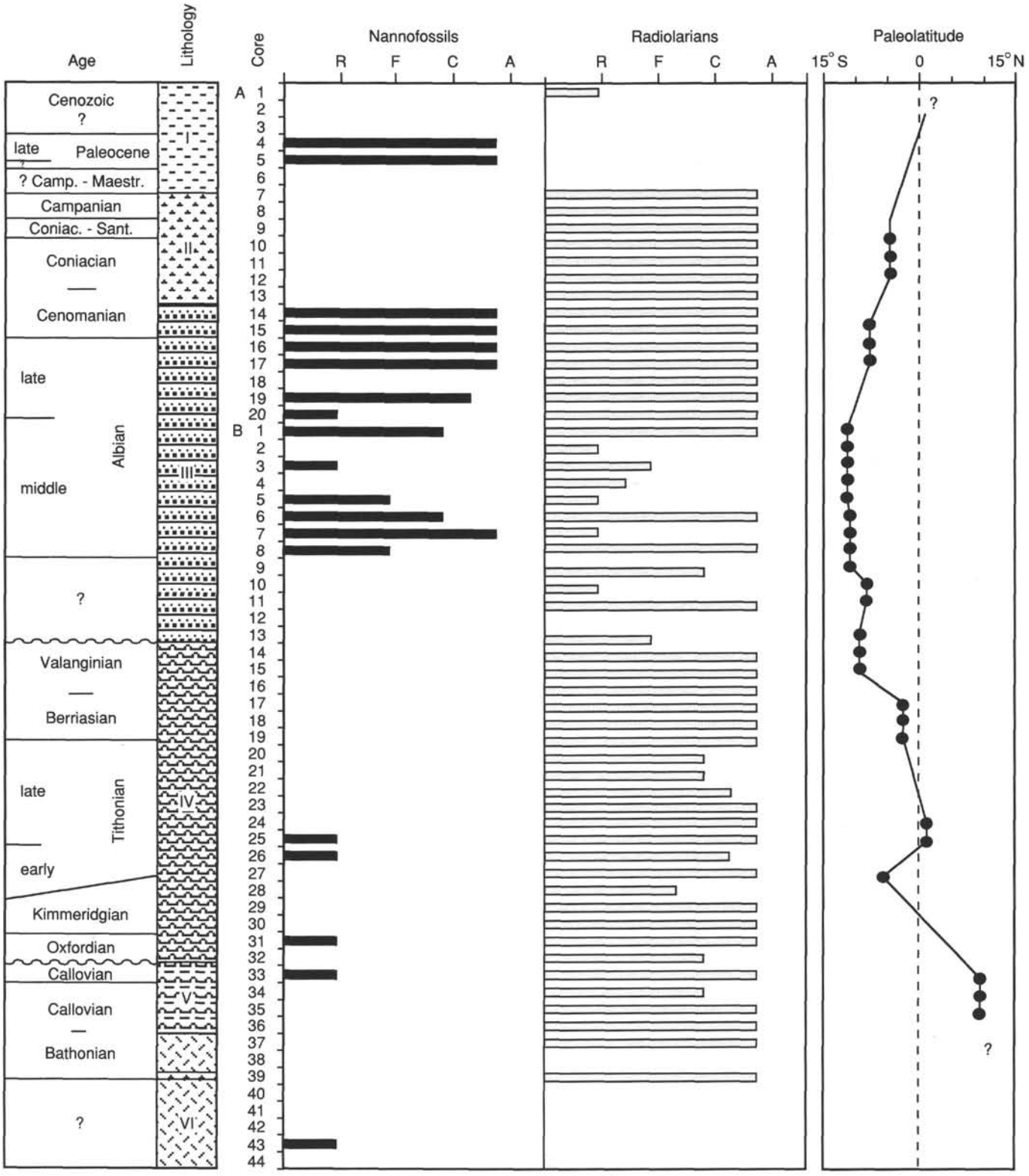

Figure 23. Abundance of calcareous nannofossils and radiolarians plotted against age, lithostratigraphy, and paleolatitude in Holes 801A and 801B. Relative abundance is denoted as follows: rare (R), few (F), common (C), and abundant (A). See "Explanatory Notes" chapter (this volume) for further discussion of abundance parameters.

sity (number of species) is usually proportional to total abundance, reaching maxima in the Cenomanian-uppermost Albian and lower middle Albian sediments.

Cores 129-801A-1R to -3R are barren of calcareous nannofossils. Samples between Sections 129-801A-4R-CC and 129-801A-5R-1, 28 cm, contain an abundant and moderately preserved mixture of nannofloras which range in age from latest Campanian to latest Paleocene. The Paleocene assemblage is characterized by abundant *Fasciculithus* spp. and *Fasciculithus tympaniformis*, common *Discoaster multiradiatus*, and rare *Heliolithus kleinpellii*, while the age-diagnostic Cretaceous species include common to few *Ceratolithoides aculeus, Micula decussata, M. murus, Quadrum sissinghii, Q. trifidum*, and *Aspidolithus parcus constrictus*. No species of *Tribrachiatus* were encountered but *D. multiradiatus* was abundant in some samples, so we assign this interval to the latest Paleocene *D. multiradiatus* (NP9) Zone of Martini (1971). The core catcher of Core 129-801A-5R contains rare Paleocene nannofossils, including *Coccolithus* sp. and *Fasciculithus tympaniformis*.

All samples examined from the core catcher of Core 129-801A-6R to the core catcher of Core 129-801A-13R are barren of nannofossils. Sample 129-801A-14R-1, 62–63 cm, contains common, moderately preserved Cretaceous nannofossils. The occurrence of the diagnostic species *Eiffellithus turriseiffelii, Prediscosphaera columnata, Cruciellipsis chiastia, Axopodorhabdus albianus*, and *Lithraphidites alatus* allows determination of the upper Albian-Cenomanian *E. turriseiffelii* Zone of Thierstein (1971, 1973, 1976), Zone NC10 of Roth (1978), and Zone CC9 of Sissingh (1977). The absence of *Microrhabdulus decoratus, Lithraphidites acutus* and any younger taxa, and the occurrence of *C. chiastia* corroborate the zonal and age assignment.

This nannofloral assemblage remains unchanged down to Sample 129-801A-19R-CC where we placed the lower limit of the *E. turriseiffelii*/NC10/CC9 Zone. The absence of *Rucinolithus irregularis* throughout this interval prevents determination by nannofossils of the Albian/Cenomanian boundary, which was recognized on the basis of planktonic foraminifers. The upper/middle Albian boundary is slightly older than the base of the *E. turriseiffelii*/NC10/CC9 Zone.

Subsequent samples down to Core 129-801A-20R contain only rare, non-diagnostic nannofossils.

As mentioned in the introduction of this chapter, Hole 801B was washed down to the approximate depth that Hole 801A was terminated. Sample 129-801B-1R-1, 30–31 cm, contains only rare, non-diagnostic nannofossils, whereas in Sample 129-801B-1R-1, 59–60 cm, a common, diverse assemblage was observed. The occurrence of *P. columnata* and the absence of *E. turriseiffelii* indicate the Albian *P. columnata* Zone of Thierstein (1971, 1973, 1976), Zones NC8–NC9 of Roth (1978), and Zone CC8 of Sissingh (1977).

The abundance of nannofossils in the interval between Sections 129-801B-1R-CC and 129-801B-4R-CC fluctuates from barren to rare and only non-diagnostic taxa were encountered.

Sections 129-801B-5R-1, 75 cm, through 129-801B-8R-CC contain frequent to common, diverse nannofossils. The assemblage is composed of *P. columnata, C. chiastia, Lithastrinus floralis, Parhabdolithus angustus, Rucinolithus terebrodentarius*, and *R. irregularis*, along with several other less diagnostic species. We assigned this interval to the Albian *P. columnata* Zone of Thierstein (1971, 1973, 1976), Zones NC8–NC9 of Roth (1978), and Zone CC8 of Sissingh (1977). The persistent occurrence of *Tranolithus orionatus* throughout this zone indicates a middle Albian age (Perch-Nielsen, 1985). This age assignment is corroborated by planktonic foraminiferal data.

No more calcareous nannofossils were observed in the remainder of the sedimentary section (Cores 129-801B-9R to -43R), with the exception of five samples. Sample 129-801B-25R-CC contains a diverse nannoflora despite the low total abundance. Rare *Polycostella beckmannii, Hexalithus noelae, Umbria granulosa minor, Cyclagelosphaera margerelii, Watznaueria barnesae, Watznaueria communis, Watznaueria manivitae, Zygodiscus erectus, Biscutum constans, Discorhabdus rotatorius, Vagalapilla stradneri, Rucinolithus* sp., *Cretarhabdus* sp., *Paleopontosphaera* sp., and *Parhabdolithus* sp. were observed. Although we are conscious that a zonal assignment based on a single sample from otherwise barren cores is difficult to substantiate, we tentatively assign this sample to the middle Tithonian *Hexalithus noelae* Subzone of Bralower et al. (1989).

In Sample 129-801B-26R-CC rare nannofossils occur. They include *W. barnesae, W. manivitae, B. constans, C. margerelii, Cretarhabdus* sp., and *P. beckmannii*. The latter taxon is a marker species restricted to the late early to late Tithonian.

Sample 129-801B-31R-CC contains a single specimen of *Biscutum erismaticum*. This species was first described from the Oxfordian of the Falkland Plateau (Wise and Wind, 1976), but its range has subsequently been extended back to the Toarcian (Perch-Nielsen, 1985). Rare specimens of the non-diagnostic species *Watznaueria barnesae* were observed in Sample 129-801B-33R-1, 58 cm.

The lowermost nannofossils observed from Hole 801B, two specimens of *W. manivitae*, were encountered in Sample 129-801B-43R-3, 80–81 cm, from claystones entrapped within pillow lavas of Unit VI (see "Lithostratigraphy and Sedimentology" section, this chapter).

Foraminifers

Twelve core-catcher samples and nine additional samples within the cores were examined in Hole 801A. Only 14 core-catcher samples could be examined for foraminifers in Hole 801B since the lithology was predominantly chert. Of the 35 samples investigated, 10 contain assemblages of foraminifers. Four of the foraminiferal assemblages display good preservation, and specimen abundance is within the range of "few" to "common." The remaining foraminiferal assemblages show poor to moderate preservation, and are of low abundance ("rare" to "few" categories).

Foraminifers are absent from Samples 129-801A-1R-CC through 129-801A-3R-CC. The core catcher from Core 129-801A-4R contains one specimen of *Recurvoides* sp. and several very small specimens (about 100 μm) of the calcareous benthic genus *Nuttallides*. Specimens are similar to *Nuttallides truempyi* except for their small size. The species *Nuttallides truempyi*, regarded as having had a cosmopolitan distribution throughout its Campanian to late Eocene range, is believed to be a lower bathyal to abyssal paleobathymetric indicator (Morkhoven et al., 1986). On the basis of the associated nannofossils, the foraminiferal assemblage in Sample 129-801A-4R-CC is assigned an upper Paleocene age.

Good recovery in Core 129-801A-5R allowed investigation of four additional samples. Sample 129-801A-5R-1, 83–87 cm, contains a low-diversity assemblage of finely agglutinated foraminifers that roughly correspond to those seen in the *Haplophragmoides* Assemblage A at Site 800, and include the following forms: *Haplophragmoides* sp., *Paratrochamminoides* sp., *Praecystammina globigerinaeformis, Bolivinopsis parvissimus*, and *Recurvoides deflexiformis*. Samples 129-801A-5R-3, 59–61 cm, 129-801A-5R-5, 41–46 cm, and 129-801A-5R-5, 76–78 cm, are characterized by an increase in the abundance of primitive tubular agglutinated foraminifers and a corresponding decrease in abundance of the coiled forms

typical of the *Haplophragmoides* Assemblage A. Specimens from Sample 129-801A-5R-CC are dominated by primitive tubular foraminifers. Core 129-801A-5R is assigned to the Paleocene on the basis of associated nannofossils.

The core catcher from Core 129-801A-6R contains a more diverse assemblage of foraminifers that correspond well to those seen in the *Haplophragmoides* Assemblage B of Site 800. This assemblage is principally characterized and distinguished from *Haplophragmoides* Assemblage A by more numerous species of *Haplophragmoides* (for example, *Haplophragmoides multicamerata, H. fraudulentus, H. constrictus,* and *H. pervagatus*), and is assigned to the Upper Cretaceous on the basis of the age of this assemblage at Site 800. The presence of Campanian radiolarians in Core 129-801A-7R suggests a Campanian or younger age for Core 129-801A-6R.

The implication of the biostratigraphy outlined above is that the K/T boundary lies within Core 129-801A-6R. The nature of the deep-water benthic foraminiferal assemblages is of interest to proponents of the widely reported extinctions seen among other fossil groups at the K/T boundary. A number of scientists argue that deep-water benthic foraminifers may have been little, if at all, affected by the K/T boundary "event" and its associated faunal extinctions. Moullade et al. (1988), on the other hand, observe a significant faunal break in deep-water foraminifers coinciding with the K/T boundary in the North Atlantic Plantagenet formation where the Paleocene foraminiferal assemblages are impoverished in comparison to those of the Upper Cretaceous. A similar trend is observed in our sequences. Additionally, the vertical change from an astrorhizid-dominated foraminiferal assemblage in Section 129-801A-5R-CC to a more diverse assemblage higher in the pelagic clay could be evidence of recolonization of the seafloor following an event that disrupted the community structure. Alternatively, such assemblages could result from hydrodynamic sorting by bottom-water or turbidity currents as was suggested for the astrorhizid-dominated assemblage of Core 129-800A-27R. Because of poor recovery from this interval, however, we are unable to investigate the effects of the so called K/T boundary "event" on the deep marine benthic foraminifers of the Pigafetta Basin in more detail.

Sample 129-801A-7R-1, 124–129 cm, contains a foraminiferal assemblage similar to that referred to as the *Haplophragmoides* Assemblage B of Site 800, but differing by the presence of abundant *Praecystammina globigerinaeformis*. The latter species seems to be of stratigraphic value in high latitude abyssal assemblages in the Atlantic Ocean (Moullade et al., 1988), where it is reported to have a last occurrence datum near the Coniacian/Santonian. In lower latitudes, on the other hand, it has also been reported from abyssal assemblages of the uppermost Cretaceous (Hemleben and Troester, 1984). Rare finds of *Praecystammina globigerinaeformis* in Paleocene sediments in Hole 801A extends the range of this species to the lowermost Tertiary in abyssal assemblages of low latitudes. Gradstein et al. (1988) observed a very similar form, which they determined as *Cystammina* aff. *globigeriniformis,* in bathyal Paleocene wells of the central North Sea. A planned comparison of our specimens with those from the North Sea may resolve any taxonomic difficulties with these forms.

Samples 129-801A-7R-2, 51–53 cm, 129-801A-7R-2, 94–99 cm, and 129-801A-7R-3, 134–139 cm, contain only a few specimens of the *Haplophragmoides* Assemblage B species. The sparsity of foraminifers in these samples may be partly the result of the dilution effect of the increasingly abundant radiolarians seen downhole.

Core-catcher samples from Cores 129-801A-7R to -15R are barren of foraminifers. Sample 129-801A-16R-CC contains the planktonic foraminifers *Ticinella roberti, Globigerinelloides bentonensis,* and *Hedbergella delrioensis* in low abundance and of poor to moderate preservation. The presence of *Ticinella roberti* allows the sample to be dated as upper Albian, as the last occurrence of this species is found within the lower *Rotalipora appenninica* Zone (uppermost Albian) of Caron (1985).

The core-catcher samples of Cores 129-801A-17R to 129-801B-5R are barren of foraminifers. Sample 129-801B-5R-CC contains a single specimen of *Ticinella bejaouensis,* indicating a middle Albian age (Caron 1985). Core-catcher samples from Cores 129-801B-6R and -7R contain the species *Hedbergella infracretacea, H. globigerinelloides, H. planispira, H. simplex,* and *Globigerinelloides bentonensis,* all of which are common in the middle Albian. The first occurrence of *Globigerinelloides bentonensis* in the *Ticinella primula* Zone (middle Albian) of Caron (1985) excludes an early Albian or older age for the sample. No more foraminifers were encountered in the remainder of the cores in Hole 801B.

Radiolarians

Twenty core-catcher samples and 32 additional samples within the cores were examined in Hole 801A. Thirty-seven core-catcher samples and 76 additional samples within the cores were investigated in Hole 801B. No Cenozoic radiolarians were obtained from this site.

Samples 129-801A-1R-CC to 129-801A-6R-CC are barren of radiolarians. Cores 129-801A-7R to -20R yielded abundant but poorly preserved radiolarians. Samples 129-801A-7R-CC, 129-801A-8R-1, 31–33 cm, and 129-801A-8R-CC contain *Dictyomitra koslovae,* a species restricted to the upper *Amphipyndax pseudoconulus* Zone and lower *Amphipyndax tylotus* Zone. *Theocampe urna* was obtained from Samples 129-801A-8R-1, 31–33 cm, 129-801A-8R-CC, 129-801A-9R-1, 13–15 cm, and 129-801A-9R-CC. The occurrence of *T. urna* is confined to the *T. urna* Zone and the next younger *A. pseudocolunus* Zone. The co-occurrence of *T. urna* and *D. koslovae,* which was recognized in Samples 129-801A-8R-1, 31–33 cm, and 129-801A-8R-CC indicates the upper part of the *A. pseudocolunus* Zone, assignable to the middle Campanian. The first occurrence of *T. urna* defines the boundary between the *T. urna* Zone and the next older *Obesacapsula somphedia* Zone, situated within the Coniacian. The interval between Samples 129-801A-12R-CC and 129-801A-20R-CC contains few to common *Pseudodictyomitra pseudomacrocephala* associated with rare *Thanarla elegantissima.* The co-occurrence of *P. pseudomacrocephala* and *T. elegantissima* characterizes the upper *Acaeniotyle umbilicata* to lower *Obesacapsula somphedia* Zones (upper Albian to Cenomanian). The boundary between the *A. umbilicata* and *O. somphedia* Zones is regarded to correspond to the Albian/Cenomanian boundary (Sanfilippo and Riedel, 1985). Although no diagnostic radiolarians were found that enabled definition of the boundary between these two zones, the boundary may be inferred as lying above Sample 129-801A-16R-CC, dated by planktonic foraminifers as late Albian.

In Samples 129-801B-1R-CC to 129-801-13R-CC, radiolarian abundance appears to depend on lithology. Coarse volcaniclastic sediments contain sparse radiolarian tests, if any, whereas fine-grained pelagic sediments are generally rich in radiolarians. The poor preservation does not permit zonal assignment of this interval.

The brown radiolarites and cherts of Cores 129-801B-14R to -32R yielded common to abundant and poorly to moderately preserved radiolarians. This interval is divided into four radiolarian zones on the basis of the first occurrence of marker species: *Cecropus septemporatus, Pseudodictyomitra carpat-*

ica, Pseudodictyomitra primitiva, and *Cinguloturris carpatica* Zones in descending order. The bases of the *C. septemporatus* and *P. carpatica* Zones are situated within the Valanginian and upper Tithonian, respectively. The zonal boundary between the *P. primitiva* and *C. carpatica* Zones is drawn near the Oxfordian/Kimmeridgian boundary. This interval is therefore tentatively assigned to the Oxfordian to Valanginian.

Samples 129-801B-14R-1, 14–15 cm, and 129-801B-14R-1, 47–49 cm, contain only a few poorly preserved radiolarians. Sample 129-801B-14R-CC contains species found in both the *C. septemporatus* and the younger *D. thytthopora* Zones, including *C. septemporatus, Acanthocircus dicranacanthos,* and *P. carpatica.* However, the faunal composition itself appears to be more typical of the *C. septemporatus* Zone, supported by the absence of *C. septemporatus* from samples below Sample 129-801B-14R-CC. Although the interval between Cores 129-801B-9R and -13R could not be dated by microfossils, we speculate that a hiatus may be present between Cores 129-801B-13R and -14R, corresponding to the boundary between the lithologic Units III and IV.

The red and brown radiolarites between Samples 129-801B-33R-1, 8–10 cm, and 129-801B-39R-CC contain abundant but poorly to moderately preserved radiolarians assignable to the *Stylocapsa(?) spiralis* and *Tricolocapsa conexa* Zones. Samples 129-801B-33R-1, 131–133 cm, 129-801B-33R-2, 14–17 cm, and 129-801B-33R-CC include abundant specimens of *S.(?) spiralis, T. conexa,* and *Stichocapsa robusta.* The dominance of the latter three species in this assemblage, combined with the absence of *Stichocapsa naradaniensis,* typical of the upper part of the *S.(?) spiralis* Zone, suggests that only the lower half of the zone is present. The implication of this is that a hiatus may be present between Cores 129-801B-32R and -33R, corresponding to the boundary between lithologic Units IV and V. This hiatus may correspond to the lower Oxfordian. The interval below the hiatus (129-801B-33R-1, 131 cm, to 129-801B-33R-CC) is therefore tentatively assigned to the Callovian.

Samples 129-801B-34R-CC to 129-801B-35R-CC yield *T. conexa, Stylocapsa tecta,* and *Stylocapsa oblongula,* which in the absence of *S.(?) spiralis* is characteristic of the upper part of the *T. conexa* Zone. In Sample 129-801B-37R-1, 16–20 cm, *T. conexa* and *Guexella nudata* occur, whereas *S. tecta* does not, indicating the middle part of the *T. conexa* Zone. From Core 129-801B-39R, five samples (129-801B-39R-1, 7–9 cm, 16–18 cm, 20–21 cm, 26–28 cm, and -CC) were examined. All samples yielded common to abundant, poorly preserved radiolarian assemblages, although those from Sample 129-801B-39R-1, 16–18 cm, are better preserved and of similar composition to the assemblage in Sample 129-801B-37R-1, 16–20 cm, indicating a Callovian-Bathonian age.

Sample 129-801B-44R-1, 127–128 cm, is red claystone intercalated with the basalt. It contains a small number of radiolarians, but these are of extremely poor preservation and cannot be assigned an age.

Palynomorphs

Fifty-seven core-catcher samples and 51 additional samples were investigated from Site 801. All samples of Site 801 are barren of palynomorphs. Cores 129-801B-16R through -32R contain rare to abundant amorphous organic matter, but no palynomorphs.

Sedimentation Rates

Figure 24 shows the sedimentation rates for Site 801, as determined on the basis of nannofossil, radiolarian, and foraminiferal biostratigraphy. A hiatus was depicted at the top of the Valanginian corresponding to the boundary between lithologic Units III and IV. Another hiatus was determined at the base of the Oxfordian and it coincides with the boundary between lithologic Units IV and V.

Discussion

The paleoenvironment of Site 801 is interpreted as abyssal with deposition below the CCD during the late Cenomanian through the Tertiary, based principally on the presence of abundant radiolarians and *in-situ* deep-water agglutinated foraminifers. The allochthonous calcareous nannofossils seen in the Paleocene samples support deposition below the CCD. Rare planktonic foraminifers and abundant, apparently autochthonous nannofossils in the Albian to Cenomanian volcaniclastic intervals (lithologic Unit III, see "Lithostratigraphy and Sedimentology" section, this chapter) may suggest deposition above the CCD, but we lack benthic foraminiferal evidence to support this. Paleobathymetry for the Jurassic interval cannot be determined from radiolarians and nannofossils alone.

Preliminary data regarding the abundance of calcareous nannofossils and radiolarians are plotted in Figure 23 against ages, lithostratigraphy, and paleolatitude. The distribution of each group appears somewhat mutually exclusive, and possibly relates to paleolatitude. Highest nannofloral abundance and diversity corresponds to a decrease in abundance of radiolarians in the interval correlated to the southernmost paleolatitude.

Nannofossil assemblages in the Tithonian sediments of Site 801, while scarce and found in only two samples, may be suggestive of high-fertility conditions. In fact, they contain similar numbers of *Watznaueria* and *Biscutum.* The occurrence of a significant number of *Biscutum* relative to the number of *Watznaueria* is considered to indicate high-fertility conditions in Cretaceous sediments (e.g., Roth and Krumbach, 1986; Erba, 1987; Premoli-Silva et al., 1989). However, the reliability of this relative abundance indicator for Jurassic and for Pacific fertility conditions is not yet known.

PALEOMAGNETISM

Methods

All sediment cores from Holes 801A and 801B (except for most of the brown pelagic clay interval, lithologic Unit I) were measured and alternating field (AF) demagnetized with the shipboard automated cryogenic magnetometer. Much of the recovery from this hole was in the form of discrete fragments of sedimentary rock rather than continuous core. Of the 55 cores recovered, only 14 were composed of continuous or semicontinuous sedimentary material. Therefore, most of the Site 801 remanent magnetization shipboard measurements were accomplished by individually taping these fragments into the magnetometer tray at spaced intervals. All pieces that had well-defined bedding planes and were larger than 20 cm^3 were measured. The pieces were oriented in the magnetometer so that the bedding planes were perpendicular to the horizontal (z) axis of the magnetometer, spaced about 10 cm apart (the width of the magnetometer sensor regions). The core volume parameter in the magnetometer program was adjusted each time to the average volume of the collection of fragments being measured. In sections of good core recovery, whole cores were measured.

Magnetic Behavior

After measurement of the natural remanent magnetization (NRM), samples were stepwise AF-demagnetized generally

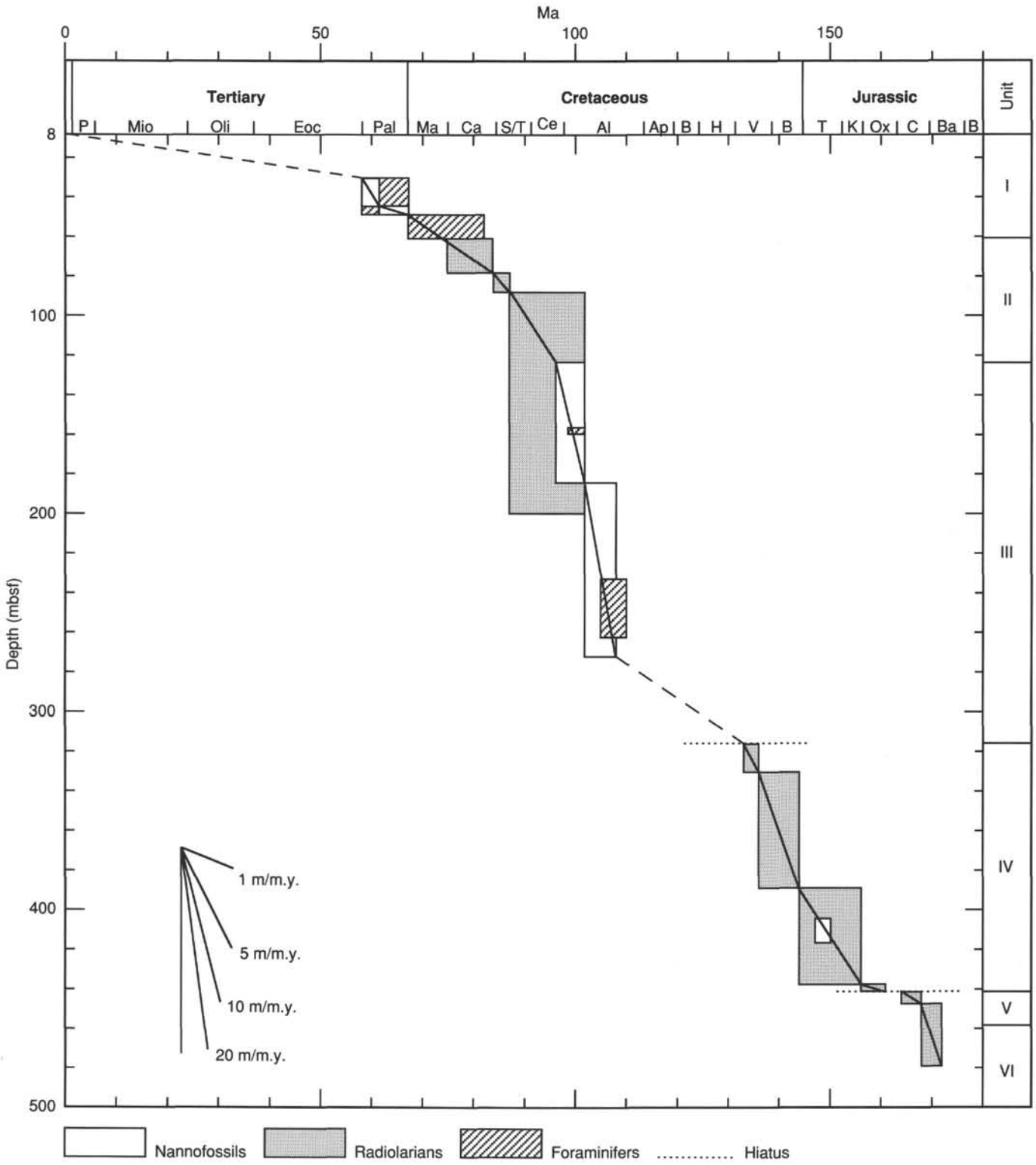

Figure 24. Sedimentation rates for Holes 801A and 801B. (Note: No recovery between 0 and 8 mbsf.)

using field strengths of 5, 10, and 15 mT, chosen on the basis of our experience with Site 800 sediments. Susceptibility was measured on all cores prior to splitting. Susceptibility and AF demagnetization response varied with the lithologic variations. Therefore, properties will be discussed on the basis of lithologic units.

The brown pelagic clay interval from Cores 129-801A-1R through -7R (lithologic Unit I) shows evidence of both homogenization due to mixing and viscous plastic flow in the nonhomogenized material within the core liner. Consequently, these cores have mixed lithologies and partially or wholly obscured bedding. The red-brown color of the cores

indicates the probable presence of hematite or iron hydroxides which are not susceptible to AF demagnetization. For these reasons, this interval could not provide much data. Susceptibility measurements from Cores 129-801A-5R and -7R show a range from 65 to 126 SI units and average approximately 85 SI units. AF demagnetization of two of the least disturbed cores yielded no coherent data.

The properties of the brown chert and porcellanite interval from the base of Section 129-801A-7R-4 through Core 129-801A-13R (lithologic Unit II) have susceptibilities ranging from 13 to 46 SI units, averaging approximately 33 units. NRM intensities average about 6 mA/m and AF demagnetization in fields of about 11 mT results in the loss of approximately half of the remanence. Demagnetization vectors do not decay directly to the origin when viewed on orthogonal axis plots; this in conjunction with the large remanence remaining after 15 mT demagnetization suggests the presence of two vectors that cannot be separated by low field AF demagnetization.

The volcaniclastic turbidites from Cores 129-801A-14R through 129-801B-13R (lithologic Unit III) are distinct in magnetic character from the overlying cherty interval. NRM intensity ranges from 2.6 to greater than 200 mA/m; susceptibility also showed great variability, ranging from less than 50 SI units to greater than 300. The variation may be due, at least in part, to the large range in grain size within the turbidites; larger values for susceptibility seem to be associated with the coarser grained fractions. The response to AF demagnetization was generally poorer in the coarser materials than in the fine-grained sediments. Most of the coarse sediments show considerable overlap in coercivity spectra and, in both fine- and coarse-grained materials, mean demagnetizing fields are quite high and generally not revealed with the low level of alternating fields available in the shipboard magnetometer system.

The underlying sedimentary unit, the brown radiolarite of Cores 129-801B-14R through -32R (lithologic Unit IV), showed a markedly lower NRM intensity, approximately 8 mA/m, and a susceptibility of only 16 SI units. In the upper portion of this interval (Subunit IVA; see "Lithostratigraphy and Sedimentology" section, this chapter), more than 90% of the magnetization of this lithology was removed by the first or second AF step (by 10 mT). The demagnetization behavior is difficult to interpret, possibly because of the weak sample intensities and/or the overlap of coercivity spectra. On orthogonal axes plots, trends move beyond the origin, possibly due to the presence of reversed polarity. The lower, more clay-rich portion of the unit (lithologic Subunit IVB) contains samples exhibiting clearer demagnetization behavior, indicative of both normal and reversed polarities. However, large overlaps in coercivity spectra of the lower portion make inclination values somewhat unreliable.

The lowest unit, the alternating claystone-radiolarite interval from Cores 129-801B-33R through -35R (lithologic Unit V), is not represented by much material. Susceptibilities and NRM intensities are similar to the previous unit, but AF demagnetization causes little change in directions or decay of intensities. One or more magnetizations of high coercive force are indicated by the lack of response to AF, consistent with the bright red color that suggests the presence of hematite, goethite, or other iron hydroxides.

Magnetostratigraphy

Despite the poor recovery of much of the sediment of Holes 801A and 801B, key biostratigraphic markers made possible the recognition of certain polarity intervals. The methods used to define polarity intervals were similar to those discussed for Site 800. The youngest or stratigraphically highest reversals were encountered in Core 129-801A-7R. The reversals in Sections 129-801A-7R-4 and 129-801A-7R-CC appear to be two different intervals separated by a distinct normal polarity zone. The biostratigraphic evidence suggests that the reversed Sample 129-801A-7R-4, 30 cm, is probably of Maestrichtian age and may represent interval 31R or 32R, whereas the lowermost reversed sample, 129-801A-7R-CC, 7 cm, is probably Campanian in age and therefore representative of interval 33R. Interval 33R was also observed at Site 800 (see "Site 800" chapter, this volume).

The next reversed interval was not observed until well down in Hole 801B, in Core 129-801B-14R. The normal polarity interval between this core and Core 129-801A-7R most likely represents the Cretaceous long normal polarity interval (Helsley and Steiner, 1969; Irving and Pullaiah, 1976; Kent and Gradstein, 1986). Beginning at Core 129-801B-14R, reversals become more common. Although in most cases reversed intervals are based on single discrete samples, these are nonetheless thought to reliably indicate geomagnetic field polarity because of the large declination changes in their AF demagnetization responses. The polarity interpretation of Cores 129-801B-13R through -28R is shown in Figure 25.

Cores 129-801B-21R through -30R are biostratigraphically constrained by the radiolarian zone *P. primitiva* as Tithonian to Kimmeridgian in age. The presence of diagnostic nannofossils allows further narrowing of the time of deposition for the majority of these cores (see "Biostratigraphy" section, this chapter). The first and last occurrences of the nannofossil *P. beckmannii* place Cores 129-801B-25R and -26R within an interval including Chrons M19–M21 (Bralower et al., 1989). Further, Core 129-801B-25R contains an assemblage of nannofossils of the *H. noelae* Subzone (see "Biostratigraphy" section, this chapter). As the base of this subzone is placed within Chron M20R, and in conjunction with the implications of the occurrence of *P. beckmannii,* the reversals of Cores 129-801B-25R and -26R likely represent either Chrons M19 or M20. These correlations and observations suggest the tentative chron assignments shown in Figure 25.

Reversals observed within the Kimmeridgian to Callovian part of Hole 801B (Cores 129-801B-29R through -36R) could not be identified with recognized polarity chrons because of the poor recovery and insufficiently detailed paleontologic data.

Paleolatitude

Determination of the paleolatitudes of this site is hampered by both the low recovery and the relative ineffectiveness of AF demagnetization on much of the material recovered. Furthermore, except for the volcaniclastic interval (lithologic Unit III), the amount of material for which uphole orientation was known was small. In both the chert-porcellanite interval (lithologic Unit II) lying above the volcaniclastics and the radiolarites lying below (lithologic Units IV and V), recovery was of small pieces in which only about 50% had known up-directions. We adopted the approach of measuring and demagnetizing the unoriented pieces in addition to the oriented ones, in the hope of inferring polarity from their demagnetization behavior, as explained in the "Site 800" chapter (this volume). The polarity, in combination with the sign of the inclinations, should indicate the hemisphere of origin, thus allowing us to determine paleolatitudes for the site. Nevertheless, because the plate was near the equator, the shallowness of the inclinations combined with incomplete removal of secondary magnetization (which generally ap-

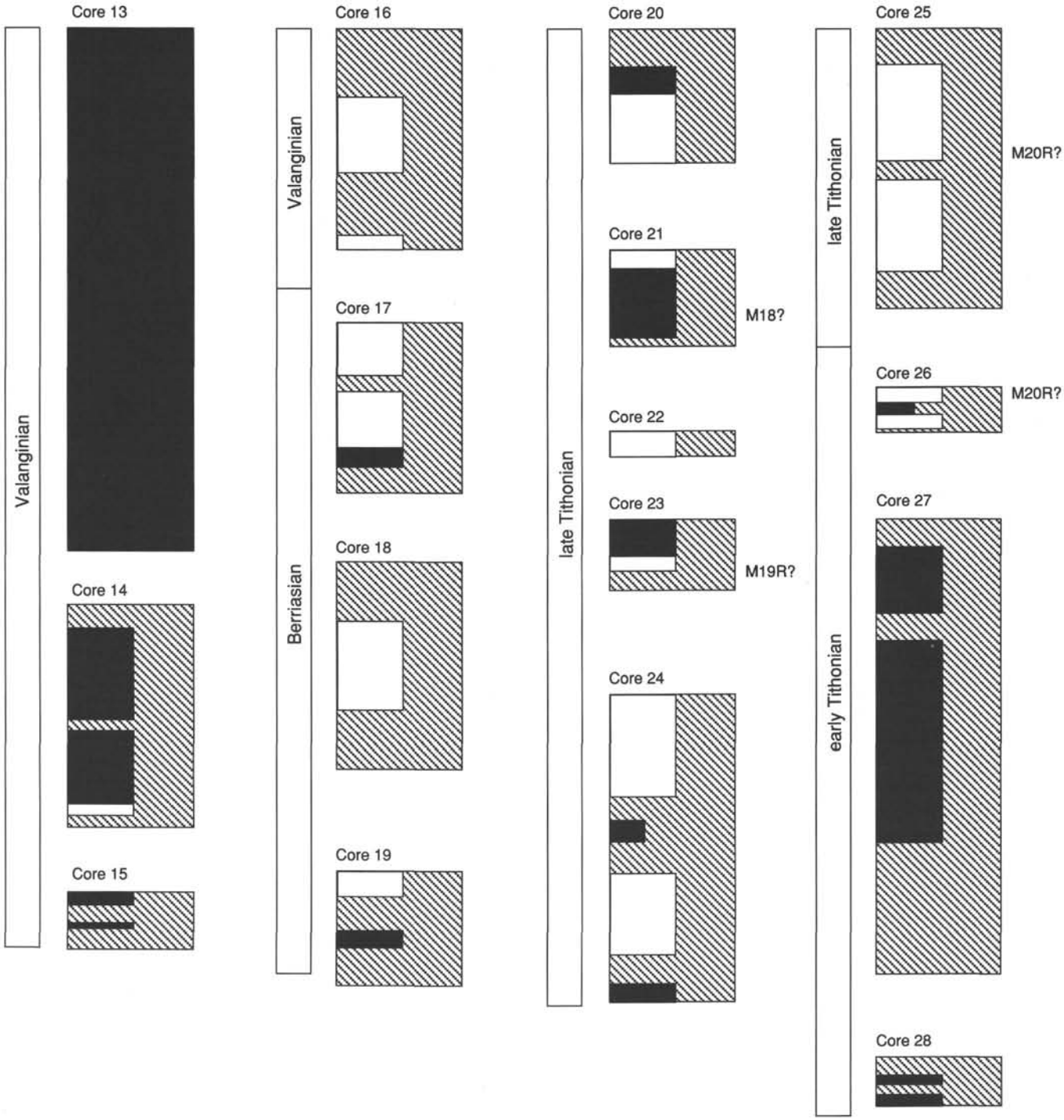

Figure 25. Interpretations of polarity and tentative identification of Tithonian polarity chrons. Each segment represents the recovered portion of individual, numbered cores from Hole 801B. Black bars indicate normal polarity, white is reversed polarity, half-filled columns reflect polarity interpretations made from discrete fragments rather than continuous recovery, one-quarter filling indicates fragments with uncertain polarity identifications, and hachured areas represent areas of no data.

peared to be a late Tertiary direction from the similarity of removed inclinations to that of the present direction of the Earth's field at this site), made distinguishing between the Northern and Southern hemispheres somewhat difficult. An additional uncertainty in paleolatitude determinations for this site was introduced by a significant dip to the beds in the lower part of both holes, but particularly in Hole 801B. More than half of the discrete pieces measured were too large to allow correction for the dip of the beds by simple positioning in the magnetometer tray; for these pieces, careful measurement of the dip and orientation were made and used to correct the magnetization directions.

The resulting data set displays a large amount of dispersion, which may be attributed to a combination of incomplete demagnetization, uncertainty in the up-direction, and possibly some uncertainties in the correction for the tilt of the strata. Nevertheless, despite the scatter, a pattern is apparent in the data. To view this pattern, all inclinations initially were converted to their corresponding latitudes and plotted against depth (Fig. 26A).

A concave band of data points south of the equator is observed. The data are generally concentrated in southern latitudes with dispersion toward and into northern latitudes. The relatively well-grouped data between 180 and 260 mbsf are from the volcaniclastic sequence of lithologic Unit III. The scattered data on either side represent the porcellanites and radiolarites. In an attempt to determine the source of the scatter, all samples for which stratigraphic up was unknown were removed. The result is a much-reduced data base (Fig. 26B) that retains the same general pattern, with only slightly less dispersion. The pattern is somewhat more evident, but the persistence of the dispersion suggests that incomplete demagnetization is probably a significant factor in this data.

Most of the samples of Figure 26B are of normal polarity and overprinting of normal directions in the Southern Hemisphere with the direction of the present field would bias the data toward apparently shallower, southerly paleolatitudes and to apparent northern paleolatitudes, up to the latitude of the site (18.6°N). The characteristic magnetization of many of the chert/porcellanite and radiolarite samples could not be completely separated from the secondary magnetization by AF demagnetization. These particularly give results dispersed to the north, supporting this as the probable origin of the dispersion. Therefore, the true paleolatitudes are probably approximated by the southern edge of the data band of Figure 26B.

We were reluctant to average data containing so many obviously contaminated data points, but the true mean paleolatitudes cannot be determined by picking the midpoint of the lower part of the data band of Figure 26B. This is because paleomagnetic inclinations are distributed in a manner analogous to a circular Gaussian distribution. When declination is not known, as is the case in rotary cores in which azimuth is unknown, simple numerical averaging of the inclinations gives undue weight to the higher values, and paleolatitudes thus generated are a few degrees steeper than the true paleolatitude. Kono (1980) developed a statistical method to average such data to obtain true mean inclinations. Mean values were calculated with the Kono method from inclination groupings apparent within the data. Paleolatitudes computed from the mean inclinations are shown in Figure 27, along with their associated standard deviations.

The youngest data obtained suggest that Site 801 was probably still in the Southern Hemisphere during Campanian time. Cores 129-801A-7R to -10R, 60–97 mbsf (Fig. 26), yielded southern paleolatitude values. The northern paleolatitudes in this same interval (responsible for the "7-10" point in Fig. 27) are most probably an expression of strongly overprinted data, as the 15°N to 20°N values in Figure 26B bracket the present 18°N latitude of the site. Figures 26 and 27 indicate that the maximum southern latitude of the site occurred between middle Albian and Valanginian time (about Cores 129-801B-5R through -16R). The site appears to have been in the Southern Hemisphere through the Late Jurassic. The incomplete demagnetization make the data inconclusive re-

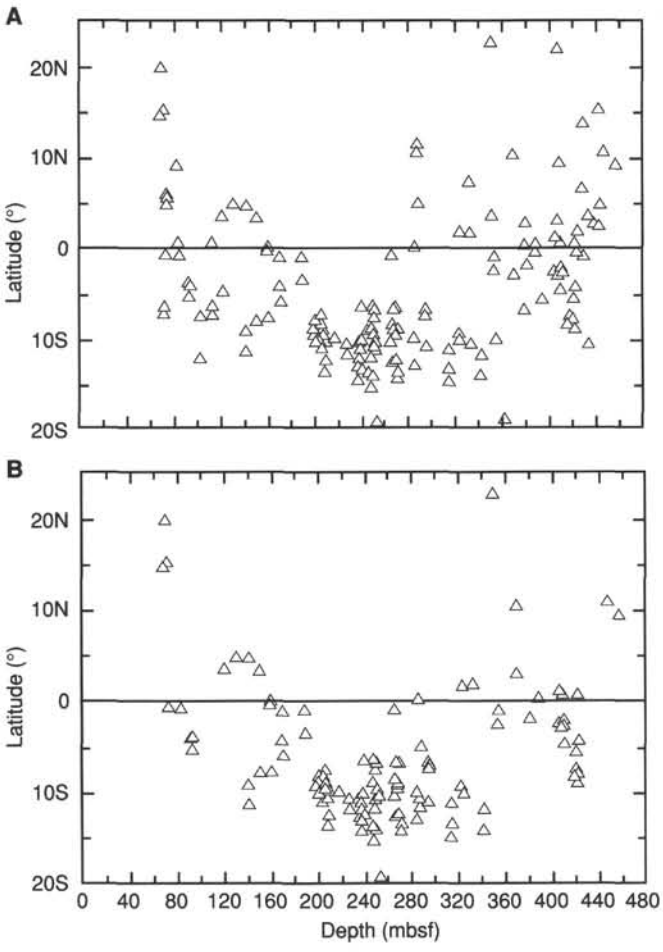

Figure 26. Paleolatitude values for individual samples, plotted against their depth (mbsf). **A.** All data plotted. **B.** Plot displaying only those samples in which stratigraphic "up" is known.

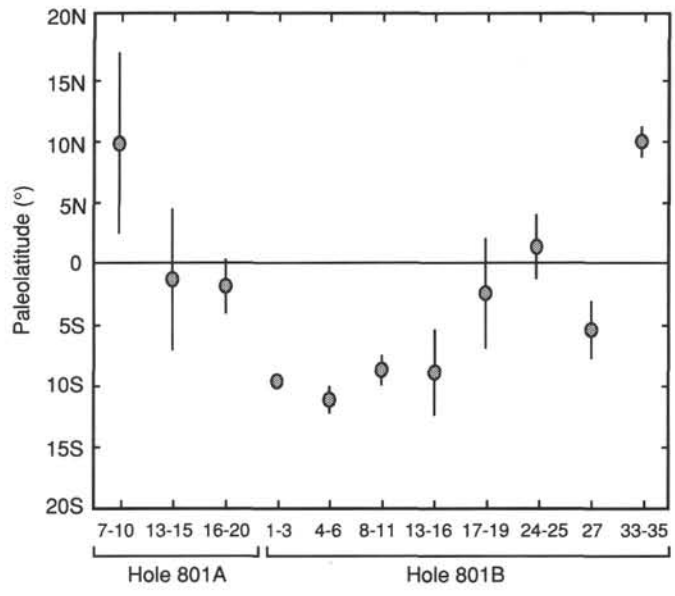

Figure 27. Paleolatitudes of Site 801 plotted for groups of cores. Error bars are one standard deviation of the mean.

garding whether (and when) the site may have crossed the equator in the Jurassic. Because significant secondary magnetization remains, particularly in the Berriasian through Tithonian samples (points 17-19 and 24-25 in Fig. 27) and in the red Callovian-Bathonian samples (point 33-35), the most probable interpretation of this data is that the site was in the Southern Hemisphere from Callovian-Bathonian time onward. However, it cannot be ruled out that those northern paleolatitudes in the Callovian-Bathonian samples (point 33-35, Fig. 27) have some validity and thus that the site may have been in the Northern Hemisphere during the Middle Jurassic. Shore-based analysis of thermally demagnetized samples will resolve this ambiguity.

Basalt Magnetism

Segments of basaltic basement from Site 801 were analyzed with the cryogenic magnetometer. NRM measurements of core segments were followed by AF demagnetization using a variety of field steps. The highest field used was 20 mT but treatment to 15 mT was more common. Volume susceptibility was routinely measured on all cores.

The cryogenic magnetometer appeared to be able to measure most of the basalt in Hole 801B, but in Hole 801C the basalts generally exceeded the range of the magnetometer. In addition, measurements at Hole 801C were complicated by an apparent electronic chip failure in the magnetometer. NRM intensities of the basalts in Hole 801B were low for submarine basalt, about 0.1 mA/m. Response to AF demagnetization was quite varied and thus the data are difficult to interpret. Both normal and reversed polarity appear to be present, although it not possible at this time to determine whether both are characteristic. Normal polarity with shallow, near-zero inclinations was often observed in the finer-grained materials; reversed polarity with steeper (positive) inclinations was observed in the coarser grained units. However, while these were general observations, other coarse- and fine-grained units gave results inconsistent with these.

Only a few of the basalts from Hole 801C could be successfully measured with the cryogenic magnetometer, both because of the high intensities and malfunction of the magnetometer. Time did not permit discrete sampling and measurement with the spinner magnetometer. Samples of these basalts will be investigated onshore.

Susceptibility measurements of the basalts lead to some interesting results. Although preliminary, values of susceptibility seem to correlate with the alteration state of the basalts. Four major susceptibility horizons are recognized. The first of these horizons is composed of Cores 129-801B-37R through -44R and Cores 129-801C-1R through -2R. Susceptibilities in this interval are generally low, averaging approximately 100 SI, but range widely from 30 to 1600 SI. Although the range in values is high, the variation seems confined to specific zones that, at present, appear to correlate with lithologic boundaries or alteration phenomena (described in the "Igneous Petrology" section, this chapter).

The second and most obvious horizon occurs immediately above, into, and below the hydrothermal deposit from Core 129-801C-3R through -7R. Here the susceptibility not only outlines the hydrothermal deposit itself, but perhaps the entire event. The zone is characterized by extremely low susceptibility with the lowest values, approximately 2 to 16 SI, registered by the hydrothermal deposit. Immediately above and below the unit (Cores 129-801C-3R and Section 129-801C-5R-3) values for susceptibility rise to only a range of 15 to 87 SI. Beneath Section 129-801C-5R-3, values begin to rise to greater than 100 SI in Section 129-801C-5R-4. This marks the beginnings of the third or transition horizon beginning in Section 129-801C-5R-4 and continuing to Section 129-801C-7R-2. This horizon has much the same properties as the first interval described.

The final horizon begins at Section 129-801C-7R-3 and continues to the base of the hole, Section 129-801C-12R-3. Susceptibilities in this horizon, with minor exceptions (e.g., Core 129-801C-8R) have values consistently above 1000 SI and reaching as high as 3500 SI. These high susceptibility values may reflect the visibly relatively fresh, unaltered state of the basalt in this interval.

INORGANIC GEOCHEMISTRY

Interstitial water samples were squeezed from sediment cores from seven depths in Holes 801A and 801B. The samples came only from the brown pelagic clay of lithologic Unit I, the volcaniclastic turbidites of Unit II, and the red radiolarite and claystone of Unit V. Because the chert and porcellanite of Unit II and the brown radiolarite of Unit IV have very low water content and were poorly recovered, no samples came from these units. Chemical analyses are summarized in Table 4 and presented in Figures 28 and 29. Yields from squeezing, in mL/cm of whole-round core, varied between lithologies: nearly 8 mL/cm in Unit I, nearly 1.5 mL/cm in Unit III, and 2 mL/cm in Unit V. Pollution by drilling fluids (see Table 3, "Inorganic Geochemistry" section, "Site 800," this chapter) is difficult to rule out for the samples at 23 and 44 mbsf, as these waters have chemical composition close to seawater. For the deeper samples, the very low potassium content of the samples suggests that fluid contamination is unlikely.

Results

Interstitial waters are very similar to seawater at 23 and 44 mbsf in the brown clays of Unit I. Only silicon and sulfate significantly increase at 44 mbsf. Below Unit II (brown chert and porcellanite), interstitial waters extracted from the volcaniclastic turbidites at 175, 233, and 265 mbsf display a general depletion in magnesium, potassium, sodium, and an enrichment in calcium. The overall depletion in cations is balanced by alkalinity, and sulfate decreases while chlorine remains constant. Magnesium is reduced to 28%–35% of seawater content, potassium to 21%–34%, sodium (Na*) to about 95%, and calcium increases to 450%–538% of seawater content. From 175 to 265 mbsf, manganese content increases gradually from 51 to 123 μmol/L, silicon sinks rapidly from 427 to 233 mmol/L and strontium is variable between 280 and 543 mmol/L. Between 444 and 454 mbsf (below Unit IV), magnesium is less depleted than between 175 and 233 mbsf and calcium is less enriched (respectively, 68% and 390%, relative to seawater). Potassium decreases to about 2 mmol/L, whereas sodium increases to near its initial value. Silicon remains constant and manganese is highly depleted compared to concentrations between 444 and 454 mbsf.

Concentration profiles of magnesium, calcium, and potassium display a clear variation from samples from Unit I to samples from Unit III. As in Hole 800A, it is the presence of a lithological barrier for diffusion over sediments undergoing diagenetic reactions (cherts over volcaniclastic turbidites) that generates these breaks. This effect is caused by to the low water content and low porosity of Unit II (3%–10% and 8%–21%, respectively (see "Physical Properties" section, this chapter). A similar barrier to diffusion probably operates in the radiolarites of Unit IV in the interval where water content remains between 1% and 3.8%, between 365 and 396 mbsf. Despite the absence of large concentration gradients between Units III and V, the fact that magnesium and sodium are higher and calcium is lower in Unit V than in Unit III is

Table 4. Chemical composition of interstitial water extracted from sediments in Holes 801A and 801B.

Core, section, interval (cm)	Depth (mbsf)[a]	Alkalinity (meq/L)	Cl (mmol/L)	SO_4 (mmol/L)	pH	Salinity (‰)	Ca (mmol/L)	Mg (mmol/L)	K (mmol/L)	Na* (mmol/L)	Mn (μmol/L)
129-801A-											
3R-2, 145–150	23	2.8	562.0	29.3	7.5	35.5	10.9	52.0	11.2	483	l.d.
5R-3, 145–150	44	2.9	564.0	37.2	7.6	36.0	12.0	53.2	11.6	496	3.7
19R-1, 65–73	175	0.7	560.0	19.3	8.0	34.0	53.2	15.1	3.8	457	51.4
129-801B-											
5R-2, 0–10	233	0.5	569.0	16.1	7.7	35.5	56.1	14.9	2.7	455	87.1
8R-3, 115–125	265	0.6	543.0	16.8	8.1	34.5	46.6	18.6	2.4	442	123.0
33R-1, 143–150	444	1.4	586.0	17.5	7.5	36.2	40.9	35.3	1.9	465	27.8
35R-2, 0–10	454	1.3	572.0	21.0	8.0	35.2	40.4	36.0	2.0	458	25.2

[a] Depth rounded to the nearest meter.
Note: Na* is calculated by charge balance; l.d. = less than detection level.

likely to be related to the presence of the low water content level.

The changes in calcium and magnesium are typical of gradients in sediment pore waters controlled by alteration reactions in underlying basalts (e.g., Gieskes and Johnson, 1981). In Unit III the presence of altered volcanic glass, plagioclase, and green magnesian smectite (see "Lithology and Sedimentology" section, this chapter) suggest that *in-situ* alteration and diagenetic reactions uptake magnesium and release calcium. In contrast, no mineral subject to calcium release has been identified in Unit V. Calcium and magnesium concentrations in Unit V are therefore more likely to be related to alteration of the underlying basement than by *in-situ* reactions.

The potassium concentration profile shows depletion below 175 mbsf in Unit III. Formation of clinoptilolite, observed in Unit II as well as in Unit III, certainly represents the major sink for potassium. In Unit V no zeolites have been recognized, and potassium, as for calcium and magnesium, may be controlled by reactions in the basement.

Sodium is depleted only in the samples of Unit III and, as in Hole 800A, it is probably the *in-situ* formation of zeolite which uptakes sodium.

A silica increase in Unit I is probably due to diffusion from the chert and porcelanite of Unit II. In Unit III, the silica decrease between 175 and 233 mbsf is certainly due to silicon uptake during the formation of authigenic clays and zeolites. The high concentration at 175 mbsf is likely to be linked to the presence of silicified radiolarian claystones at about 183 mbsf in Core 129-801A-20R. Hence, it should be only a local high concentration due to a particular change in lithology.

Manganese reaches significant concentrations only in Unit III, which reflects (1) the general reducing conditions in the volcaniclastic turbidites and (2) the oxidizing conditions in the red claystones of Unit V. Manganese oxides related to fractures are frequent in Unit V.

Conclusions

In sediments of Site 801, the presence of cherts and radiolarites with very low porosity (10%–20%) in Units II and IV appears to isolate the three sampled lithologic units. In Unit I, interstitial water composition is very close to that of seawater and only the silica diffusing from the underlying radiolarite increases significantly. In the volcaniclastics of Unit III, *in-situ* diagenetic and alteration reactions deplete the waters in magnesium, potassium, silicon, and sodium, and release calcium. In Unit V, the magnesium-calcium exchange is more likely to be related to alteration in basement than to *in-situ* reactions. In contrast to Hole 800A, chloride concentration remains constant at all depths.

PHYSICAL PROPERTIES

Physical properties measurements were collected on discrete sediment and rock samples recovered at Site 801. These measurements are presented in Tables 5, 6, and 7 for Holes 801A, 801B, and 801C, respectively, and include index properties (wet-bulk density, porosity, water content, and grain density), compressional-wave velocity, and thermal conductivity. Continuous GRAPE density and *P*-wave velocity measurements, on the multisensor track, were not collected due to coring disturbance and incomplete filling of core liners. However, GRAPE density measurements were made on discrete sediment and rock samples. The above measurements were obtained on average once every other section. Methodologies and equipment used in collecting these data are described in the "Explanatory Notes" chapter (this volume).

Index Properties

Porosity measurements were determined from gravimetric measurements, except where only GRAPE analysis was employed. Wet-bulk density measurements were determined by gravimetric and 2-min GRAPE methods. Grain densities were determined mostly from solid pieces, but for 18 samples, measurements were determined using powdered samples (Tables 5, 6, and 7).

The pelagic brown clays of Unit I (8.0–63.8 mbsf), recovered in Cores 129-801-1R to -7R and sampled for physical properties in Cores 129-801-1R, -3R, -4R, -5R, and -7R, were highly disturbed as a result of rotary coring. The porosity, wet-bulk density, and grain density of these sediments average 75.6%, 1.41 g/cm^3, and 2.56 g/cm^3, respectively. Porosity and wet-bulk density values should be viewed with caution because of the drilling disturbance. Overall, porosity decreases downsection, ranging from 84.0% to 60.1%, whereas wet-bulk density increases with depth and ranges from 1.27 to 1.69 g/cm^3 (Fig. 30).

Brown chert and porcellanite are the dominant lithologies recovered in Unit II (63.8–126.5 mbsf) and show downsection trends of increasing porosity (8.3%–36.1%) and grain density (2.15–2.44 g/cm^3), with wet-bulk density values averaging 2.05 g/cm^3 (Fig. 30, Tables 5 and 6). The increase in porosity and grain density with depth may be related to a downward increase in abundance of calcareous beds (see "Lithostratigraphy and Sedimentology" section, this chapter).

The volcaniclastic turbidite sequences of lithologic Unit III (126.5–318.3 mbsf) are characterized by highly variable physical properties (Fig. 30). Porosity and grain density range from

Table 4 (continued).

Si (μmol/L)	Sr (μmol/L)	Lithology
200	84	Pelagic brown clay
323	8	Pelagic brown clay
427	289	Volcanogenic silty claystone
249	280	Volcanogenic silty claystone
233	543	Volcanogenic silty claystone
212	274	Red clay
218	280	Red clay

21.7% to 71.9% and 2.44 to 2.98 g/cm³, respectively, with wet-bulk density ranging from 1.50 to 2.17 g/cm³. Textural variations, ranging from claystone to sandstone, account for the high variation within these volcaniclastic sediments. Fine-grained pelagic interbeds are common in the upper part of this unit (126–208 mbsf) and also account for the greater variability in porosity, grain density, and wet-bulk density. Porosity, grain density, and wet-bulk density range from 21.7% to 71.9%, 2.29 to 2.98 g/cm³, and 1.50 to 2.05 g/cm³, respectively, in this part of Unit III (Tables 5 and 6).

Pelagic interbeds and volcaniclastic sandstones are less common in the central part of the volcaniclastic unit (208–278 mbsf). The index properties of volcaniclastic siltstones and claystones, which dominate this part of Unit III, are more closely grouped (Fig. 30). Porosity and grain density range from 56.9% to 68.4% and 2.68 to 2.86 g/cm³, respectively. Wet-bulk density values range from 1.59 to 1.81 g/cm³ (Tables 5 and 6).

The lower part of Unit III (278–318 mbsf) is a transition zone between overlying volcaniclastic sediments and underlying brown radiolarites of Unit IV. It consists of volcaniclastic turbidites interbedded with radiolarian claystones (see "Lithostratigraphy and Sedimentology" section, this chapter). Such an assemblage produces a wide range of values for porosity (25.9%–61.5%), grain density (2.57–2.74 g/cm³), and wet-bulk density (1.69–2.03 g/cm³). A sharp decrease in porosity and grain density and an increase in wet-bulk density characterize the base of this transition zone, with respective values of 37.6%, 2.64 g/cm³, and 2.03 g/cm³ at 280.27 mbsf (Fig. 30, Table 6).

The radiolarites and cherts of Unit IV yielded wide-ranging values for porosity (2.5%–49.6%), and wet-bulk density (1.91–2.61 g/cm³). Grain density is more nearly constant, averaging 2.68 g/cm³, and ranging from 2.60 to 2.85 g/cm³ throughout this unit (Table 6). The radiolarites have a high porosity, ranging from 35.3% to 49.6%, relative to the cherts, which have a range of 2.5% to 8.9%. The wet-bulk density of the cherts ranges between 2.46 and 2.61 g/cm³ and is distinctly higher than that of the radiolarites which ranges from 1.91 to 2.21 g/cm³ (Fig. 30).

The lowermost sedimentary unit at Site 801, Unit V (442.9–461.6 mbsf), consists of interbedded red radiolarite and claystone. Claystone, sampled at 443.35 mbsf, displays values of 46.2%, 2.76 g/cm³, and 1.96 g/cm³ for porosity, grain density, and wet-bulk density, whereas radiolarite, sampled at 453.61 mbsf, is characterized by values of 46.8%, 2.73 g/cm³, and 1.93 g/cm³ (Table 5).

The interbedded basalts and silicified claystones of the upper part (above 563 mbsf) of lithologic Unit VI (461.6–90.9 mbsf) show more variation in physical properties (Table 6) than the basalts of the lower part (below 563 mbsf). Index

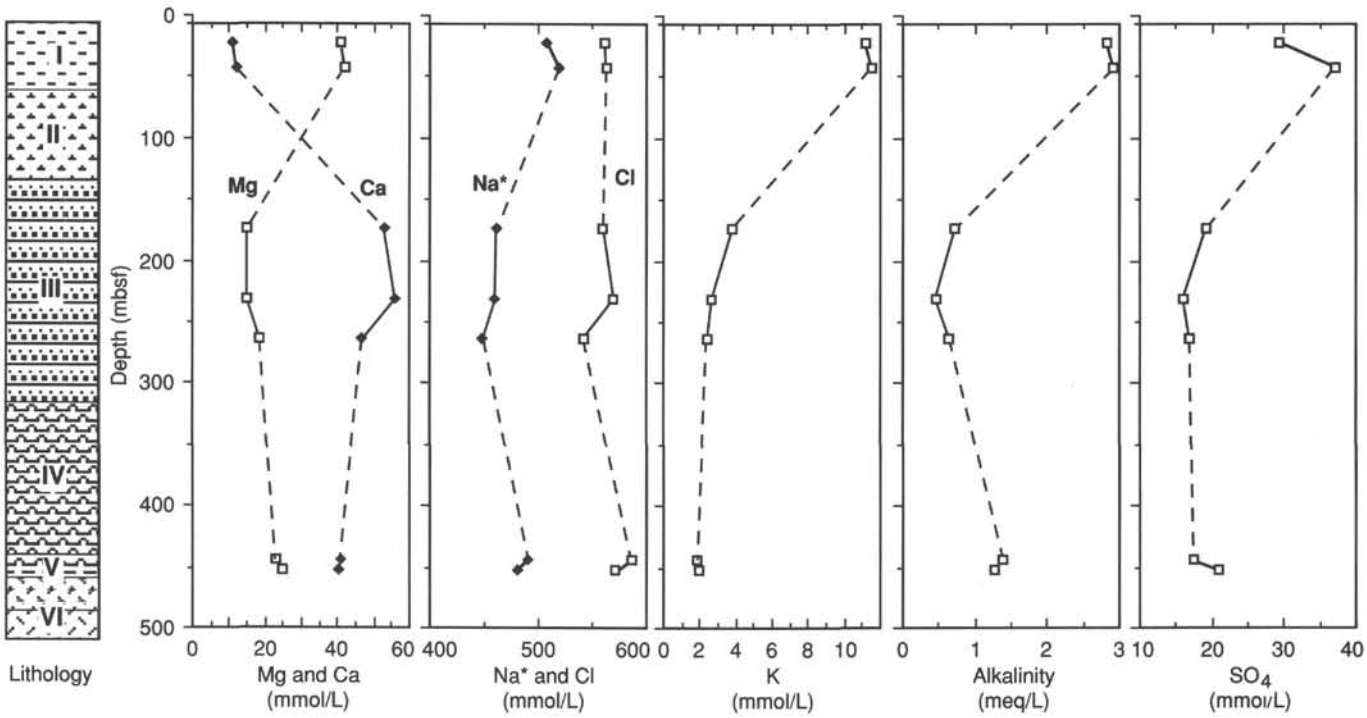

Figure 28. Concentration vs. depth profiles for Mg, Ca, Na*, Cl, K, alkalinity, and SO_4 in interstitial water extracted from sediments in Holes 801A and 801B. Connection lines are dashed for the intervals 44–175 mbsf and 265–444 mbsf because of low porosities in Units II and IV. The lithostratigraphic column refers to the lithologic units defined in the "Lithostratigraphic and Sedimentology" section (this chapter). Unit I, brown pelagic clay; Unit II, brown chert and porcelanite; Unit III, volcaniclastic turbidites; Unit IV, brown radiolarite; Unit V, red radiolarite and claystone; and Unit VI, aphyric basalts.

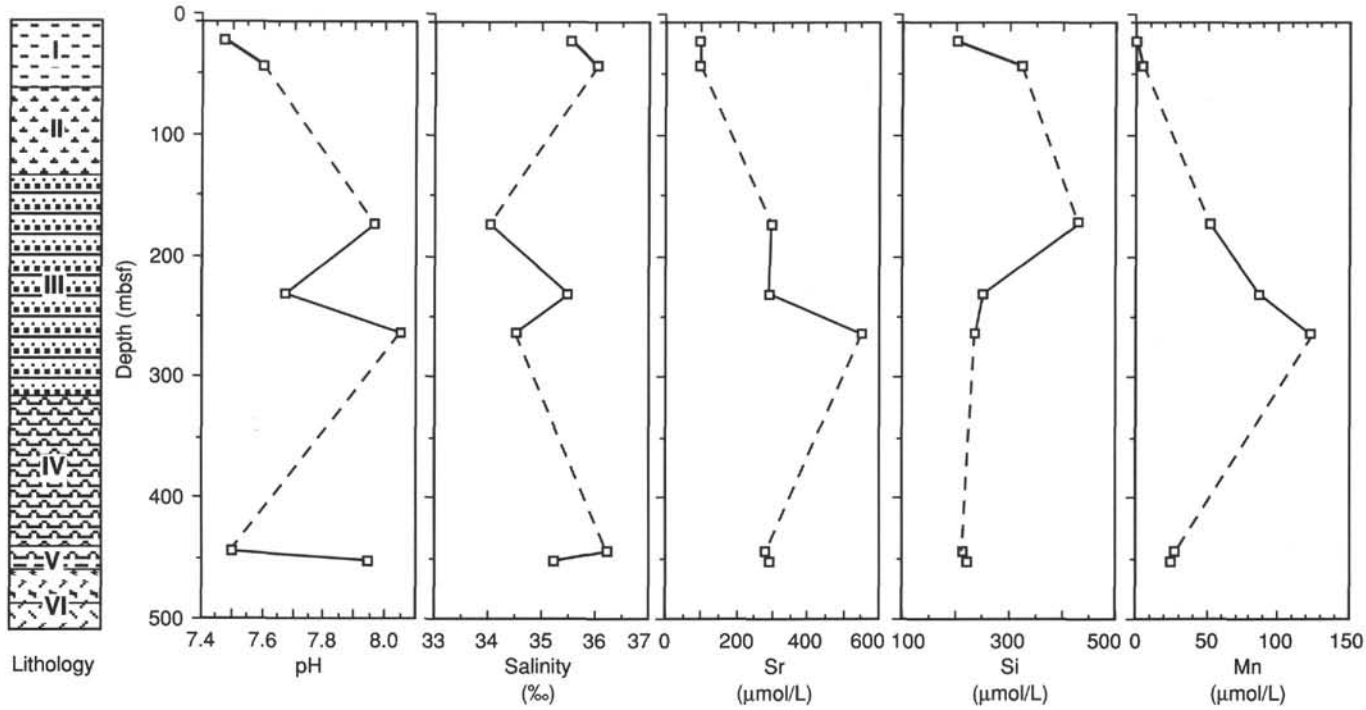

Figure 29. Profiles of depth vs. pH, salinity, and Sr, Si, and Mn concentrations in interstitial water extracted from sediments in Holes 801A and 801B. See Figure 28 for legend.

Table 5. Physical properties summary for Hole 801A.

Core, section, interval (cm)	Depth (mbsf)	Wet-bulk density: Gravimetric (g/cm³)	Wet-bulk density: GRAPE (g/cm³)	Grain density[a] (g/cm³)	Porosity (%)	Water content (%)	Vertical velocity (m/s)	Horizontal velocity (m/s)	Velocity anisotropy (%)	Thermal conductivity (W/m · K)	Remarks
129-801A-											
1R-1, 60–61	8.60	1.28		2.58	83.8	66.7				0.90	Pelagic clay
3R-1, 76–79	21.16	1.27		2.38	81.8	65.3	1517			1.02	Pelagic clay
3R-3, 94–97	24.34	1.32		2.34	77.4	59.5	1494			0.96	Pelagic clay
4R-1, 77–79	30.77	1.27		2.54	84.0	67.4	1508			0.89	Pelagic clay
4R-2, 50–50	32.00									0.94	Pelagic clay
5R-1, 74–76	40.34	1.69		2.70	60.1	36.2	1556			1.04	Nannofossil ooze
5R-3, 74–76	43.34	1.44		2.60	73.5	51.8	1527			0.95	Pelagic clay
5R-5, 74–76	46.34	1.45		2.62	73.3	51.4	1550			1.04	Pelagic clay
7R-1, 75–77	59.75	1.47		2.61	72.3	50.3				0.94	Pelagic clay
7R-3, 76–78	62.76	1.46		2.67	73.9	51.7				0.97	Pelagic clay
7R-CC, 11–13	64.06	2.33	2.22	2.29(2.45)	8.3	3.6	4116	4638	3.0	1.69	Radiolarian chert
9R-1, 17–19	78.37	1.93	2.01	2.15	19.2	10.0	3468	3605	1.0	1.91	Radiolarian chert
10R-1, 22–24	87.72	1.97	2.01	2.23	21.7	11.2	3577	3356	−1.6	1.82	Radiolarian porcellanite
12R-1, 1–3	106.81	1.98		2.32	26.3	13.5					Chert/porcellanite
13R-1, 13–15	116.63	2.13	1.94	2.19(2.44)	21.7	10.4	3391	3619	1.6	1.86	Radiolarian porcellanite
14R-1, 51–53	126.71	1.93	1.90	2.44	36.1	19.0	2569	2648	0.8	1.54	Radiolarian porcellanite
15R-1, 11–13	136.01	1.99	1.95	2.91	49.1	25.2	2463	2492	0.3	1.43	Volcaniclastic sandstone
16R-1, 39–41	145.99	1.80	1.76	2.97	60.6	34.4	2135	2167	0.4	1.20	Volcaniclastic sandstone
17R-1, 64–66	155.84	1.98	1.94	2.29(2.44)	32.4	16.6	2997	3156	1.3	1.70	Chert/porcellanite
18R-1, 49–51	165.49	1.70	1.68	2.80	62.0	37.2	2038	2025	−0.2	1.14	Volcaniclastic sandstone
19R-1, 33–35	175.03	1.50	1.48	2.72	71.9	48.7	1642	1667	0.4		Volcaniclastic silty claystone
20R-1, 15–17	184.55	2.09	2.12	2.38	21.7	10.6	3488	3636	1.0	1.79	Radiolarian claystone

[a] Values in parentheses were determined using powdered samples.

properties were measured using gravimetric techniques and 2-min GRAPE for all samples except three, for which only the 2-min GRAPE was used. Porosities were estimated for these three samples, using the relationship between porosity, wet-bulk density, and fluid density (see "Explanatory Notes" chapter, this volume). Porosities, ranging from 1.0% to 23.0%, characterize the basalts and dolerites of the upper part of Unit VI. The highest porosity (23.0%) occurs in a heavily altered flow unit sampled at 541.65 mbsf. The grain density of the basalts and dolerites ranges from 2.67 to 2.99 g/cm³ and wet-bulk density varies between 2.37 and 2.97 g/cm³. Chert, interbedded with basalt at 470.79 mbsf, is characterized by porosity, wet-bulk density, and grain density values of 3.3%, 2.66 g/cm³, and 2.71 g/cm³, respectively. A sedimentary hydrothermal deposit, sampled at 530.14 mbsf, has a wet-bulk density of 2.52 g/cm³, grain density of 2.65 g/cm³, and porosity of 8.0%. Between 563 and 594 mbsf, index properties are characterized by low variability (Fig. 30). Excluding a

Table 6. Physical properties summary for Hole 801B.

Core, section, interval (cm)	Depth (mbsf)	Wet-bulk density: Gravimetric (g/cm³)	Wet-bulk density: GRAPE (g/cm³)	Grain density[a] (g/cm³)	Porosity (%)	Water content (%)	Vertical velocity (m/s)	Horizontal velocity (m/s)	Velocity anisotropy (%)	Thermal conductivity (W/m · K)	Remarks
129-801B-											
1R-1, 55–57	194.55	1.83	1.81	2.71	52.3	29.1	1929	1959	0.4	1.34	Radiolarian claystone
1R-3, 81–83	197.81	2.01	1.99	2.98	49.7	25.2	2421	2481	0.6	1.33	Volcaniclastic sandstone
2R-1, 92–94	204.42	2.05	2.03	2.82	43.1	21.4	2625	2618	−0.1	1.38	Volcaniclastic sandstone
3R-CC, 0–2	214.06	1.59	1.56	2.78(2.82)	68.4	43.9	1802	1881	1.1		Clayey siltstone
4R-1, 17–19	222.47	1.70	1.70	3.20(2.83)	62.7	37.8	1894	1919	0.3	1.22	Volcaniclastic sandy claystone
5R-1, 64–66	232.34	1.80	1.80	2.91(2.84)	57.0	32.3	1739	2021	3.8	1.43	Volcaniclastic claystone
5R-2, 145–147	234.65	1.69	1.68	3.02(2.75)	61.2	36.9	1820	1860	0.5	1.29	Volcaniclastic sandstone
6R-1, 12–14	241.42	1.68	1.68	2.86	64.6	39.3	1711	1836	1.8	1.25	Volcaniclastic silty sandstone
6R-3, 6–8	244.36	1.81	1.80	2.84	56.9	32.0	1736	1960	3.0	1.38	Volcaniclastic sandy siltstone
6R-4, 10–12	245.90	1.71	1.69	2.73	60.2	36.0	1887	2046	2.0	1.23	Volcaniclastic clayey siltstone
7R-1, 3–5	251.03	1.81	1.82	2.84	57.1	32.2	1728	1904	2.4	1.43	Volcaniclastic claystone
8R-2, 24–26	262.44	1.76	1.68	2.77	57.7	33.4	1808	2027	2.9	1.35	Volcaniclastic silty claystone
8R-4, 126–128	266.46	1.59	1.58	2.69(2.68)	65.7	42.2	1763	1864	1.4	1.14	Volcaniclastic silty claystone
10R-1, 27–29	280.27	2.03	2.03	2.64	37.6	18.8	2454	2779	3.1		Calcareous siltstone
11R-1, 22–24	289.92	2.17	2.00	2.57	25.9	12.2	3076	3914	6.0		Clayey radiolarite
12R-1, 15–17	299.45	1.92	1.91	2.82	50.2	26.6	2362	2303	−0.6	1.31	Volcaniclastic siltstone
13R-1, 47–49	309.47	1.69	1.68	3.24(2.74)	61.5	37.3	1899	1977	1.0	1.22	Volcaniclastic claystone
14R-1, 19–21	318.49	1.91	1.74	2.78	49.6	26.5	1927	2028	1.3	1.39	Clayey radiolarite
16R-1, 30–32	337.50	2.54	2.48	2.54(2.60)	3.7	1.5	5072	5078	0.0	2.31	Radiolarian chert
17R-1, 346.60	346.60	1.96	1.93	2.63	42.1	21.9	2355	2153	−2.2	1.61	Radiolarite
18R-1, 17–19	355.97	1.99	1.95	2.66	41.3	21.2	2198	2304	1.2	1.55	Radiolarite
19R-1, 26–28	365.56	2.61	2.73	2.60(2.65)	2.5	1.0	5280	4987	−1.4		Chert
20R-1, 21–23	374.71	2.61	2.51	2.58(2.65)	2.5	1.0	5173	5305	0.6		Chert
21R-1, 10–12	383.80	2.46	2.42	2.47(2.60)	8.9	3.7	4568	4250	−1.8	2.16	Chert
23R-CC, 13–15	396.03	2.58	2.47	2.54(2.65)	4.5	1.8	5035	4904	−0.7		Chert
25R-1, 41–43	405.61	1.95	1.89	2.73	45.7	23.9	1965	2016	0.6	1.50	Clayey radiolarite
27R-1, 37–39	415.07	1.95	1.93	2.68	44.3	23.1	2059	2155	1.1	1.72	Clayey radiolarite
31R-1, 25–27	433.85	2.21	2.07	2.85	35.3	16.3	2389	2562	1.7	1.68	Clayey radiolarite
33R-1, 55–57	443.35	1.96	1.93	2.76	46.2	24.0	1840	1945	1.4	1.39	Claystone with radiolarians
35R-1, 131–133	453.61	1.93	1.94	2.73	46.8	24.6	1761	1861	1.4	1.66	Radiolarite
37R-1, 56–58	462.04	2.38	2.34	2.75(2.70)	19.3	8.3	3461	3622	1.1	1.50	Aphyric basalt
39R-1, 9–11	470.79	2.66	2.52	2.60(2.71)	3.3	1.3	5035	5138	0.5		Chert
40R-1, 38–40	477.28		2.42		19.1[b]		3805	3565	−1.6	1.65	Aphyric basalt
41R-2, 95–97	485.45		2.63		11.6[b]		4843	4451	−2.1	1.76	Aphyric basalt
42R-2, 95–97	490.00	2.71	2.65	2.85(2.89)	9.6	3.6	4838	4694	−0.8	1.75	Aphyric dolerite
43R-1, 42–44	492.62		2.61		12.7[b]		4945	4889	−0.3	1.80	Phyric basalt
43R-3, 121–123	496.19	2.63	2.54	2.69(2.81)	9.8	3.8	5105	4902	−1.0	1.80	Phyric basalt
44R-1, 54–56	502.24	2.65	2.57	2.77(2.83)	10.2	3.9	4766	4515	−1.4	1.67	Aphyric basalt

[a] Values in parentheses were determined using powdered samples.
[b] Porosity determined from GRAPE wet-bulk density.

moderately high-porosity (9.4%), low-density sample at 588.00 mbsf, ranges for porosity, wet-bulk density, and grain density are 2.1% to 3.3%, 2.85 to 2.92 g/cm³, and 2.91 to 2.97 g/cm³, respectively (Table 7).

Compressional-Wave Velocity

Compressional-wave velocities, measured perpendicular and horizontal to bedding on discrete samples in the Hamilton Frame Velocimeter, show considerable variation downsection. These changes in velocity correspond with variations in index properties and lithologies. Unless otherwise noted the velocities cited are for the vertical propagation direction.

Throughout lithologic Unit I (soft brown pelagic clay), the compressional-wave velocities are closely grouped (Fig. 31). Velocity averages 1525 m/s and ranges from 1494 to 1556 m/s (Table 5).

Compressional-wave velocities in Unit II decrease downsection from a maximum of 4116 m/s at 64.06 mbsf to a low of 3391 m/s at the base of the unit (116.63 mbsf), with an overall unit average of 3638 m/s. The highest velocity and velocity anisotropy in Unit II occur in chert near the top of the unit (Fig. 31). Values for both parameters decrease downsection in Unit II.

In Unit III, sonic velocity is highly variable in the upper part of the unit (126–208 mbsf), low and less variable in the central part of the unit (208–278 mbsf), and high with a distinct trend decreasing downsection in the lower part of the unit (278–318 mbsf) (Fig. 31). The scatter in the data from the upper part of Unit III can be attributed to a variety of textural and physical changes in lithologies (Tables 5 and 6, Fig. 31). Compressional-wave velocities range from 1642 m/s in volcaniclastic silty claystone, at 175.03 mbsf, to 3488 m/s in radiolarian claystone, at 184.55 mbsf. Consistently low velocities occur within the volcaniclastic siltstones and claystones of the central part of Unit III. These velocities range from 1711 to 1894 m/s and average 1789 m/s. These velocity values are associated with high porosities (ranging from 56.9%–68.4%) and low wet-bulk densities (ranging from 1.59–1.81 g/cm³). Velocity anisotropy for these sediments ranges from 0.5% to 3.8% and maintains a higher overall average (1.92%) than the upper and lower parts of this unit (Fig. 31). The lower part of Unit III is characterized by higher velocities, associated with the occurrence of clayey radiolarite. Velocity decreases downsection, in this part of Unit III, from 3076 m/s in clayey radiolarite at 289.92 mbsf to 1899 m/s in the volcaniclastic claystone, at 309.47 mbsf (Fig. 31).

Distinct differences in velocity values between chert and radiolarite characterize lithologic Unit IV. Velocities in chert range from 4568 m/s to 5280 m/s and average 5026 m/s. Velocities in radiolarite range from 1927 to 2389 m/s and average 2149 m/s. Variations in velocity with depth are not well defined (Fig. 31). Anisotropy for the cherts ranges from 1.8% to 0.6% and from 2.2% to 1.7% for the radiolarites. The cherts are characterized by negative anisotropy, and the

Table 7. Physical summary for Hole 801C.

Core, section, interval (cm)	Depth (mbsf)	Wet-bulk density: Gravimetric (g/cm^3)	Wet-bulk density: GRAPE (g/cm^3)	Grain density (g/cm^3)	Porosity (%)	Water content (%)	Vertical velocity (m/s)	Horizontal velocity (m/s)	Velocity anisotropy (%)	Thermal conductivity (W/m · K)	Remarks
129-801C-											
1R-1, 90–92	494.60	2.67	2.62	2.84	9.5	3.6	4589	4652	0.2	1.82	Aphyric microdolerite
1R-3, 82–84	497.13	2.59	2.6	2.77	10.4	4.1	4436	4374	−0.4	1.62	Sparely plagioclase phyric basalt
1R-5, 29–31	498.84	2.59	2.61	2.71	7.1	2.8	5154	5087	−0.3	1.91	Aphyric basalt
2R-1, 14–16	503.14	2.47	2.48	2.69	13.2	5.4	4267	4266	0.0		Sparsely plagioclase phyric basalt
2R-2, 81–83	505.19	2.63	2.65	2.8	9.6	3.7	4866	4866	0.0		Aphyric basalt
2R-4, 76–78	507.86	2.66	2.63	2.84	10.1	3.9	4757	4808	0.3	1.82	Sparsely plagioclase microphyric basalt
3R-1, 32–34	512.52	2.38	2.39	2.69	18.7	8.0	3746	3755	0.1	1.60	Aphyric basalt
4R-1, 44–46	522.14	2.52	2.49	2.65	8.0	3.2	5141	5112	−0.1	4.98	Yellow hydrothermal deposit
5R-1, 103–105	532.23	2.41	2.35	2.67	16.0	6.8	3982	3879	−0.7	1.65	Highly plagioclase megaphyric basalt
5R-2, 87–89	533.33	2.53	2.52	2.77	14.0	5.6	4510	4592	0.5	1.65	Moderately plagioclase megaphyric basalt
5R-3, 43–45	534.20	2.64	2.62	2.84	10.8	4.2	4990	4966	−0.1	1.73	Moderately plagioclase megaphyric basalt
6R-1, 115–117	541.65	2.37	2.36	2.78	23.0	9.8	3690	3479	−1.5	1.69	Sparsely plagioclase phyric basalt
6R-2, 35–37	542.14	2.80	2.79	2.85	2.4	0.9	5994	5975	−0.1	1.74	Aphyric basalt
6R-4, 111–113	545.76	2.36	2.36	2.70	20.3	8.7	3773	3879	0.7	1.49	Moderately olivine plagioclase phyric basalt
6R-5, 68–70	546.71	2.94	2.92	2.98	1.7	0.6	6313	6323	0.0	1.94	Sparsely olivine-plagioclase microphyric basalt
7R-1, 35–37	550.45	2.96	2.92	2.99	1.3	0.5	6333	6414	0.3	2.02	Aphyric basalt
7R-2, 37–39	551.92	2.67	2.71	2.81	7.9	3.0	5281	5248	−0.2	1.80	Aphyric basalt
8R-1, 65–67	560.15	2.47	2.48	2.81	18.8	7.7	4108	4088	−0.1	1.60	Aphyric basalt
8R-2, 78–80	561.35	2.97	2.94	2.99	1.0	0.3	6588	6593	0.0	1.95	Aphyric basalt
9R-1, 49–51	563.69	2.86	2.85	2.92	3.3	1.2	6367	6442	0.3	2.10	Aphyric basalt
9R-3, 121–123	567.15	2.88	2.88	2.93	2.5	0.9	6077	6364	1.2	1.95	Aphyric basalt
9R-4, 137–139	568.58	2.91	2.91	2.96	2.7	0.9	6325	6114	−0.8	1.97	Aphyric basalt
10R-2, 55–57	571.05	2.92	2.90	2.97	2.6	0.9	6218	6224	0.1	2.16	Aphyric basalt
10R-5, 3–5	574.84	2.92	2.91	2.96	2.1	0.7	6234	6275	0.2	1.99	Sparsely olivine microphyric basalt
10R-6, 65–67	576.81	2.86	2.86	2.91	2.7	1.0	6040	5981	−0.2	2.11	Sparsely olivine microphyric basalt
11R-2, 119–121	580.49	2.85	2.84	2.91	2.9	1.0	6102	6050	−0.2	2.24	Sparsely plagioclase-olivine microphyric basalt
11R-3, 40–42	581.20	2.87	2.87	2.91	2.3	0.8	6304	6204	−0.4	2.43	Aphyric basalt
12R-1, 70–72	588.00	2.59	2.66	2.75	9.4	3.6	5011	5027	0.3	1.75	Aphyric basalt
12R-2, 109–111	589.89	2.92	2.91	2.96	2.1	0.7	6178	6245	1.1	1.79	Aphyric basalt

radiolarites, other than one anomalous negative value (2.2%), display positive anisotropy.

Only two velocity measurements were obtained for rocks from Unit V (Fig. 31), 1761 m/s for red radiolarite at 453.61 mbsf and 1840 m/s for claystone at 443.35 mbsf. Both rocks display a velocity anisotropy of 1.4%.

The basalts and dolerites of the upper part of Unit VI (above 563 mbsf) have velocities ranging from 3461 to 6588 m/s with an average velocity of 4765 m/s. Low velocities occur in altered basalt flows with high porosities. Sonic velocities are highest in the vertical propagation direction at the top of Unit VI, with a trend of negative velocity anisotropy changing to positive anisotropy downsection (Tables 6 and 7, Fig. 31). Microfractures or large crystals oriented vertically could explain the high vertical velocities within this part of Unit VI. Below 563 mbsf, velocity anisotropy is nearly constant downsection, averaging 0.2%. The interbedded chert (470.79 mbsf) has a compressional-wave velocity of 5035 m/s. The hydrothermal deposit (522.14 mbsf) has a sonic velocity of 5141 m/s. The velocities of basalts in the lower part of Unit VI range from 5011 to 6367 m/s (Table 7, Fig. 31). Excluding the sample at 588 mbsf, velocities of basalt from this part of Unit IV show little variability (Table 7) and are tightly clustered about an average of 6205 m/s (Fig. 31).

The various lithologies recovered at Site 801 show a direct relationship of increasing compressional-wave velocity with increasing wet-bulk density. The soft pelagic muds have the lowest velocity/density gradient and occupy the lowest field in the velocity/density crossplot (Fig. 32). The volcaniclastic sandstones and volcaniclastic siltstones and claystones plot in similarly tight fields. However, the volcaniclastic sandstones are characterized by a higher gradient and slightly higher velocities than the volcaniclastic siltstones (Fig. 32). Radiolarites are generally tightly clustered and have a higher gradient than the volcaniclastics. The cherts and porcellanites have a moderate to high velocity/density gradient and occupy a wide field on the velocity/density crossplot. The range of velocities for the cherts overlaps that of the basalts and dolerites; however, at equivalent wet-bulk densities, chert velocities are typically higher than those of the igneous rocks. Basalts and dolerites are characterized by high velocity and density values and a very steep velocity/density gradient. These basalts are clustered into two distinct groups (see Fig. 32), one having markedly higher overall velocity values than the other.

Thermal Conductivity

Thermal conductivity was measured in soft sediments and lithified rock recovered at Site 801. Procedures for thermal conductivity measurements are described in the "Explanatory Notes" chapter (this volume). Thermal conductivity measurements are listed in Tables 5, 6, and 7, and are plotted against depth in Figure 33 and against porosity in Figure 34.

Thermal conductivity of the pelagic clays of Unit I ranges from 0.89 to 1.04 W/m · K and averages 0.97 W/m · K. A sharp increase in conductivity characterizes the boundary between Unit I and Unit II. The siliceous sediments of Unit II have an average thermal conductivity of 1.76 W/m · K with a range of 1.54 to 1.91 W/m · K. The thermal conductivity values of the

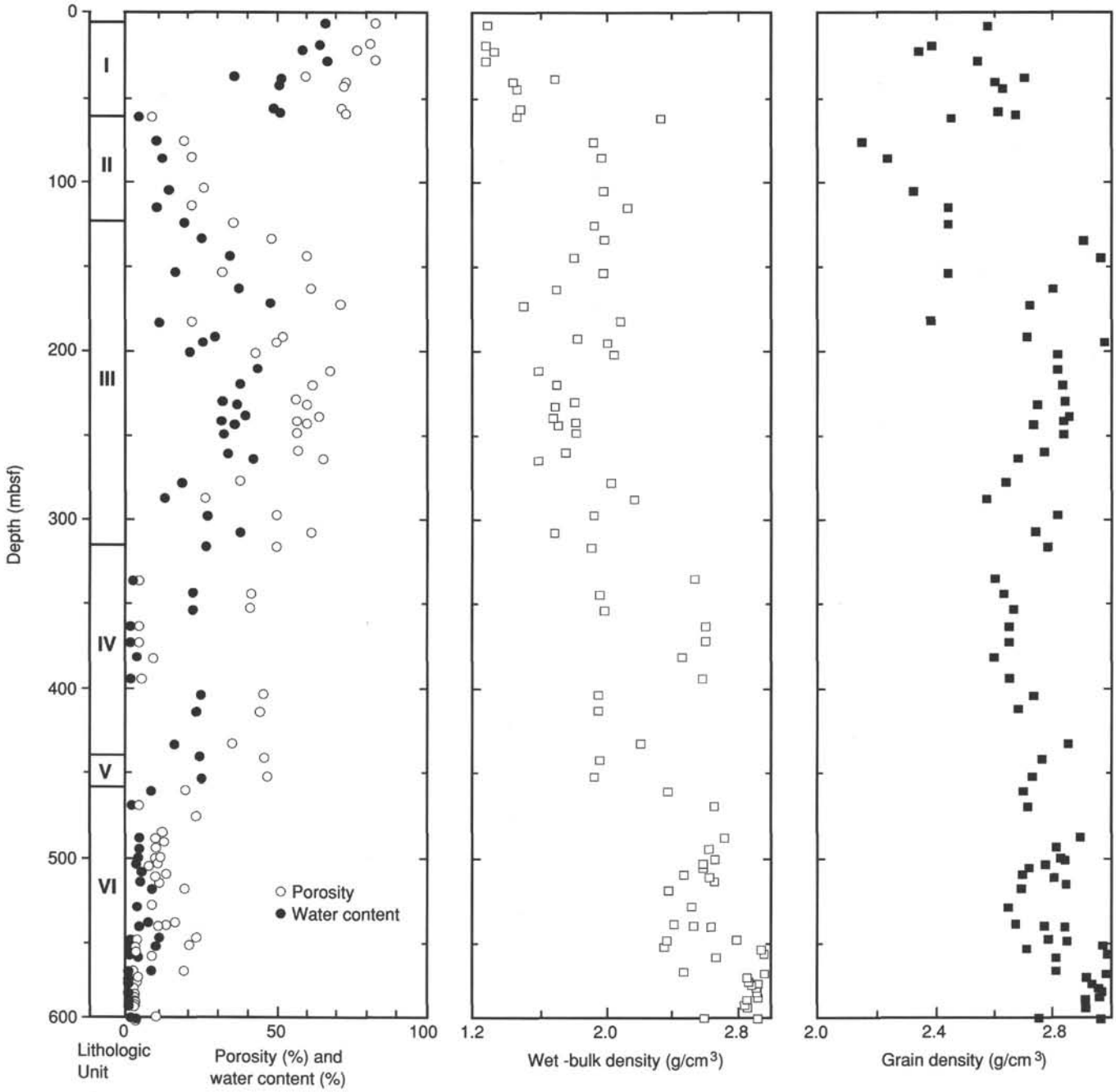

Figure 30. Index properties (porosity, wet-bulk density, and grain density) vs. depth for Holes 801A, 801B, and 801C.

upper part of the volcaniclastic Unit III (126–208 mbsf) are variable, ranging from 1.14 to 1.79 W/m · K. Thermal conductivity in the remaining parts of Unit III is less variable, ranging from 1.14 to 1.43 W/m · K. Conductivity in this interval remains nearly constant downsection. Wide-ranging thermal conductivity values characterize the biogenic silica-rich sediments of Unit IV with minimum and maximum values of 1.39 and 2.31 W/m · K, respectively. The highest conductivity values (2.16 and 2.31 W/m · K) occur in cherts at 337.50 and 383.80 mbsf in Unit IV. The thermal conductivity of Unit V is 1.39 for claystone and 1.66 for radiolarite. The thermal conductivity of the basalts of Unit VI ranges from 1.50 to 2.39 W/m · K and averages 1.73 W/m · K. The lowest conductivity (1.49 W/m · K) was measured in altered basalt sampled at 545.76 mbsf (Table 7). The hydrothermal deposit within Unit VI has an extremely high thermal conductivity (4.98 W/m · K) because of its probable high iron content. This value is highly uncertain because it is considerably above our highest calibration standard (macor 1.61 W/m · K).

A strong inverse relationship between porosity and thermal conductivity characterizes sediments and sedimentary rocks at Site 801 (Fig. 34). Basalts and dolerites with less than 5% porosity display a wide variation in thermal conductivity (1.70–2.45 W/m · K). A general inverse relationship between porosity and thermal conductivity characterizes the entire igneous rock data set. The trend of this relationship lies approximately 0.2 W/m · K below the trend for siliceous sedimentary rocks with comparable porosities (Fig. 34).

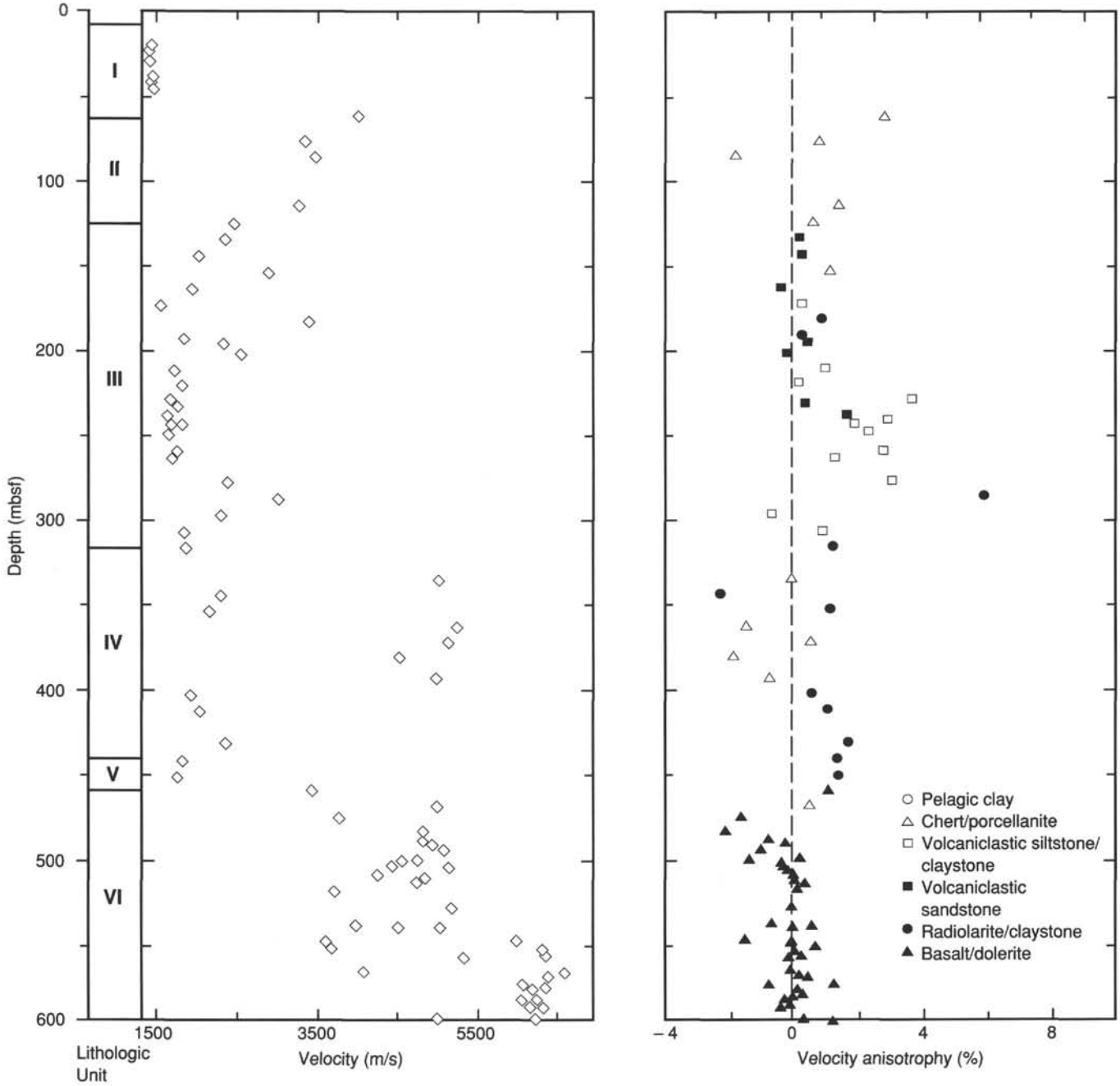

Figure 31. Compressional-wave velocity (V*v*) and velocity anisotropy vs. depth for Holes 801A, 801B, and 801C.

IGNEOUS PETROLOGY

Igneous rocks overlain by sediments that are at least late Middle Jurassic in age (~165 Ma) were recovered at Site 801 in the southern Pigafetta Basin. These igneous rocks are different from those drilled at Site 800 in the northern part of the basin, which occur below Lower Cretaceous (~140 Ma) sediments, because rock units that were recognized at Site 801 are mostly fine-grained basalts and microdolerites emplaced as lava flows (a few, possibly, as thin intrusions) whereas those at Site 800 are mainly medium-grained dolerite intruded as sills. Site 801 igneous rocks are also different from the extrusive basalts recovered at Site 802 in the East Mariana Basin because Site 802 rock units were emplaced generally as thin (<1 m) pillow lavas and occur just below middle Cretaceous (~110 Ma) sediments. Although there are no absolute age or chemical data yet available, we propose that the igneous rocks at Site 801 in the southern Pigafetta Basin represent the first Jurassic oceanic crust ever sampled *in-situ* in the Pacific Ocean because (1) the presence of extrusive lava flows indicates that the Jurassic sediments were deposited on top of a pre-existing oceanic crust and (2) even if some of Site 801 rock units were intrusives, at least a part of the intrusive event was penecontemporaneous with Jurassic sedimentation in the Pigafetta Basin.

Hole 801B

Lithology and Mode of Emplacement

A total of 15.42 m of igneous and sedimentary rocks were recovered from 462.3 mbsf to 511.2 mbsf at Hole 801B, representing an average recovery of 31.3%. Using similar

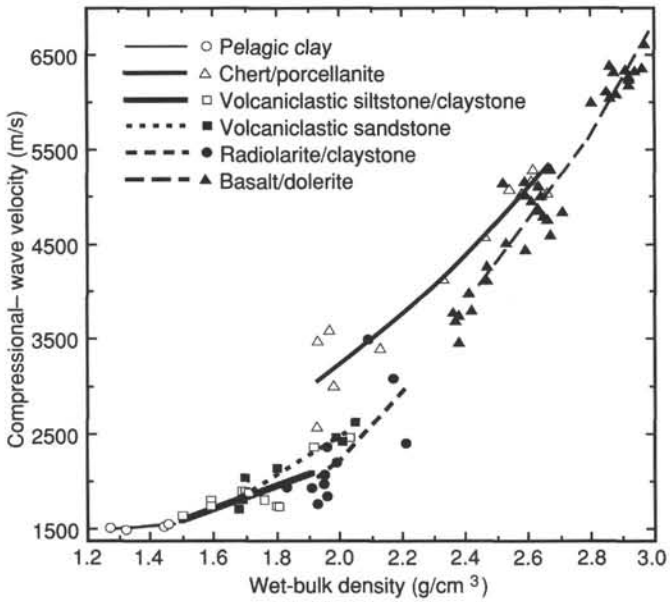

Figure 32. Wet-bulk density vs. compressional-wave velocity (V*v*) for Holes 801A, 801B, and 801C, coded according to sediment and rock type.

criteria employed in Hole 800A (see also, "Explanatory Notes" chapter, this volume), 14 cooling units were observed starting from interval 129-801B-37R-1, 18 cm, down to 129-801B-44R-3, 47 cm. A summary of the features of these units is presented in Table 8 and Figure 35.

It is very important to point out, however, that whereas all the units were identified based on actual observations, critical contacts bearing on the mode of emplacement of some of the units (i.e., Units 1, 2, 3, 4, 5, 6, 10, and 11) were not recovered. Available data suggest that Unit 9 consists of pillow lavas, Units 8 and 14 are intrusive bodies, and Units 7 and 12 are lava flows. For simplicity of presentation, however, we consider the remainder of the units as thin (~1 m but <4 m) lava flows although some of these can not be completely ruled out as parts of thin intrusive sills. A more detailed discussion of the most important features of some of the units is presented below.

Units 1 to 4 are aphyric basalts interlayered with cherts and silicified claystones. None of the actual contacts was observed, but the top portions of these units and the whole of Unit 1, which is composed of centimeter-sized basaltic fragments, are finer grained and more oxidized than the lower, recovered portions. Based on these limited data, these units could be interpreted as either thin lava flows (Anderson, Honnorez, Becker et al., 1985) or thin sills (Larson, Schlanger, et al., 1981). Some of the interlayered, silicified sediments are poorly laminated and have preserved bioturbations, whereas others have desiccation cracks that are now filled, sometimes only partially, with drusy quartz. The combined features of these interlayered sedimentary and volcanic rocks suggest that if the basalts were extruded as thin flows, then these units are undoubtedly Jurassic in age because the overlying sediments in Core 129-801B-36R were dated as late Middle Jurassic (see "Biostratigraphy" section, this chapter). On the other hand, if these were intruded as sills, then the intrusion event most probably occurred penecontemporaneously with sedimentation in the southern Pigafetta Basin.

The grain size of Unit 7 systematically increases from top to interior and then decreases again to a subrounded bottom with a chilled glassy margin. These data suggest that Unit 7 is

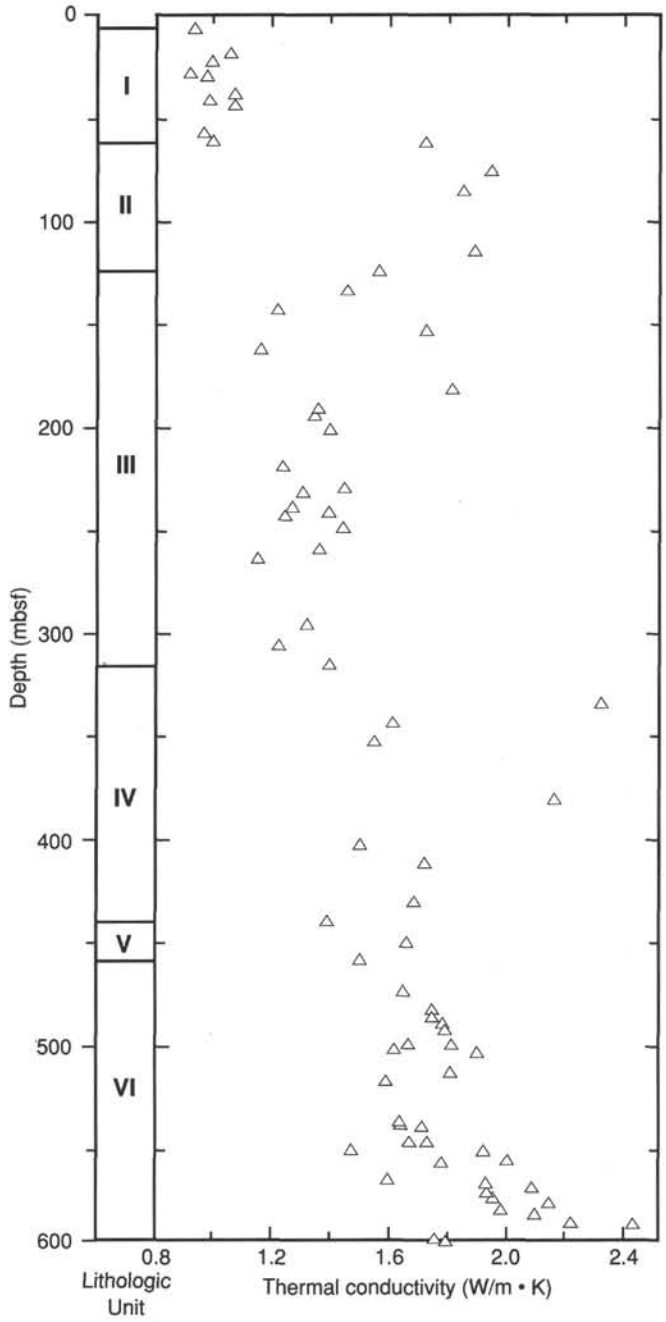

Figure 33. Thermal conductivity vs. depth for Holes 801A, 801B, and 801C.

a thin lava flow. Furthermore, the quenched bottom margin of Unit 7 is most probably a pre-existing feature that formed prior to intrusion of Unit 8, which is an irregularly shaped, thin (~8 cm at its widest), sparsely plagioclase phyric, feldspar-rich, basaltic andesite. Only a thin (~1 mm) chilled zone was observed at the margin of Unit 8 but it contains isolated fragments of Unit 7 that show the thermal effect of assimilation. Some of the xenoliths can be easily fitted back to their original positions in Unit 7. Because of its unique intrusive features and more differentiated composition, Unit 8 has been interpreted as a late-stage differentiation magma that intruded the interstices between flow units.

As noted above, Unit 8 is also in contact with Unit 9, which consists of fragments of sparsely plagioclase phyric basalts

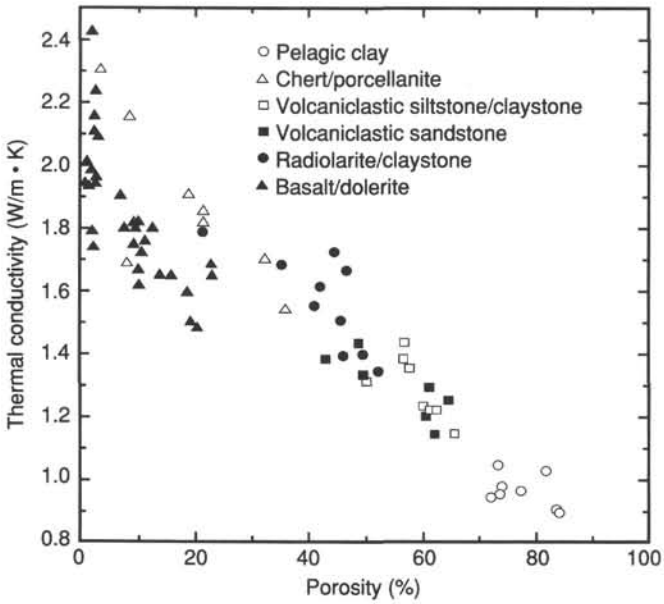

Figure 34. Porosity vs. thermal conductivity for Holes 801A, 801B, and 801C, coded according to sediment and rock type.

Table 8. Extent of igneous units actually observed in Hole 801B.

Unit	Top	Bottom	Thickness (cm)
	129-801B-	129-801B-	
1	37R-1, 18 cm	37R-1, 22 cm	4
2	37R-1, 27 cm	37R-1, 80 cm	53
3	38R-1, 14 cm	39R-1, 3 cm	14
4	40R-1, 14 cm	40R-1, 102 cm	88
5	41R-1, 6 cm	41R-2, 120 cm	264
6	42R-1, 0 cm	42R-2, 145 cm	245
7	43R-1, 0 cm	43R-3, 36 cm	327
8	43R-3, 36 cm	43R-4, 44 cm	8
9	43R-3, 44 cm	43R-4, 4 cm	109
10	43R-4, 4 cm	43R-4, 14 cm	10
11	43R-4, 14 cm	43R-4, 101 cm	87
12	44R-1, 0 cm	44R-1, 124 cm	124
13	44R-2, 23 cm	44R-3, 13 cm	140
14	44R-3, 13 cm	44R-3, 47 cm	3

Note: Total thickness of igneous rocks recovered is 15.07 m. Total core recovered from Cores 129-801B-37R to 129-801B-44R, including sediments, is 15.42 m, representing 31.3% recovery for this portion of Hole 801B.

and silica-calcite (± green clays) veinlets. The basalt fragments were interpreted as parts of pillow lavas. For example, one of the fragments (piece 14) is a pillow margin with a well-developed, subvertical holohyaline rim that grades into a curved spherulitic zone, and finally to a crystalline interior (Fig. 36). Another fragment (piece 17) contains a boundary between two pillows which is now filled with a calcite-silica veinlet. The rest of the veinlets are also probably pillow lava infill and a couple of these contain millimeter-sized claystone with very sparse, ill-preserved nannofossils of *Watznaueria manivitae* that range from Middle Jurassic to Cretaceous. Thus, Unit 9 was interpreted as a pillow lava unit based on the following observations: (1) the presence of Unit 8 filling the interstices between lava flows, (2) the presence of fragments of secondary silica-calcite veinlets carrying millimeter-sized fragments of claystone, which, similar to Unit 8, may have preferred the interstices between flows as the easiest avenues of intrusion, and (3) the presence of chilled pillow margins that are generally vertical in orientation.

Unit 12 is an aphyric basalt conformably overlying sediments and has moderately preserved, fine-grained top and bottom margins. Thus, it is probably a thin lava flow (Anderson, Honnorez, Becker et al., 1985). If this is the case, Hole 801B must have been drilled through a sequence of lava flows starting from the top of Unit 7 (Section 129-801B-42R-1, 29 cm) down to the bottom of Unit 12 (Section 129-801B-44R-1, 124 cm).

Finally, Unit 14 is a quenched, semirounded margin of a moderately plagioclase, microphyric glassy basalt. It resembles a half cross-section of a pillow lava from its shape and its hypohyaline texture with a chilled, holohyaline rim (Fig. 37). However, the overlying Unit 13, a moderately altered, aphyric basalt, apparently wraps around the relatively less altered Unit 14 and does not have a systematic grain-size coarsening away from the contact (see thin-section description below). This is somewhat surprising because Unit 13 is a massive, continuously cored, hypocrystalline to holocrystalline, aphyric basalt unit and its top contact with sediments at 129-801B-44R-2, 23 cm, does have a wide (~30 cm), well-developed, systematic fining margin. These observations suggest that Unit 14 could be intrusive (Anderson, Honnorez, Becker et al. 1985). Moreover, fragments very similar to Unit 13 are present underneath and as a xenolith within Unit 14. Finally, two clearly intrusive units, which are very similar and most probably correlative with Unit 14, were recovered at Hole 801C (see below). Thus, Unit 14 has the shape and internal texture typical of a pillow lava but other evidence suggests that it is an apophysis of an intrusive unit that penetrated the previously emplaced and crystallized Unit 13.

Petrography

Texture

Thin-section examination showed that the igneous rocks recovered in Hole 801B range in texture from glassy basalt (Sample 129-801B-44R-3, 26–27 cm, piece 3A) to predominantly medium-grained, hypidiomorphic-granular dolerite (Sample 129-801B-43R-2, 103–104 cm, piece 5C) (see also Fig. 35). A majority of the samples, however, are fine- to medium-grained, hypidiomorphic-granular microdolerites (Samples 129-801B-41R-1, 25–26 cm, piece 3; 129-801B-42R-1, 86–87 cm, piece 5C; 129-801B-43R-1, 20–21 cm, piece 4A; and 129-801B-44R-3, 25–26 cm, piece 3A). There is no systematic textural variation among the igneous units despite the general fining of grain size from interior to margins within most units. Only two of the thin sections studied are phyric: (1) the glassy basalt of Unit 14 (Sample 129-801B-44R-3, 26–27 cm, piece 3A), which originally contained as much as ~13% phenocrysts of plagioclase, olivine, and a trace of clinopyroxene, and (2) the basal margin of Unit 7 (Sample 129-801B-43R-3, 35–37 cm, piece 2B), which contains 1% plagioclase and traces of clinopyroxene and olivine. The remainder of the samples are aphyric. Almost all crystalline samples have interstitial glass or mesostasis that had been completely altered to clay and invariably contains quenched microlites of plagioclase with or without relict pyroxene.

A brief discussion of the most interesting petrographic features of a few specific units follows. The top of Unit 7 (Sample 129-801B-43R-1, 20–21 cm, piece 4A) contains euhedral to subhedral crystal outlines of olivine that are now completely filled with corrugated plates of talc(?) and brownish smectite. The pseudomorphs range in size from 0.5 to 1.5 mm and constitute as much as ~20% of the thin section, thus making this the most mafic igneous rock sampled so far from the Pigafetta Basin. Equally interesting is the basal margin of

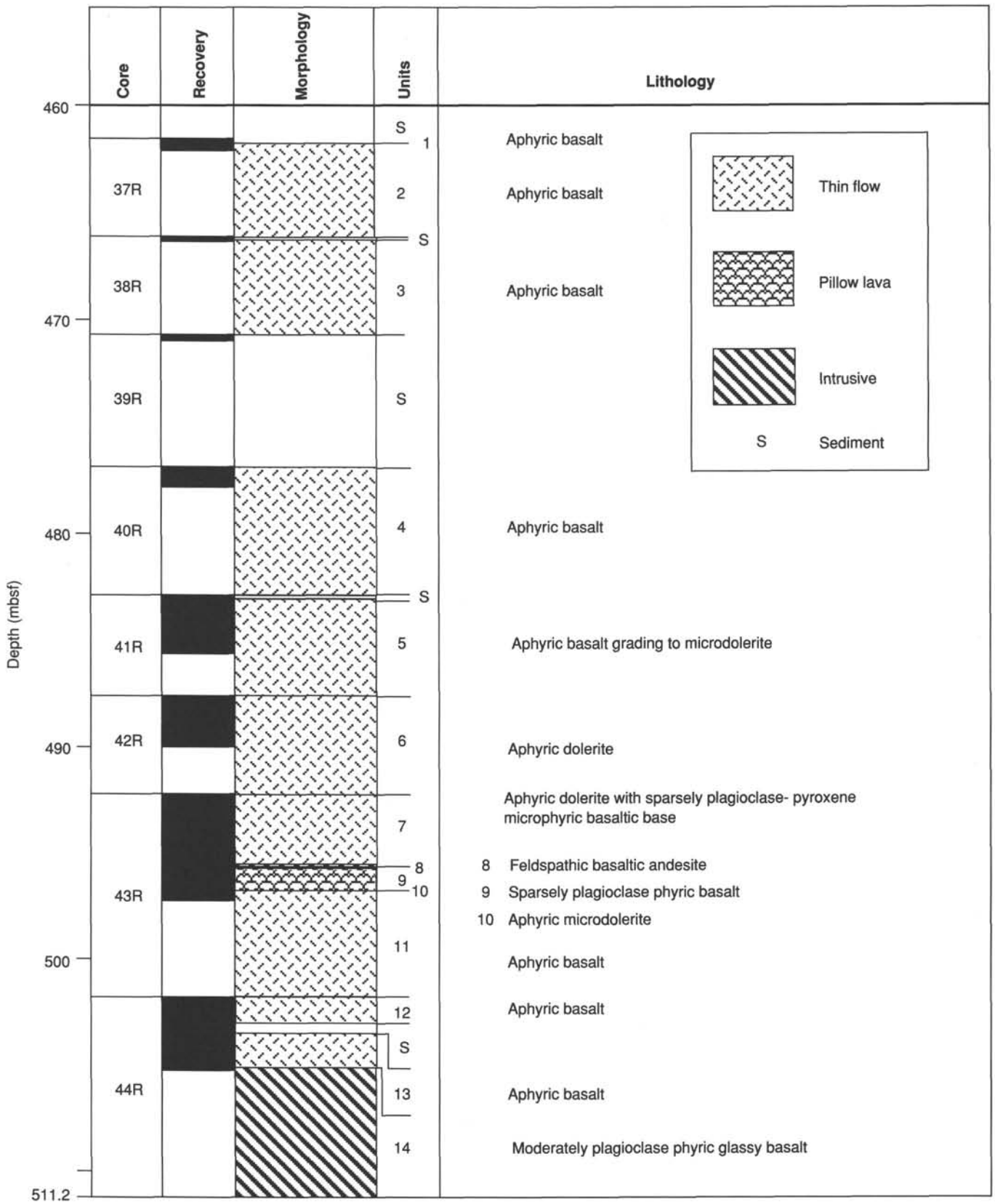

Figure 35. Summary of lithostratigraphy of igneous rocks in Hole 801B.

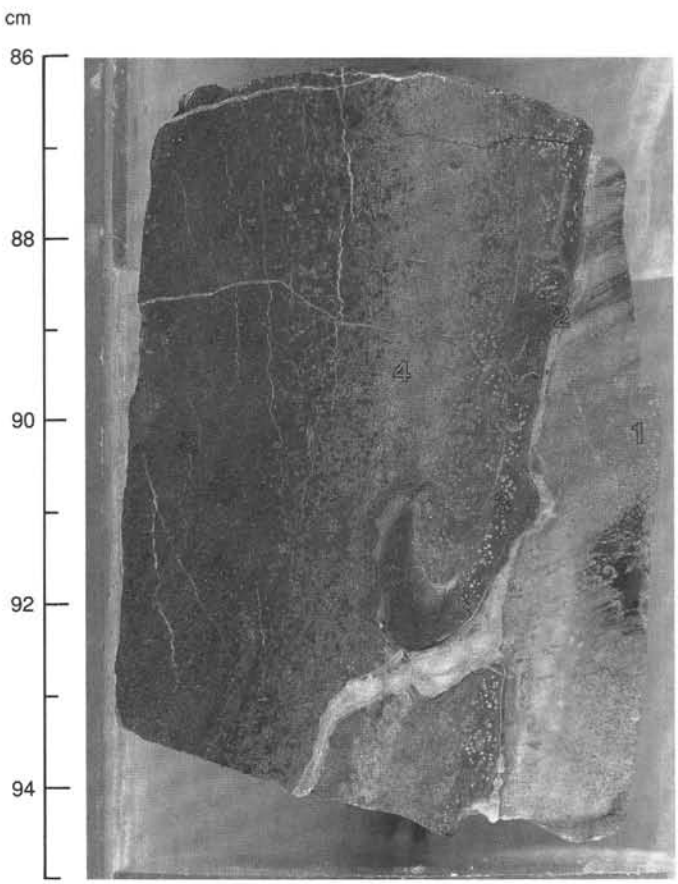

Figure 36. Photograph of a fragment of a pillow lava margin (piece 14) in interval 129-801B-43R-3, 86–95 cm. From right to left of the photograph: (1) a portion of a light gray, upright silica-calcite vein, (2) a thin (~1 mm), white calcite veinlet between the vein and the pillow fragment (this veinlet is connected to the wider (~5 mm) but irregular, diagonal, white veinlet in the lower part of the fragment), (3) a dark gray, glassy rim of the pillow fragment with a few white amygdales, (4) spherulitic zone (~1 mm) containing radiating fibers of quenched plagioclase and pyroxene, and (5) a black, hypocrystalline basalt. A moderate amount (~5%) of feathery plagioclase microlites is randomly distributed throughout the pillow fragment but especially along the glassy rim. Note that the spherulitic zone is concaved towards the hypocrystalline basalt.

this unit (Sample 129-801B-43R-3, 35–37 cm, piece 2B) because it appears to have been metamorphosed during the intrusion of Unit 8 (Sample 129-801B-43R-3, 37–39 cm, piece 2B) as discussed in the previous section. The margin starts from a convex glassy rim, which is now replaced by brown smectite and contains skeletal plagioclase microlites, and then passes to a crystallite-rich interior zone devoid of the microlites. Superimposed on the two zones are randomly oriented grains and plates of secondary biotite. The intrusive Unit 8, on the other hand, is a fine-grained, hypocrystalline basaltic andesite that contains small (a few millimeters in length), glassy xenoliths derived from Unit 7.

Petrographic examination confirmed that Unit 14 (Sample 129-801B-44R-3, 26–27 cm, piece 3A) is relatively younger than Unit 13 (Sample 129-801B-44R-3, 25–26 cm, piece 3A) as previously discussed. The contact is very sharp but cuspate because the palagonitized glassy rim of Unit 14 penetrates the moderately altered, hypocrystalline Unit 13, causing some of its plagioclase and clinopyroxene crystals to terminate

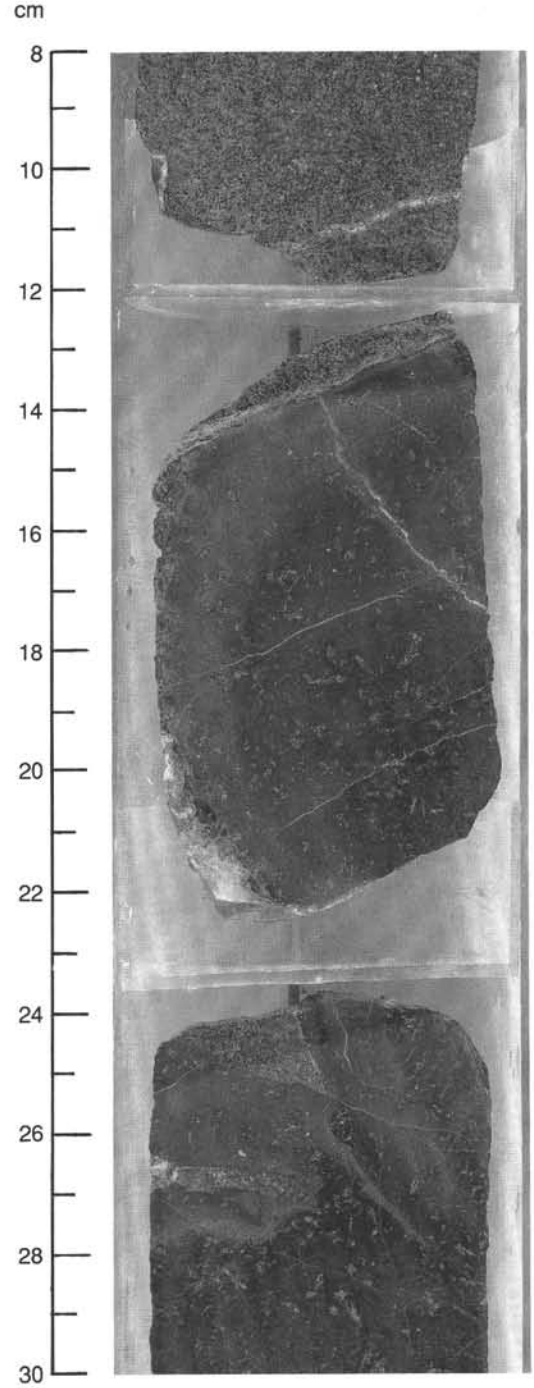

Figure 37. Photograph of pieces 1 (lower part), 2, and 3A (upper part) in interval 129-801B-44R-3, 8–30 cm. In piece 2, a subrounded portion of a moderately plagioclase, phyric, glassy basalt is partially wrapped by hypocrystalline aphyric basalt, a typical specimen of which is clearly shown in piece 1. The glassy basalt has a light grayish-brown glassy rim that grades into a dark gray, holohyaline interior. The white specks throughout the glassy basalt are quenched microlites of feathery plagioclase. The outline of the subrounded margin continues in piece 3A and cuts another fragment of glassy basalt. Note that in piece 3A, the contact between the glassy and the hypocrystalline basalt is sharp and a small fragment of hypocrystalline basalt is enclosed in the glassy basalt. The nature of the intrusive contact between the two igneous units is discussed in more detail in the text.

abruptly against the contact. There is no apparent change in texture of Unit 13 with increasing distance from the contact, whereas Unit 14 clearly changes from yellow to brown, palagonitized glass to opaque, smectite-replaced glass, and then finally to a hypohyaline interior containing variolitic plagioclase and clinopyroxene. Phenocrysts of quenched, swallow-tailed plagioclase, skeletal to euhedral relicts of olivine, and traces of clinopyroxene are randomly distributed throughout Unit 14.

Mineralogy

The approximate proportions of primary and secondary minerals actually present in thin sections of Hole 801B igneous rocks are summarized in Table 9. As expected, plagioclase is ubiquitous in all samples ranging in abundance from 25% to 60% in crystalline samples and from 1% to 35% in glassy samples. Its crystal morphology ranges from quenched spherulites in the spherulitic zone, to feathery microlites in mesostasis, and finally to well-developed, subhedral laths that are sometimes as long as 5 mm. Plagioclase laths form phenocrysts in the two phyric samples previously mentioned and groundmass phases in all the rock units. These laths range in composition from An_{38} to An_{74} but it must be noted that plagioclase is almost always oscillatory zoned to variable extent.

Pyroxene is also ubiquitous in all samples save for the most altered one (Sample 129-801B-37R-1, 36–38 cm, piece 2) but, although its variability is partly due to replacement, its abundance generally is less than that of the plagioclase (<1% to 22%). Pyroxene morphology ranges from quenched microlites in mesostasis to elongate or stubby, millimeter-sized prisms. Some pyroxene crystals are relatively long (up to 3 mm in length) and are mostly represented by optically continuous relicts separated by alteration products. Optical properties indicate that the pyroxene is mainly titanaugite.

Titanomagnetite is also present in all samples ranging from ~2% to a maximum of 8% in abundance (Table 9). A majority of titanomagnetite occurs as fine (<0.5 mm), subhedral grains but some occur as long (up to 1.5 mm in length), skeletal needles.

As noted previously, a few samples contain subhedral to euhedral pseudomorphs of olivine (Table 9). The pseudomorphs range in size from ~0.1 to 1.5 mm and occur as a major phase in a microdolerite (Sample 129-801B-43R-1, 20–21 cm, piece 4A) and as phenocrysts in glassy rims (Samples 129-801B-43R-3, 35–37 cm, piece 2B, and 129-801B-44R-3, 26–27 cm, piece 3A). Small, euhedral grains of spinel are included in these olivine pseudomorphs as well as in phenocrystic plagioclase in the same glassy rims.

The presence of groundmass olivine, titanaugite, and titanomagnetite suggests that many of the microdolerites are alkaline in character.

Alteration

All 801B igneous rocks are variably altered, from at least 10% to as high as 75%. Surprisingly, the least altered one observed in thin section was Unit 14. It still has a thin (~1 cm) palagonitized glassy rim and, despite complete alteration of its few olivine and pyroxene phenocrysts, its plagioclase phenocrysts with delicate swallow-tailed crystal morphology are moderately well preserved. The most obvious sign of alteration in this unit is the presence of almost opaque, smectite-replaced glass behind the palagonitized rim. Unit 2 (Sample 129-801B-37R-1, 36–38 cm, piece 2) is the most altered sample studied under the microscope. Except for ~25% plagioclase, the unit is essentially made up of clays (Table 9). About 2% opaques are still visible but these are also rimmed or totally replaced with iron-hydroxide (limonite?). The style of alteration of other Hole 801B samples is generally within the range of these two extremes, except perhaps for the previously described bottom margin of Unit 7, which also had been clearly contact-metamorphosed, probably during the intrusion of Unit 8.

The most common type and also the probable first stage of alteration that occurred in these rocks was the transformation of glassy rim, as well as mesostasis, into yellow-brown palagonite and then, together with pyroxene and plagioclase, into pale to opaque brown and slightly greenish smectitic clays. Olivine, whenever present, is also altered to smectite and corrugated plates of talc(?) that are always spatially

Table 9. Approximate proportions (visual estimate) of primary and secondary phases in some representative igneous samples from Hole 801B.

Core, section Sample interval (cm) Piece number	129-801B-37R-1 36–38	41R-1 25–26 3	42R-1 86–89 5C	43R-1 20–21 4A	43R-2 103–104 5C	43R-3 35–37 2B	43R-3 37–39 2B	44R-3 25–26 3A	44R-3 26–27 3A
Primary minerals									
Olivine	—	—	—	o.p.	—	o.p.	—	—	o.p.
Plagioclase	25	45	45	38	50	1	59	30	35
Clinopyroxene	—	20	20	22	8	o.p.	tr	5	10
Titanomagnetite	2	4	3	5	7	2	2	8	5
Spinel	—	—	tr	—	—	—	—	—	tr
Mesostatis[a]	—	o.p.	o.p.	o.p.	o.p.	35	tr	o.p.	tr
Secondary minerals									
Palagonite	—	—	—	—	—	—	10	—	2
Smectitic clays	70	20	27	20	31	38	16	53	44
Carbonate	tr	5	1	tr	tr	tr	tr	2	4
Zeolites	—	2	1	3	1	—	3	1	tr
Chlorite	—	1	1	tr	tr	—	5	tr	—
Biotite	—	3	2	8	3	25	2	1	tr
Pyrite	—	tr	tr	—	—	—	—	—	—
Talc	—	—	—	4	—	—	—	—	—
Limonite	3	—	—	—	—	—	3	—	—

[a] Interstitial glass generally, except in Sample 129-801B-43R-3, 37–39 cm, piece 2B, in which it is composed of crystallites.
Notes: Dashes = not observed; o.p. = originally present but now almost entirely altered to clay; and tr = trace. Some of the olivine, plagioclase, and clinopyroxene in Sample 129-801B-43R-3, 35–37 cm, piece 2B, and Sample 129-801B-44R-3, 26–27 cm, piece 3A, occur as phenocrysts. The remainder of the primary minerals occur as groundmass phases.

restricted inside olivine pseudomorphs. Zeolites are also very common alteration products. These commonly occur as subparallel, clear, acicular prisms (phillipsite?) throughout the thin section. Less commonly, a variety of zeolites (natrolite?) occurs as irregular patches of radially arranged fibers inside plagioclase laths. Opaque grains, which are most probably titanomagnetites, are often rimmed with amorphous, dirty-white leucoxene(?) and pinkish iron-hydroxides, possibly limonite. Zeolite formation and titanomagnetite alteration were probably contemporaneous with smectite formation.

Chlorite is invariably present and probably also formed during the first stage of alteration because of its common occurrence with the clays. It must be noted, however, that some chlorite may have replaced some of the clays, which makes it suspect as a slightly later-stage alteration product. In any case, the formation of the bulk of the above-mentioned secondary minerals in the igneous rocks of the southern Pigafetta Basin probably occurred during a low-grade submarine alteration event in the zeolite facies.

Carbonate (invariably calcite) is also always present but occurs in variable amounts (Table 9). It is most commonly found replacing plagioclase but it also can be traced, together with clays, in altered olivine, pyroxene, and mesostasis. It is possible that calcite was formed together with the other secondary minerals during the low-grade submarine alteration stage, but because a majority of the several generations of veinlets are also infilled with carbonate (see below), some secondary calcite was formed or introduced into these rocks in several stages.

The brown, pleochroic biotite is quite different from the above secondary minerals because it commonly occurs as tiny grains or flakes (generally <1 mm) that commonly nucleate on the opaques or replace pyroxene and secondary minerals. A few isolated subhedral crystals of biotite were also observed in some thin sections. The formation of biotite is therefore considered to be the last stage of secondary alteration of the major phases in Hole 801B igneous rocks.

Trace amounts of pyrite were observed in a couple of thin sections (Table 9) and although they were put under secondary minerals, it is also possible that these are of magmatic origin (Deer et al., 1966).

Finally, it was mentioned previously that Units 1 to 4 are the most oxidized among the units. As in Hole 800A, these are the topmost units and may imply that the oxidation was due to the downwards percolation of oxygenated seawater probably soon after their emplacement. The fact that oxidation is most intense at the top of Unit 2 and slightly decreases towards its interior is consistent with this interpretation.

Fractures and Veins

All units are cut by veinlets to varying degrees (1% to 5%), with the top three units having the fewest veins. Veinlets range in width from ~0.1 mm to as much as ~1.5 cm, and as mentioned earlier, decimeter-sized pieces of veinlets or infill materials (as much as 15%) were recovered within Unit 9. A majority of the veinlets are subhorizontal but oblique (~45° dip) to vertical ones are not uncommon. In general, these veinlets have very irregular shapes; some are braided and branching, and cross-cutting is very common, suggesting that there are several stages of vein formation.

Calcite, quartz, green clays, and a combination of these are the vein materials that were commonly observed. There is no unequivocal evidence that would suggest the paragenesis of these minerals. Black, shiny veinlets infilled with dark, submetallic materials (manganese?) are limited to the oxidized Units 2 and 3 and perhaps represent the earliest generation of veinlets, as one of these is cut by a calcite veinlet. Moreover, a thin section of Unit 2 (Sample 129-801B-37R-1, 36–38 cm, piece 2) shows a manganese veinlet almost eradicated by clay alteration, suggesting that its formation was at least contemporaneous with, if not earlier than, the pervasive submarine alteration.

Geochemistry

Table 10 shows calcium carbonate, organic carbon, and sulfur contents of representative samples from the base of Hole 801B. Sulfur content is relatively low and quite normal for these igneous rocks. Calcium carbonate content, however, is generally high, which is consistent with the persistence of secondary calcite in all thin sections (Table 9). With the exception of one sample (129-801B-38R-1, 22–25 cm), carbonate concentration is generally higher in the lower part, starting from slightly below the top of Section 129-801B-44R-1. This could be due to the higher degree of oxidation and alteration of the upper units, but probably reflects the presence of more veinlets in the lower part of the hole (see previous discussion).

Hole 801C

Lithology and Mode of Emplacement

About 61 m of mostly igneous and a few sedimentary rocks were cored from 493.7 mbsf to 594.3 mbsf in Hole 801C. This represents an average recovery of 60.2%, the highest among the holes drilled during Leg 129. Thirty-two lithologic units were identified from the cored samples but only 29 of these are volcanic cooling units (Table 11, Fig. 38). Available data suggest that Unit 17 is a sheet flow, Unit 25 is a thick (>5 m) flow, Units 4 and 6 are intrusive bodies, and Units 9, 10, 11, 20, 29, 30, and 31 are pillow lavas. Data also suggest that Units 13, 16, 21, 22, and 24 are probably thin (~1 to 4 m thick) lava flows but, as in Hole 801B, the remainder of the cooling units without well-preserved boundaries were interpreted as thin lava flows. Actual observation of a few thin lava flows with preserved boundaries in cores in which recovery is good (i.e., ~50% recovery and higher as in Cores 129-801C-5R, -6R, -7R, and -9R) lends support to this interpretation. This is in sharp contrast with Hole 802A, in which the number of cooling units (mostly glassy pillow lavas) is relatively large where core recovery is good (see "Igneous Petrology" section, "Site 802" chapter, this volume). The most important features of some the Hole 801C petrologic units are presented below.

Table 10. Carbonate, organic carbon, and sulfur analyses for igneous rocks at the base of Hole 801B.

Core, section, interval (cm)	$CaCO_3$ (wt%)	C_{org} (wt%)	S (wt%)
129-801B-			
37R-1, 54–56	0.4	0.00	0.05
37R-1, 66–71	0.5		
38R-1, 22–25	1.9		
39R-1, 9–11	0.4		
40R-1, 20–23	0.2		
40R-1, 38–40	1.7	0.00	0.05
40R-1, 85–91	9.1		
41R-1, 26–31	6.8		
41R-2, 95–97	8.2	0.03	0.03
42R-2, 93–95	1.2	0.01	0.05
43R-1, 42–44	2.0	0.00	0.04
43R-3, 119–121[a]	23.0	0.06	0.00
44R-1, 52–54	8.8	0.03	0.04

[a] Contains veinlet.

Table 11. Extent of lithologic units actually observed in Hole 801C.

Unit	Top	Bottom	Thickness (cm)
	129-801C-	129-801C-	
1	1R-1, 0 cm	1R-3, 103 cm	363
2	1R-3, 103 cm	1R-6, 131 cm	395
3	2R-1, 0 cm	2R-3, 63 cm	347
4	2R-3, 63 cm	2R-3, 110 cm	47
5	2R-3, 110 cm	2R-3, 115 cm	5
6	2R-3, 115 cm	2R-5, 118 cm	248
7	3R-1, 0 cm	3R-1, 100 cm	100
8[a]	4R-1, 0 cm	4R-2, 128 cm	264
9	5R-1, 0 cm	5R-3, 69 cm	324
10	5R-3, 69 cm	5R-3, 104 cm	35
11	5R-3, 104 cm	5R-3, 150 cm	46
12[a]	5R-4, 0 cm	5R-4, 31 cm	31
13	5R-4, 31 cm	5R-5, 130 cm	241
14	5R-5, 130 cm	5R-5, 142 cm	12
15[a]	6R-1, 0 cm	6R-1, 96 cm	96
16	6R-1, 96 cm	6R-2, 137 cm	170
17	6R-2, 137 cm	5R-2, 150 cm	13
18	6R-3, 0 cm	6R-3, 14 cm	14
19	6R-3, 14 cm	6R-3, 34 cm	20
20	6R-3, 34 cm	6R-5, 44 cm	294
21	6R-5, 44 cm	7R-1, 129 cm	195
22	7R-1, 129 cm	74-2, 143 cm	159
23	7R-3, 0 cm	8R-1, 32 cm	389
24	8R-1, 32 cm	8R-2, 142 cm	216
25	9R-1, 31 cm	10R-6, 75 cm	1345
26	10R-6, 81 cm	11R-1, 17 cm	70
27	11R-1, 17 cm	11R-2, 126 cm	248
28	11R-2, 126 cm	11R-3, 60 cm	84
29	11R-3, 60 cm	12R-1, 5 cm	102
30	12R-1, 19 cm	12R-1, 49 cm	30
31	12R-1, 49 cm	12R-1, 150 cm	101
32	12R-2, 0 cm	12R-3, 91 cm	234

[a] Not cooling unit. Unit 8 is a hydrothermal deposit, Unit 12 is an interpillow deposit, and Unit 15 is composed of basaltic fragments of questionable order and orientations.

Unit 3 in Core 129-801C-2R is an aphyric basalt and, although the actual top contact was not recovered, it had a glassy top rim with sparse plagioclase phenocrysts. It contains a few, randomly distributed, subrounded, millimeter-sized carbonate grains and is diagonally (40° inclination) intruded by 47-cm-thick Unit 4, which has dense, brownish, moderately plagioclase, microphyric glassy top and bottom margins (Fig. 39). It is interesting to note that Unit 13 in Hole 801B has textural features very similar to Unit 3 of Hole 801C and, although at a higher level, is intruded by a 34-cm-thick subrounded apophysis of Unit 14, which is a dense, brownish, moderately plagioclase phyric glassy basalt (see previous discussion and Fig. 37). Moreover, Unit 13 of Hole 801B and Unit 3 of Hole 801C are at about the same level below seafloor and are only several meters apart (see "Operations" section, this chapter). Based on these observations, these four units were used as the basis for correlating the few overlapping cooling units of Hole 801B and 801C (Fig. 39).

Unit 6 is separated from Unit 4 by 5-cm-thick Unit 5, which is an aphyric basalt probably separated from Unit 3 during the intrusion of Unit 4 (Fig. 40). Unit 6 also intruded Unit 5 and has an inclined, dense, brownish, sparsely plagioclase phyric glassy rim quite similar to the glassy margin of Unit 4. Thus, both Units 4 and 6 may have come from the same body although the latter grades to an aphyric microdolerite because it is relatively thick (248 cm; Table 11).

A highly silicified, yellow hydrothermal deposit (Unit 8) was the only sample recovered in Core 129-801C-8R. It is important to note that, although not a cooling unit, the formation of this deposit may have affected the style of alteration of the underlying units, and surprisingly, the overlying Unit 7 as well (see below). If this is the case, then the hydrothermal activity that deposited Unit 8 must have continued for some period of time even if the deposit had been covered by later lava flows.

Subrounded margins of pillow lavas rimmed with devitrified glass were recovered in Units 9, 10, and 11 (Fig. 41). These are in contact with reddish and white carbonate ± greenish clay (e.g., Unit 12), which are probably previous interpillow sediments but are now almost totally replaced. The pillow lavas are interbedded with thin lava flows. A devitrified sheet flow (Unit 17) occurs below the sequence of pillows and flows in Core 129-801C-5R.

Unit 25 is an unusually thick (~13.5 m) lava flow that was fully recovered in Cores 129-801C-9R and -10R (Fig. 38). This unit contains several interesting features, interpreted as the result of flow differentiation, that also characterize some of the thin flows directly above and below this unit. It is a fine-grained, aphyric basalt but it contains variable patches or layers with sparse plagioclase and/or olivine microphenocrysts. It also contains subrounded to rounded vesicles that range in size from 0.1–0.6 mm and in amount from 0%–5%, generally distributed at random at different levels within the unit. The vesicles are always infilled with green, smectitic(?) clays or white calcite ± fine pyrite. Although it is not uncommon to find smectite and calcite (and even pyrite, but in a much lesser amount) to be concentrically interlayered within a single vesicle, it is important to note that calcite- and smectite-infilled vesicles usually occur at separate levels within the unit. This usually gives the flow units alternating, conspicuous, white and very dark green spotted zones. The only characteristic feature of the vesicles that was not observed in the flows, other than in Unit 25, is that these attain sizes up to 5 mm in diameter. These large vesicles are almost exclusively infilled with white calcite and occur in a ~2-m section just 1 m above the base of Unit 25.

Petrography

A majority of the cooling units are fine-grained, aphyric basalts, particularly those in the lower portion of Hole 801C (Fig. 38). Samples from the lower portion of the hole are slightly finer in grain size, less variable in texture, and as previously mentioned, more vesicular than those in the upper portion. The overall texture of the upper cooling units (i.e., Units 1 to 6) in Hole 801C are similar to those of the lower units in Hole 801B. For example, Units 3 and 4 of Hole 801C are texturally very similar to Units 13 and 14 of Hole 801B, as already mentioned. Moreover, the coarsest unit recovered in Hole 801C is the aphyric microdolerite Unit 1, which has a very similar texture and degree of alteration (e.g., presence of secondary biotite in Sample 129-801C-1R-1, 119–120 cm, piece 2G) to some of the aphyric basalts and microdolerite units in Cores 129-801B-41R to -44R (Table 9).

Except for Unit 9, which contains 6% to 10% plagioclase phenocrysts that are up to 4 mm in size, the rest of the units generally range from sparsely to moderately microphyric (1% to 4% phenocrysts), and contain fine-grained (~1 mm on the average) crystals of plagioclase and olivine or only plagioclase. These are typically set in a hypocrystalline groundmass consisting of plagioclase, pyroxene, olivine, titanomagnetite, and mesostasis. The estimated proportions of glass, mesostasis, crystallites, and primary minerals in thin sections are shown in Table 12.

Another important feature shown by the thin-section data is that a majority of Hole 801C basalts have olivine, at least in the groundmass (Table 11). Moreover, one of the samples

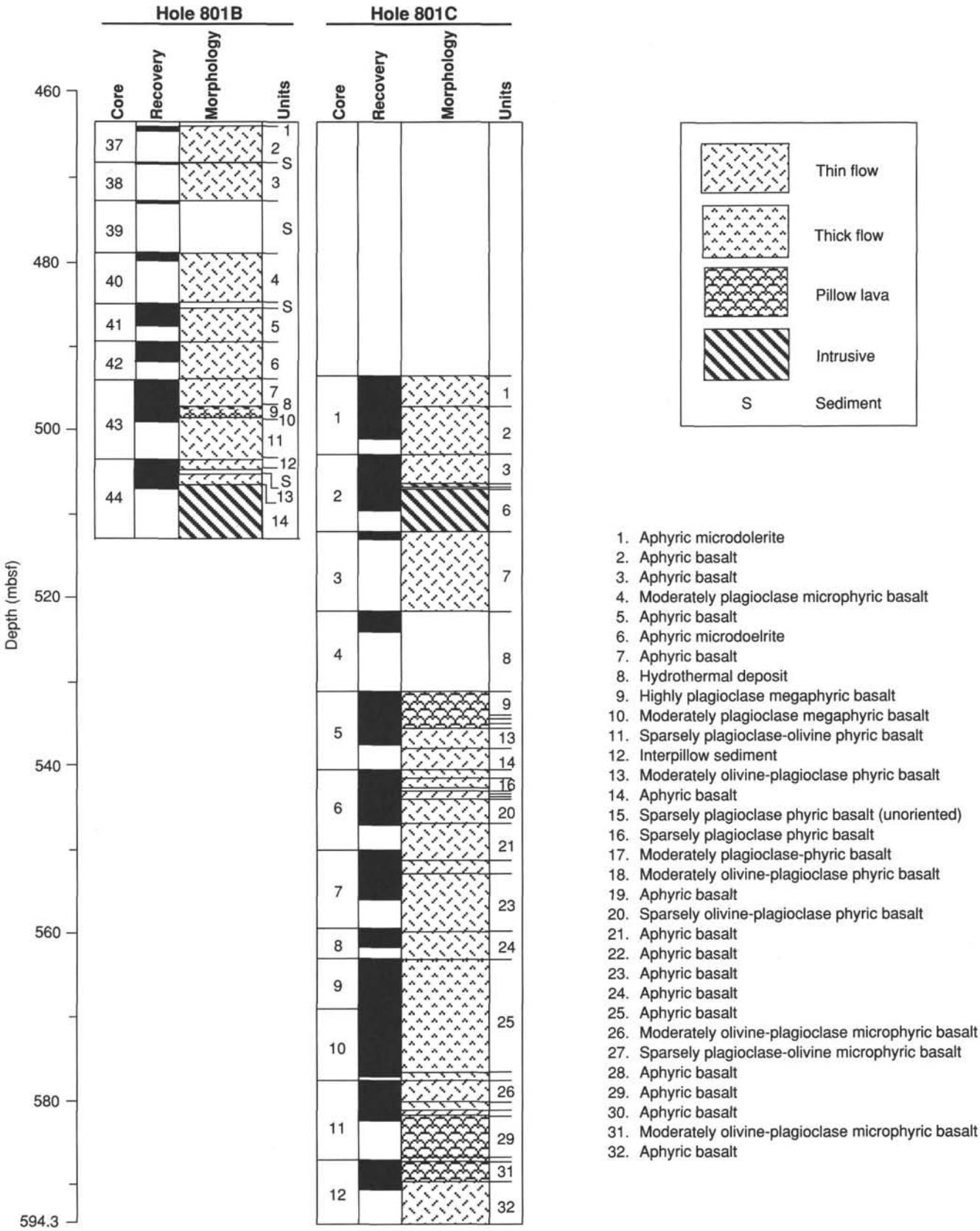

1. Aphyric microdolerite
2. Aphyric basalt
3. Aphyric basalt
4. Moderately plagioclase microphyric basalt
5. Aphyric basalt
6. Aphyric microdoelrite
7. Aphyric basalt
8. Hydrothermal deposit
9. Highly plagioclase megaphyric basalt
10. Moderately plagioclase megaphyric basalt
11. Sparsely plagioclase-olivine phyric basalt
12. Interpillow sediment
13. Moderately olivine-plagioclase phyric basalt
14. Aphyric basalt
15. Sparsely plagioclase phyric basalt (unoriented)
16. Sparsely plagioclase phyric basalt
17. Moderately plagioclase-phyric basalt
18. Moderately olivine-plagioclase phyric basalt
19. Aphyric basalt
20. Sparsely olivine-plagioclase phyric basalt
21. Aphyric basalt
22. Aphyric basalt
23. Aphyric basalt
24. Aphyric basalt
25. Aphyric basalt
26. Moderately olivine-plagioclase microphyric basalt
27. Sparsely plagioclase-olivine microphyric basalt
28. Aphyric basalt
29. Aphyric basalt
30. Aphyric basalt
31. Moderately olivine-plagioclase microphyric basalt
32. Aphyric basalt

Figure 38. Summary of lithostratigraphy of igneous rocks in Holes 801B and 801C.

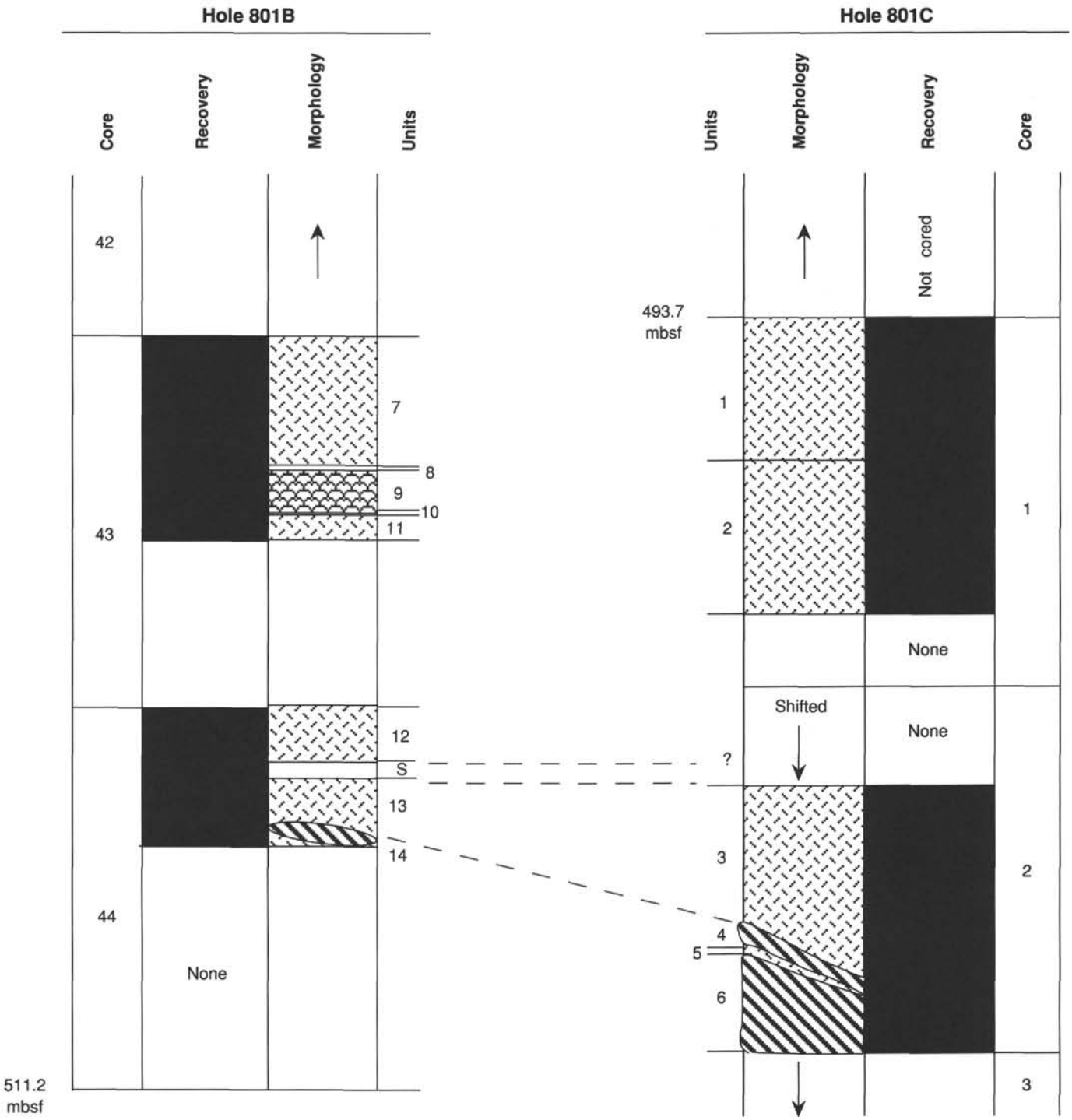

Figure 39. A tentative correlation between Units 13 and 14 of Section 129-801B-44R-3 and Units 3 and 4 of Sections 129-801C-2R-1 to -2R-3. See text for explanation. Stratigraphic correlation above these units is difficult to make because of a lack of close similarities among the other recovered units. See Figure 38 for explanation of symbols. Recovered samples were shifted into the lower portion of Core 129-801C-2R in order to match the top of the presumably flat-lying lava flows in Sections 129-801B-44R-3 (Unit 13) and 129-801C-2R-1 (Unit 3).

studied (129-801C-5R-5, 70–71 cm, piece 3D) has brown, spinel microphenocrysts (up to ~0.4 mm in size), which are either free-floating or enclosed in phenocrystic olivine. These data suggest that olivine (± spinel) is a liquidus phase in a majority of Hole 801 basalts and that their crystallization sequence is olivine (± spinel)-clinopyroxene-plagioclase, which is typical of primitive mid-ocean ridge basalts. Groundmass olivine is typically granular whereas phenocrystic olivine ranges from hopper-shaped to subhedral- and even euhedral-shaped crystals.

The margins of pillow lavas (Fig. 41) and thin lava flows (Fig. 42) appear to have well-preserved glassy rims. However, thin-section examination also showed that all of these had been completely devitrified and altered to brown, almost opaque smectitic clays. These glassy rims generally grade to a variolitic to spherulitic zone and finally to a hypocrystal-

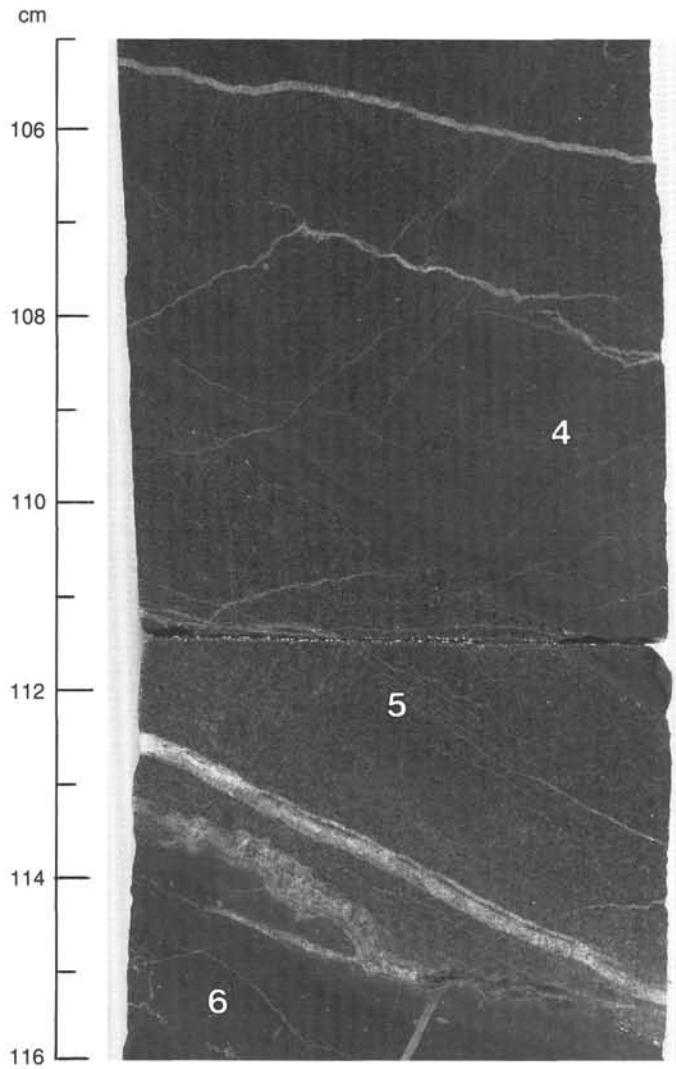

Figure 40. Photograph illustrating the contacts between Units 4 and 5, and between Units 5 and 6. Interval 129-801C-2R-3, 105–116 cm. (Numbers in the photograph correspond to respective units.) The contact of Unit 4 with Unit 5 is relatively sharp and originally glassy, whereas that of Unit 6 with Unit 5 is cuspate although originally glassy. The texture of Unit 5 is generally constant; except in thin section, its crystals are clearly cut or abruptly terminated by the opaque brown, smectitic rims of Units 4 and 6.

line interior, which is typical of submarine extrusive lavas. The typical texture of the interior of Hole 801C pillow and flow basalts range from intergranular to intersertal.

Alteration

The thin flows and pillow lavas of Hole 801C are moderately to highly altered and exhibit a higher degree and a wider range of alteration features than seen previously in samples from the other holes. Apart from typical, low-grade submarine alteration of the matrix and ubiquitous carbonate-smectite veinlets, there are hydrothermal breccia zones and vesicles infilled with secondary minerals. In general, however, the degree of alteration is often highly variable from core to core, and shows no clear relationship to depth or cooling unit type. For example, although the most highly altered basalts occur immediately below the hydrothermal deposit (see below) in the pillow lavas and thin flows of Units 9 to 13 (Core

Figure 41. Subrounded portions of pillow lavas separated by interpillow material that has altered to smectite and carbonate. Note the light gray-colored, relatively sharp, originally glassy margins of the pillows. Interval 129-801C-5R-3, 118–147.

129-801C-5R), units above (including those in Hole 801B) and below this zone are slightly to moderately altered. The intensity and type of alteration can also vary considerably within any cooling unit, such that the upper segment may show a high proportion of smectitic clays, whereas the central and lower part is dominated by relatively minor carbonate replacement (e.g., Units 9 and 24).

A late, oxidative type of alteration, which is typically absent from the other sites, is particularly well developed at

Table 12. Visual estimate (in vol%) of proportion of primary and secondary minerals from thin-section studies, Hole 801C.

Core, section	129-801B-1R-1	2R-2	2R-3	5R-1	5R-1	5R-5	7R-3
Sample interval (cm)	119–120	2–3	64–68	12–13	124–125	70–71	64–66
Piece number	2G	1A	2A	2A	4	3B	3A
Phenocrysts							
Olivine	—	—	o.p.	o.p.	o.p.	o.p.	—
Plagioclase	—	—	o.p.	o.p.	o.p.	—	—
Spinel	—	—	—	—	—	tr	—
Primary minerals							
Olivine	o.p.	o.p.	—	o.p.	o.p.	o.p.	o.p.
Plagioclase	50	60	—	10	20	35	30
Clinopyroxene	12	7	—	tr	0	35	15
Opaques	8	4	1	1	tr	1	3
Glass + spherulites[a]	o.p.	o.p.	40	o.p.	o.p.	—	o.p.
Spinel	—	—	—	—	—	tr	—
Apatite	tr	—	—	—	—	—	—
Secondary minerals							
Clays	25	18	50	66	60	27	51
Carbonate	—	10	5	3	5	—	1
Zeolites	4	1	—	—	—	—	—
Chlorite	tr	—	—	—	10	—	—
Limonite	—	—	4	20	5	—	—
"Iddingsite"	—	—	—	tr	tr	tr	—
Talc	—	—	—	tr	tr	—	—
Quartz	—	—	—	tr	tr	—	—
Prehnite	tr	tr	—	—	—	—	—
Biotite	1	tr	—	—	—	—	—
Hematite	—	—	—	—	—	2	—

[a] Includes mesostasis glass.
Notes: Dashes = not observed; o.p. = originally present but totally altered; and tr = trace.

the top of Unit 9 (interval 129-801C-5R-1, 0–35 cm). In Unit 9, there exists a sharp boundary between the upper brownish oxidized zone (with limonite and hematite) and the lower, adjacent light gray colored zone (with carbonate and smectite) (Fig. 43). The oxidative alteration is post-clay production as the green smectites are colored red, and being related to the top of the unit, indicates the oxidizing fluid was downward percolating seawater. This oxidized flow top may represent either a pause in a fairly rapid and continuous extrusion of lavas to allow time for alteration by seawater or, alternatively, may be directly related to the hydrothermal activity that formed the deposit just directly above Unit 9. Either case is consistent with the general lack of interflow oxidized zones throughout the lava pile except that the presence of a similar, but definitely smaller, type of oxidative alteration in the reverse order (i.e., brownish oxidized zone below and light gray-colored zone above) in Unit 7 directly above the hydrothermal deposit tends to favor the latter scenario. The presence of scattered pristine pyrite in most cooling units of Hole 801C indicates a predominantly reducing environment was (and has been) maintained throughout the lavas.

In general, alteration affected a number of different domains and environments within the Hole 801C lava sequence: matrix (including phenocrysts and mesostasis), vesicles, interpillow material, veins, and brecciated zones. Some of the typical features exhibited are described below.

Matrix

Matrix color often provided a visible means to the presence and domination of secondary minerals, such that strong green indicates smectite replacement, whereas pale gray indicates carbonate replacement. Color zonation is characteristic of some of the units directly below the hydrothermal deposit of Unit 8. Both groundmass and microphenocrystic olivine was always totally replaced, either by dirty green smectite with iddingsitic (or limonitic) veinlets or irregular carbonate patches within smectite. Depending on the degree of alteration, plagioclase was variably replaced by pale green and brown to opaque smectites, minor limonite, carbonate, zeolite, and prehnite. Clinopyroxene is often fresh, but under extreme conditions can be totally replaced by clays and limonite. Other secondary matrix minerals include two types of zeolite, one forming hemispheres of radiating fibers replacing mesostasis glass (natrolite?) and the other, acicular clear prisms (phillipsite?) piercing plagioclase laths. The devitrified glass along the rims of cooling units and spherulite zones directly below these are always replaced by brown smectites. In medium-grained hypocrystalline basalts in the upper units of Hole 801C, biotite may be developed from elongate titanomagnetite needles (e.g., Sample 129-801C-1R-1, 119–120 cm, piece 2G), but is relatively rare. Mesostasis glass is totally replaced by brown smectite or sometimes a radiate zeolite.

Vesicles

Thin-section examination confirmed the presence of small, subrounded to rounded vesicles, infilled with either smectite or carbonate. Some of the infilling materials are zoned with a thin, pale green, granular smectite rim and an interior of either dark green radiating fibers of smectite or carbonate plates or more rarely, pyrite. A few rare examples were observed of vesicle walls decorated with scattered pyrite granules and an interior of smectite. Based on observation, the general order of development and replacement within vesicles appears to be (1) pale smectite, (2) dark green smectite, (3) pyrite, and, finally, (4) carbonate.

Figure 42. A typical recovered margin of a volcanic cooling unit in Hole 801C. Interval 129-801C-1R-3, 103–109. From top to bottom, a thin glassy rim, a spherulitic zone, and a hypocrystalline interior. The glass is totally replaced by brown smectitic clays and the spherulitic zone and the hypocrystalline interior are also in various degrees of alteration.

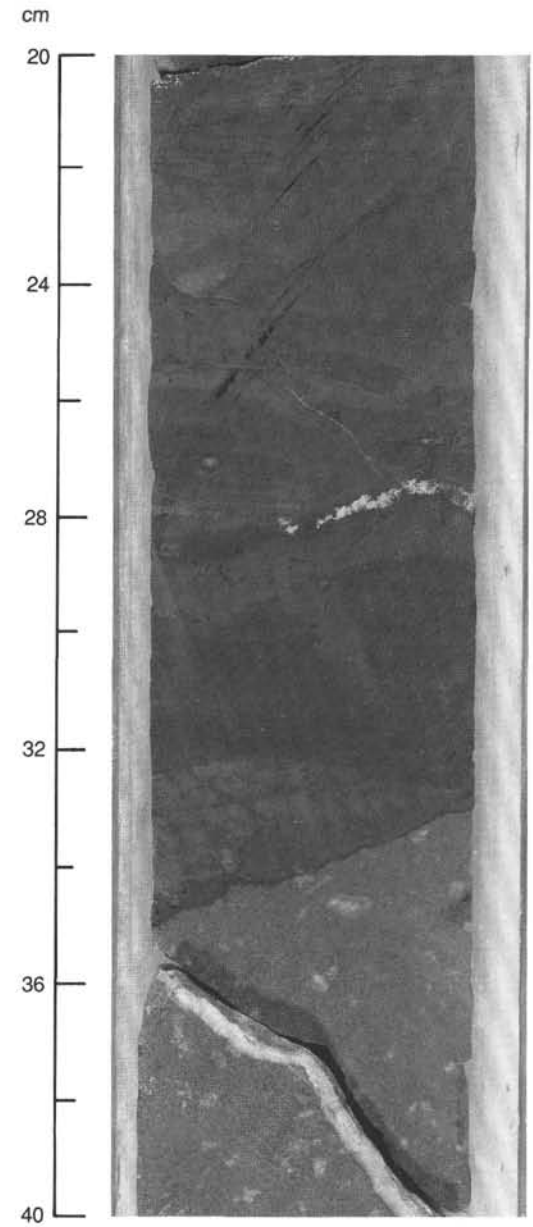

Figure 43. Sharp demarcation of the lower margin of the oxidized zone at the top of Unit 9. The white crystals in the lower part of the photograph are carbonate-replaced plagioclase megaphenocrysts. Interval 129-801C-5R-1, 20–40 cm.

Because of the hydrostatic pressure of seawater at normal depths of mid-ocean ridges (3–4 km), vesiculation caused by the exsolution of water vapor from basaltic lava is generally inhibited; thus, the presence of a small volume of vesicles in some Hole 801C lavas implies either a "shallow" active axis or possibly the presence of gases (e.g., carbon dioxide) other than water vapor.

Interpillow Material

Altered material fills the spaces between the pillows of Unit 11 (Section 129-801C-5R-3) and is composed of greenish, smectite-replaced, glassy, spherulitic fragments derived from the pillow margins during rapid quenching (Fig. 44). Unit 12 (interval 129-801C-5R-4, 0–31 cm) is entirely composed of interpillow sediments and, in this case, consists of a reddish, highly calcareous material with relicts of small fragments of brown claystone hydrothermal deposit similar to that in Unit 8, and basalt.

Veins

Small, ramifying, cross-cutting veinlets of widely varying widths (0.1–80.0 mm) are very common throughout the lava sequence. These are generally randomly oriented and are commonly infilled with either carbonate or smectite. If there is a mixture of both phases, the carbonate generally is later and occupies the central portion of the larger veins. Pyrite may also occur as minute veinlets or lines the walls of the fractures infilled with smectite or carbonate. Some veinlet halos (e.g., in Units 27, 28, and 29) consisting of more clay-rich groundmass also contain very finely disseminated pyrite. In more oxidized sections, limonite and hematite, which the likely result of oxidation of pyrite, are present, forming a yellowish or brownish margin to the veinlets. Larger veins (up to 30 mm) may have multiple or zoned deposits of carbonate, smectite, pyrite, and quartz, suggesting a number of stages of fracturing and infilling.

Brecciated Zones

Units 9, 13, and 24 contain highly irregular (10–35 mm wide), subvertical breccia zones filled with angular basaltic material derived from the adjacent lavas and cemented by late green smectite and carbonate. Brecciation in Unit 9 extends over 1 m of core, with large, angular, displaced blocks at the base, ending in a close-fitting mosaic of smectite netveined fragments, and may be related to the hydrothermal activity that formed Unit 8 directly above it. However, the presence of brecciated zones in other zones away from Unit 8 may also be

Figure 44. A close-up photograph of the interpillow material shown in Figure 41. The material is altered to smectite and carbonate, with glassy pillow fragments showing spherulitic texture (white dots).

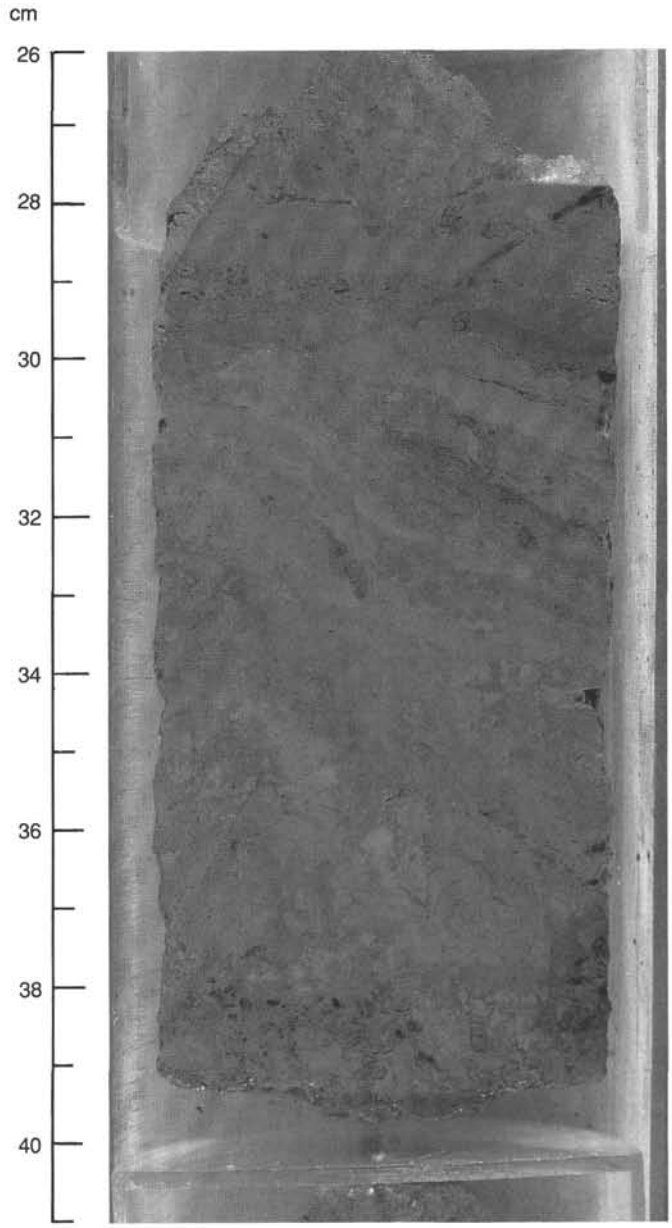

Figure 45. Disrupted, color-zoned, irregular laminations within the yellow hydrothermal deposit. Interval 129-801C-4R-2, 26–40 cm.

interpreted as small, hydrothermally brecciated pipes produced by the sudden release of water-rich volatiles possibly trapped within pillows or flows.

Hydrothermal Deposit

Unit 8 (Sections 129-801C-4R-1 and 129-801C-4R-2) within the basalt lavas is a bright yellow, ochrous material cemented by silica and interpreted as a hydrothermal, iron-rich precipitate. It is composed of somewhat irregular, yellow bands which may show botryoidal hemispheres or radiate coalesced spheres on the upper surface of the bands that merge together downward. Much of the banding is disrupted, however, with broken and disorientated fragments apparently suspended in a silica matrix (Fig. 45). Some fragments are color zoned with paler yellow margins and exhibit minute, internal shrinkage cracks. Without X-ray-diffraction analysis confirmation, it was considered that the yellow material was probably some form of Fe oxyhydroxide.

Thin-section examination revealed growth patterns and a number of development stages for the hydrothermal deposit. Much of the yellow, iron-rich material is composed of small interlocking platelets with a dark red granular core, and occasional star-shaped shrinkage cracks. Other morphologies show hemispherical or small columnar forms with circular and asymmetric growth rings, respectively, nucleated on an opaque growth point. Many of the better-developed hemispheres and almost spherical bodies exhibit a radial fibrous structure. This preliminary examination suggests a possible sequence of events as follows: The forms exhibiting growth rings appear to be the original material, deposited layer by layer, possibly from a colloid that subsequently devitrified with the development of radially disposed fibers. Further development is represented by the formation of fine shrinkage

cracks that define the edges of the yellow platelets subsequently formed by recrystallization of the original growth-ring bodies. Relicts of hemispheres and their growth point may sometimes be seen within a group of adjacent platelets. After this stage, the crudely layered deposit was partly replaced by silica, which contains relicts of the platelets within patches of small equant quartz crystals. The apparently forceful invasion by silica-rich solutions also disrupted the layering, enclosing angular yellow fragments within a silica "matrix." Finally, the iron-silica deposit was fractured and further siliceous solutions formed the coarser grained quartz veins that traverse the whole deposit. Some veins have a vuggy interior lined with the inward pointing terminations of quartz crystals.

It seems likely that this approximately 3-m-thick (after recovery) iron-silica-rich deposit was formed by precipitation from seawater enriched by hydrothermal solutions ultimately derived from Jurassic "black smokers" situated in an active ridge system. However, the apparent lack of associated metalliferous sediments or sulfides in the deposit could imply that it was formed some distance away from the active axial zone. Alternatively, it is possible that this deposit was formed near silica-rich "white smokers" on the ridge flanks.

Geochemistry

Table 13 shows calcium carbonate contents of representative samples from Hole 801C. Similar to the samples from the bottom portion of Hole 801B, calcium carbonate contents of Hole 801C samples are generally high except for that from the hydrothermal deposit (Sample 129-801C-4R-1, 44–46 cm). Some of the higher values may be due to the nearness of the sample analyzed to a carbonate veinlet, but even if these were excluded, Hole 801C and Hole 801B samples, on the average, have the highest carbonate contents among the basaltic rocks from all sites. This is confirmed by the presence of moderate amounts of secondary carbonate (up to 10 vol%) in a majority of thin sections examined (Table 11).

Summary and Conclusion

1. Site 801 igneous rocks were recovered from below Middle Jurassic (~165 Ma) sediments.

2. Fourteen cooling units were observed in Hole 801B and 29 in Hole 801C. A vast majority of these units are basalts and the rest are dolerites, microdolerites, and a basaltic andesite.

3. Cooling unites in Holes 801B and 801C are morphologically and petrographically similar to typical ocean ridge lavas. These were emplaced as lava flows and pillow lavas with variably altered glass along their rims and all the textures typical of basalts erupted in a marine environment. The units contain predominantly plagioclase, varying proportions of clinopyroxene and titanomagnetite. Olivine (± spinel) occur only in a few samples from Hole 801B but are more common in samples from Hole 801C.

4. Site 801 igneous rocks are moderately to highly altered. The stratigraphically higher Hole 801B units were variably affected by low-grade alteration in the zeolite facies. The main alteration products are clays (mostly smectite), carbonate, zeolites, chlorite, iron-hydroxides, and talc(?). Biotite is also present but its formation probably occurred later and possibly at a slightly higher grade of alteration. The stratigraphically lower Hole 801C units exhibit a wider range and generally higher degree of alteration features. In addition to the type of alteration observed in Hole 801B, Hole 801C units are generally more vesicular and contain secondary features, which are probably related to hydrothermal activities.

5. Calcium carbonate contents of Site 801 igneous rocks generally increase downward in Hole 801B and remain generally high throughout Hole 801C, except in the hydrothermal deposit. Calcium carbonate contents of Site 801 basaltic rocks are the highest among the sites drilled in Leg 129.

6. Based on these observations, we propose that Site 801 basaltic rocks represent a piece of Pacific oceanic crust that was formed in the Jurassic.

DOWNHOLE MEASUREMENTS

Operations

On 14 December 1989, after reaching a total depth (TD) of 511.2 mbsf in Hole 801B, a complete wiper trip was made and salt water was circulated in preparation for logging. The bit was dropped at the bottom of the hole and pipe was raised to 77.6 mbsf. The last circulation into Hole 801B was at 0200 hr UTC on 15 December. Logging operations began at 0515 hr on 15 December 1989 and were completed at 0430 hr on 16 December, corresponding to a total logging time of 23.25 hr (Table 14). The pipe was pulled to 78 mbsf for the beginning of

Table 13. Carbonate content of basaltic samples from Hole 801C.

Core, section, interval (cm)	$CaCO_3$ (wt%)
129-801C-	
1R-1, 90–92	3.5
1R-3, 82–84	8.0
1R-5, 29–31	3.4
2R-1, 14–16	6.0
2R-2, 81–83	8.6
2R-4, 76–78	11.4
3R-1, 32–34	3.4
4R-1, 44–46	0.1
5R-1, 103–105	7.2
5R-2, 87–89	13.3
5R-3, 43–45	7.2
6R-1, 115–117	17.7
6R-2, 35–37	5.9
6R-4, 111–113	3.4
6R-5, 68–70	5.7
7R-1, 35–37	3.0
7R-2, 37–39	7.7
8R-1, 65–67	11.9
8R-2, 78–80	6.7

Table 14. Actual time schedule (UTC) for logging operations at Hole 801B, including a list of tools used during each logging run.

Tool String	Time	Procedure
Quad Combination (TCCB-LSS-HLDT-NGT-DIL-TLT)	RIH 0515 hr UTC 15 December 1989 POOH 1145 hr	Log down to 470 mbsf, log up to 64.4 mbsf. Log down to 167 mbsf, log up to 64.4 mbsf.
Formation Microscanner (FMS-TCCB-NGT-TLT)	RIH 1330 hr POOH 1950 hr	Run down to 470 mbsf, log up to 64.4 mbsf. Run down again to 470 mbsf, log up to 64.4 mbsf.
Geochemical Combination (TCCB-NGT-ACT-GST)	RIH 2100 hr POOH 0430 hr 16 December 1989	Run down to 452 mbsf, log up to 54.1 mbsf. Run down to 166 mbsf, log up to 54.1 mbsf.

Notes: Total logging time is 23.25 hr, including initial rig-up and final rig-down of tool strings. Abbreviations are as follows: TCCB = telemetry tool; FMS = formation microscanner; LSS = long-spaced sonic tool; ACT = aluminum clay tool; HLDT = lithodensity tool; GST = induced gamma-ray spectrometry tool; NGT = natural gamma-ray spectrometry tool; RIH = run in to hole; DIL = dual induction tool; POOH = pull out of hole; TLT = Lamont temperature tool.

each logging run and raised to approximately 64 mbsf while logging uphole.

The quad combination tool string included, from top to bottom, telemetry, long-spaced sonic, lithodensity, natural gamma-ray spectrometry, dual-induction resistivity tools, and the Lamont temperature tool (TLT). These tools were rigged at 0515 hr on 14 December, creating a tool string 30.72 m long. At 0655 hr this string was run down to 6.5 m below the mud line and held stationary for 3 min to obtain a bottom-water calibration point for the TLT. The depth to the end of pipe recorded on this logging run was within 2.1 m of that calculated by the driller. As logging continued downhole it was reported that the wireline heave compensator (WHC) was not operating. The WHC again had checked out without any additional load applied and failed under full tensional load. Down-going data were recorded while the tool string was lowered downhole until a bridge was encountered at 470 mbsf. Logging data were recorded successfully as the tool string moved uphole at 300 m/hr from 470 to 64.4 mbsf (Fig. 46) with a repeat section taken from 167 to 64.4 mbsf. The bottom of the pipe was encountered at approximately 64.4 mbsf and another bottom-water temperature calibration point for the TLT was obtained inside the pipe at 14.5 m below the mud line. The quad combination tool string was returned to the rig floor at 1145 hr on 15 December. The TLT was then taken from the rig floor to the downhole measurements lab, opened, and hard-wired to the Masscomp computer to download the recorded temperature/time measurements.

The formation microscanner (FMS) string included telemetry, natural gamma-ray spectrometry, general-purpose inclinometer, the FMS, and the TLT. This tool string was rigged and in the hole at 1330 hr on 15 December. This tool combination was lowered down the pipe and held stationary for 3 min at 14.5 m below the mud line to obtain a bottom-water calibration point for the TLT. Two full passes of FMS data were recorded uphole at 260 m/hr from 470 to 64.4 mbsf with no problems. The FMS tool string was run twice with the hope that the tool would be rotated on the second run relative to the first in order to obtain greater coverage of the borehole wall, and indeed this was the case. Another bottom-water temperature calibration point for the TLT was obtained inside the pipe at 14.5 m below the mud line. The WHC was also successfully operating during both of the FMS runs but failed to operate during the subsequent geochemical logging run. The FMS tool string was returned to the drill floor at 1950 hr on 15 December.

The final run at Site 801 was with the geochemical combination tool string, which included telemetry, natural gamma-ray spectrometry, aluminum clay, and induced gamma-ray spectrometry tools. The string was rigged at 2100 hr on 15 December, creating a tool string 18.13 m long. The tool string encountered the bridge at 470 mbsf and logging data were recorded from 452 mbsf up into pipe at 64.1 mbsf as the tool string moved uphole at 200 m/hr (Figs. 47 and 48). A repeat logging run beginning at 166 mbsf was also completed.

This final logging run ended at 0430 hr on 16 December with all tools off of the wireline and secured on deck. All logging runs were shifted by the Schlumberger engineer relative to the quad combination logging run using the natural gamma-ray log response. The geochemical and FMS runs were shifted to shallower depths by 4.27 m and 7.9 m, respectively. All logs were then tied into the drill-string depth.

Log Quality

The logs are generally of good quality (Figs. 46, 47, and 48). The raw sonic data, however, required significant shipboard processing and editing in an attempt to create a useful sonic log (Figs. 46 and 49). The data recorded from the induced gamma-ray spectrometry tool require post-cruise processing; references made to silicon, calcium, and iron are therefore only broadly qualitative. In contrast, the natural gamma-ray spectrometry tool produces reliable values for the concentration of potassium, thorium, and uranium, and the aluminum clay log is generally little improved through post-cruise processing. The quad combination and geochemical logs are not obviously affected by the ship's heave; the small degree of elasticity within the wireline summed over its extreme length (6000 m) may have acted to slightly decouple these logging tools from the heave of the ship. The WHC was operational only during the FMS logging run and effectively decoupled the FMS tool string from the heave of the ship. No adverse effects from the ship's motion are apparent on the raw FMS records; however, the FMS data will still require significant shore-based image-processing to achieve an interpretable record.

Summary log figures appear at the end of this chapter. The FMS images are presented on microfiche in the back of this volume.

Logging Units

Five logging units were identified in Hole 801B (Figs. 46 to 50), based on log response and analyses of recovered cores, but are not to be confused with the lithologic units defined previously (see "Lithostratigraphy and Sedimentology" section, this chapter). The boundaries between adjacent logging units were placed at significant inflection points resulting from simultaneous variations on at least several of the logs illustrated in Figures 46 to 50. These units display consistent log responses or distinct overall trends. In general, the logging unit boundaries in Hole 801B are characterized by a single shift in the log values rather than the sinusoidal log responses observed at Site 800. The potassium values displayed much greater variability at this site than at Site 800 and were used effectively to choose logging boundaries, whereas the calcium values were more uniform at this site and less useful for defining logging units.

Core recovery was poor throughout most of the logged interval (less than 10%) and only fragments of the most indurated portions of the formation were usually recovered. The lithologies for unrecovered intervals have been inferred from the logs based on the broad assumption that the logging tools responded to varying proportions of the primary constituents in samples actually recovered (e.g., biogenic silica, carbonate, pelagic clay, and volcanogenic clay) and to their relative porosity.

Logging Unit 1 (64.4–126 mbsf)

Logging Unit 1 is characterized by generally high sonic velocity (2.1–2.6 km/s), resistivity (2–6 ohm-m), density (1.8–2.0 g/cm^3), silicon content, and variable but relatively high sulfur content along with relatively low values of aluminum (.5 wt%), iron, and total gamma-ray counts (22–30 API). Logging Unit 1 is also uniquely distinguished by relatively low thorium (1.2–1.8 ppm) and potassium (.4–.8 wt%) concentrations and relatively high uranium values (.5–1.25 ppm). This kind of log response is indicative of a diagenetic interval in which pore spaces are filled with recrystallized silica where the mobile uranium ion was concentrated. The overall log responses suggest that the porcellanite and chert fragments recovered in this section accurately reflect the most indurated portion of this formation. The variability in the above-mentioned logs indicates the presence of unrecovered clay-rich intervals (e.g., pelagic clay, 98–103 mbsf, and volcanogenic clay, 111–116 mbsf). The boundary between logging Unit 1 and Unit 2 is marked by a sharp unidirectional shift to lower velocity, resistivity, density, sulfur, and silicon content along with increasing aluminum content and total gamma-ray counts.

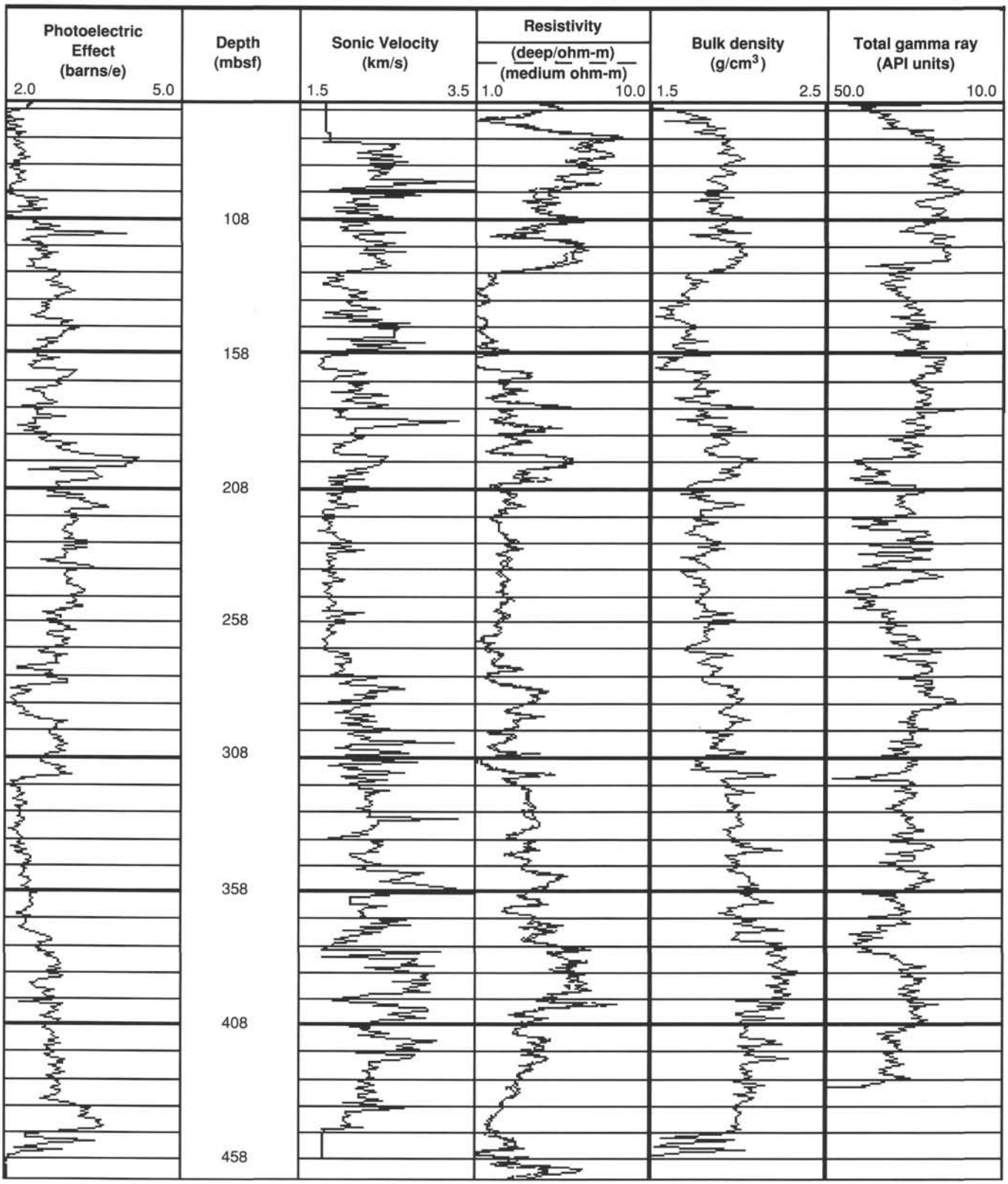

Figure 46. Selected downhole logs from the quad combination tool string for the interval 64.4 to 466 mbsf in Hole 801B: Photoelectric effect, sonic velocity, resistivity, bulk density, and total gamma ray. Stratigraphic units defined by logging data (logging units) are shown in Figure 50. Sonic velocity, resistivity, and density reflect the porosity of the formation and therefore the degree of lithification or cementation (e.g., chert vs. radiolarite).

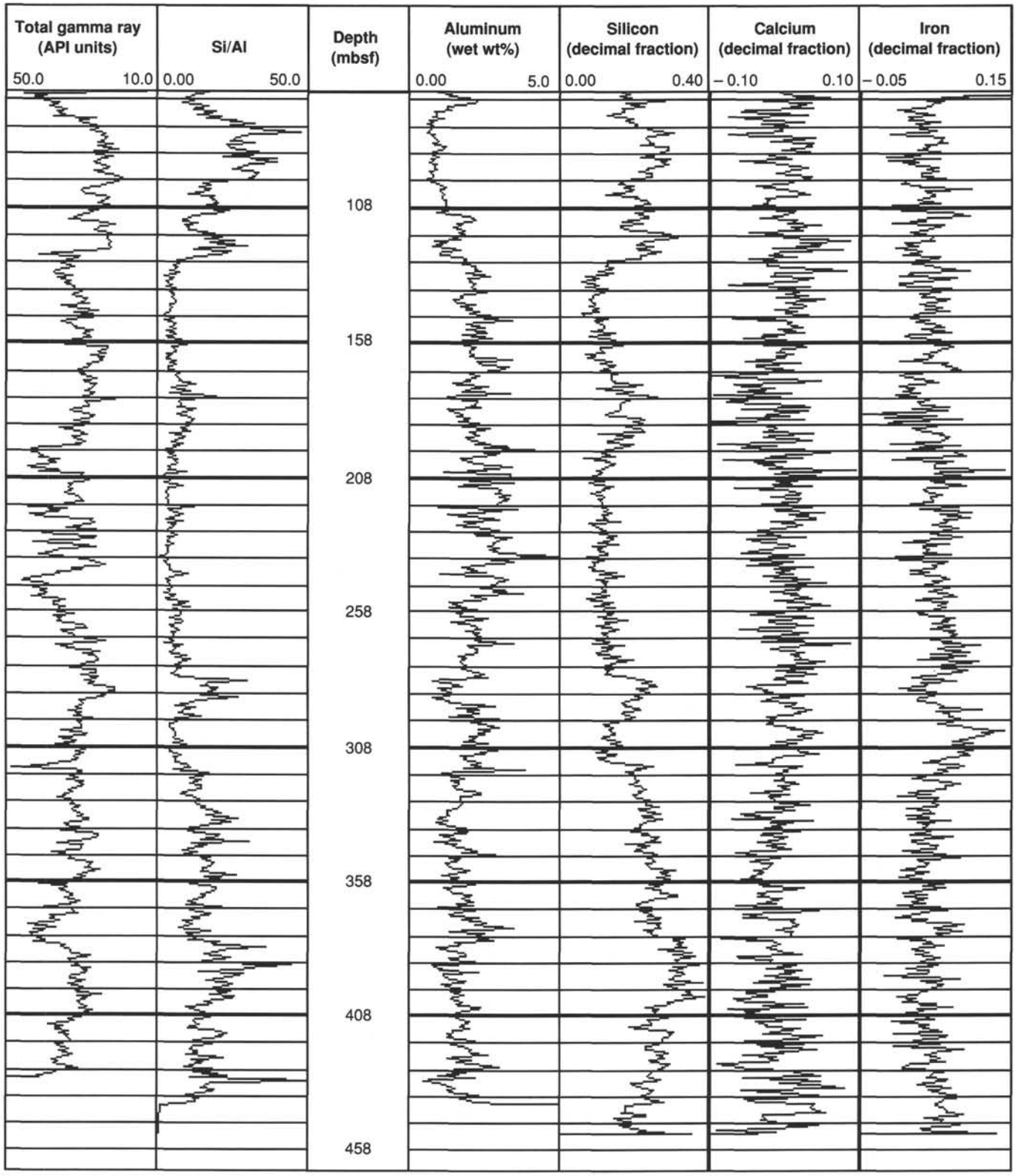

Figure 47. Selected downhole logs from the geochemical tool string for the interval from 64.4 to 466 mbsf in Hole 801B: Total gamma ray, silicon/aluminum ratio, aluminum, silicon, calcium, and iron. Stratigraphic units defined by logging data (logging units) are shown in Figure 50. The relative abundances of these elements serve to identify the primary constituents that distinguish the major lithologies recovered from Hole 801B (e.g., biogenic silica and carbonate, pelagic clay, and volcanogenic material, including clay). The silicon/aluminum ratio helps define intervals dominated by pelagic or volcanogenic sedimentation.

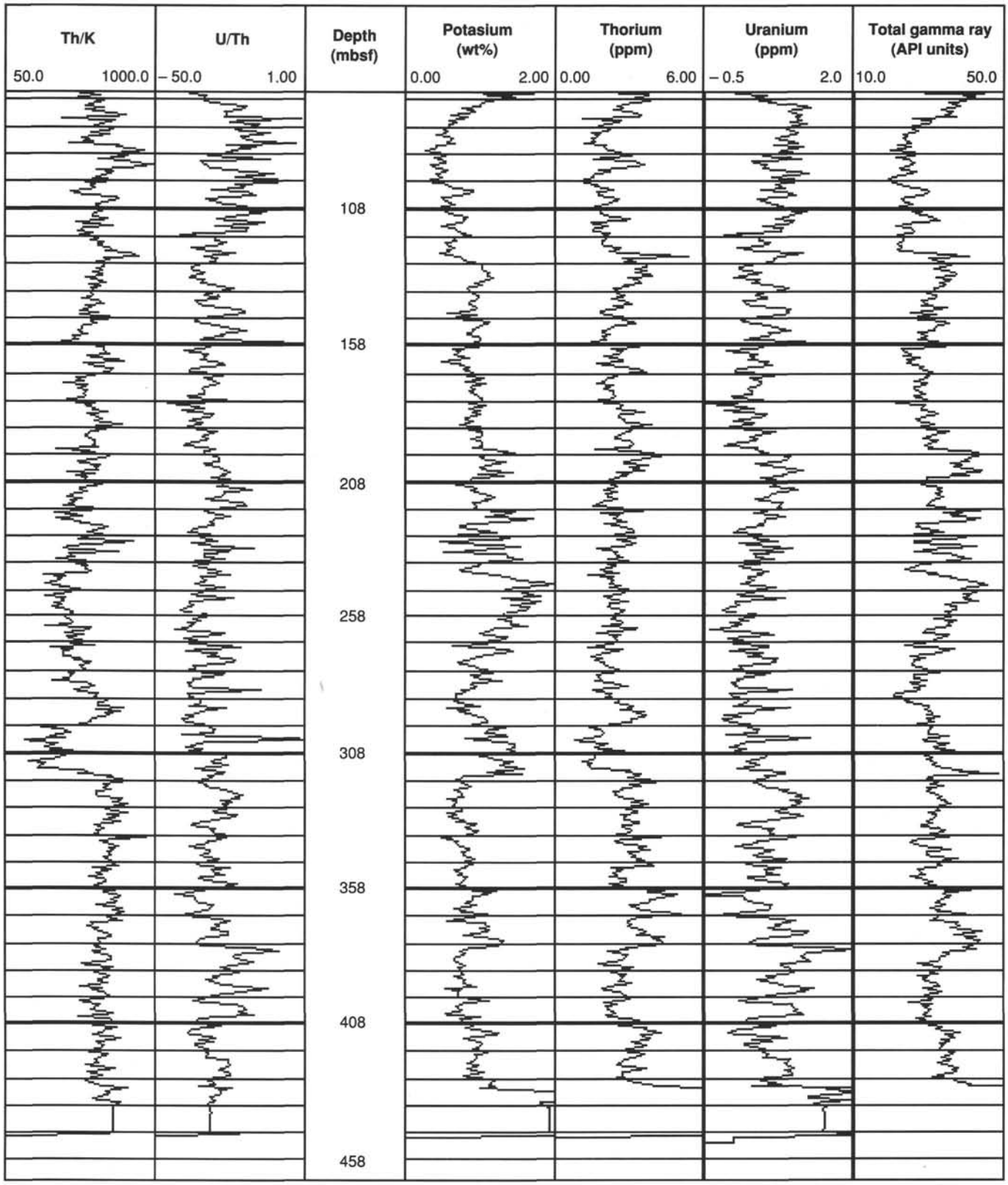

Figure 48. Downhole logs from the natural gamma-ray spectrometry tool on the geochemical tool string for the interval from 64.4 to 466 mbsf in Hole 801B: Thorium/potassium ratio, uranium/thorium ratio, potassium, thorium, uranium, and total gamma ray. Stratigraphic units defined by logging data (logging units) are shown in Figure 50.

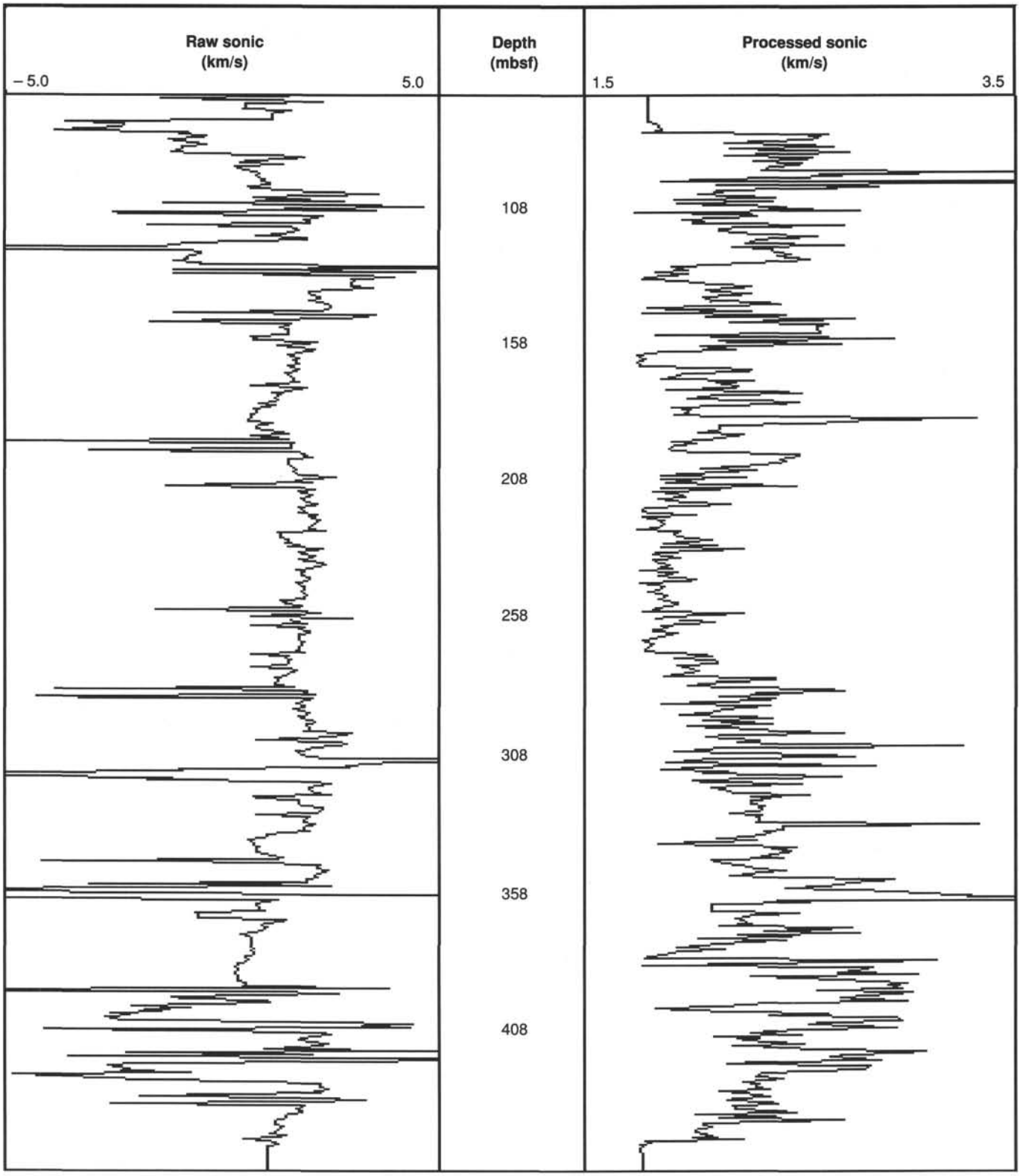

Figure 49. Comparison of observed "raw" (left column) and processed (right column) velocity logs for Hole 801B. Covariation of the processed sonic log with resistivity, gamma ray, and bulk density logs occurs where logging unit boundaries were chosen (Figs. 46 and 50), indicating that a useful velocity log was produced. There are still several intervals where significant velocity variations occur with no covarying response from other logs, making it difficult to confidently interpret a synthetic seismogram made from this sonic log.

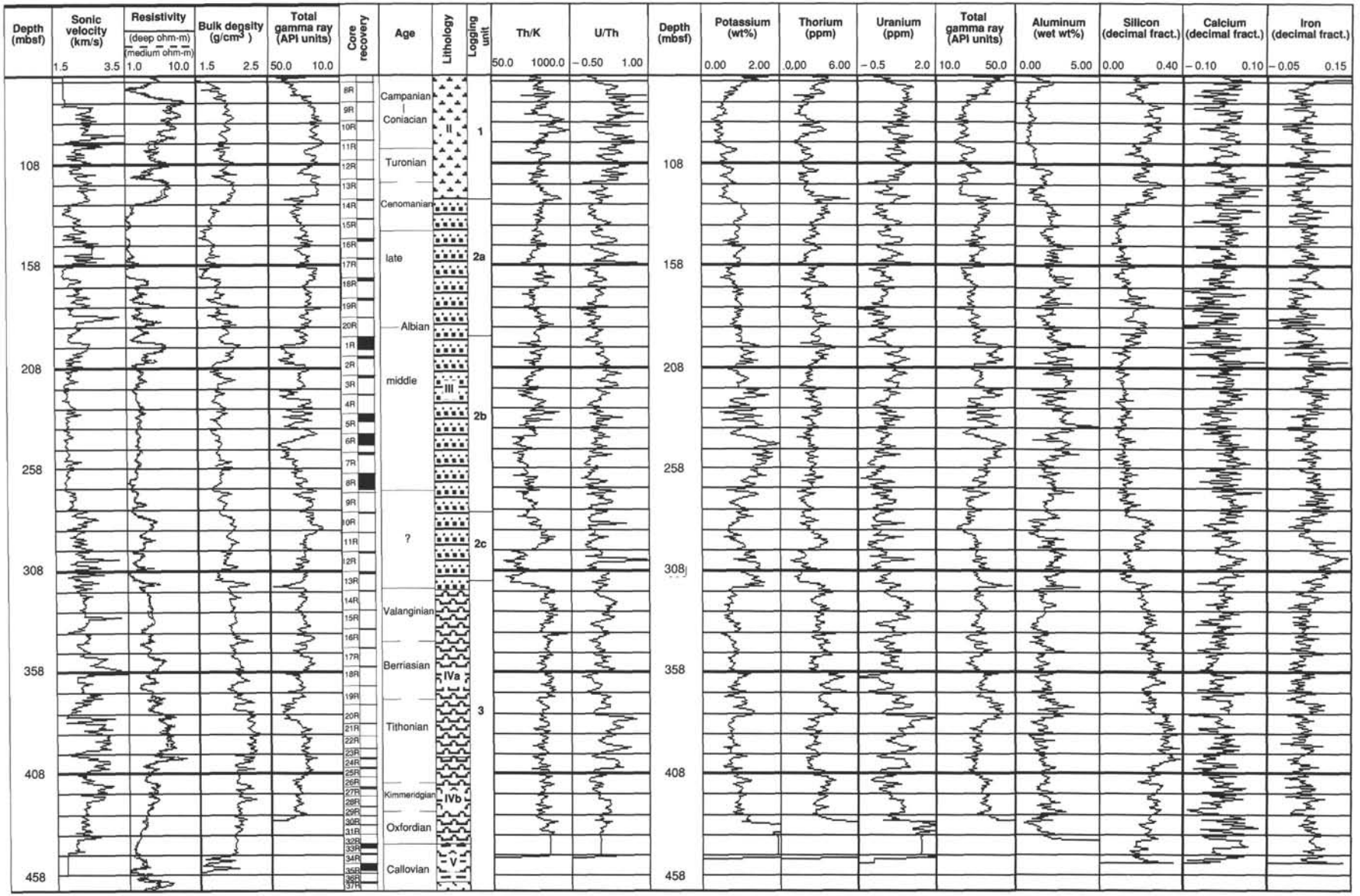

Figure 50. Summary compilation of downhole logs, intervals of core recovery, lithology, and downhole logging units at Hole 801B. Lithologic units are based on coring results (see "Lithostratigraphy and Sedimentology" section, this chapter).

This boundary is also characterized by abrupt shifts toward higher potassium and thorium and lower uranium content. The log responses at this boundary argue for an abrupt contact at 126 mbsf between the diagenetic pelagic sediments (64–126 mbsf) and an underlying volcanic clay-rich, chert-poor sequence. The logging data correlate well with lithofacies Unit II (see "Lithostratigraphy and Sedimentology" section, this chapter), with the base of logging Unit 1 and lithofacies Unit II coinciding exactly.

Logging Unit 2A (126–193 mbsf)

Logging Unit 2A is characterized initially by the lowest resistivities (1 ohm-m), densities (<1.8 g/cm^3), and silicon content observed at Hole 801B, and by relatively high total gamma ray (42 API) decreasing to 30 API at 158 mbsf. There is also a local minima in velocity, density, silicon, aluminum, potassium, and thorium values from 158 to 166 mbsf with calcium and iron displaying no change in trend. Sulfur content is variable but steadily decreases through Unit 2A, reaching an absolute minimum value at the base of this logging unit (193 mbsf). The remaining portion of Unit 2A from 166 to 193 mbsf is distinguished by variable but generally increasing resistivity (1.5 to 3.0 ohm-m), density (1.8–2.1 g/cm^3), and silicon content with generally lower calcium values of higher frequency variability. The lower boundary of logging Unit 2A at 193–198 mbsf is marked by an abrupt, sinusoidal variation on several logs at 193 mbsf with local minima in velocity (1.9 km/s), resistivity (1.2 ohm-m), and density (1.8 g/cm^3) juxtaposed against local maxima in these logs along with maximum values for potassium, thorium, uranium, and aluminum at 198 mbsf.

The logging responses defining logging Unit 2A from 126 to 158 mbsf are interpreted to result from poorly cemented, clay-rich volcanogenic material. Nannofossils become abundant in this interval but the relative concentration of calcium remains essentially the same as in logging Unit 1, which is barren of nannofossils. Radiolarians are abundant in both Unit 1 and Unit 2A but the relative concentration of silicon reaches a minimum in Unit 2A where no recrystalization of silica is evident. The logging response at 158 to 166 mbsf strongly indicates a clay-poor (both volcanic and pelagic) as well as poorly cemented interval that corresponds with the coarser-grained volcanic sandstone (probably high porosity) recovered at this level (e.g., Core 129-801A-18R). The log response over the interval from 166 to 193 mbsf indicates a trend toward greater siliceous and lower calcareous pelagic input within the still dominant volcanics, resulting in a somewhat less porous, better cemented interval that is punctuated by chert/porcellanite lenses (e.g., 178 mbsf). This lowermost interval is also observed to contain greater abundances of radiolarians and is barren of nannofossils (see "Biostratigraphy" section, this chapter). Finally, the simultaneous variation on nearly all the logs, which distinguishes the lower boundary of logging Unit 2A at 193–198 mbsf, is interpreted to indicate a well-indurated sequence of altered volcanics possibly including high-potassium zeolites with recrystallized calcium carbonate rather than silica as the dominant cementing agent. Logging Unit 2A is considered a transition zone between logging Unit 1 and underlying Unit 2B and, as such, corresponds quite well with the lithologies and trends reported in the upper portion of lithologic Unit III (i.e., Cores 129-801A-14R to 129-801B-1R; see "Lithostratigraphy and Sedimentology" section, this chapter).

Logging Unit 2B (193–280 mbsf)

Logging Unit 2B is distinguished by a relatively uniform and extended zone of low velocity (<1.9 km/s), resistivity (1.5 ohm-m), density (1.7–1.9 g/cm^3,) and silicon content. This unit is also characterized by variable but generally the most elevated concentrations of potassium (>.8%), aluminum, and iron.

This type of logging response is interpreted to result from a sequence dominated by volcaniclastics and various alteration products such as clays and high potassium zeolites. This interval appears to have the least amount of pelagic input (especially silica) over the entire interval logged at Site 801, and corresponds to the interval where radiolarians are least abundant (see "Biostratigraphy" section, this chapter).

Logging Unit 2C (280–313 mbsf)

The boundary between logging Units 2B and 2C is marked by a unidirectional shift to higher velocities (2.1–2.5 km/s), resistivities (1.9 ohm-m), densities (1.9–2.0 g/cm^3), and silicon values along with local minima in calcium, iron, aluminum, and total gamma-ray counts. The remainder of logging Unit 2C is characterized by steadily decreasing silicon content matched by increasing iron, aluminum, and potassium. The interval from 298 to 313 mbsf is uniquely characterized by the highest relative concentration of iron along with elevated potassium content, relative minima in silicon, and an absolute minima in thorium. The lower boundary of Unit 2C is marked at 313 mbsf by relative minima in resistivity, density, silicon, iron, and calcium.

The log response defining Unit 2C from 280 to 298 mbsf is representative of a restricted interval of low porosity resulting from silicification within a unit where pelagic sedimentation temporarily dominates redeposited volcanics. The logging reaction from 313 to 298 mbsf is indicative of altered, poorly cemented volcanogenic material. The relatively extreme values observed for potassium, thorium, and iron suggest that some unusual rock type may be present. This depth interval corresponds to Cores 129-801B-12R and -13R, which contain the only recovered occurrence of closely spaced bands of white crystalline material within green volcaniclastics (see "Lithostratigraphy and Sedimentology" section, this chapter). The white crystalline bands are interpreted to be zeolites and anhydrite, and their unusual abundance may create the distinctive logging response that marks the lower boundary of Unit 2C. Logging Unit 2C corresponds to the base of lithologic Unit III and illustrates the transition from nonvolcanogenic lithologies to a sequence dominated by volcanogenic turbidites.

Logging Unit 3 (313–448 mbsf)

Logging Unit 3 begins at 313 mbsf and terminates at 448 mbsf approximately 20 m above the TD for logging operations at Site 801. This unit is distinguished by variable but relatively high velocities, resistivities (1.9–4.6 ohm-m), densities (1.9–2.3 g/cm^3), and silicon concentrations along with reduced aluminum (<0.2%) and iron concentrations and generally low total gamma-ray counts. This type of log response is interpreted to result from variations in porosity because of varying degrees of silicification within the sediments. Intervals of lower silica, resistivity, velocity, and density are considered to be dominated by poorly cemented radiolarite sand rather than chert, and in the instances where an increase in aluminum and total gamma-ray counts are observed (e.g., 373–378 mbsf), volcanic clays are expected to be present. In general, logging Unit 3 is quite similar to Unit 1. However, Unit 1 appears to be nearly free of any volcanic influence (e.g., lowest aluminum values), whereas Unit 3 exhibits evidence for some volcanogenic components.

A distinctive interval occurs within Unit 3 from 378 to 403 mbsf which is marked by the highest relative concentrations of silicon and uranium (2 ppm) and the highest densities (2.3 g/cm^3) recorded by logging tools at Site 801. This interval also displays uniformly high velocities (2.9 km/s) and resis-

tivities (3.7 ohm-m) along with low potassium (0.8%) and thorium (<3 ppm) concentrations. This interval, which is interpreted to contain the greatest percentage of chert at Site 801, is sandwiched between a radiolarite, pelagic clay-rich layer at 403 mbsf and an interval of radiolarite with volcanic clay at 378 mbsf. Paleomagnetic studies on cores from this interval indicate that these diagenetically altered sediments were deposited during an equatorial crossing (see "Paleomagnetism" section, this chapter). The Jurassic/Cretaceous boundary coincides with the clay and radiolarite layer at 370 mbsf, and directly overlies the chert-rich interval that marks the equatorial crossing (see "Biostratigraphy" section, this chapter).

Synthetic Seismogram

The raw sonic log at this site is of considerably poorer quality than the sonic log recorded at Site 800, and the results of our initial processing of this raw sonic log are considered unsatisfactory for production of a useful synthetic seismogram (Fig. 49). A synthetic seismogram will be produced for Site 801 after further shore-based processing that will incorporate physical properties data and a repicking of traveltimes using the full sonic waveform (Borehole Research Group, 1988).

Summary

A suite of eight different downhole logs was successfully recorded at Site 801, resulting in the identification of five distinct logging units. Compositional trends and boundaries were inferred from these logs through intervals of poor recovery by assuming that unrecovered intervals are composed of varying proportions of recovered materials. The logs were most useful in defining boundaries and in characterizing the unrecovered majority of the formation.

SITE GEOPHYSICS AND SEISMIC STRATIGRAPHY

Site Geophysics

Site selection for Leg 129 was based on the multichannel seismic (MCS) surveys described in the "Site Geophysics and Seismic Stratigraphy" section, "Explanatory Notes" chapter (this volume). Underway geophysical data were collected as we approached all sites and provided the correlations with principal MCS sections needed to position the ship at preferred locations.

Site 801 (proposed site PIG-3A) in the central Pigafetta Basin is located within the Jurassic magnetic quiet zone (JQZ) near the intersection of lines 6 and 10 of an MCS survey obtained during the MESOPAC II expedition aboard the *Le Suroit* in August-September 1989. Because Leg 129 began less than three months after the *Le Suroit* cruise, only single-channel, real-time records of both water-gun and air-gun data, as well as sonobuoy refraction data obtained during MESOPAC II, were used to locate proposed site PIG-3A (Figs. 51 and 52). The location of these MESOPAC II MCS profiles was dictated by an earlier MCS expedition aboard the *Fred H. Moore* (FM35-12, November-December 1987). Although the proposed site is not located on an FM35-12 profile, the MCS basement images and velocity structure derived from sonobuoy data (specifically, SB-22) obtained during the FM35-12 expedition provided the regional seismic framework for locating Site 801. Proposed site PIG-3A was specifically located at 0600 hr UTC on 26 August 1989 along MESOPAC II line 10 approximately 3 km southeast of its intersection with MESOPAC II line 6. MESOPAC II sonobuoys 6m (45 km south of Site 801), 4m (93 km east of Site 801), and FM35-12 sonobuoy 22 (located 55 km northeast of Site 801) were used to constrain basement depth and velocity structure (Fig. 56). The only other seismic data in the area are a few widely spaced single-channel air-gun analog profiles (e.g., C1005).

Single-channel seismic (SCS) reflection and 3.5-kHz and 12-kHz profiling were conducted both during the approach of the *JOIDES Resolution* to Site 801 and upon departure for Site 802 (see "Operations" section, this chapter, for detailed approach plan). The actual site is located on the approaching SCS water-gun profile at 1600 hr on 7 December 1989 and on the departing SCS profile at 0110 hr on 23 December 1989 (Figs. 51 and 54) within 0.4 km of the proposed site location on MESOPAC II line 10. Unfortunately, only 0.5 s (7.5–8.0 s two-way traveltime, or twt) of SCS data were recorded digitally during the approach because of a mistake in setting the deep-water delay, but a full 5 s of SCS data were recorded across the site upon departure.

The water-gun data collected during Leg 129 (two 80-in.^{3}) and MESOPAC II (six 80-in.^{3}), and the FM35-12 air-gun data (2819 in.^{3}) are corroborative, and together with 3.5-kHz and sonobuoy data, provided the following seismic criteria for locating Site 801:

1. The relatively thick (53–79 ms) transparent layer over acoustic basement imaged with an excellent 3.5-kHz record (Fig. 55) indicated that enough soft sediment is present over the first cherts to provide lateral support for the drill string during spud-in.
2. A high-amplitude reflection imaged regionally at 0.41 to 0.48 s below the seafloor (bsf) corresponds to the onset of velocities characteristic of oceanic crust as recorded on sonobuoys 4m and 6m (MESOPAC II) and 22 (FM35-12), indicating that approximately 410 to 480 m of sediment overlies oceanic crust in this area.
3. This high-amplitude reflection appears rough, undulating, and diffractive, resulting in an image characteristic of the top of oceanic crust.

Seismic Stratigraphy

The acoustic stratigraphy of large portions of the western Pacific consists of four units originally defined by Ewing et al. (1968): (1) an upper transparent layer, (2) an upper opaque layer, (3) a lower transparent layer, and (4) acoustic basement. These seismic facies descriptions were made from observations of SCS analog air-gun profiles. Acoustic basement has been characterized by the presence of a prominent zone of flat-lying ("smooth"), high amplitude, and closely spaced reflections referred to as "horizon B" by Ewing et al., (1968), the "deep opaque layer" (Heezen, MacGregor, et al., 1973) and as the "reverberant layer" by Houtz et al., (1970) and Houtz and Ludwig (1979). It is now recognized that the reverberant nature of acoustic basement in such profiles is usually the result of a trailing bubble pulse oscillation reflecting from a single high-impedance boundary (Shipley et al., 1983). This characteristic of the air-gun source is now routinely compensated for through the use of tuned air-gun arrays and deconvolution techniques. The use of water-guns in these surveys provides a much more implosive and bubble pulse-free source signature that provides a high-resolution record with little processing effort (Hutchinson and Detrick, 1984).

Although modern acquisition and processing techniques have allowed a more detailed and quantitative assessment of the stratigraphic units originally proposed by Ewing et al. (1968) (especially acoustic basement), these units can still serve to describe the general seismic character of the Pigafetta Basin. It is understood that the following qualitative seismic facies descriptions are largely controlled by the type of seismic source (air gun vs. water gun), processing, and display

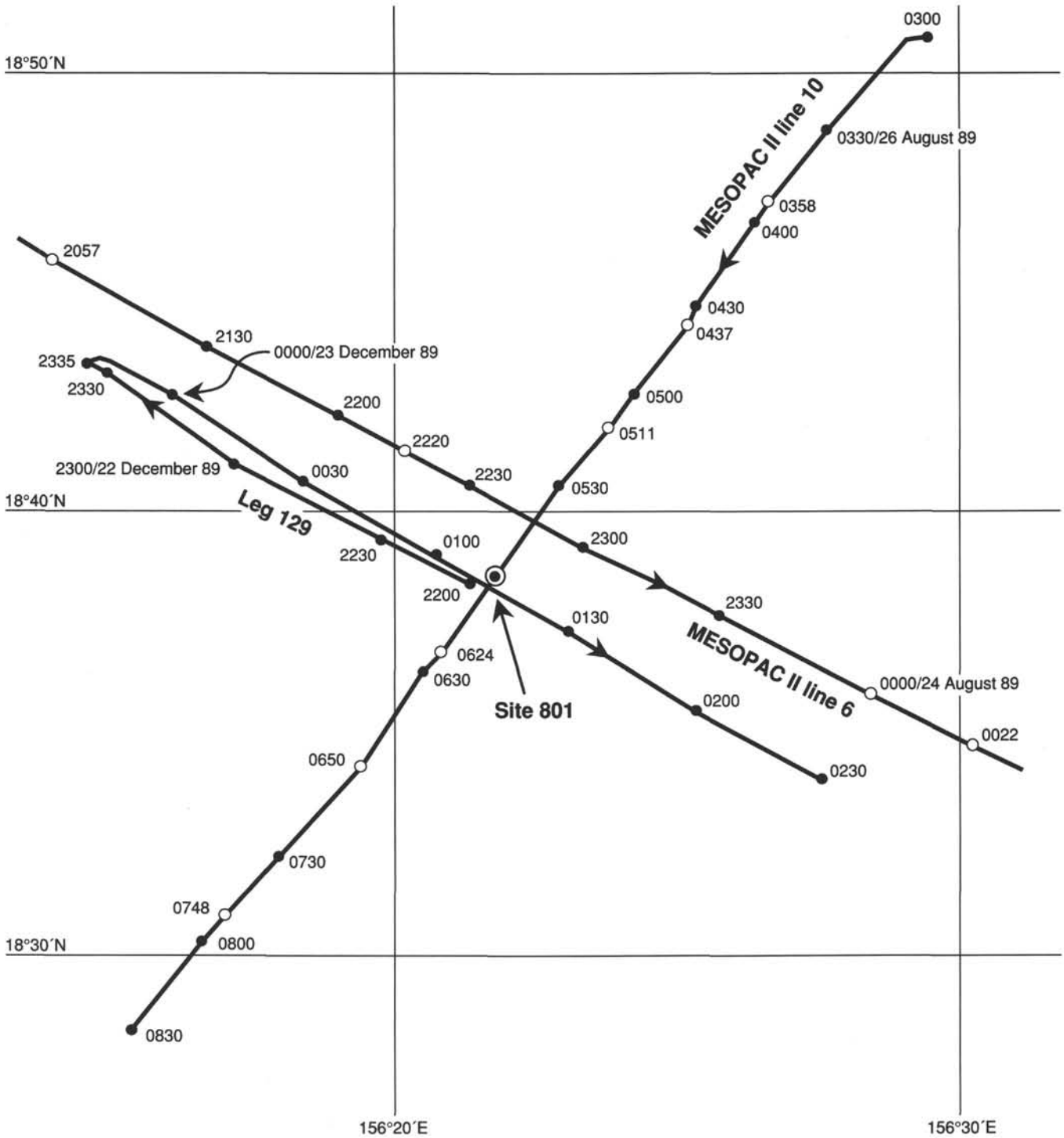

Figure 51. Track chart of expeditions MESOPAC II and Leg 129 showing the location of Site 801 at the intersection of MESOPAC II line 10 (0600 hr UTC, 26 August 1989) and Leg 129 SCS line (0110 hr, 23 December 1989) within 400 m of the location of originally proposed site PIG-3A.

parameters. The final seismic facies identification and interpretation will be made after the MESOPAC II MCS data have been stacked and properly displayed and a synthetic seismogram has been generated.

The lowermost sequence, the reverberant layer, is composed of closely spaced, high-amplitude, continuous reflections that directly overlie a less continuous, more diffractive surface. This most prominent horizon is continuous, flat-lying, and shallow (250–300 ms bsf) in the southeastern Pigafetta Basin and is observed to monotonically deepen (400–480 ms bsf), becoming fragmented or absent altogether, revealing rougher, undulating reflections beginning approximately 130 km south of and including Site 801. To the northeast (but still within the JQZ) this horizon appears tectonized, often exhibiting smooth, block-faulted slabs that have an apparent dip to the northeast. This distinctive lowermost horizon is associated with the onset of velocities characteristic of oceanic crust as determined from sonobuoy data collected during FM35-12

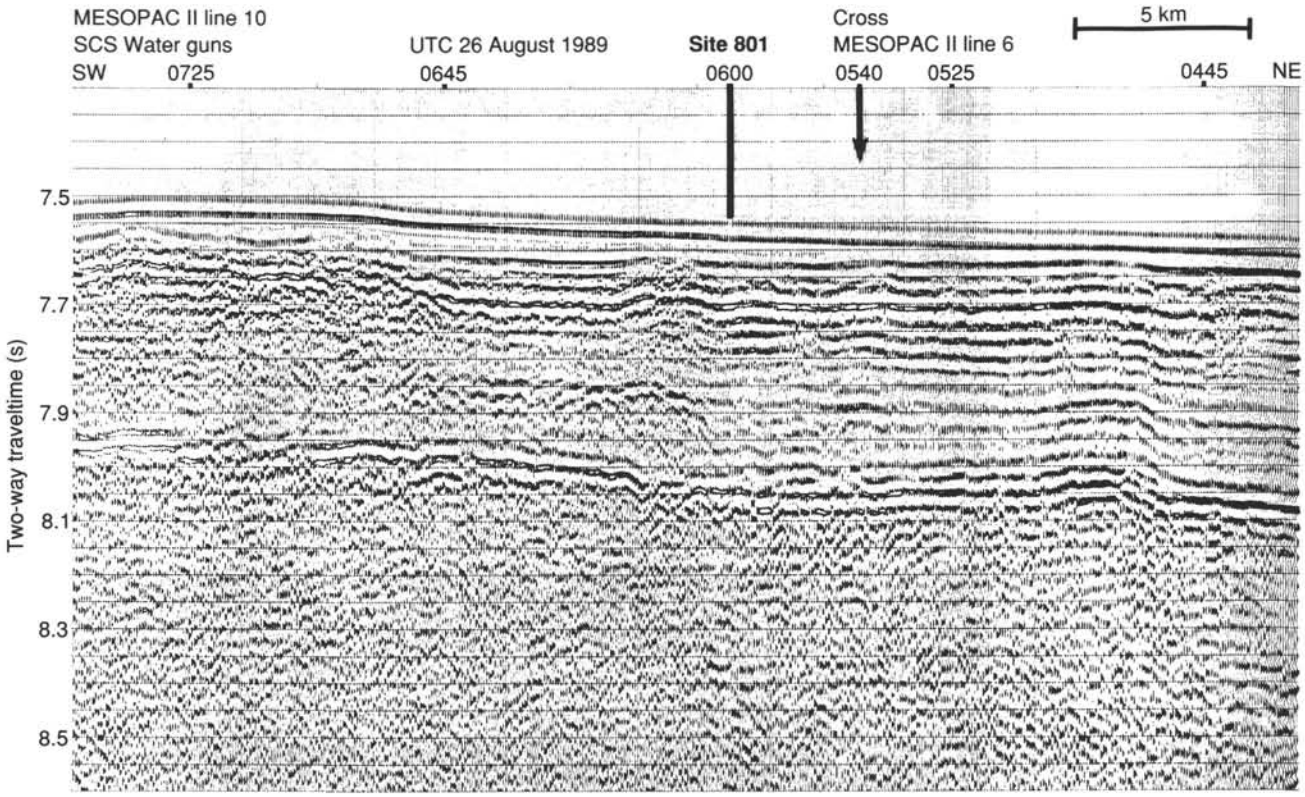

Figure 52. MESOPAC II line 10 SCS record (six 80-in.^{3} water guns) showing location of Site 801 (0600 hr UTC, 26 August 1989) at the intersection with Leg 129 SCS (0110 hr, Fig. 54), and the intersection with MESOPAC II line 6 (Fig. 53). The top of oceanic crust and total depth at Site 801 lie at approximately 8.0 and 8.064 s twt, respectively. This near-channel record was processed and displayed with the following parameters: water velocity F/k migration, mute, 2-trace mix, band-pass filter 25–100 Hz, 500 ms AGC, and vertical exaggeration ~22× at 1.5 km/s.

and MESOPAC II (Abrams et al., 1988). At Site 801, the reverberant sequence ranges from 50 to 100 ms in thickness beginning at 8.0 s twt or 460 ms bsf (Figs. 52, 53, and 54). This lowermost sequence of reflections does not appear as the typical, flat-lying, smooth horizon that is one of the primary characteristics of the reverberant layer and may be better termed "the basement reflector." However, this surface does appear to be contiguous with such a flat-lying horizon that extends for hundreds of kilometers to the southeast. Immediately overlying this interval is the lower transparent layer which is characterized by lower amplitude, widely spaced, and less continuous reflections that range from 250 to 460 ms bsf (7.79–8.00 s twt) and may extend as high as 140 ms bsf. This relatively transparent layer appears to thin to the southeast as the underlying reverberant layer rises in the section and changes to its more typical, flat-lying, smooth appearance. The lower transparent layer includes a distinct high-amplitude, quite continuous reflection that mimics the underlying relief and appears to be draping deposit. In the immediate vicinity of Site 801 this high-amplitude reflection at 310 ms bsf (7.85 s twt) appears to divide the lower transparent layer in two (e.g., Fig. 53) and in other instances it seems to mark the base of an overlying opaque layer or becomes part of an opaque layer that extends all the way to basement (e.g., left side of Fig. 52). The lower transparent layer is bounded on top by a distinctly higher amplitude, more continuous sequence of reflections that also appear to drape over underlying relief. This unit appears to maintain a fairly uniform thickness throughout extended portions of the Pigafetta Basin.

The upper transparent zone as envisioned by Ewing et al., (1968) is very much attenuated in the Pigafetta Basin and extends from 0 to approximately 79 ms bsf (7.54–7.619 s twt) at Site 801. This interval is best displayed on the 3.5-kHz records obtained during Leg 129 (Fig. 55) and MESOPAC II, but is also apparent on SCS records. These four seismic facies are essentially identical on the SCS monitor records of both Leg 129 and MESOPAC II.

Correlation between Seismic Stratigraphy and Lithology at Site 801

DSDP Legs 6, 17, 61, and 89 had instances during which a flat-lying, high-amplitude "acoustic basement" or "reverberant layer" was correlated to middle Cretaceous volcanic material (sills, flows, and volcanogenic turbidites) which, according to magnetic lineations, significantly post-date the formation of oceanic crust. However, the physical nature of a similar seismic facies observed throughout the East Mariana and Pigafetta basins had not been determined before Leg 129.

The reverberant layer at Site 800, located on a correlatable magnetic anomaly (M33) in the northern Pigafetta Basin is created by a massive chert overlying a series of dolerite sills and appears as a flat-lying sequence of reflections approximately 100 ms thick (see "Site Geophysics and Seismic Stratigraphy" section, "Site 800" chapter, this volume). This type of smooth, flat-lying, high-velocity horizon is characteristic of much of the Pigafetta Basin and the majority of the East Mariana Basin (Abrams et al., 1988). In contrast, the

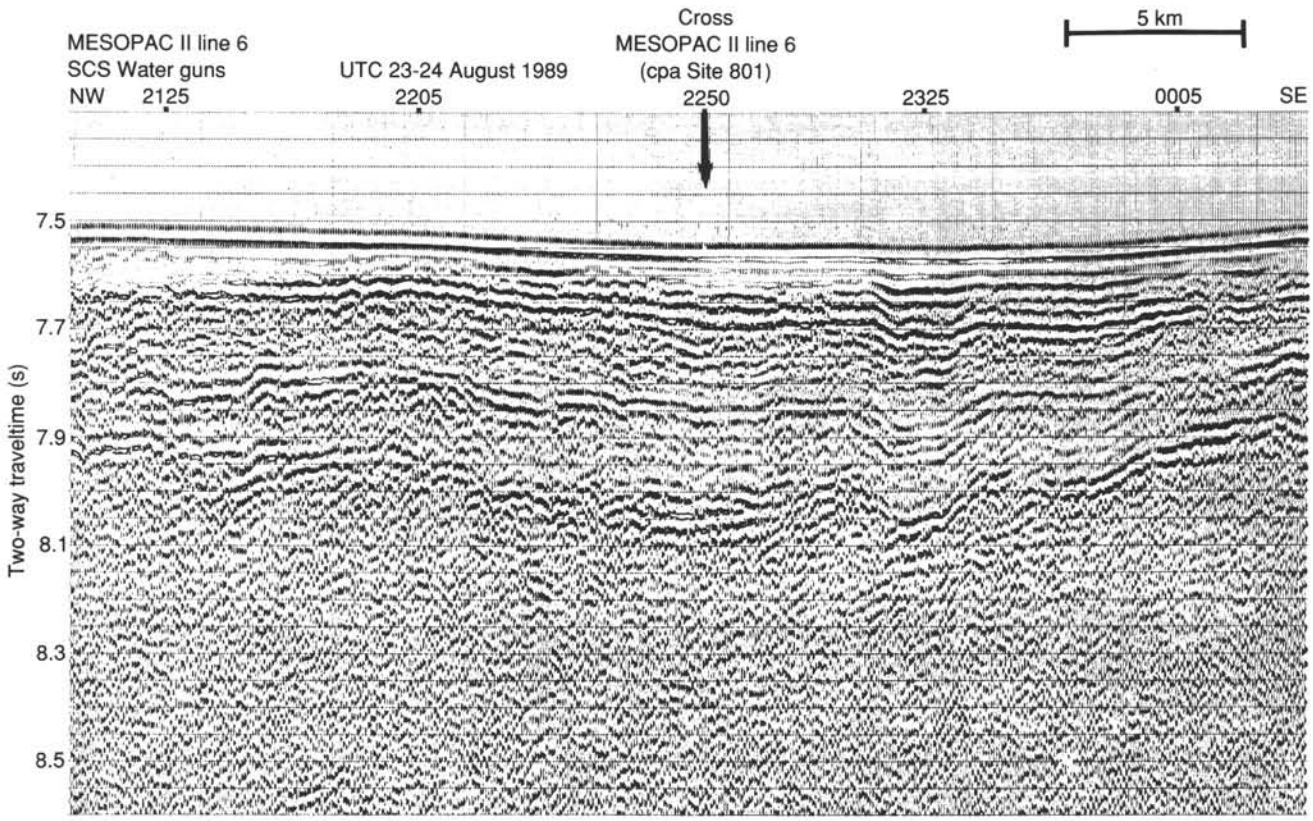

Figure 53. MESOPAC II line 6 SCS record (six 80-in.^{3} water guns) showing intersection with MESOPAC II line 10 (Fig. 52) approximately 3 km northeast of Site 801. The basement reflection along this inferred flow-line profile varies from 7.85 to 8.0 s twt, displaying the relief that characterizes buried abyssal hill bathymetry. This "rough" basement reflection is coincident with the onset of velocities and velocity gradients characteristic of oceanic crust (Fig. 56). Processing and display parameters are identical to those given for Figure 52.

reverberant layer at Site 801, located well within the JQZ, appears as a rough, undulating horizon that is created by interbedded basalt and chert overlying a series of contiguous basalt flow units (see "Igneous Petrology" section, this chapter). This seismic facies is interpreted to result primarily from a single impedance contrast between the radiolarite clays and the top of chert overlying basalt at 461 mbsf.

The velocity structure of this area of the Pigafetta Basin is well constrained by refraction data from three long-range sonobuoys that produce nearly identical velocity vs. depth solutions (Fig. 56). These solutions show velocities and velocity gradients characteristic of "normal" oceanic crust beginning from 410 to 440 ms bsf, which correlates to the reverberant layer imaged regionally at 410 to 480 ms bsf. The high-relief horizon penetrated in Holes 801B and 801C is interpreted to be the top of oceanic crust. In the areas where the reverberant horizon becomes flat-lying and shallow, cherts overlying sills and/or flows which are significantly younger than those recovered at Site 801 are expected to overlie oceanic crust. This observation has significant implications for the lateral extent of middle Cretaceous deep-sea volcanism within the "Jurassic" western Pacific, considering that most of the Pigafetta and East Mariana basins is characterized by such a flat-lying, high-amplitude, high-velocity basement reflection.

This distinctive change in the seismic character of the reverberant layer from smooth to rough can also be correlated to a change in magnetic anomaly amplitudes and field strength that was first observed in the aeromagnetics data of Handschumacher et al. (1988) and also displayed on the shipboard magnetics of FM35-12 and MESOPAC II. The "rough-smooth" reverberant horizon boundary corresponds to a change in magnetic anomalies from higher field/low amplitude anomalies to lower field/high amplitude anomalies. A comparable boundary within the East Mariana Basin, which is characterized by the nearly ubiquitous presence of the high-amplitude, flat-lying reverberant layer, is not apparent (see "Site Geophysics and Seismic Stratigraphy" section, "Site 802" chapter, this volume).

The lower transparent layer correlates with the thin (18 m) sequence of red radiolarite and claystone and brown radiolarite between 318.3 and 461.6 mbsf (lithologic Units IV and V), as well as the lower portion of the volcaniclastic turbidites (about 193 to 318 mbsf). The high-amplitude reflection dividing the transparent layer in half at 310 ms bsf is believed to correspond to an unrecovered massive chert layer (abrupt decrease in drilling rate and apparent on logs), which marks the beginning of a transition from nonvolcanogenic lithologies below 318 mbsf to an overlying sequence dominated by volcanogenic turbidites. The low-amplitude reflections are created by small impedance contrasts within two different but internally homogenous intervals. The lower pelagic interval shows uniformly low porosity (inferred from logs) punctuated by variations in porosity because of radiolarite-rich or chert-rich intervals. The overlying turbidites display uniformly high porosity with well-developed graded bedding structures and variations in calcite cementation that may create relatively low-amplitude reflections (see "Downhole Measurements" and "Lithostratigraphy and Sedimentology" sections, this chapter).

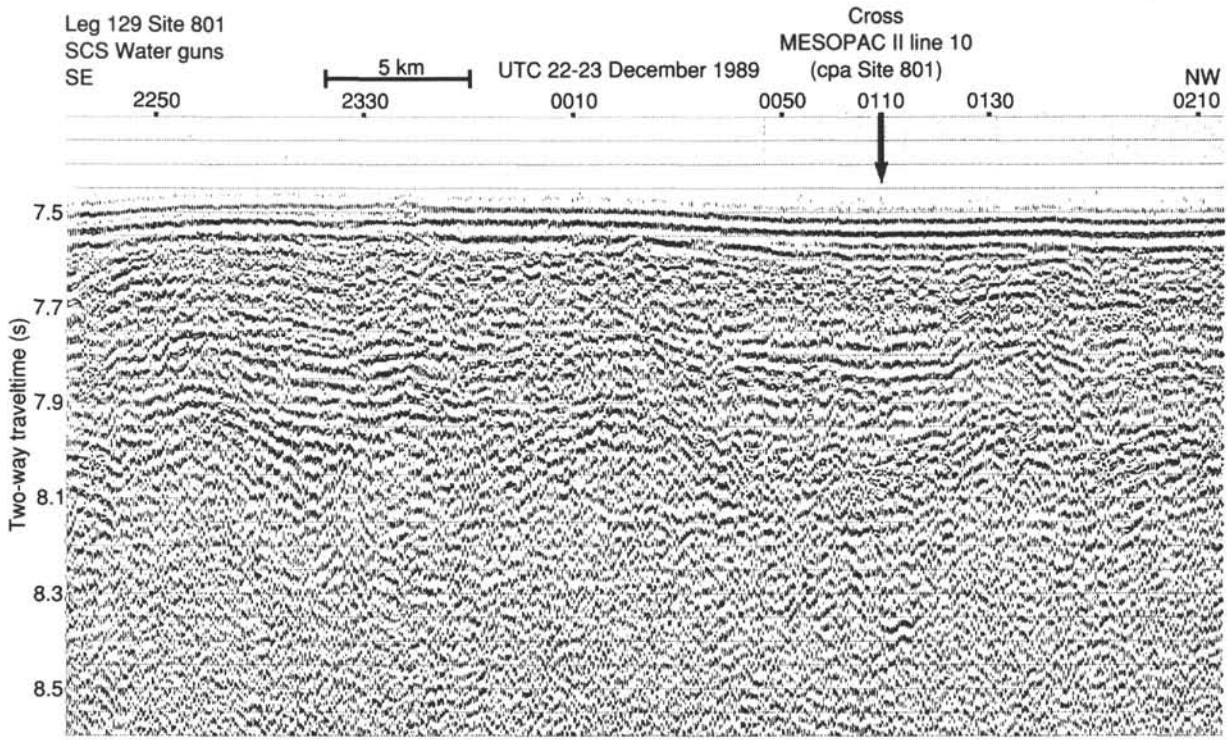

Figure 54. The entire SCS profile (two 80-in.^{3} water guns) obtained upon departure from Site 801 (0110 hr UTC, 23 December 1989) during Leg 129. This SCS profile crosses MESOPAC II line 10 (Fig. 52) at 0110 hr at its closest approach to Site 801. This seismic record is obviously of poorer quality than that obtained at Sites 800 and 802 during Leg 129 because of problems during digital acquisition (for details, see "Site Geophysics and Seismic Stratigraphy" section, "Explanatory Notes" chapter, this volume). This record is displayed with the following parameters: mute, 2-trace mix, band-pass filter 30–100 Hz, 500 ms AGC, vertical exaggeration ~22× at 1.5 km/s.

A transition zone (logging Unit 2A), which consists of both volcanogenic and pelagic material at approximately 193 mbsf, correlates to the relative increase in reflection amplitude that marks the change from lower transparent to upper opaque seismic facies. The distinctive high-amplitude reflection at 160 ms bsf correlates to a chert-rich interval at 178 mbsf interbedded with volcaniclastic claystone. This chert-rich interval lies beneath a poorly cemented volcaniclastic sandstone (see "Lithostratigraphy and Sedimentology" section, this chapter). These high-amplitude reflections also encompass the overlying pelagic interval where impedance contrasts occur between interbedded chert/porcellanite and pelagic clay.

The transparent nature of the uppermost 79 ms bsf (upper transparent layer) is indicative of a relatively homogenous interval containing no significant impedance contrasts. This interval correlates to pelagic brown clay (8–61 mbsf) underlain by the uppermost cherts.

The depths of specific horizons mentioned in the above correlation of seismic facies with lithofacies within the sedimentary section were assigned without the guidance and constraints provided by a log-generated synthetic seismogram and should be considered only as general estimates (see Fig. 57). A synthetic seismogram will be used to accurately tie the drilled sequence in the hole to seismic reflection data over the site.

SUMMARY AND CONCLUSIONS

Jurassic in the Pacific (At Last)

Site 801 is the first site to have reached the Jurassic in the Pacific, and it might remain the only one for a long time. This simple statement does not really do justice to the importance of the discovery considering the years of hope, effort, and frustration spent in the search for the oldest record of the world's Jurassic "superocean." Site 801 represents a milestone in our quest for the earliest evolution of the part of the world's oceanic record that is still accessible. Given the relatively small size of the Pacific plate in the Middle to Late Jurassic, compared to the enormous size of the ocean at that time, we admittedly have only a very partial view of Jurassic oceanic paleoenvironments. Nevertheless, we have broken entirely new ground at this site, which will certainly represent a reference for the Mesozoic history of the Pacific and of the world ocean. The site has been continuously cored to the basement. Unfortunately, core recovery was rather poor in most of the pelagic sediments, because of the abundance of chert interlayered in relatively soft claystones. On the other hand, despite technical mishaps that made operations quite acrobatic toward the end of the leg, we achieved substantial penetration (131 m) into the oldest *in-situ* oceanic crust of the world and were blessed with good basement recovery and particularly interesting discoveries.

Site 801 lies in the Jurassic quiet zone, almost 150 nmi southeast of the oldest magnetic anomaly ever recognized in an ocean basin (M37). The age of the crust falls almost exactly on the predictive plot derived from a simple linear extrapolation of the ages of the M-series (See Fig. 3). This finding provides indisputable proof that the quiet zone is indeed of Jurassic age, and that it is not the result of subsequent erasure of magnetic anomalies by middle Cretaceous volcanic events. Despite the fact that this site was not located on a magnetic lineation, this finding also indirectly confirms the Late Jurassic age of the sequence of magnetic anomalies from M17 through M37. This confirmation is of extreme importance because the "type locality" of the M-series magnetic reversal stratigraphy is the western Pacific, although the oldest well-

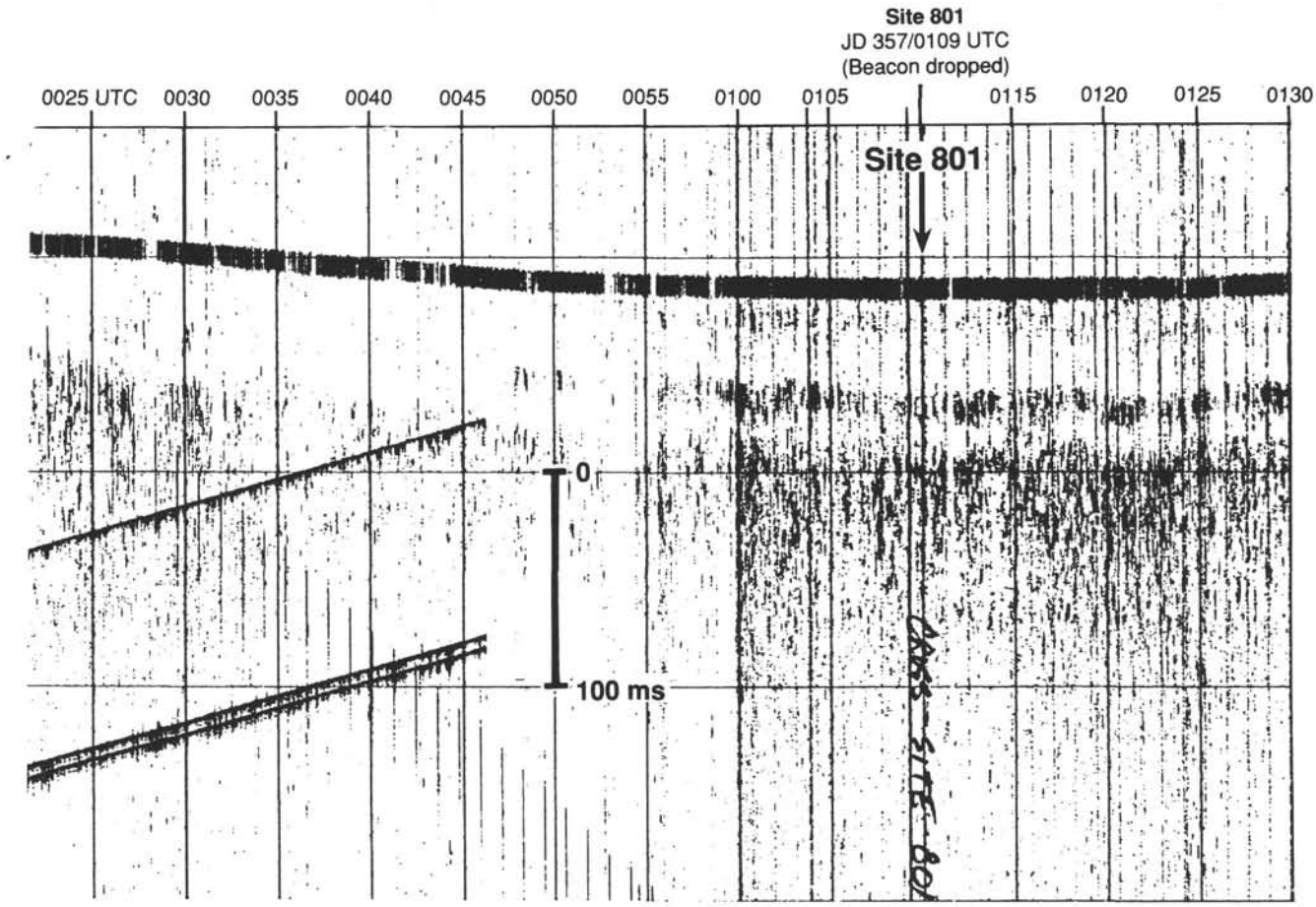

Figure 55. The 3.5-kHz record collected upon departure from Site 801. Horizontal lines represent 100-ms intervals. Acoustic basement on this record marks the top of the first chert and indicates 79 ms of pelagic clay. A weak intermittent reflection is also visible at 53 mbsf. The 53-m thickness for the pelagic interval overlying the first chert is derived from the drillers' determination of the mud line to the depth of the first impenetrable interval encountered during jet-in tests. A thickness of 53 m over 79 ms results in an unreasonable interval velocity of 1.34 km/s. During camera-guided re-entry operations at Site 801, depth to mud line was observed to be 8 m shallower, making the actual thickness of pelagic clay 61 m, which results in a more reasonable interval velocity of 1.544 km/s. The thickness of the pelagic clay layer measured from jet-in tests at Site 800 was probably also underestimated by 10 m (see "Site Geophysics and Seismic Stratigraphy" section, "Site 800" chapter, this volume).

dated magnetic lineation in this area is M9 on the Japanese sequence, dated as Hauterivian at DSDP Site 304. The seismic profiles from the recent MCS surveys provided excellent continuity between Sites 800 and 801, and we anticipated a sediment section roughly similar at both sites except for the lowermost levels. The acoustic basement in particular was inviting as a target when compared to that of Site 800. It presented all the characteristics of oceanic crust and certainly appeared to be the best possible prospect, together with Site 802 farther to the southwest in the Mariana Basin.

The Jurassic Crust

A total of 131 m of igneous basement section was penetrated at Holes 801B and 801C, and a 20-m overlap is included at the bottom of Hole 801B and top of Hole 801C. Most of this section consists of interlayering lava flows of varying thicknesses and pillow basalts. The pillow basalts exhibit chilled margins, variolitic textures, and microcrystalline interiors. There is a minor amount of baked and silicified claystone near the top of the section, and a 3-m-thick sill is present at 510 mbsf. There is little doubt on the basis of its physical appearance that this igneous section consists of basalts extruded under submarine conditions. Because it underlies sediments dated as Callovian-Bathonian in age, it is at least Middle Jurassic in age.

A total of 40 physical units were recovered from the complete crustal section, including the overlap. Most of this material is extrusive flow units varying from 0.2 to 7 m in thickness. These flows are mainly composed of aphyric basalts, although a significant fraction of moderately olivine/plagioclase, microphyric/phyric basalt is present. A few of the flows have an aphyric, microdoleritic texture.

There is a remarkable hydrothermal deposit included in the basement section at 520 to 530 mbsf. It is chrome yellow and consists of iron oxides/hydroxides that are well cemented, and largely replaced, by silica. It is directly underlain by highly altered pillow basalts, apparently the result of hydrothermal solutions percolating up through the basement section that deposited the hydrothermal concretion. Obvious cracks and fissures are present which acted as conduits for part of this circulation system.

It is likely that this entire hydrothermal system was buried beneath the uppermost basalt flows soon after its deposition, which allowed its preservation. Beneath these altered basalts, the flows become markedly fresher and are often characterized by vesicles up to 1.5 cm in diameter. Although such

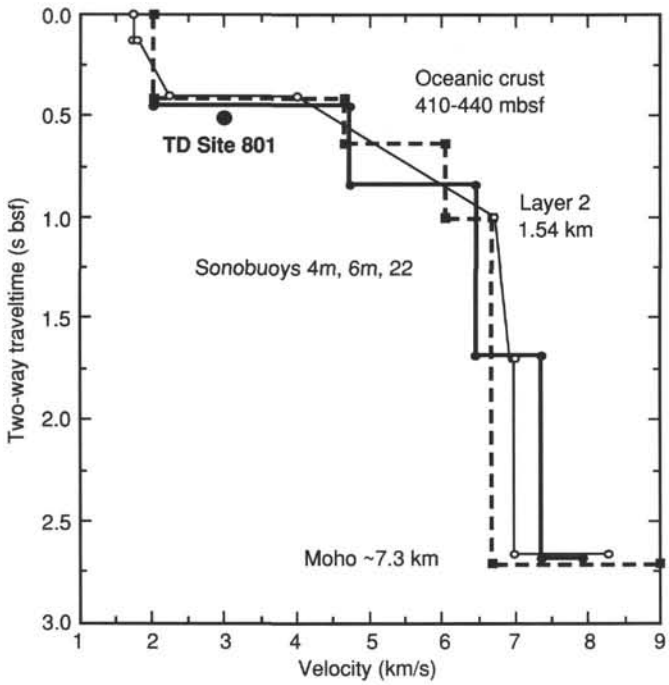

Figure 56. Velocity vs. two-way traveltime below seafloor (bsf) from sonobuoy data collected during FM35-12 and MESOPAC II. The onset of velocities and velocity gradients characteristic of oceanic crust at approximately 410 to 440 mbsf corresponds to the reflection imaged at approximately 8.0 s twt in Figures 52, 53, and 54.

vesicles are not unknown from modern ridge crests, they are less common than at Hole 801C, possibly indicating an anomalously shallow ridge-crest depth.

Radiometric dating of this basement sequence will be of great interest from two independent points of view. First, there is the question of a possible age progression that could be recognized from bottom to top which would yield insight into the history of the hydrothermal system and its subsequent burial. Second, the youngest radiometrically dated rocks with an extrusive character can be considered as contemporaneous with the overlying Callovian-Bathonian sediments, and thus will provide valuable, absolute calibration for that part of geological time, as well as for the magnetic reversal time scale. This calibration is especially critical because (1) it provides the oldest point that can be dated on a marine magnetic anomaly reversal sequence and (2) the Middle Jurassic is heretofore the most poorly calibrated part of the last 200 m.y. of geologic time.

We also note that Hole 801C is cased through the entire sediment section and cemented into basement. Through a combination of luck and persistence, it is free of any drilling junk in the hole. Thus, a golden opportunity exists for future expeditions to deepen this hole into the oldest crustal section in the world's ocean basins and subsequently to conduct logging and downhole measurements that were not accomplished during this expedition.

Early History of the Pacific

Data from Site 801 pertain only to a rather small, low-latitude area of the Mesozoic Pacific, at least with respect to the Jurassic. Cores from Holes 801A and 801B sampled only deep-water facies, so that our view of the early evolution of the Pacific plate remains limited.

The earliest sediments found just on top of the Jurassic crust are reddish brown radiolarites interbedded with claystones in a more or less rhythmic fashion. This facies is reminiscent of the radiolarites of the Tethys and circum-Pacific regions, even if actual "ribbon radiolarites" are not present. These sediments indicate relatively high productivity that may be associated with the proximity of the site to the equatorial zone. Rates of accumulation, however, remained rather low until the latest Jurassic-earliest Cretaceous, when a peak in biogenic silica is well documented both in the cores and in the geochemical logs. It is too early to determine with confidence whether the variations in the abundance of radiolarians or chert in the sediments directly reflect the transit of the site across the equatorial zone or whether they correspond with fluctuations in the productivity of the surface waters. In any case the conditions of sedimentation for the Late Jurassic and early Neocomian times reflect a deep-water environment characterized by a relatively elevated CCD and a moderate style of bottom-water circulation, nevertheless sufficient to maintain permanent oxidizing conditions. The absence of carbonates in the sediments found directly above the ridge crest basalts, presumed to have erupted in water depths averaging 2800 m, seems to be better explained by reduced production of calcareous plankton in the surface waters than by accelerated dissolution on the seafloor.

Paleolatitudes and Plate Motion

Paleomagnetic measurements performed on the sediments aboard the ship provide a preliminary estimate of the successive paleolatitudes occupied by Site 801 that confirms the trends already observed at Site 800. The distribution of various sediment facies in time shows a relatively good agreement with the paleomagnetic determination. The combination of the two data sets helps to explain the relative variations in the abundance of biogenic silica in the sediments. In particular, results from this site document again the latitudinal reversal in plate motion that seems to have occurred sometime between the Valanginian and the Aptian. Prior to the Valanginian, Site 801 may have been close to the equator for most of its early history, although paleomagnetic data are too preliminary to determine if the site actually formed in the Northern Hemisphere during the Middle Jurassic. The youngest equatorial crossing seems to have occurred during the Campanian according to the paleomagnetic data, although they show some dispersion for that interval. The sediment record, which shows a predominance of chert from the Turonian through at least the Campanian, appears to agree well with this estimate.

Middle Cretaceous Volcanic Events

A pulse of volcanic activity was recorded at Site 801. This pulse was characterized by massive redeposition of volcanogenic material shed from the slopes of seamounts when they nearly reached the surface of the sea. These active volcanos were probably the major seamounts lying less than 100 nmi north and south of Site 801. The beginning of the volcanic pulse is not accurately dated because the lowermost redeposited beds are barren of age-diagnostic microfossils. These beds may be of Aptian age because they lack magnetic reversals, but a more precise determination will require more shore-based work. Variations in the volume of the redeposited volcaniclastics suggest that there were several pulses of volcanic activity. The major one seems to have occurred during the Albian and is recorded by a turbidite sequence over 4 m thick and by possible debris flows that confer a proximal character to most of this interval. Fragments of shallow-water fossils (red algae and echinoderms) confirm that the nearby seamounts had reached very near the surface by the late Albian.

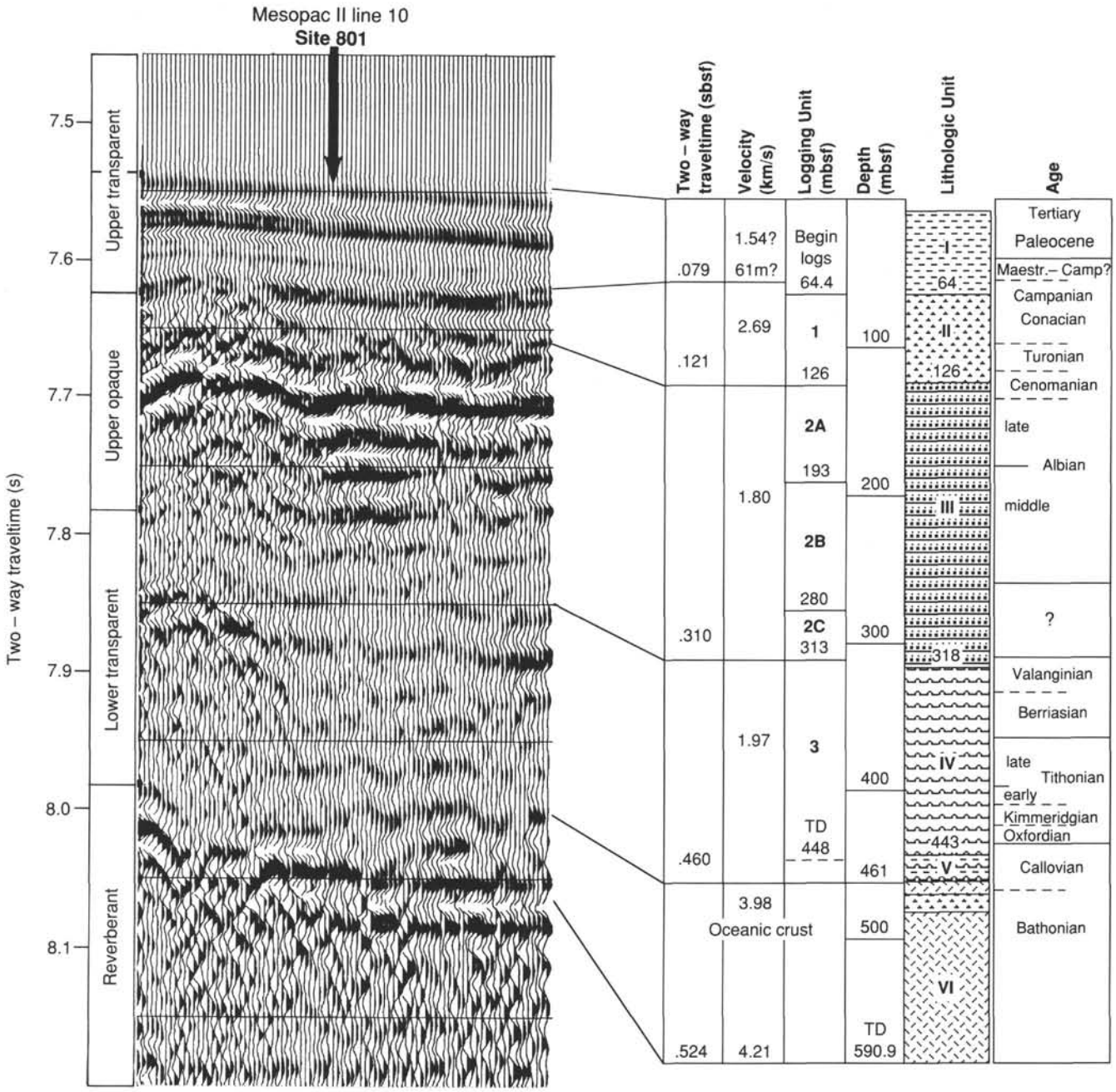

Figure 57. Summary of seismic stratigraphy at Site 801 showing correlations with logging units, lithologic units, ages, and depths. These correlations were made without the constraints provided by a log-generated seismogram, and should be considered only as a best estimate. The crustal velocities given are based on traveltime modeling of sonobuoy data. The 2.69 km/s velocity is based on the interval between 56.4 and 118 mbsf. See Figure 55 for an explanation of 1.54-km/s pelagic-clay velocity. This SCS water-gun record is displayed with a vertical exaggeration of ~33× at 1.5 km/s with the same parameters as described in the caption for Figure 52.

Volcanic activity lasted throughout the Albian and apparently ended sometime during the Cenomanian. Thus, the record from Sites 800 and 801 indicates that most of the seamounts surrounding the Pigafetta Basin may have been built during the middle Cretaceous. The relation between edifice-building and deep-basin sill-intrusion processes remains a mystery, however, and the original Jurassic crust may be generally covered with Cretaceous intrusives. In retrospect, we may have found at Site 801 one of the very rare "windows" allowing us a peek into the well-defended Jurassic.

REFERENCES

Abrams, L. J., Larson, R. L., Shipley, T., and Lancelot, Y., 1988. Cretaceous volcanic sequences and Jurassic(?) crust in the western Pacific. *Trans. Am. Geophys. Union,* 69:1442.

Adachi, M., Koshi, Y., and Ryuichi, S., 1986. Hydrothermal chert and associated siliceous rocks from the northern Pacific: their geological significance as an indication of ocean ridge activity. *Sediment. Geol.,* 47:125–148.

Anderson, R. N., Honnorez, J., Becker, K., et al., 1985. *Init. Repts. DSDP,* 83: Washington (U.S. Govt. Printing Office).

Baumgartner, P. O., 1987. Age and genesis of Tethyan radiolarites. *Eclogae Geol. Helv.*, 80:831–879.

Bernoulli, D., 1972. North Atlantic and Mediterranean Mesozoic facies: a comparison. *In* Hollister, C. D., Ewing, J. I., et al., *Init. Repts. DSDP*, 11: Washington (U.S. Govt. Printing Office), 801–871.

Bonatti, E., 1981. Metal deposits in the oceanic lithosphere. *In* Emiliani, C. (Ed.), *The Sea* (Vol. 7): New York (Wiley), 639–686.

Borehole Research Group, 1988. *Ocean Drilling Program Wireline Logging Manual:* New York (Lamont-Doherty Geological Observatory, Columbia Univ.).

Boström, K., and Peterson, M.N.A., 1965. Precipitates from hydrothermal exhalations on the East Pacific Rise. *Econ. Geol.*, 61:1258–1265.

Bralower, T. J., Monechi, S., and Thierstein, H. R., 1989. Calcareous nannofossil zonation of the Jurassic-Cretaceous boundary interval and correlation with the geomagnetic polarity timescale. *Mar. Micropaleontol.*, 14:153–235.

Caron, M., 1985. Cretaceous planktonic foraminifera. *In* Bolli, H. M., Saunders, J. B., and Perch-Nielsen, K. (Eds.), *Plankton Stratigraphy:* Cambridge (Cambridge Univ. Press), 17–86.

Cotillon, P., 1984. Tentative world-wide correlation of Early Cretaceous strata by limestone-marl cyclicities in pelagic deposits. *Bull. Geol. Soc. Den.*, 33:91–102

Cotillon, P., 1985. Les variations à différentes échelles du taux d'accumulation sédimentaire dans les séries pélagiques alternantes du Crétacé inférieur, conséquences de phénomènes globaux. Essai d'évaluation. *Bull. Soc. Géol. Fr.*, Ser. 8, 1:59–68.

Deer, W. A., Howie, R. A., and Zussman, J., 1978. *An Introduction to the Rock Forming Minerals:* New York (Longman Group).

Erba, E., 1987. I Nannofossili calcarei nell'Aptiano-Albiano (Cretacico inferiore): biostratigrafia, paleoceanografia e diagenesi degli Scisti a Fucoidi del pozzo Piobbico (Marche) [Ph.D. dissert.], Univ. of Milan.

Ewing, J., Ewing, M., Aitken, T., and Ludwig, W. J., 1968. North Pacific sediment layers measured by seismic profiling. *In* Drake, C. L., and Hart, P. J. (Eds.), *The Crust and Upper Mantle of the Pacific Area*. Am. Geophys. Union. Monogr., 12:147–173.

Garrison, E. D., 1974. Radiolarian cherts, pelagic limestones and igneous rocks in eugeosynclinal assemblages. *In* Hsü, K. J., and Jenkyns, H. C. (Eds.), *Pelagic Sediments on Land and Under the Sea*. Spec. Publ. Int. Assoc. Sedimentol., 1:367–399.

Gieskes, J. M., and Johnson, J., 1981. Interstitial water studies, Leg 58. *In* Larson, R. L., and Schlanger, S. O., *Init. Repts. DSDP*, 61: Washington (U.S. Govt. Printing Office), 607–611.

Gradstein, F. M., Kaminski, M. A., and Berggren, W. A., 1988. Cenozoic foraminiferal biostratigraphy of the Central North Sea. *Abh. Geol. Bundensanst. Austria.*, 41:97–108.

Gradstein, F. M., and Sheridan, R. E., 1983. On the Jurassic Atlantic Ocean and a synthesis of results of DSDP Leg 76. *In* Gradstein, F. M., and Sheridan, R. E., *Init. Repts. DSDP*, 76: Washington (U.S. Govt. Printing Office), 913–943.

Handschumacher, D. W., and Gettrust, J. F., 1985. Mixed polarity model for the Jurassic "Quiet Zones": new oceanic evidence of frequent pre-M25 reversals. *Eos*, 66:867.

Handschumacher, D. W., Sager, W. W., Hilde, T.W.C., and Bracey, D. R., 1988. Pre-Cretaceous tectonic evolution of the Pacific Plate and extension of the geomagnetic polarity reversal time scale with implications for the origin of the Jurassic "Quiet Zone." *Tectonophysics*, 155:365–380.

Harland, W. B., Cox, A. V., Llewellyn, P. G., Pickton, C.A.G., Smith, D. G., and Walters, R., 1982. *A Geologic Time Scale:* Cambridge (Cambridge Univ. Press).

Heezen, B. C., MacGregor, I. D., and DSDP Leg 20 Scientific Party, 1973. Mesozoic chalks beneath the Caroline abyssal plain: DSDP Site 199. *In* Heezen, B. C., MacGregor, I. D., et al., *Init. Repts. DSDP*, 20: Washington (U.S. Govt Printing Office), 65–85.

Helsley, C. E., and Steiner, M. D., 1969. Evidence for long intervals of normal polarity during the Cretaceous period. *Earth Planet. Sci. Lett.*, 5:325–332.

Hemleben, C., and Troester, J., 1984. Campanian-Maestrichtian deep-water foraminifers from Hole 534A, Deep Sea Drilling Project. *In* Biju-Duval, B., Moore, J. C., et al., *Init. Repts. DSDP*, 78A: Washington (U.S. Govt. Printing Office), 509–532.

Houtz, R. E., J. Ewing, and P. Buhl, 1970. Seismic data from sonobuoy stations in the northern and equatorial Pacific, *J. Geophys. Res.*, 75:5093–5111.

Houtz, R. E., and Ludwig, W. J., 1979. Distribution of reverberant subbottom layers in the southwest Pacific basin. *J. Geophys. Res.*, 84:3497–3505.

Hutchinson, D. R., and Detrick, R. S., 1984. Water gun vs. air gun: a comparison. *Mar. Geophys. Res.*, 6:295–310.

Irving, E., and Pullaiah, G., 1976. Reversal of the geomagnetic field, magnetostratigraphy and relative magnitude of palaeosecular variation in the Phanerozoic. *Earth-Sci. Rev.*, 12:35–64.

Karpoff, A. M., 1989. Les faciès pélagiques condensés cénozoiques des océans Pacifique et Atlantique: témoins des grandes crises géodynamiques [Thèse Doc. ès Sci.], Univ. Louis Pasteur, Strasbourg.

Karpoff, A. M., Walter, A. V., and Pflumio, C., 1988. Mettaliferous sediments within lava sequences of the Sumail ophiolite (Oman): mineralogical and geochemical characterization, origin and evolution. *Tectonophysics*, 151:223–245.

Kent, D. V., and Gradstein, F. M., 1985. A Cretaceous and Jurassic geochronology. *Geol. Soc. Am. Bull.*, 96:1419–1427.

_____, 1986. A Jurassic to Recent chronology. *In* Tucholke, B. E., and Vogt, P. R. (Eds.), *The Geology of North America: The Western Atlantic Region*. Geol. Soc. Am. DNAG Ser., 1:45–50.

Kono, M., 1980. Statistics of paleomagnetic inclination data. *J. Geophys. Res.*, 85:3878–3882.

Lancelot, Y., 1973. Chert and silica diagenesis in sediments from the central Pacific. *In* Winterer, E. L., Ewing, J. I., et al. *Init. Repts. DSDP*, 17: Washington (U.S. Govt. Printing Office), 377–405.

_____, 1978. Relation entre évolutions sédimentaire et tectonique de la plaque Pacifique depuis le Crétacé inférieur. *Mem. Soc. Geol. Fr.*, Nelle Ser., 134.

Lancelot, Y., Hathaway, J. C., and Hollister, C. D., 1972. Lithology of sediments from the western from the western North Atlantic. *In* Hollister, C. D., Ewing, J. I., et al., *Init. Repts. DSDP*, 11: Washington (U.S. Govt. Printing Office): 901–949.

Lancelot, Y., and Larson, R. L., 1975. Sedimentary and tectonic evolution of the northwestern Pacific. *In* Larson, R. L., Moberly, R., et al., *Init. Repts. DSDP*, 32: Washington (U.S. Govt. Printing Office), 925–939.

Larson, R. L., and Hilde, T.W.C., 1975. A revised time scale of magnetic reversals for the Early Cretaceous and Late Jurassic. *J. Geophys. Res.*, 80:2586–2594.

Larson, R. L., and Lowrie, W., 1975. Paleomagnetic evidence for motion of the Pacific plate from Leg 32 basalts and magnetic anomalies. *In* Larson, R. L., Moberly, R., et al., *Init. Repts. DSDP*, 32: Washington (U.S. Govt. Printing Office), 571–577.

Larson, R. L., Schlanger, S. O., et al., 1981. *Init. Repts. DSDP*, 61: Washington (U.S. Govt. Printing Office).

Lynn, D. C., and Bonatti, E., 1965. Mobility of manganese in diagenesis of deep-sea sediments. *Mar. Geol.*, 3:457–474.

Martini, E., 1971. Standard Tertiary and Quaternary calcareous nannoplankton zonation. *In* Farinacci, A. (Ed.), *Proc. 2nd Planktonic Conf. Roma:* Rome (Ed. Technosci.), 2:739–785.

Matsuoka, A., and Yao, S., 1986. A newly proposed radiolarian zonation for the Jurassic of Japan. *Mar. Micropaleontol.*, 11:91–105.

McCave, I. N., 1979. Depositional features of organic-carbon-rich black and green mudstones at DSDP Sites 386 and 387, western North Atlantic. *In* Tucholke, B. E., Vogt, P. R., et al., *Init. Repts. DSDP*, 43: Washington (U.S. Govt. Printing Office): 411–416.

Morkhoven, F.P.C.M. van, Berggren, W. A., and Edwards, A. S., 1986. Cenozoic cosmopolitan deep-water benthic foraminifera. *Mem. Cent. Rech. Explor. Prod. Elf Aquitaine*, 11:1–421.

Moullade, M., Kuhnt, W., and Thurow, J., 1988. Agglutinated benthic foraminfers from Upper Cretaceous vareigated clays of the North Atlantic Ocean (DSDP Leg 93 and ODP Leg 103). *In* Boillot, G., Winterer, E. L., et al., *Proc. ODP, Sci. Results*, 103: College Station, TX (Ocean Drilling Program), 349–377.

Ogg, J. G., Robertson, A.H.F., and Jansa, L. F., 1983. Jurassic sedimentation history of Site 534 (western North Atlantic) and the Atlantic-Tethys seaway. *In* Sheridan, R. E., Gradstein, F. M., et al., *Init. Repts. DSDP*, 76: Washington (U.S. Govt. Printing Office), 829–884.

Perch-Nielsen, K., 1985. Mesozoic calcareous nannofossils. *In* Bolli, H., Saunders, J. B., and Perch-Nielsen, K. (Eds.), *Plankton Stratigraphy:* Cambridge (Cambridge Univ. Press), 329–426.

Premoli-Silva, I., Erba, E., and Tornaghi, M. E., 1989. Paleoenvironmental signals and changes in surface fertility in mid-Cretaceous C_{org}-rich pelagic facies of the Fucoid Marls (central Italy). *Geobios,* 11:225–236.

Roth, P. H., 1978. Cretaceous nannoplankton biostratigraphy and oceanography of the northwestern Atlantic Ocean. *In* Benson, W. E., Sheridan, R. E., et al., *Init. Repts. DSDP,* 44: Washington (U.S. Govt. Printing Office), 731–759.

Roth, P. H., and Krumbach, K. R., 1986. Middle Cretaceous calcareous nannofossil biogeography and preservation in the Atlantic and Indian Oceans: implications for paleoceanography. *Mar. Micropaleont.* 10:235–266.

Sanfilippo, A., and Riedel, W. R., 1985. Cretaceous radiolaria. *In* Bolli, H. M., Saunders, J. B., and Perch-Nielsen, K. (Eds.), *Plankton Stratigraphy:* Cambridge (Cambridge Univ. Press), 573–630.

Shipboard Scientific Party, 1973. Site 167. *In* Winterer, E. L., Ewing, J. I., et al., *Init. Repts. DSDP,* 17: Washington (U.S. Govt. Printing Office), 145–234.

Shipboard Scientific Party, 1976. Site 319. *In* Yeats, R. S., Hart, S. R., et al., *Init. Repts. DSDP,* 34: Washington (U.S. Govt. Printing Office), 19–80.

Shipley, T. H., Whitman, J. M., Dunnebier, F. K., and Peterson, L. D., 1983. Seismic strtigraphy and sedimentation history of the East Mariana Basin, Western Pacific. *Earth Planet. Sci. Lett.,* 64:257–275.

Sissingh, W., 1977. Biostratigraphy of Cretaceous calcareous nannoplankton. *Geol. Mijnbouw,* 56:37–65.

Tamaki K., Nakanishi, M., Sayanagi, K., and Kobayashi, K., 1987. Jurassic magnatic anomaly lineations of the western Pacific Ocean and the origin of the Pacific plate. *Eos,* 68:1493.

Thierstein, H. R., 1971. Tentative Lower Cretaceous nannoplankton zonation. *Eclogae Geol. Helv.,* 64:459–488.

_____, 1973. Lower Cretaceous calcareous nannoplankton biostratigraphy. *Abh. Geol. Bundesanst. Austria,* 29:1–52.

_____, 1976. Mesozoic calcareous nannoplankton biostratigraphy of marine sediments. *Mar. Micropaleontol.,* 1:325–362.

Tsunogai, S., and Kusakabe, M., 1982. Migration of manganese in the deep-sea sediments. *In* Fanning, K. A., and Manheim, F. T. (Eds.), *The Dynamic Environment of the Ocean Floor:* Lexington, MA (Lexington Books), 257–273.

Wise, S. W., and Wind, F. H., 1977. Mesozoic and Cenozoic calcareous nannofossils recovered by Deep Sea Drilling Project Leg 36 drilling on the Falkland Plateau, Southwest Atlantic sector of the Southern Ocean. *In* Barker, P., Dalziel, I.W.D., et al., *Init. Repts. DSDP,* 36: Washington (U.S. Govt. Printing Office), 269–491.

Zotto, M., Drugg, W. S., and Habib, D., 1987. Kimmeridgian dinoflagellate stratigraphy in the Southwestern North Atlantic. *Micropaleontology,* 33:193–213.

Ms 129A-103

NOTE: All core description forms ("barrel sheets") and core photographs have been printed on coated paper and bound as Section 3, near the back of the book, beginning on page 247.

Hole 801B: Density-Caliper-Gamma Ray Log Summary

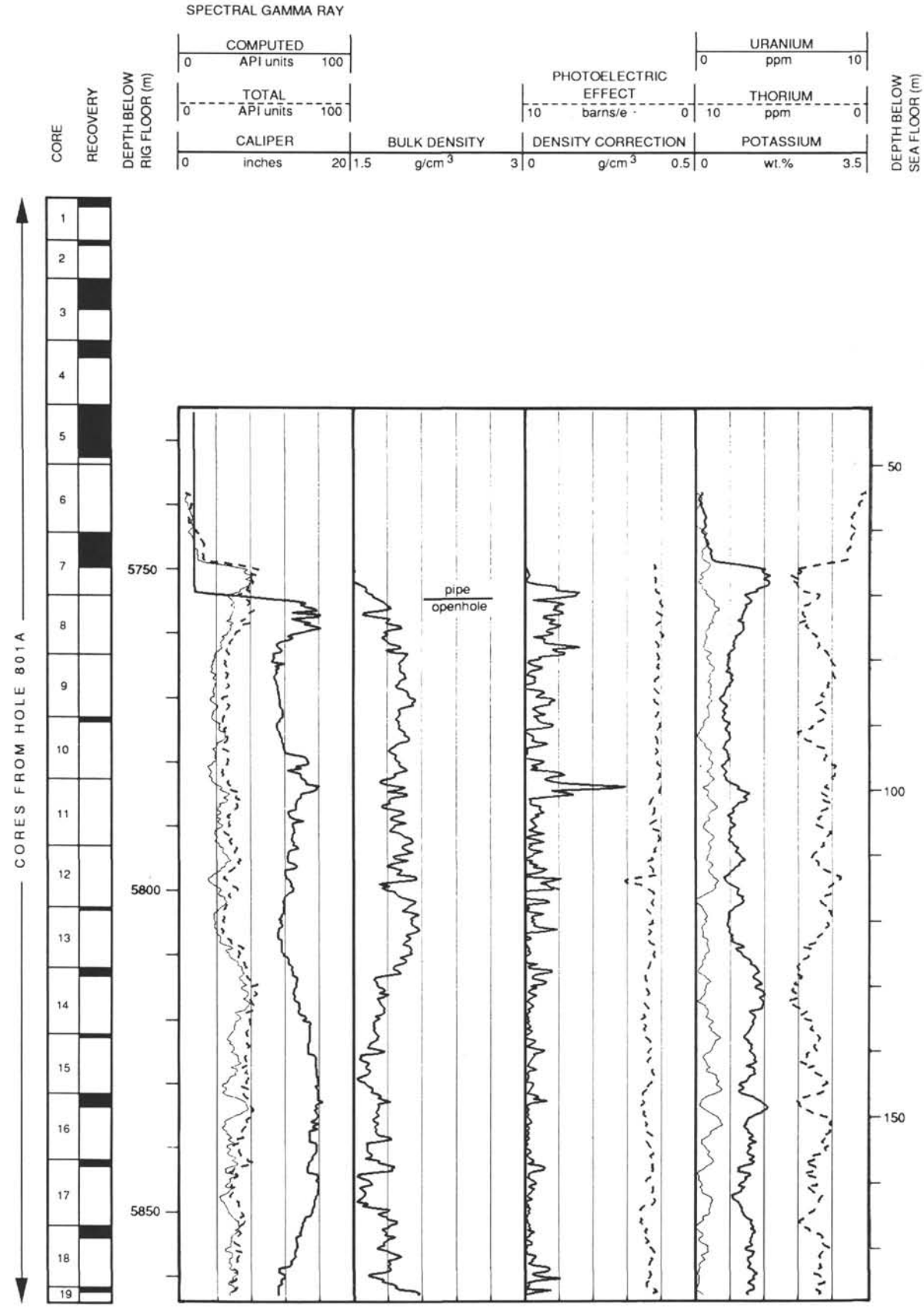

Hole 801B: Density-Caliper-Gamma Ray Log Summary (continued)

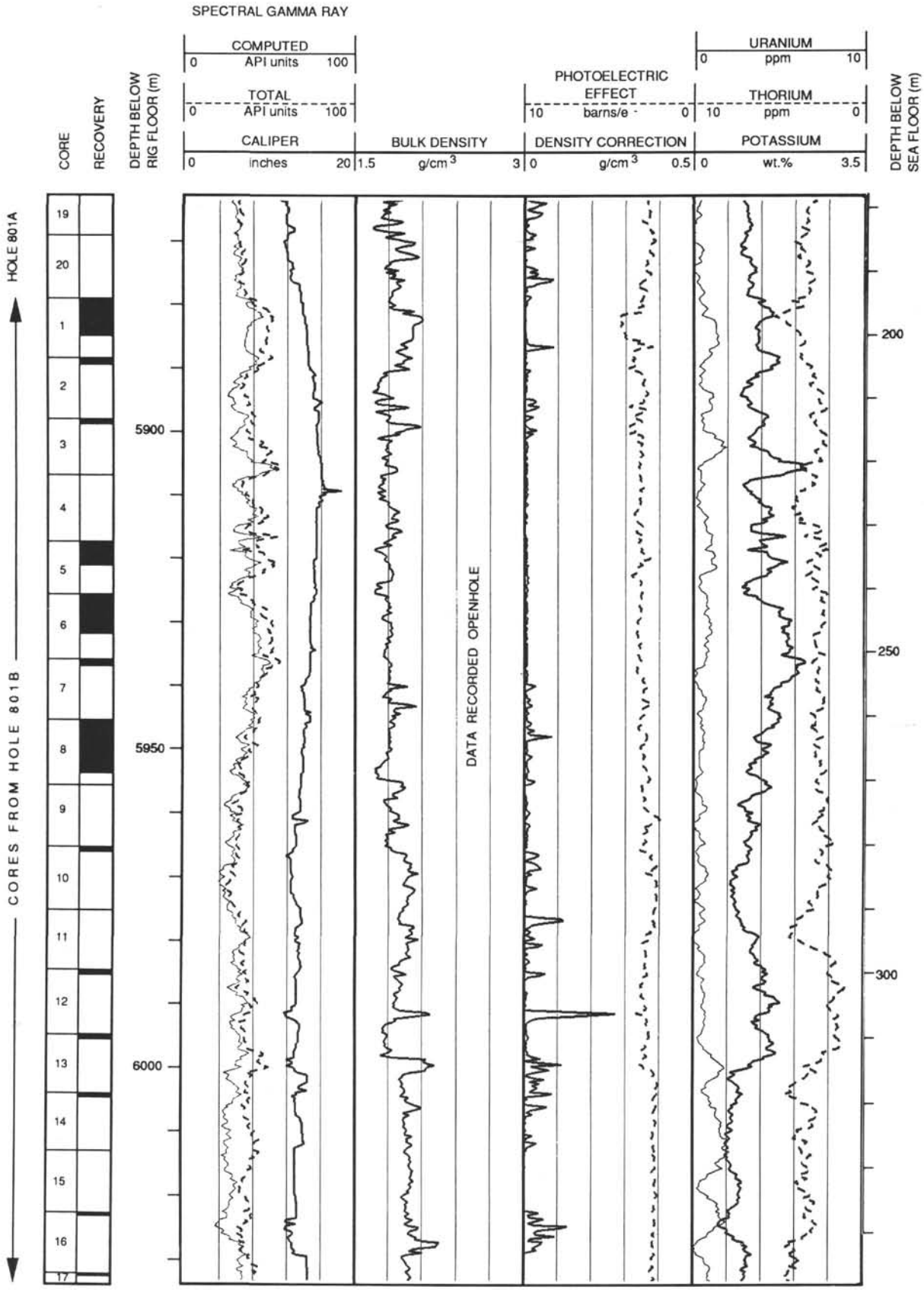

Hole 801B: Density-Caliper-Gamma Ray Log Summary (continued)

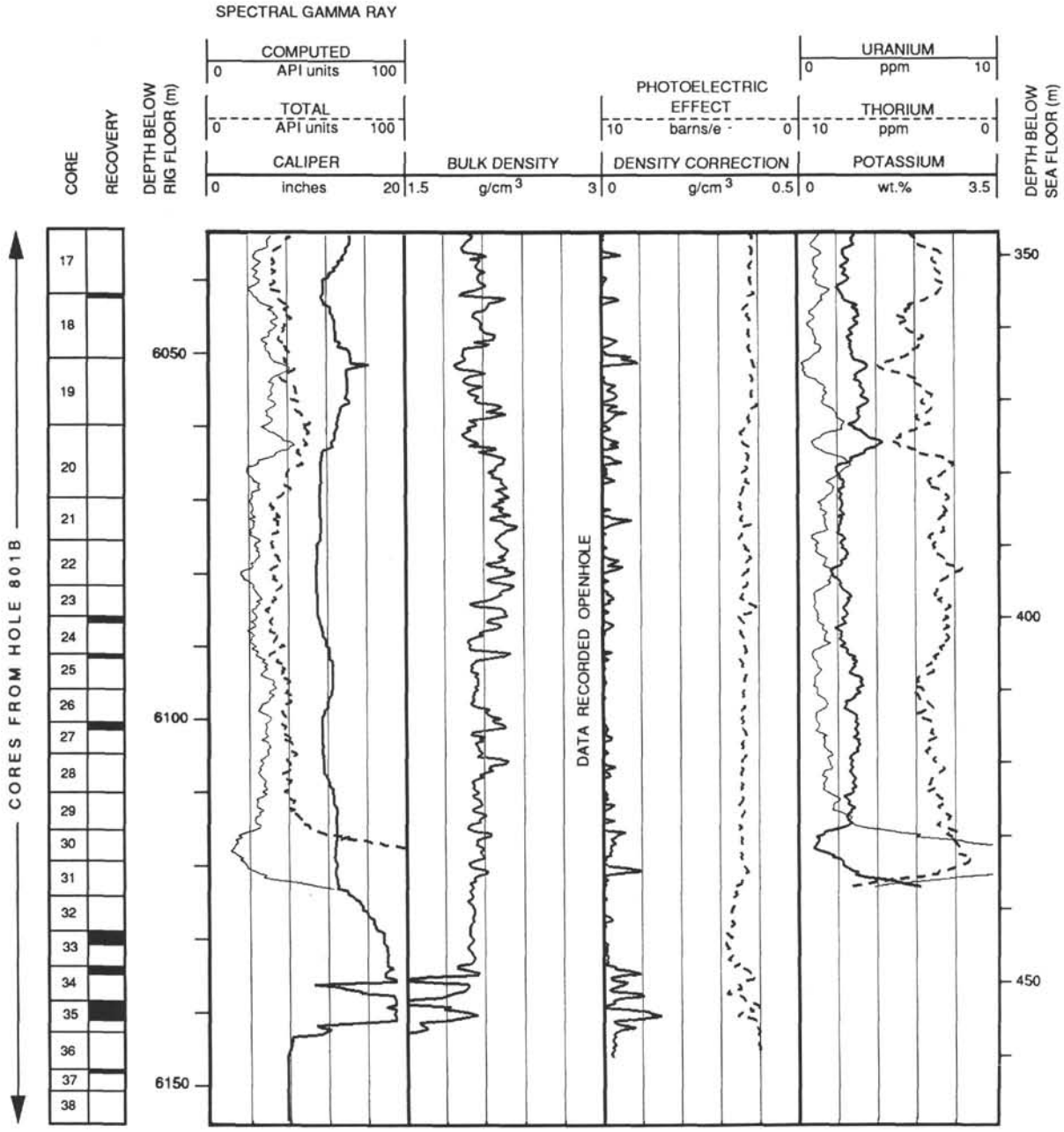

Hole 801B: Geochemical Log Summary

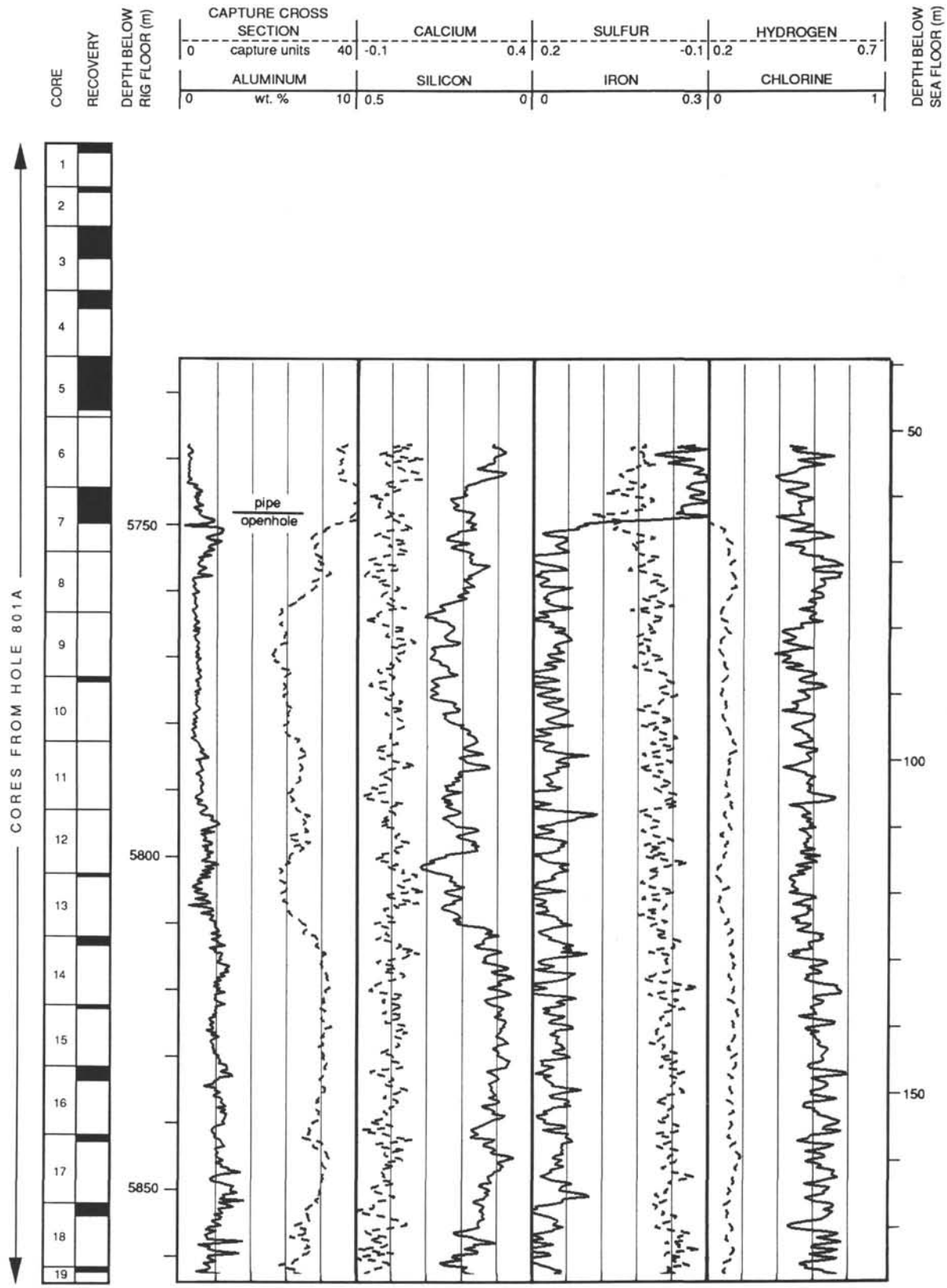

Hole 801B: Geochemical Log Summary (continued)

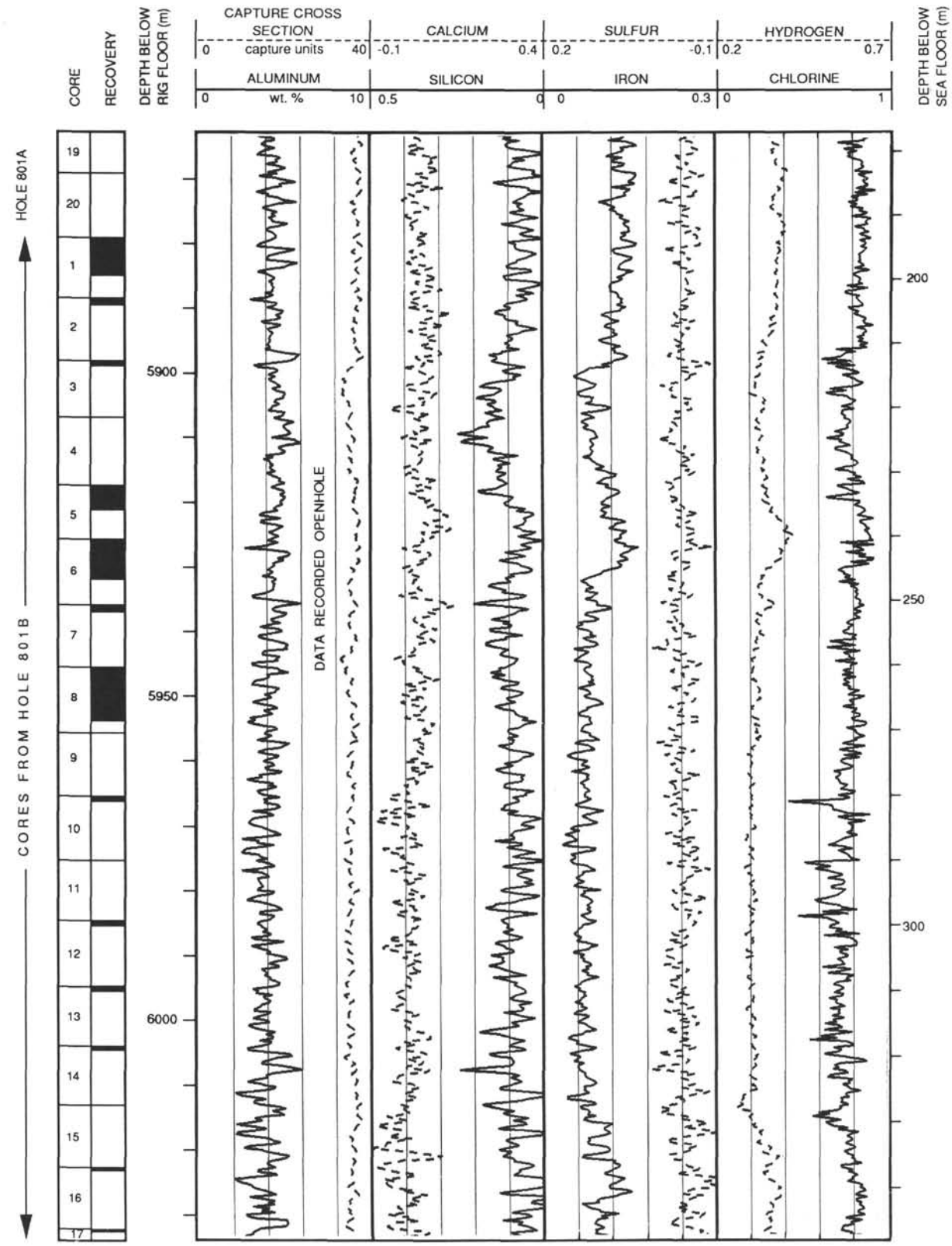

Hole 801B: Geochemical Log Summary (continued)

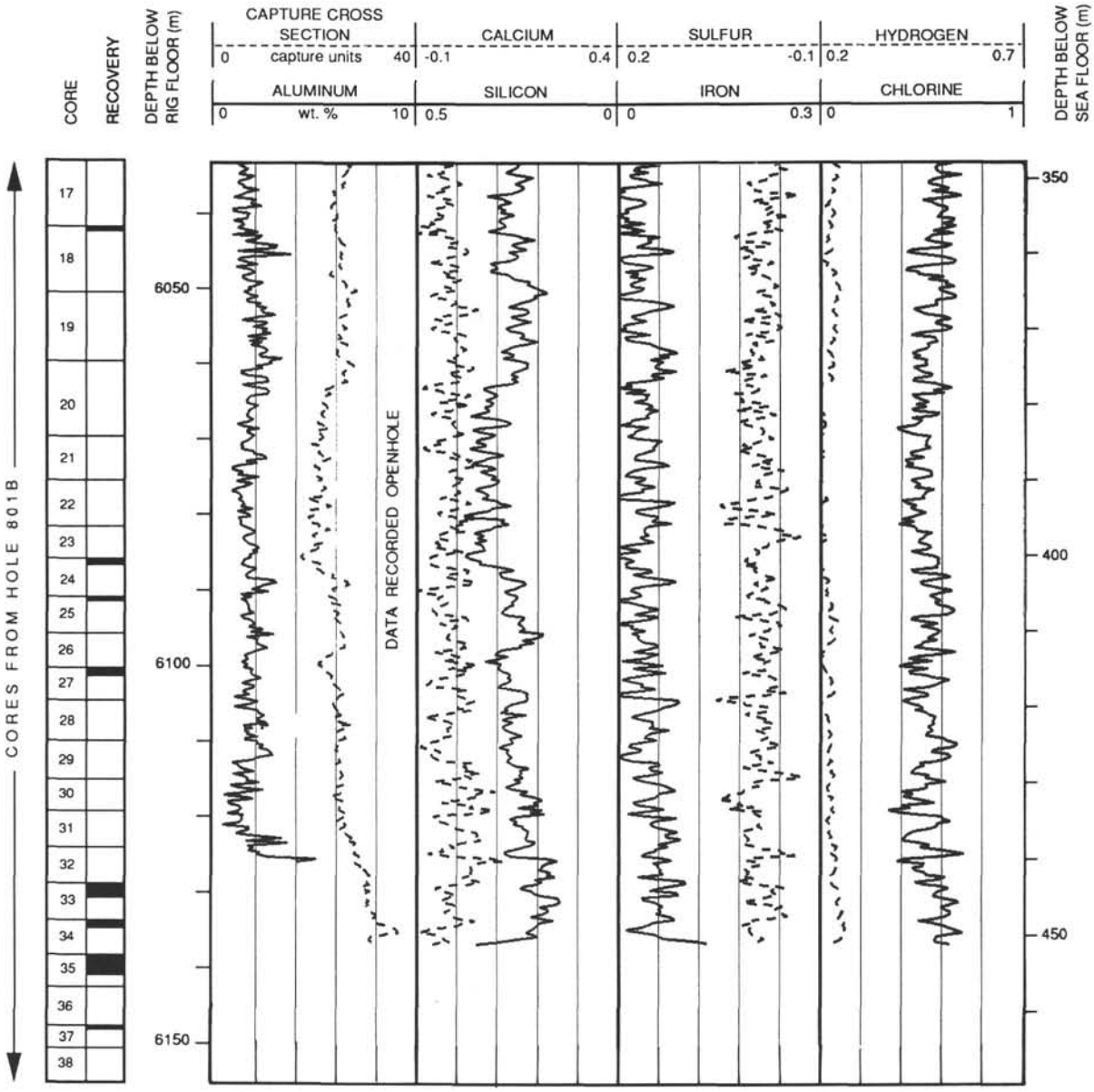

Hole 801B: Resistivity-Sonic-Gamma Ray Log Summary

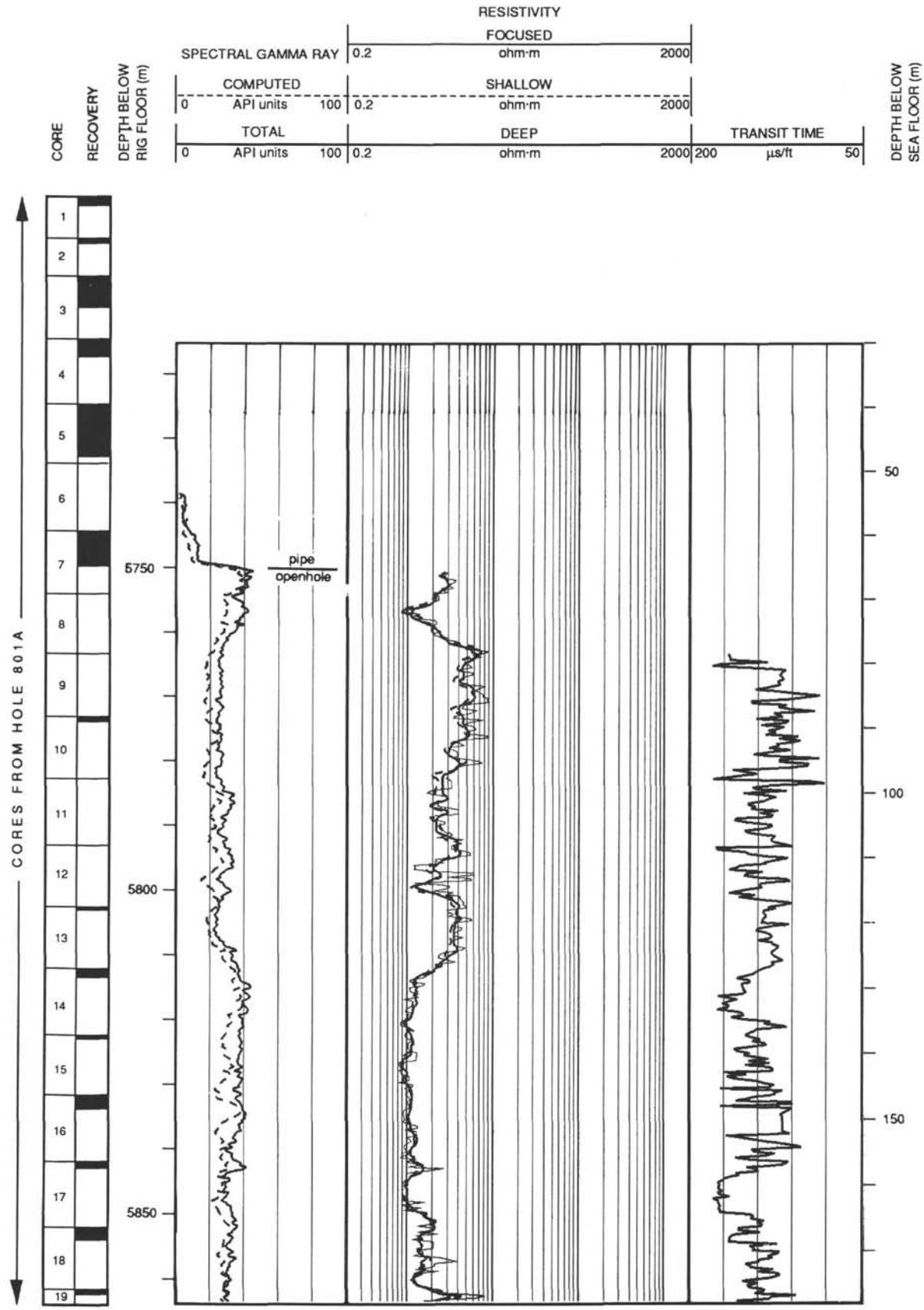

Hole 801B: Resistivity-Sonic-Gamma Ray Log Summary (continued)

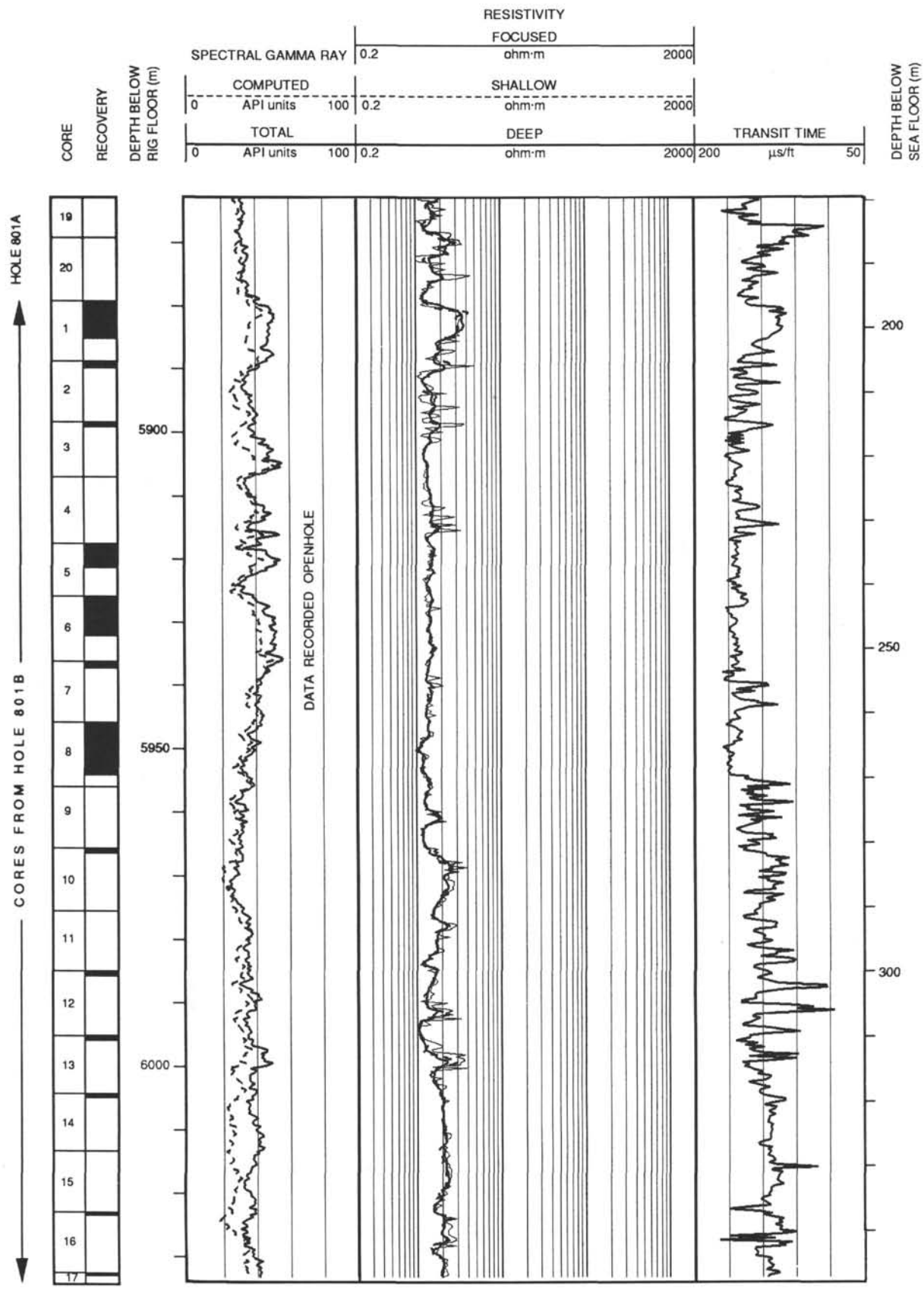

Hole 801B: Resistivity-Sonic-Gamma Ray Log Summary (continued)